

# **CYTOTOXICITY AND TOXICOKINETICS OF NEW PSYCHOACTIVE SUBSTANCES**

Dissertation

zur Erlangung des Grades

des Doktors der Naturwissenschaften

der Naturwissenschaftlich-Technischen Fakultät

der Universität des Saarlandes

von

**Tanja Maria Gampfer**

Saarbrücken

2022

**Tag des Kolloquiums:** 08. Februar 2023

**Dekan:** Prof. Dr. Ludger Santen

**Berichterstatter:** Prof. Dr. Markus R. Meyer  
Prof. Dr. Marc Schneider

**Akad. Mitglied:** Dr. Daniel Krug

**Vorsitz:** Prof. Dr. Veit Flockerzi

## **VORWORT**

Die nachfolgende Arbeit entstand unter der Anleitung von Herrn Univ.-Prof. Dr. Markus R. Meyer in der Abteilung für Experimentelle und Klinische Toxikologie der Fachrichtung Experimentelle und Klinische Pharmakologie und Toxikologie der Universität des Saarlandes in Homburg von Oktober 2018 bis Oktober 2022.

## **Danksagung**

Insbesondere möchte ich mich bei meinem Doktorvater Herrn Professor Markus R. Meyer bedanken für das entgegengebrachte Vertrauen und die herzliche Aufnahme in seinen Arbeitskreis, die Vergabe dieses interessanten, und herausfordernden Dissertationsthemas, der hervorragenden Betreuung sowie seiner stets sachlichen und konstruktiven Kritik und die Ermöglichung der aktiven Teilnahme an nationalen und internationalen Fachkongressen. Besonders zu schätzen lernte ich die immer offene und freundliche Arbeitsatmosphäre, seine stets lösungsorientierte Denkweise, sowie seinen Ansporn über sich hinaus zu wachsen.

Herrn Professor Marc Schneider danke ich für die Übernahme des Koreferats, sowie Herrn Professor Hans H. Maurer für seine Diskussionsbereitschaft und fachliche Unterstützung während der Seminare.

Frau Dr. Lea Wagmann danke ich für ihre wissenschaftliche Expertise, die Begleitung und Anleitung der Arbeit und die fachliche Diskussionsbereitschaft.

Zudem möchte ich Herrn Professor Veit Flockerzi danken für die Ermöglichung der Zellkulturversuche.

Meinen Kolleginnen und Kollegen möchte ich neben dem wichtigen wissenschaftlichen Austausch besonders für das angenehme Arbeitsklima und die gute Zusammenarbeit trotz Corona-Pandemie, schlafloser Dienstächte oder nahender Kongressdeadlines danken.

Meiner ehemaligen Kollegin Frau Dr. Frederike Nordmeier aus der Abteilung der Rechtsmedizin danke ich für ihre fachliche Unterstützung und Zusammenarbeit, sowie der daraus resultierenden guten Freundschaft.

Außerdem danke ich Herrn Armin A. Weber und Herrn Martin Simon-Thomas für ihre unermüdliche Einsatzbereitschaft und Unterstützung bei allen technischen Fragestellungen, Frau Heidi Löhr und Frau Ute Soltek für ihre tatkräftige Unterstützung in der Zellkultur, Frau Gabriele Ulrich, Frau Michelle Backes und Herrn Carsten Schöder für ihre gewissenhaft ausgeführte Laborarbeit, sowie den Auszubildenden für die gute Zusammenarbeit im Labor.

Meinen Freunden (insbesondere Frederike, Sandra und Selina) danke ich für das stets offene Ohr, den Zusammenhalt trotz aller durchlebter Höhen und Tiefen während der Promotion, und den Wiederaufbau nach Rückschlägen auch über große Entfernungen hinweg.

Zudem möchte ich meinem Partner danken, der die Endphase meiner Promotionszeit miterleben durfte wie kein anderer, aber trotzdem nicht müde wurde mir geduldig zuzuhören und mich mit konstruktiven Ratschläge seelisch und moralisch aufzubauen.

Die letzten Worte dieser Danksagung möchte ich meiner Familie widmen: Lieber Papa, Liebe Mama, und Liebe Sis, ohne euren grenzlosen Rückhalt und eure Unterstützung in schwierigen Zeiten wäre all das nicht möglich gewesen. Danke euch!

Homburg, Oktober 2022

Tanja Maria Gampfer

“LIFE BEGINS AT THE END OF YOUR COMFORT ZONE.”

*Neale Donald Walsch*



## ZUSAMMENFASSUNG

Zur Erforschung der toxikokinetischen und cytotoxischen Eigenschaften von neuen psychoaktiven Substanzen (NPS) wurden verschiedene in vitro und in vivo Tests (weiter-)entwickelt und an strukturell unterschiedlichen Verbindungen angewendet. Mittels Stoffwechselversuchen wurden unter anderem analytische Zielmoleküle für Urinuntersuchungen identifiziert. Um mögliche Interaktionen mit anderen NPS oder Drogen zu untersuchen, wurden die am Metabolismus beteiligte Isoenzyme sowie die Plasmaproteinbindung bestimmt. Im letzten Schritt ging es um die Optimierung eines bestehenden Hochdurchsatzverfahrens zur Bestimmung der zytotoxischen Eigenschaften von NPS an HepG2 Zellen. Synthetische Cannabinoide zeigten einen ausgeprägteren Metabolismus als synthetische Opioide, welches sich auch in der Anzahl der daran beteiligten Isoenzyme widerspiegelte. Die Plasmaproteinbindung der untersuchten NPS lag über 70%, weshalb Wechselwirkungen mit anderen Drogen nicht ausgeschlossen werden können. Mittels des optimierten Zytotoxizitäts-Assays konnten sieben NPS als potenziell zytotoxisch eingestuft werden. In zwei Fällen konnte somit eine zuvor beschriebene in vivo Hepatotoxizität in vitro bestätigt werden. Außerdem wurden Metabolismus-basierte Effekte an der Zytotoxizität zweier NPS beobachtet.



## SUMMARY

To expand the knowledge about toxicokinetic and cytotoxic properties of new psychoactive substances (NPS), different *in vitro* and *in vivo* tests were (further) developed and applied on structurally different compounds. First, *in vitro* and *in vivo* models were used to determine the metabolic stability (*in vitro* half-life) and the metabolic fate to elucidate targets for urine-based screenings. Investigations on isozymes, which contribute to their metabolism, and on the plasma protein binding were conducted to identify potential interactions with other NPS or drugs (of abuse). Finally, an existing cytotoxicity high-content screening assay (HCSA) using HepG2 cells was optimized to specify the cytotoxic potential of NPS. Synthetic cannabinoids showed a more extensive metabolism compared to synthetic opioids, which was in accordance with the number of involved isozymes. Since plasma protein binding values exceeded 70% in all cases, relevant drug-drug interactions cannot be excluded. Based on the optimized HCSA, a cytotoxic potential was assigned for seven NPS. Therefore, for two NPS a previously reported *in vivo* hepatotoxicity can be confirmed *in vitro*. Furthermore, metabolism-based effects on their cytotoxicity were observed for two NPS.



# Table of Contents

<b>Vorwort</b>	<b>I</b>
<b>Zusammenfassung</b>	<b>V</b>
<b>Summary</b>	<b>VII</b>
<b>1. General Part</b>	<b>1</b>
1.1 New Psychoactive Substances.....	1
1.2 Toxicokinetics.....	2
1.2.1 <i>METABOLISM AND METABOLIC STABILITY</i> .....	3
1.2.2 <i>PLASMA PROTEIN BINDING</i> .....	5
1.3 Cytotoxicity Testing .....	6
1.3.1 <i>MEASUREMENT PRINCIPLES AND EVALUATION CRITERIA</i> .....	7
<b>2. Aims and Scope</b>	<b>11</b>
<b>3. Publication of the Results</b>	<b>13</b>
3.1 Toxicokinetics and analytical toxicology of the abused opioid U-48800—in vitro metabolism, metabolic stability, isozyme mapping, and plasma protein binding <sup>63</sup> .....	13
3.2 Toxicokinetic Studies and Analytical Toxicology of the New Synthetic Opioids Cyclopentanoyl-Fentanyl and Tetrahydrofuranoyl-Fentanyl <sup>64</sup> .....	23
3.3 Toxicokinetics and toxicodynamics of the fentanyl homologs cyclopropanoyl-1-benzyl-4'-fluoro-4-anilinopiperidine and furanoyl-1-benzyl-4-anilinopiperidine <sup>65</sup> .....	54

3.4 Cytotoxicity, metabolism, and isozyme mapping of the synthetic cannabinoids JWH-200, A-796260, and 5F-EMB-PINACA studied by means of in vitro systems <sup>66</sup> .....	72
3.5 A simplified strategy to assess the cytotoxicity of new psychoactive substances in HepG2 cells using a high content screening assay - Exemplified for nine compounds <sup>67</sup> .....	92
<b>4. Discussion and Conclusions</b>	<b>117</b>
<b>5. References</b>	<b>125</b>
<b>6. Abbreviations</b>	<b>133</b>

# 1. GENERAL PART

## 1.1 New Psychoactive Substances

Consumption of plant-based psychoactive substances is as old as human history, for instance, opium, cannabis, or cocaine were used for treatment of pain or in religious rituals to expand the consciousness. However, it was not until the serious consequences of opium smoking in the late 19th century became visible, which eventually led to enactment of the Single Convention on Narcotic Drugs in 1961 regulating traditional narcotic drugs.<sup>1,2</sup> In 1971, strict regulations on further psychoactive substances were promulgated by the Convention on Psychotropic Substances followed by the Convention against Illicit Traffic in Narcotic Drugs and Psychotropic Substances in 1988.<sup>2</sup> Even though these Conventions still form the basis for international drug control, new synthetic drugs are elusive.<sup>2</sup> These substances are collectively defined by the United Nations Office on Drugs and Crime (UNODC) as new psychoactive substances (NPS).<sup>2,3</sup> Their main purpose on the market is to bypass existing legislations of controlled substances by slight structural modifications. This results in legal substances retaining or even increasing dose-response effects of their illegal counterparts. Usually, manufacturing of NPS takes place in clandestine laboratories distributed around the globe.<sup>4</sup> Afterwards, they are sold as so-called ‘legal highs’, ‘research chemicals’ or ‘bath salts’ by open trading on the internet.<sup>5</sup>

By the end of 2020, more than 1,047 NPS were reported to the UNODC.<sup>6</sup> Even though the number of NPS recorded each year stagnates, there is a growing regional diversity of substances.<sup>6</sup> On the European drug market, for instance, most of the monitored NPS belong to the classes synthetic cannabinoid (SC) receptor agonists, stimulants such as cathinones or phenethylamines, opioids, and hallucinogens such as tryptamines.<sup>7</sup> Particular alarming is the ever-changing pool of NPS flooding the drugs (of abuse) market entailed by constant

law changes to control recently emerged NPS. This leads to the appearance of new compounds but also to the disappearance of other's.

Nevertheless, NPS pose a growing health concern by causing adverse effects and fatalities as indicated by hospital emergency admissions.<sup>8</sup> NPS users are generally placed at high risk of unintentional overdoses, since the content of active ingredients in NPS products vary widely. Moreover, NPS are often present as adulterants in products containing traditional drugs or they are falsely sold under the name of other NPS or illicit drugs.<sup>9</sup> In contrast to therapeutic drugs, NPS are distributed without implemented (pre-)clinical studies, resulting in a lack of information on their effects and harms. Hence, clinical and forensic toxicologists are faced with challenging tasks not only regarding analytical problems to confirm NPS exposure but also to assess possible drug interactions and toxic risks.

## 1.2 Toxicokinetics

Pharmacokinetics is a core discipline in the drug-development process of every lead compound. Its primary objective is to obtain a clinical candidate, which fulfills the desired efficacy and safety profile.<sup>10,11</sup> Such pharmacokinetic studies describe the disposition and fate of compounds in the living organism by considering processes such as absorption, distribution, metabolism, and excretion (ADME).<sup>12</sup> However, a series of fast and cost effective in vitro tests may serve as surrogates of the in vivo ADME properties of compounds.<sup>12</sup> Since NPS should not be considered as therapeutic drugs, the term "toxicokinetic" should be used instead for these compounds.<sup>13</sup> As mentioned above, there is usually a severe knowledge gap regarding NPS's safety and thus also about their threats for public health. Therefore, a timely investigation of toxicokinetics of NPS after their first emergence on the market seems crucial.

### 1.2.1 Metabolism and Metabolic Stability

One of the first steps in toxicokinetics is the investigation on the drug's metabolic pattern and stability. Knowledge about metabolites is fundamental to detect NPS in human biosamples such as blood or urine. In particular, because a reliable detection of parent compounds is not always possible, since some NPS undergo extensive biotransformation mainly in the liver.<sup>14-16</sup> Metabolic biotransformation converts lipophilic compounds into more hydrophilic ones by phase I or II reactions to facilitate their excretion mostly via urine or bile.<sup>17</sup> Although metabolic reactions mainly correspond to detoxification processes, the formation of toxic metabolites is also possible.<sup>18,19</sup> Phase I enzymes, such as the cytochrome P450 (CYP) isoenzymes, catalyze reactions, which result in the introduction or exposure of functional groups by oxidization, hydroxylation, hydrolysis, dealkylation, epoxidation, or reduction reactions. By phase II reactions, polar groups such as glucuronic acid, sulfate, glutathione, or amino acids are conjugated to phase I metabolites or directly to parent compounds. These biotransformations are mostly catalyzed by transferases, e.g., by UDP-glucuronyltransferases (UGT), sulfotransferases (SULT), or glutathione S-transferases.<sup>20</sup> Even though metabolites may be detectable in blood, urine is the matrix of choice for drug testings or presumed NPS intoxication cases. As urine features a larger number of metabolic targets, prolonged detection window, a higher analyte concentration and its collection is non-invasive.<sup>21,22</sup> Controlled human trials would certainly be best suited to identify urinary biomarkers, but these are not feasible due to ethical concerns and the absence of (pre-)clinical safety data.<sup>23</sup> Consequently, different approaches have been established distinguishing between *in vitro* and *in vivo* models. Primary human hepatocytes (PHH) are considered as the “gold standard” for *in vitro* metabolism studies as they reflect the natural enzyme clusters and drug transporters of the human liver.<sup>24</sup> However, their phenotypic instability and restricted accessibility has greatly contributed to the use of

immortalized cell lines, e.g., HepG2 or HepaRG, which originated from hepatic tumors.<sup>25</sup>

The disadvantage of immortalized cell lines is that they acquire mutations over time, which are associated with a loss of functionality found in the parental cells. For instance, HepG2 cells express lower levels of several CYP enzymes as well as single UGT.<sup>26,27</sup>

Furthermore, subcellular systems such as pooled human liver microsomes (pHLM) or pooled human liver S9 fractions (pHLS9) are commonly used in vitro preparations for metabolism studies.<sup>28,29</sup> These two models differ in the number and quantity of metabolizing enzymes since pHLM merely consist of membrane-bound enzymes, e.g., CYP isoforms or UGT, while pHLS9 additionally include enzymes contained in the cytosol such as SULT. Compared to cell-based models, pHLM and pHLS9 preparations are less expensive and time-consuming and no skilled staff is required for conducting the experiments.<sup>30</sup>

Biotransformation of xenobiotics leads to the appearance of metabolites while the parent compound simultaneously disappears over time. This is considered as metabolic stability and is usually determined by substrate depletion assays in pHLM.<sup>31-33</sup> Metabolic stability is defined via the in vitro half-life ( $t_{1/2}$ ) and intrinsic clearance ( $CL_{int}$ ). Based on this data, in vivo toxicokinetic parameters such as bioavailability and half-life can be estimated and predicted.<sup>34</sup> For example, poorly metabolic stable compounds may produce relevant amounts of toxic metabolites. By contrast, a slowly metabolized compound can remain for a longer period in the body and provoke toxicity by interactions with other drugs.<sup>35</sup>

In general, in vitro systems have the drawback that identified metabolites may not correspond entirely to those found in humans.<sup>36</sup> An explanation for this effect may be that any in vitro model is considered as a static closed system, while a whole organism is rather complex enabling the biotransformation of a drug on multiple reaction stages. Physiological processes can be reproduced best using in vivo models, however, any in vivo

model other than human may result in a dissimilar metabolic pattern by species differences.<sup>37</sup>

Rats are a traditionally established in vivo model, which has been broadly used in the past to study NPS metabolism.<sup>38</sup> However, an ethical approval is required to perform these experiments. The zebrafish (*Dario rerio*) model has been implemented more recently since their metabolism is expected to be similar to mammals holding several metabolic enzymes as direct orthologues in human. While either the adult fish or the larvae may be used as organism, the latter one is not regarded as animal experiment until five days post-fertilization according to the European Directive 2010/63/EU and thus requires no ethical approval.<sup>39</sup> On the downside, establishing and maintaining a zebrafish culture platform is expensive and experienced staff is indispensable.<sup>30,40</sup>

### 1.2.2 Plasma Protein Binding

Another important parameter in drug-development programs is the determination of plasma protein binding (PPB) since compounds can either be bound to proteins or they are freely available in plasma. Based on the free drug theory, the extent of protein binding may have an impact on their efficacy and toxicity as it is generally assumed that only the unbound drug can interact with the target receptor to achieve a pharmacological effect.<sup>41-44</sup> Thus, drugs with high binding affinity may not be distributed in the body, metabolized, or excreted. Consequently, PPB may influence toxicokinetic parameters such as volume of distribution and clearance of compounds. The prevailing binding proteins in plasma are albumin,  $\alpha$ 1-acid-glycoprotein, and lipoprotein with the largest share of almost 60% accounting for albumin of the total protein content.<sup>44,45</sup> Although the albumin concentration in plasma is usually steady, it decreases rapidly after severe injuries or surgery.<sup>43</sup> The concentration of  $\alpha$ 1-acid glycoprotein, an acute-phase-protein, increases in different

diseases such as cardiovascular diseases, inflammation and infection.<sup>43</sup> Equilibrium of bound and unbound drug concentration depends on changes in pH value, temperature, and the concentration of plasma proteins as well as competitive drugs. Besides, other factors such as renal impairment, hepatic dysfunction, or pregnancy can also alter plasma proteins and result in an acute toxicity.<sup>46</sup> Competition of different drugs for the same binding site may result in a displacement of bound molecules, which has been implicated as the causative mechanism in many drug-drug interactions.<sup>47</sup>

### **1.3 Cytotoxicity Testing**

In the early stage of drug discovery, toxicity testing is essential to identify potential candidates showing cytotoxic effects for a risk assessment of drug-induced organ injury in humans. As cytotoxicity testing of NPS is usually not in the interest of pharmaceutical industry, in most cases their (cyto)toxic properties remain unknown until reports are published about acute organ damages after ingestion.<sup>48-51</sup> Reported clinical symptoms range from an impairment of the central nervous system, e.g., seizures, aggression, or acute psychosis to the cardiovascular system such as arrhythmia but also a liver toxicity has been associated with the use of NPS.<sup>51</sup>

Historically, *in vitro* cytotoxicity assays have been found to predict human toxicity far less accurately in comparison to animal models. Driven by ethical and scientific concerns, considerable developments in technology and progress in cell biology led to the identification of numerous appropriate “cytobiomarkers”.<sup>52</sup> Thus, multiple parameters can be analyzed concerning the viability and proliferation activity of cells, e.g., cell count, leakage of intracellular components from injured cells such as lactate dehydrogenase, dysfunction of mitochondrial membrane potential, increase or loss of mitochondrial redox

activity, rise in intracellular calcium levels, or apoptosis by caspase activation or increase in cell membrane permeability.<sup>52,53</sup>

Over the years different liver-derived cell-based models have been employed to monitor drug-induced hepatotoxic effects such as HepG2, HepaRG, or PHH.<sup>26,54</sup> As already mentioned above, PHH mimic the in vivo human features most precisely as they hold different cell types present in the liver, e.g., hepatocytes, Kupffer cells, and hepatic stellate cells.<sup>55</sup> However, isolation of these cells are often complicated and isolated cells have relatively short lifetime for continuous experiments. Alternatively, differentiated HepaRG cells can be cultured for some weeks expressing gene levels of almost all metabolic enzymes similar to PHH except for CYP2D6.<sup>26,27</sup> Besides their above mentioned metabolic limitations, HepG2 cells are, compared to PHH and HepaRG, almost unlimited in lifespan, relatively simple in cell culture, and cost-effective.<sup>47</sup> Concerning the in vivo hepatotoxic predictivity of the presented cell models, some studies report about an inferiority of HepG2 cells compared to the other cell models, whereas others observed no differences in their predictivity.<sup>26,52,54</sup>

Most commonly used cell culture systems to assess a cytotoxicity are based on two-dimensional (2D) cell monolayers, however, recently three-dimensional (3D) spheroid culture models has become more popular. In general, 3D cultivation improves many shortcomings stated for the 2D cultures and also restores hepatic functions, thus it may pose a genuine future perspective.<sup>56</sup>

### **1.3.1 Measurement Principles and Evaluation Criteria**

Different imaging-based techniques have been implemented to measure drug-induced changes on cellular parameters. Multiplate readers are frequently used to determine parameters depending on absorbance, fluorescence, or luminescence intensity. Another

approach is based on flow cytometry, which detects and counts single fluorescent-labeled cells in front of a laser beam. The main disadvantage of both multiplate readers and flow cytometry is their limited spatial resolution of cells, that means effects are often only visualized on a well or whole cell level, which may lead to false positive or negative results.<sup>57</sup> In turn, fluorescence microscopy measures effects on subcellular levels. Therefore, changes on intracellular processes can be directly monitored at the target compartment. Thus artifacts can be reduced such as background fluorescence.<sup>52</sup>

Basically, two different test strategies are applied, namely conventional assays or high-content screening assays (HCSA). Conventional assays often measure single endpoint parameters in individual experiments, which can be laborious in handling, expensive, and time consuming.<sup>52</sup> Motivated by the pharmaceutical industry, fluorescence-based HCSA have been developed to minimize costs by a higher sample throughput due to a fully automatized analysis.<sup>52</sup> These allow the simultaneous analysis of several endpoints in one single run leading to an enhanced cytotoxic predictivity than single conventional assays, which resulted in their more widespread use in recent years.<sup>52,53,58,59</sup> However, as both strategies measure parameters at a fixed time at the end of the experiment, potentially not all cytotoxic processes are considered. Therefore, real-time measurement systems have been developed lately to enable the analysis of cells during the whole experiment in the incubator. Particular in combination with endpoint assays, the use of real-time analyzers with its special focus on proliferation and morphological changes seems to be a promising approach.<sup>60</sup>

To evaluate a potential cytotoxicity, intracellular concentrations of drugs would be the best indicator, however, they are difficult to quantify in humans.<sup>61</sup> Thus, typically maximum blood or serum concentrations are used as surrogate measure to assess a cytotoxic potential of drugs.<sup>52</sup> Since known maximum blood or serum concentrations of NPS are rare for

reasons stated above, accurate assessment criteria are hard to determine. Some studies base their evaluation criteria on case reports or common consumer dosages for a first hepatotoxic estimation.<sup>53,62</sup> Additionally, toxicokinetic parameters such as ADME should be considered to predict cytotoxic properties as accurately as possible.



## 2. AIMS AND SCOPE

This thesis aimed to (further) develop and apply a set of in vitro and in vivo toxicokinetic tests and cytotoxicity screenings to gain a comprehensive picture about NPS's toxicity as depicted in Fig. 1. Fentanyl and non-fentanyl derived NPS were studied regarding their in vitro metabolic stability to calculate  $t_{1/2}$  and  $CL_{int}$ . In vitro metabolic pattern of these fentanyl and non-fentanyl derived NPS and SC were investigated to identify metabolic biomarkers for urine screenings. Studies on PPB were conducted for fentanyl and non-fentanyl derivatives to evaluate possible drug-drug interactions. Metabolites identified by in vitro models were compared to the those detected using the in vivo zebrafish larvae model for two fentanyl-homologs. Finally, the hepatotoxic propensity of 12 NPS belonging to different classes were investigated by a HCS approach to roughly assess the risk of in vivo liver toxicity.

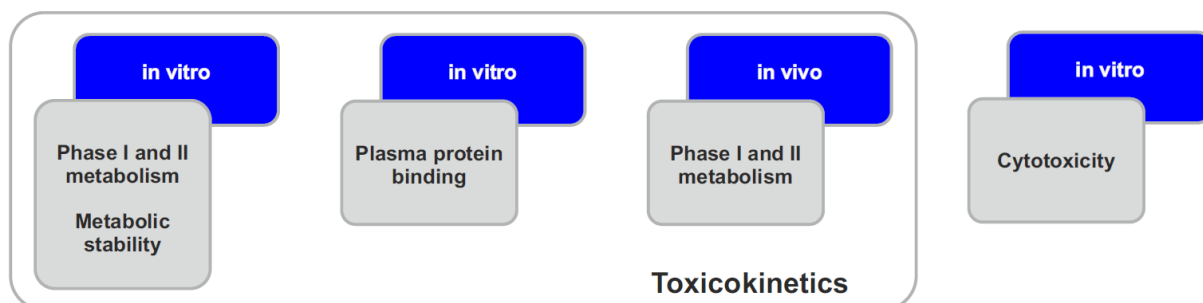


Fig. 1: In vitro and in vivo tests used in this work.

The constitutions of this thesis are:

- Determination of in vitro metabolic stability of five NPS using human liver preparations and liquid chromatography coupled to high-resolution tandem mass spectrometry (LC-HRMS/MS)
- Identification of phase I and II metabolites of eight NPS using in vitro pHLM or pHLS9
- Mapping of human CYP isozymes involved in the initial metabolic steps of eight NPS
- Evaluation of PPB for five NPS and calculation of hepatic clearances
- Development of a method to detect three new synthetic opioids (NSO) in rat urine using a precipitation procedure or glucuronidase cleavage coupled with solid phase extraction (SPE) by LC-HRMS/MS
- Investigation on the in vivo metabolic fate of the fentanyl homologs cyclopropanoyl-1-benzyl-4'-fluoro-4-anilinopiperidine (4F-Cy-BAP) and furanoyl-1-benzyl-4'-fluoro-4-anilinopiperidine (Fu-BAP) using a zebrafish larvae model in comparison to in vitro models
- Optimization and simplification of an existing cytotoxicity HCSA using HepG2 cells
- Investigation on the cytotoxic potential including metabolism-based effects of 12 NPS from four different chemical classes using HepG2 cells

### 3. PUBLICATION OF THE RESULTS

The results of this thesis are published in the following articles:

#### 3.1 Toxicokinetics and analytical toxicology of the abused opioid U-48800—in vitro metabolism, metabolic stability, isozyme mapping, and plasma protein binding<sup>63</sup>

(DOI: 10.1002/dta.2683)

**Authors Contributions** Tanja M. Gampfer conducted the experiments, evaluated the data, and wrote the manuscript; Lilian H. J. Richter developed the incubation using pooled human liver S9 fractions and supported with scientific discussions; Jan Schäper characterized and provided the investigated new psychoactive substance U-48800 and supported with scientific discussion; Markus R. Meyer and Lea Wagmann supported with scientific discussion, the design of the experiments, and research supervision.

## RESEARCH ARTICLE

# Toxicokinetics and analytical toxicology of the abused opioid U-48800 – in vitro metabolism, metabolic stability, isozyme mapping, and plasma protein binding

Tanja M. Gampfer<sup>1</sup> | Lilian H.J. Richter<sup>1</sup> | Jan Schäper<sup>2</sup> | Lea Wagmann<sup>1</sup> |  
Markus R. Meyer<sup>1</sup> 

<sup>1</sup>Department of Experimental and Clinical Toxicology, Institute of Experimental and Clinical Pharmacology and Toxicology, Center for Molecular Signaling (PZMS), Saarland University, Homburg, Germany

<sup>2</sup>State Bureau of Criminal Investigation Bavaria, Munich, Germany

**Correspondence**

Markus R. Meyer, Department of Experimental and Clinical Toxicology, Institute of Experimental and Clinical Pharmacology and Toxicology, Center for Molecular Signaling (PZMS), Saarland University, Homburg, Germany.  
Email: markus.meyer@uks.eu

**Abstract**

Due to the risk of new synthetic opioids (NSOs) for human health, the knowledge of their toxicokinetic characteristics is important for clinical and forensic toxicology. U-48800 is an NSO structurally non-related to classical opioids such as morphine or fentanyl and offered for abuse. As toxicokinetic data of U-48800 is not currently available, the aims of this study were to identify the in vitro metabolites of U-48800 in pooled human liver S9 fraction (pS9), to map the isozymes involved in the initial metabolic steps, and to determine further toxicokinetic data such as metabolic stability, including the in vitro half-life ( $t_{1/2}$ ), and the intrinsic ( $CL_{int}$ ) and hepatic clearance ( $CL_H$ ). Furthermore, drug detectability studies in rat urine should be done using hyphenated mass spectrometry. In total, 13 phase I metabolites and one phase II metabolite were identified. *N*-Dealkylation, hydroxylation, and their combinations were the predominant metabolic reactions. The isozymes CYP2C19 and CYP3A4 were mainly involved in these initial steps. CYP2C19 poor metabolizers may suffer from an increased U-48800 toxicity. The in vitro  $t_{1/2}$  and  $CL_{int}$  could be rated as moderate, compared to structural related compounds. After administration of an assumed consumer dose to rats, the unchanged parent compound was found only in very low abundance but three metabolites were detected additionally. Due to species differences, metabolites found in rats might be different from those in humans. However, phase I metabolites found in rat urine, the parent compound, and additionally the *N*-demethyl metabolite should be used as main targets in toxicological urine screening approaches.

**KEYWORDS**

LC–HRMS/MS, metabolic stability, new synthetic opioids, pooled human liver S9 fraction

This is an open access article under the terms of the Creative Commons Attribution-NonCommercial-NoDerivs License, which permits use and distribution in any medium, provided the original work is properly cited, the use is non-commercial and no modifications or adaptations are made.

© 2019 The Authors. Drug Testing and Analysis published by John Wiley & Sons Ltd



added. The amount of organic solvent was below 1%.<sup>13</sup> All given concentrations are concentrations in the final incubation mixture (final volume: 300  $\mu$ L).

Reactions were started by adding U-48800. The maximum incubation time was 360 minutes and 30  $\mu$ L aliquots were taken after 1, 15, 30, 45, 60, 75, 90, 180, and 360 minutes. Reactions were terminated by addition of 10  $\mu$ L ice-cold acetonitrile containing trimipramin- $d_3$  (5  $\mu$ M) as internal standard (IS). Afterwards, the tubes were cooled for 30 minutes at  $-20^\circ\text{C}$ , centrifuged at  $18,407 \times g$  for 2 minutes, the supernatants transferred to autosampler vials, and analyzed by liquid chromatography coupled to high-resolution tandem mass spectrometry (LC-HRMS/MS). Blank incubation (without substrate) and control incubation (without pS9) were done to confirm the absence of interfering compounds and to identify not metabolically formed compounds. All incubations were performed in duplicate.

Metabolic stability was evaluated by substrate depletion. Statistical analysis was done using GraphPad Prism 5.00 (GraphPad Software, San Diego, CA, USA). The natural logarithm of the area ratio of the analyte to the IS was plotted versus incubation time (1–90 minutes). The slope of the linear regression was used to calculate in vitro half-life. A t-test was performed to confirm that the  $\ln[\text{peak area ratio}]_{\text{initial}}$  of the remaining analyte was not significantly different from the  $\ln[\text{peak area ratio}]$  of the control incubation without pS9. The following settings were used: unpaired; two-tailed; significance level, 0.05; confidence intervals, 99%.

Following equations were used according to Baranczewski and Obach<sup>14,15</sup>:

$$t_{1/2} = \frac{\ln 2}{k \text{ (min)}} \quad (1)$$

$$\ln[\text{peak area ratio}]_{\text{remaining}} = \ln[\text{peak area ratio}]_{\text{initial}} - k \times t \quad (2)$$

$$CL_{\text{int}} = \frac{\ln 2}{t_{1/2} \text{ (min)}} \times \frac{[V]_{\text{incubation}} \text{ (ml)}}{[P]_{\text{incubation}} \text{ (mg)}} \times \frac{[\text{Liver}] \text{ (g)}}{[\text{BW}] \text{ (kg)}} \times \text{SF} \left( \frac{\text{mg}}{\text{g}} \right) \quad (3)$$

$$CL_{\text{h}} = \frac{Q \times f_u \times CL_{\text{int}}}{Q + f_u \times CL_{\text{int}}} \quad (4)$$

$$CL_{\text{h}} = \frac{Q \times CL_{\text{int}}}{Q + CL_{\text{int}}} \quad (5)$$

(well-stirred model with<sup>4</sup> and without<sup>5</sup> free fraction in plasma)

$$CL_{\text{h}} = Q \times \left( 1 - e^{\left( \frac{-f_u \times CL_{\text{int}}}{Q} \right)} \right) \quad (6)$$

$$CL_{\text{h}} = Q \times \left( 1 - e^{\left( \frac{-CL_{\text{int}}}{Q} \right)} \right) \quad (7)$$

(parallel tube model with<sup>6</sup> and without<sup>7</sup> free fraction in plasma)

with  $k$  = slope of the linear regression fit,  $t_{1/2}$  = in vitro half-life,  $CL_{\text{int}}$  = intrinsic clearance,  $[V]_{\text{incubation}}$  = incubation volume = 0.3,  $[P]_{\text{incubation}}$  = amount of S9 protein in the incubation = 0.6,  $[\text{Liver}]$

$[\text{BW}]$  = liver weight normalized by body weight = 26,<sup>16</sup> and SF = scaling factor S9 protein per gram of liver = 121,<sup>17</sup>  $CL_{\text{h}}$  = hepatic clearance,  $Q$  = hepatic blood flow rate in human = 20 mL/min/kg,<sup>18</sup>  $f_u$  = free fraction in plasma.

### 2.3 | Isozyme mapping

Monoxygenases activity screening was performed in accordance to a previous study with minor modifications.<sup>19</sup> U-48800 (2.5  $\mu$ M) was incubated with CYP1A2, CYP2A6, CYP2B6, CYP2C8, CYP2C9, CYP2C19, CYP2D6, CYP2E1, CYP3A4, CYP3A5 (50 pmol/mL each), or FMO3 (0.25 mg protein/mL) for 30 minutes at  $37^\circ\text{C}$ . All given concentrations are concentrations in the final incubation mixture (final volume: 250  $\mu$ L). Furthermore, the incubation mixtures contained 90mM phosphate buffer (pH 7.4), 5mM  $\text{Mg}^{2+}$ , 5mM isocitrate, 1.2mM NADP+, 0.5 U/mL isocitrate dehydrogenase, and 200 U/mL superoxide dismutase. For incubations with CYP2A6 or CYP2C9, phosphate buffer was replaced by 90mM tris buffer, according to the manufacturer's recommendation. The reactions were initiated by addition of the respective enzyme and terminated after 30  $\mu$ L aliquots were taken at 1, 5, 10, 15, 20, 25, and 30 minutes by addition of 10  $\mu$ L ice-cold acetonitrile. Afterwards, the samples were centrifuged at  $18,407 \times g$  for 5 minutes, the supernatants transferred to autosampler vials, and analyzed by LC-HRMS/MS. Blank incubation with CYP2E1 and without substrate and a negative control without enzyme were done to confirm the absence of interfering compounds and to identify not metabolically formed compounds. All incubations were performed in duplicate.

### 2.4 | Plasma protein binding studies

Two-chambered Centrifree devices from Merck (Darmstadt, Germany) were used for determination of PPB and  $f_u$ . According to published procedures,<sup>20,21</sup> 450  $\mu$ L fresh human plasma samples were spiked with 50  $\mu$ L U-48800 methanolic solution (final concentration: 0.5  $\mu$ M) and incubated for 30 min at  $37^\circ\text{C}$  ( $n = 3$ ). Before filtration, a 100  $\mu$ L aliquot (global approach, GA) was transferred to a new reaction tube. After filtration for 35 minutes at  $37^\circ\text{C}$  and  $1,600 \times g$ , 100  $\mu$ L of the ultrafiltrate (UF) was also transferred to a new reaction tube. All reactions were terminated by addition of 50  $\mu$ L ice-cold acetonitrile containing trimipramin- $d_3$  (2.5  $\mu$ M) as IS. Afterwards, samples were cooled for 30 minutes at  $-20^\circ\text{C}$ , centrifuged for 2 minutes at  $18,407 \times g$ , transferred into autosampler vials and analyzed by LC-HRMS/MS. Calculation of lipophilicity was done using ChemDraw Professional 16.0.1.4 (PerkinElmer, Waltham, MA, USA). The PPB was calculated using the following equations:

$$f_u = \frac{\text{peak area ratio} \left( \frac{U48800_{\text{UF}}}{IS_{\text{UF}}} \right)}{\text{peak area ratio} \left( \frac{U48800_{\text{GA}}}{IS_{\text{GA}}} \right)} \quad (8)$$

$$\text{PPB, \%} = (1 - f_u) \times 100 \quad (9)$$

## 2.5 | Rat urine samples

As reported earlier,<sup>22</sup> drug detectability studies were performed using rat urine samples from male Wistar rats (Charles River, Sulzfeld, Germany) for toxicological diagnostic reasons according to the corresponding German animal protection law. The rat dosage was based on a common consumer U-47700 dosage (<http://drugs.tripsit.me/>) due to unavailable consumer data of U-48800. After a single 0.6 mg/kg body mass dose administration, urine and feces were collected separately over 24 hours. Blank urine was collected before drug administration to confirm the absence of interfering compounds. Creatinine was measured in blank urine and after administration by an immunoassay. Samples were stored at -20°C until use.

## 2.6 | Sample preparation for drug detectability studies in rat urine

Urine precipitation (UP) was done in accordance to Wissenbach et al.<sup>23</sup> A volume of 200 µL rat urine was precipitated with 1 mL ice-cold acetonitrile, shaken for 2 minutes, and centrifuged at 18 407 × g for 2 minutes. The supernatant was evaporated to dryness at 70°C under nitrogen stream, and reconstituted in 100 µL eluent mixture A and B (50:50 v/v, Section 2.7). The samples were analyzed using both the mass spectrometry settings described in Section 2.7 and by standard urine screening approach (SUSA) in switching mode and without inclusion list with minor modifications.<sup>24</sup>

## 2.7 | LC-HRMS/MS conditions

A Thermo Fisher Scientific (TF, Dreieich, Germany) Dionex UltiMate 3000 RS pump consisting of a degasser, a quaternary pump, and an UltiMate autosampler, coupled to a TF Q-Exactive Plus system equipped with a heated electrospray ionization (HESI)-II source were used. A mass calibration was done according to the manufacturer's recommendations using external mass calibration prior to analysis. Injection volume was 1 µL for all samples. Gradient elution was performed according to a previous study<sup>24</sup> on a TF Accucore PhenylHexyl column (100 mm × 2.1 mm, 2.6 µm). The mobile phases consisted of 2mM aqueous ammonium formate containing formic acid (0.1%, v/v, pH 3, eluent A) and 2mM ammonium formate solution with acetonitrile: methanol (1:1, v/v), water (1%, v/v), and formic acid (0.1%, v/v, eluent B). The initial flow rate was set to 500 µL/min (0–10 minutes) and 800 µL/min (10–13.5 minutes). The gradient was stepped as follows: 0–1.0 minute hold 99% A, 1–10 minute to 1% A, 10–11.5 minute hold 1% A, and 11.5–13.5 minute hold 99% A. The HESI-II source conditions were as follows: heater temperature, 320°C; ion transfer capillary temperature, 320°C; spray voltage, 4.0 kV; ionization mode, positive; sheath gas, 60 arbitrary units (AU); auxiliary gas, 10 AU; sweep gas, 0 AU; and S-lens RF level, 50.0. Mass spectrometry was performed using full scan data and a subsequent data-dependent acquisition (DDA) with priority to mass-to-charge ratios (*m/z*) of parent compounds and their expected metabolites. The settings for full

scan data acquisition were the following: resolution, 35 000; microscans, 1; automatic gain control (AGC) target, 1e6; maximum injection time (IT), 120 ms; and scan range, *m/z* 50–750. The settings for the DDA mode with an inclusion list of U-48800 and its expected metabolites were as follows: option “pick others,” enabled; dynamic exclusion, 5 seconds; resolution, 17500; microscans, 1; isolation window, 1.0 *m/z*; loop count, 5; AGC target, 2e5; maximum IT, 250 ms; high collision dissociation cell with stepped normalized collision energy, 17.5, 35.0, 52.5; exclude isotopes, on; spectrum data type, profile; and underfill ratio, 1%. The inclusion list contained *m/z* values of likely formed metabolites such as *N*-dealkyl and hydroxy metabolites (phase I) as well as sulfates, glucuronides, methoxy metabolites (phase II), and combinations thereof. ChemSketch 2010 12.01 (ACD/Labs, Toronto, Canada) was used to draw structures of hypothetical metabolites and to calculate the exact masses. TF Xcalibur Qual Browser software version 2.2 SP1.48 (TF, Dreieich, Germany) was used for data handling. The following automated peak integration settings were used: peak detection algorithm, INCOS; baseline window, 40; area noise factor, 5; and peak noise factor, 10.

## 3 | RESULTS AND DISCUSSION

### 3.1 | In vitro metabolic stability, half-life, intrinsic clearance, and hepatic clearance

Metabolic stability was determined by a substrate depletion assay using a low protein concentration of 2 mg/mL to minimize non-specific protein binding.<sup>14</sup> Furthermore, a low substrate concentration (2.5 µM) was used to ensure a linear metabolite formation during incubation time. The *t*-test confirmed no significant difference between the natural logarithms of the peak area ratios of incubations after 1 minute and control incubations.

Metabolic stability data are summarized in Table Table S1 in the Supporting Information. The calculated in vitro *t*<sub>1/2</sub> of 54.5 minutes was longer than previously published for the structurally related compound AH-7921.<sup>11</sup> The CL<sub>int</sub> was calculated to be 20 mL/min/kg, which can be considered as intermediate in accordance to McNaney et al.<sup>25</sup> To predict human hepatic clearance (CL<sub>h</sub>), two different models (well-stirred, parallel tube) were used. Calculation using the well-stirred model including *f*<sub>u</sub> yielded 1.4 mL/min/kg and parallel tube model 1.5 mL/min/kg. In the case of basic substances, the calculated in vitro CL<sub>h</sub> values are in higher agreement with in vivo clearance data without considering the PPB.<sup>15</sup> The calculated CL<sub>h</sub> without considering *f*<sub>u</sub> was 10.0 mL/min/kg based on the well-stirred model and 12.6 mL/min/kg based on the parallel tube model. The results obtained by the two models were comparable within the with and without considering *f*<sub>u</sub> groups. Within one model, the clearance was much lower considering *f*<sub>u</sub> than without *f*<sub>u</sub>. This would lead to an underestimation of the measured in vivo clearance.

### 3.2 | Identification of in vitro metabolites

Twelve phase I metabolites were tentatively identified in pS9 or CYP isozyme incubations by comparison of their MS<sup>2</sup> spectra to the MS<sup>2</sup> spectrum of U-48800. The measured accurate masses of precursor ion (PI) and characteristic fragment ions (FI), relative intensities in MS<sup>2</sup>, calculated exact masses, elemental compositions, mass deviation errors, and retention times (RT) of U-48800 and its metabolites are listed in Table S2. The metabolites were sorted by increasing mass and RT. Only calculated exact masses will be used in the following chapter for discussion of in vitro phase I metabolites. The MS<sup>2</sup> spectra of U-48800 and the most abundant metabolites in pS9 and in monooxygenase activity studies are given in Figure 2. The MS<sup>2</sup> spectra of all other metabolites are given in Figure S1. The metabolic pathways detected in all investigated models are given in Figure 3.

The MS<sup>2</sup> spectrum of U-48800 (PI at  $m/z$  343.1338), showed FI at  $m/z$  298.0759, which originated from the separation of the tertiary amine. A cleavage of the cyclohexyl ring led to FI at  $m/z$  218.0133, followed by FI at  $m/z$  158.9762 generated after the amide cleavage. FI at  $m/z$  112.1120 contained the cyclohexyl ring coupled with the methylated amine. The cyclohexyl ring was represented by the FI at  $m/z$  81.0698. M2 (PI at  $m/z$  329.1181), formed by *N*-demethylation of the tertiary amine, had the same FIs as the parent compound. M1 (PI at  $m/z$  315.1025), originated from *N,N*-bisdemethylation of the tertiary amine, was characterized by the FI at  $m/z$  298.0759, which was identical with the FI in the MS<sup>2</sup> spectrum of the parent compound. M8, M11, and M12 (PI at  $m/z$  359.1287) were hydroxylated at the cyclohexyl ring indicated by the FI at  $m/z$  110.0964, which consisted of the cyclohexyl ring with the primary amine shifted by two hydrogen after loss of water. M9, M10 and M13 (PI at  $m/z$  359.1287) were formed by hydroxylation of the phenyl ring characterized by the FI at  $m/z$  234.0083, which corresponded to the FI at  $m/z$  218.0133 shifted by an oxygen. The *N*-demethyl hydroxy metabolite M4 (PI at  $m/z$  345.1131) showed the same FI pattern as the corresponding hydroxy metabolites (M9, M10, M13). M5 and M6 (PI at  $m/z$  345.1131) are the corresponding *N*-demethyl hydroxy isomers of M8, M11, M12 and their FIs are in accordance with each other. M3 (PI at  $m/z$  331.0974) originated from a hydroxylation at the cyclohexyl ring and *N,N*-bisdemethylation at the tertiary amine, which was identified by the FI at  $m/z$  114.0913, which corresponded to the FI at  $m/z$  128.1069 altered in one CH<sub>2</sub> group. The absence of interfering compounds was confirmed by blank incubations. M2 was also identified in negative control incubations, but with much lower intensity than in the pS9 and single isozyme incubations, most probably due to degradation processes during storage.

M3, M4, M5, M6, M8, M9, M10, and M13 were only identified in CYP isozyme incubations. This was most probably due to higher total CYP concentrations in incubations with recombinant CYP isozymes in comparison to pS9 incubations. However, as pS9 represents the relative CYP isozyme amounts within the human liver, the metabolites which were only detected in CYP isozyme incubations may be

expected to be minor metabolites in vivo. Another reason could be suppression or enhancement effects in the different matrices, which could not be excluded.

### 3.3 | Isozyme mapping

All metabolites previously identified in pS9 and eight additional metabolites were found in the isozymes incubations in total (Table S3). The *N*-demethylation, the most abundant step in vitro, was catalyzed by several isozymes (CYP2B6, CYP2C19, CYP2D6, CYP3A4, CYP3A5). Furthermore, CYP2C19 was involved in all other metabolic steps. M3, M4, M8, M10, and M13 were only identified in CYP2C19, while M5 and M9 was formed only in CYP3A4 incubations. Besides the *N,N*-demethyl metabolite (M1), the *N*-demethyl-hydroxy metabolite (M5), and the hydroxy metabolite (M9), the formation of the *N*-demethyl-hydroxy isomer (M6) and the hydroxy isomer (M11) was catalyzed by CYP3A4. Thus, CYP2C19 and CYP3A4 are the predominant isozymes involved in the metabolism of U-48800. The changes in the U-48800 amount and the formation rates of the three most abundant metabolites in pS9, CYP2C19, and CYP3A4 incubations are given in Figure 4. Inhibition of one or both of these two isozymes, for example by drug–drug interactions or varying activity due to different CYP2C19 expression levels may cause an increased U-48800 concentration and thus toxicity.

### 3.4 | Determination of plasma protein binding

As classical ultrafiltration may have the non-specific binding as disadvantages compared to equilibrium dialysis,<sup>26</sup> the used filtration membrane consisted of regenerated cellulose, which was shown to avoid this issue.<sup>27</sup> Free fraction of U-48800 represents unbound drug ( $f_u$ ) and was calculated to be 0.078, which resulted in a PPB of 92% (log P value of 3.4). Amongst other factors, for example ionization state, there is a high correlation between lipophilicity and PPB.<sup>28,29</sup> It is expected that a PPB over 70% would have significant effects on the pharmacokinetics and pharmacodynamics such as lower clearance.<sup>30</sup> However, this effect will depend on the elimination route and/or active transport into the hepatocytes,<sup>31</sup> which were not part of this study. Therefore, further studies are encouraged.

### 3.5 | Detectability of metabolites in rat urine

The only metabolite that could be automatically identified in urine by automated SUSA was M7. Therefore, a more sensitive but targeted approach was additionally used to allow the identification of more than one biomarker. The metabolic pathways in rats are shown in Figure 3. Two phase I (M5, M7) and one phase II metabolite (M14) could be detected using the settings described in Section 2.7, whereas M5 has already been identified in vitro. M7 (PI at  $m/z$  345.1131) is the *N*-demethyl-hydroxy isomer of M4 with identical MS<sup>2</sup> pattern. The MS<sup>2</sup> spectrum of M14 (PI at  $m/z$  375.1236) is given in Figure S2. M14 was formed by *N*-demethylation of the

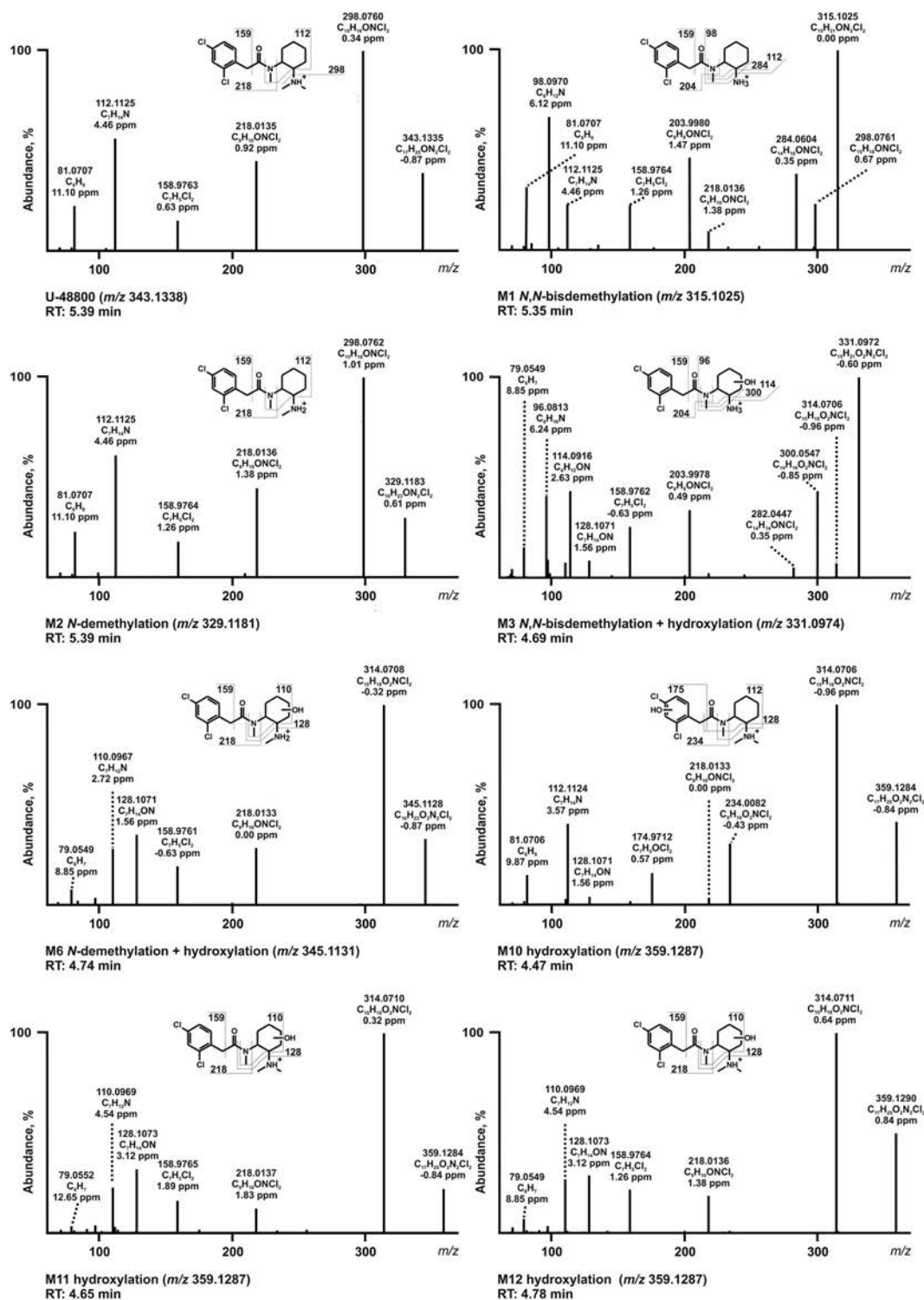


**FIGURE 2** MS<sup>2</sup> spectra of U-48800 and seven proposed major phase I metabolites in pooled human S9 fraction (pS9) and monooxygenases incubations sorted by precursor ions and retention time (RT)

tertiary amine and dihydroxylation at the phenyl ring followed by methylation of one hydroxy group, characterized by the FI at *m/z* 344.0814, which showed a shift of a CH<sub>3</sub> and NH<sub>2</sub> moiety. In comparison to the listed metabolites, the unchanged parent compound was only found at a very low abundance in urine. By comparing these findings in rat urine to findings in human urine of structural

related compounds, except the *N*-demethyl-hydroxy-methoxy metabolite, the two phase I metabolites were identified.<sup>11,32</sup> Therefore, analytical procedures should include the parent compound and the described phase I metabolites. Additionally, the *N*-demethyl metabolite only identified in vitro should be considered due to the high abundance in the investigated human urine.<sup>32</sup> The absence of

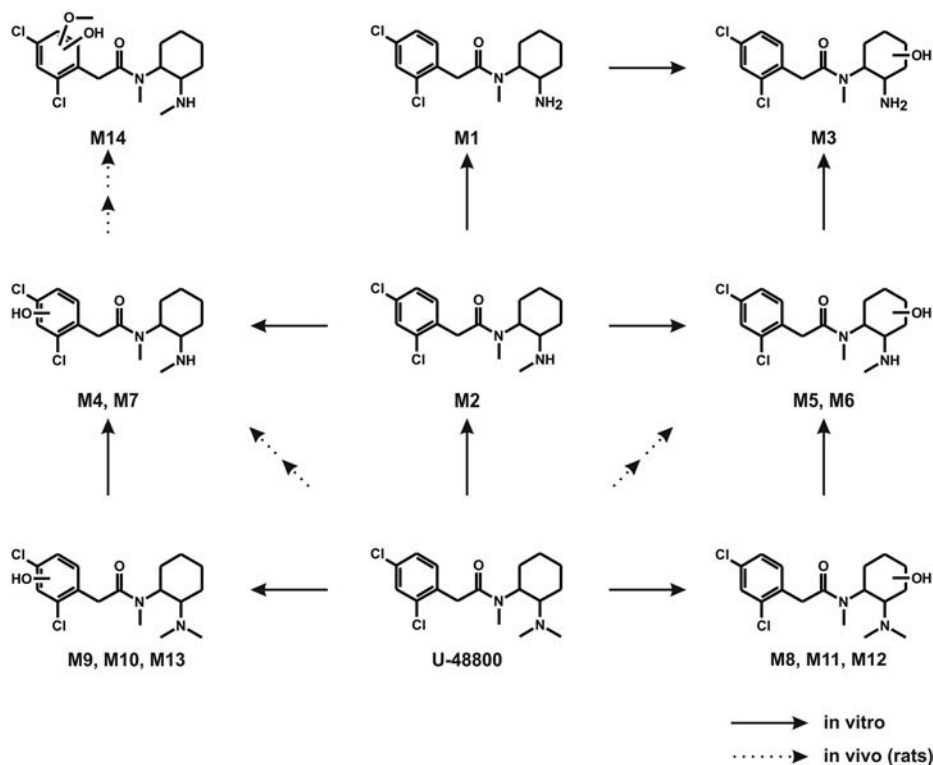


**FIGURE 3** In vitro and in vivo (rats) metabolic pathways of U-48800

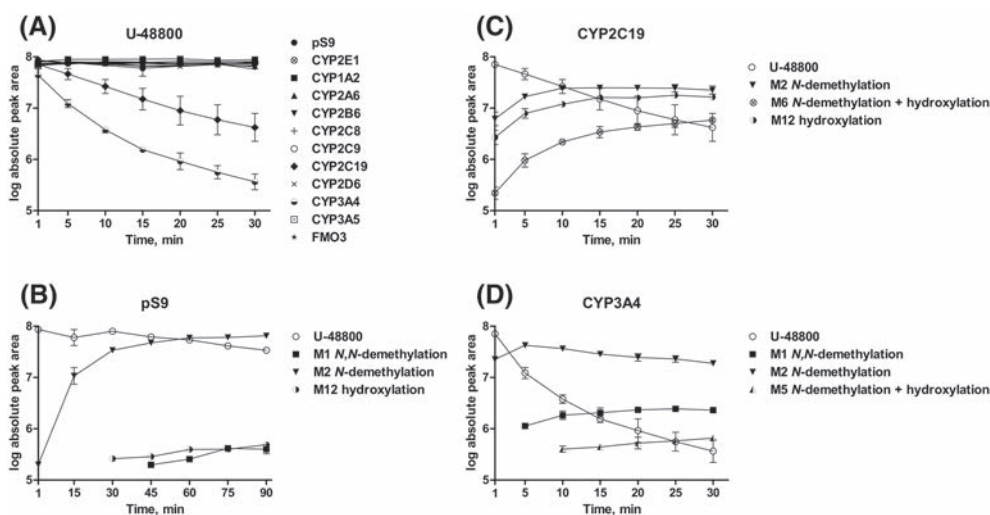


**FIGURE 4** Changes of the U-48800 amount in pS9 and isozymes in A and incubations and the formation rates of the most abundant metabolites compared to parent compound in B, pS9; C, CYP2C19; and D, CYP3A4. Logarithm of the absolute peak areas were plotted against time (min)

interfering compound was confirmed by analysis of blank urine. Creatinine values of blank urine and after dose administration were 76 mg/dL and 87 mg/dL.

## 4 | CONCLUSIONS

The present study describes the in vitro toxicokinetics and in vivo detectability of the NSO U-48800. In total, 14 metabolites were

tentatively identified. *N*-dealkylation, hydroxylation, and combinations thereof were the main metabolic reactions. The CYP isozyme mapping revealed the predominant involvement in the initial steps of CYP2C19 and CYP3A4. CYP2C19 polymorphisms could therefore lead to increased drug concentrations and subsequent toxicity cannot be excluded. Predicted  $CL_{int}$  and  $t_{1/2}$  is rated as intermediate in comparison to another NSO. Detection of a U-48800 intake in human urine should be possible by LC-HRMS/MS-based urine screening approaches. Both phase I metabolites found in rat urine, the parent

compound, and additionally the most abundant in vitro metabolite N-demethyl-U48800 should be considered as main targets.

## ACKNOWLEDGEMENTS

The authors like to thank Matthias J. Richter, Gabriele Ulrich, and Armin A. Weber for their support.

## CONFLICT OF INTEREST

The authors declare that there is no conflict of interest.

## ORCID

Markus R. Meyer  <https://orcid.org/0000-0003-4377-6784>

## REFERENCES

- UNODC. Global SMART Update Volume 17. 2017.
- EMCDDA. European Drug Report 2018. Publications of the European Union. 2018. [http://www.emcdda.europa.eu/system/files/publications/8585/20181816\\_TDAT18001ENN\\_PDF.pdf](http://www.emcdda.europa.eu/system/files/publications/8585/20181816_TDAT18001ENN_PDF.pdf).
- Fentanils and synthetic cannabinoids: driving greater complexity into the drug situation. An update from the EU Early Warning System. EMCDDA; 2018. <http://www.emcdda.europa.eu/system/files/publications/8870/2018-2489-td0118414enn.pdf>. Accessed 10/07/2018.
- Muller D, Neurath H, Neukamm MA, et al. New synthetic opioid cyclopropylfentanyl together with other novel synthetic opioids in respiratory insufficient comatose patients detected by toxicological analysis. *Clin Toxicol (Phila)*. 2019;57(9):806-812.
- Garneau B, Desharnais B, Beauchamp-Dore A, Lavallee C, Mireault P, Lajeunesse A. Challenges related to three cases of fatal intoxication to multiple novel synthetic opioids. *J Anal Toxicol*. 2019;n/a. <https://doi.org/10.1093/jat/bkz018> epub ahead of print
- Sharma KK, Hales TG, Rao VJ, NicDaeid N, McKenzie C. The search for the "next" euphoric non-fentanyl novel synthetic opioids on the illicit drugs market: current status and horizon scanning. *Forensic Toxicol*. 2019;37(1):1-16.
- Beardsley PM, Zhang Y. Synthetic opioids. *Handb Exp Pharmacol*. 2018;252:353-381.
- Fabregat-Safont D, Carbon X, Ventura M, et al. Updating the list of known opioids through identification and characterization of the new opioid derivative 3,4-dichloro-N-(2-(diethylamino)cyclohexyl)-N-methylbenzamide (U-49900). *Sci Rep*. 2017;7(1):6338.
- Loew G, Lawson J, Toll L, Frenking G, Berzetei-Gurske I, Polgar W. Structure activity studies of two classes of beta-amino-amides: the search for kappa-selective opioids. *NIDA Res Monogr*. 1988;90:144-151.
- Solimini R, Pichini S, Pacifici R, Busardo FP, Giorgetti R. Pharmacotoxicology of non-fentanyl derived new synthetic opioids. *Front Pharmacol*. 2018;9:654.
- Wohlfarth A, Scheidweiler KB, Pang S, et al. Metabolic characterization of AH-7921, a synthetic opioid designer drug: in vitro metabolic stability assessment and metabolite identification, evaluation of in silico prediction, and in vivo confirmation. *Drug Test Anal*. 2016;8(8):779-791.
- Richter LHJ, Maurer HH, Meyer MR. New psychoactive substances: studies on the metabolism of XLR-11, AB-PINACA, FUB-PB-22, 4-methoxy-alpha-PVP, 25-I-NBOMe, and meclonazepam using human liver preparations in comparison to primary human hepatocytes, and human urine. *Toxicol Lett*. 2017;280:142-150.
- Chauret N, Gauthier A, Nicoll-Griffith DA. Effect of common organic solvents on in vitro cytochrome P450-mediated metabolic activities in human liver microsomes. *Drug Metab Dispos*. 1998;26(1):1-4.
- Baranczewski P, Stanczak A, Sundberg K, et al. Introduction to in vitro estimation of metabolic stability and drug interactions of new chemical entities in drug discovery and development. *Pharmacol Rep*. 2006;58(4):453-472.
- Obach RS. Prediction of human clearance of twenty-nine drugs from hepatic microsomal intrinsic clearance data: an examination of in vitro half-life approach and nonspecific binding to microsomes. *Drug Metab Dispos*. 1999;27(11):1350-1359.
- Davies B, Morris T. Physiological parameters in laboratory animals and humans. *Pharm Res*. 1993;10(7):1093-1095.
- Houston JB, Galetin A. Methods for predicting in vivo pharmacokinetics using data from in vitro assays. *Curr Drug Metab*. 2008;9(9):940-951.
- Boxenbaum H. Interspecies variation in liver weight, hepatic blood flow, and antipyrine intrinsic clearance: extrapolation of data to benzodiazepines and phenytoin. *J Pharmacokinet Biopharm*. 1980;8(2):165-176.
- Wagmann L, Meyer MR, Maurer HH. What is the contribution of human FMO3 in the N-oxygenation of selected therapeutic drugs and drugs of abuse? *Toxicol Lett*. 2016;258:55-70.
- Fung EN, Chen YH, Lau YY. Semi-automatic high-throughput determination of plasma protein binding using a 96-well plate filtrate assembly and fast liquid chromatography-tandem mass spectrometry. *J Chromatogr B Analyt Technol Biomed Life Sci*. 2003;795(2):187-194.
- Mardal M, Gracia-Lor E, Leibnitz S, Castiglioni S, Meyer MR. Toxicokinetics of new psychoactive substances: plasma protein binding, metabolic stability, and human phase I metabolism of the synthetic cannabinoid WIN 55,212-2 studied using in vitro tools and LC-HR-MS/MS. *Drug Test Anal*. 2016;8(10):1039-1048.
- Welter J, Kavanagh P, Meyer MR, Maurer HH. Benzofuran analogues of amphetamine and methamphetamine: studies on the metabolism and toxicological analysis of 5-APB and 5-MAPB in urine and plasma using GC-MS and LC-(HR)-MS(n) techniques. *Anal Bioanal Chem*. 2015;407(5):1371-1388.
- Wissenbach DK, Meyer MR, Remane D, Weber AA, Maurer HH. Development of the first metabolite-based LC-MS(n) urine drug screening procedure-exemplified for antidepressants. *Anal Bioanal Chem*. 2011;400(1):79-88.
- Helfer AG, Michely JA, Weber AA, Meyer MR, Maurer HH. Orbitrap technology for comprehensive metabolite-based liquid chromatographic-high resolution-tandem mass spectrometric urine drug screening - exemplified for cardiovascular drugs. *Anal Chim Acta*. 2015;891:221-233.
- McNaney CA, Drexler DM, Hnatyshyn SY, et al. An automated liquid chromatography-mass spectrometry process to determine metabolic stability half-life and intrinsic clearance of drug candidates by substrate depletion. *Assay Drug Dev Technol*. 2008;6(1):121-129.
- Barre J, Chamouard JM, Houin G, Tillement JP. Equilibrium dialysis, ultrafiltration, and ultracentrifugation compared for determining the plasma-protein-binding characteristics of valproic acid. *Clin Chem*. 1985;31(1):60-64.
- Kratzer A, Kees F, Dorn C. Unbound fraction of fluconazole and linezolid in human plasma as determined by ultrafiltration: impact of membrane type. *J Chromatogr B Analyt Technol Biomed Life Sci*. 2016;1039:74-78.
- Fauber BP, Rene O, de Leon Boenig G, et al. Reduction in lipophilicity improved the solubility, plasma-protein binding, and permeability of tertiary sulfonamide RORc inverse agonists. *Bioorg Med Chem Lett*. 2014;24(16):3891-3897.

29. Zhivkova ZD. Quantitative structure - pharmacokinetics relationships for plasma protein binding of basic drugs. *J Pharm Sci.* 2017;20(1):349-359.
30. Lindup WE, Orme MC. Clinical pharmacology: plasma protein binding of drugs. *Br Med J (Clin Res Ed).* 1981;282(6259):212-214.
31. Howard ML, Hill JJ, Galluppi GR, McLean MA. Plasma protein binding in drug discovery and development. *Comb Chem High Throughput Screen.* 2010;13(2):170-187.
32. Krotulski AJ, Mohr ALA, Papsun DM, Logan BK. Metabolism of novel opioid agonists U-47700 and U-49900 using human liver microsomes with confirmation in authentic urine specimens from drug users. *Drug Test Anal.* 2018;10(1):127-136.

## SUPPORTING INFORMATION

Additional supporting information may be found online in the Supporting Information section at the end of the article.

**How to cite this article:** Gampfer TM, Richter LHJ, Schäper J, Wagmann L, Meyer MR. Toxicokinetics and analytical toxicology of the abused opioid U-48800 – in vitro metabolism, metabolic stability, isozyme mapping, and plasma protein binding. *Drug Test Anal.* 2019;11:1572–1580. <https://doi.org/10.1002/dta.2683>

### 3.2 Toxicokinetic Studies and Analytical Toxicology of the New Synthetic Opioids Cyclopentanoyl-Fentanyl and Tetrahydrofuranoyl-Fentanyl<sup>64</sup>

This is a pre-copyedited, author-produced version of an article accepted for publication in Journal of Analytical Toxicology following peer review. The version of record<sup>64</sup> and the Electronic Supplement Material is available online at:

(DOI: 10.1093/jat/bkaa010; accepted by mail of 26.12.2019)

**Authors Contributions** Tanja M. Gampfer conducted the experiments, analyzed the data, and wrote the manuscript; Matthias J. Richter developed the method for the detection of NSO in urine after glucuronidase cleavage and SPE and supported with scientific discussions; Svenja Fischmann and Folker Westphal characterized and provided the new psychoactive substance cyclopentanoyl-fentanyl and supported with scientific discussion; Markus R. Meyer and Lea Wagmann supported with scientific discussions, the design of the experiments, and research supervision

# **Toxicokinetic studies and analytical toxicology of the new synthetic opioids cyclopentanoyl-fentanyl and tetrahydrofuranoyl-fentanyl**

**Tanja M. Gampfer<sup>1</sup>, Lea Wagmann<sup>1</sup>, Matthias J. Richter<sup>1</sup>, Svenja Fischmann<sup>2</sup>, Folker Westphal<sup>2</sup>, Markus R. Meyer\*<sup>1</sup>**

<sup>1</sup>Department of Experimental and Clinical Toxicology, Institute of Experimental and Clinical Pharmacology and Toxicology, Center for Molecular Signaling (PZMS), Saarland University, Homburg, Germany

<sup>2</sup>State Bureau of Criminal Investigation Schleswig-Holstein, Kiel, Germany

\* Author to whom correspondence should be addressed. Markus R. Meyer, Department of Experimental and Clinical Toxicology, Institute of Experimental and Clinical Pharmacology and Toxicology, Center for Molecular Signaling (PZMS), Saarland University, 66421 Homburg, Germany, [markus.meyer@uks.eu](mailto:markus.meyer@uks.eu)

## Abstract

The growing number of new synthetic opioids (NSO) on the new psychoactive substances (NPS) market bears new challenges in toxicology. As their toxicodynamics and particularly their toxicokinetics are usually unknown, impact on human health is not yet fully understood. Detection of the two NSO cyclopentanoyl-fentanyl (CP-F) and tetrahydrofuranoyl-fentanyl (THF-F) was first reported in 2016. Both were involved in several fatal intoxication cases but no detailed information about their toxicological characteristics is available so far. The main purpose of this study was therefore to investigate the *in vitro* toxicokinetics and *in vivo* analytical toxicology of CP-F and THF-F by means of liquid chromatography high-resolution tandem mass spectrometry (LC-HRMS/MS). These studies included metabolic stability, phase I and II metabolism, isozyme mapping, plasma protein binding, and detectability in LC-HRMS/MS standard urine screening approaches (SUSA) using rat urine samples. In total, 12 phase I metabolites of CP-F and 13 of THF-F were identified, amongst them nine metabolites described for the first time. Overall, *N*-dealkylations, hydroxylations, and dihydroxylations were the main metabolic reactions. The cytochrome P450 (CYP) isozymes mainly involved were CYP2D6 and CYP3A4, leading to elevated drug levels and intoxications in CYP2D6 poor metabolizers. CP-F showed a high plasma protein binding of 99%, which may increase the risk of toxicity by simultaneous intake of other highly bound drugs. Detectability studies showed that neither the parent compounds nor their metabolites were detectable in rat urine using LC-HRMS/MS SUSA. However, a more sophisticated analytical strategy was successfully applied and should be used for analytical confirmation of an intake of CP-F and/or THF-F.

## Introduction

Although the annual appearance of new psychoactive substances (NPS) stagnated or even declined (1, 2), the subgroup of new synthetic opioids (NSO) is still growing (3). Usually, only little is known about the pharmacological and toxicological effects of NPS, leading to unpredictable risks for human health. Thus, an increasing number of fatal causalities was associated with consumption of fentanyl analogues in Europe and in the US (4, 5). This underlines the need for toxicological investigations of NSO. Toxicokinetic information is particularly relevant regarding analytical questions, such as whether parent compound or metabolites are traceable in real toxicological cases and for prediction of possible interactions e.g. after simultaneous intake of multiple drugs. Cyclopentanoyl-fentanyl (CP-F) and tetrahydrofuranoyl-fentanyl (THF-F), two fentanyl-related NSO, differ only in one oxygen atom in the ring next to the amide from each other. In Figure 1 their chemical structures are given in comparison to fentanyl. Both were first reported in 2016 and since then associated with several fatal and non-fatal intoxications (6, 7). No opioid receptor binding study of CP-F has been done so far but the alicyclic analogue cyclopropanoyl-fentanyl showed a similar potency as fentanyl (8). Another study indicated that aliphatic derivatives might be less potent than fentanyl (9). THF-F has been proved to bind with high affinity at the  $\mu$ -receptor (10). However, it was not as potent as fentanyl. Comparable pharmacological effects to fentanyl such as respiratory depression, sedation, euphoria, and miosis were described (7). By now, several toxicokinetic studies of fentanyl-related NSO were performed (6, 11-13). Though most of them investigated solely their qualitative metabolism without considering further toxicokinetic parameters such as isozyme mapping, which is essential for prediction of drug-drug interactions or influence of interindividual

variations. Therefore, the purpose of this study was to investigate the metabolic stability of CP-F and THF-F including in vitro half-lives ( $t_{1/2}$ ), intrinsic clearances ( $CL_{int}$ ), and prediction of the hepatic clearances ( $CL_h$ ) using well-stirred model, parallel tube model, and hepatic extraction ratio ( $ER_h$ ). Furthermore, the identification of phase I and II metabolites by liquid chromatography high-resolution tandem mass spectrometry (LC-HRMS/MS) after pooled human liver S9 fraction (pHLS9) incubation was included. Mapping of the involved isozymes, elucidation of the free fractions in plasma ( $f_u$ ), and calculation of the respective plasma protein binding (PPB) was also performed. Finally, the detectability of CP-F, THF-F, and/or their metabolites in rat urine after administration of a presumed consumer dosage by using LC-HRMS/MS standard urine screening approaches (SUSA) was determined.

## Materials and Methods

### Chemicals, enzymes, and materials

CP-F was characterized and provided for research purposes from the EU-project ADEBAR/State Bureau of Criminal Investigation Schleswig-Holstein (Kiel, Germany). THF-F was purchased by LGC standards (Wesel, Germany). Stock solutions were freshly prepared in methanol (1 mg/mL) before each experiment. Isolute HXC cartridges (130 mg, 3 mL) were obtained from Biotage (Uppsala, Sweden) and Centrifree devices from Merck (Darmstadt, Germany). The creatinine immunoassays for the P.I.A.<sup>2</sup> device were from Protzek Diagnostic (Lörrach, Germany). Isocitrate, isocitrate dehydrogenase, superoxide dismutase, 3'-phosphoadenosine-5'-phosphosulfate (PAPS), *S*-(5'-adenosyl)-L-methionine (SAM), dithiothreitol (DTT), reduced glutathione (GSH), magnesium chloride ( $MgCl_2$ ), potassium dihydrogenphosphate ( $KH_2PO_4$ ), dipotassium hydrogenphosphate ( $K_2HPO_4$ ), tris hydrochloride, and

trimipramine-d<sub>3</sub> were obtained from Sigma Aldrich (Taufkirchen, Germany) and NADP<sup>+</sup> from Biomol (Hamburg, Germany). BG Turbo glycerol free (1 mg/mL β-glucuronidase) and instant buffer I were from Kura Biotec (Rancho Dominguez, USA). Acetonitrile (LC-MS grade), methanol (LC-MS grade), ammonium formate (analytical grade), formic acid (LC-MS grade), and all other reagents and chemicals (analytical grade) were purchased by VWR (Darmstadt, Germany). The baculovirus-infected insect cell microsomes (Supersomes) containing 1 nmol/mL of the human cDNA-expressed cytochrome P450 (CYP) isozymes CYP1A2, CYP2A6, CYP2B6, CYP2C8, CYP2C19, CYP2D6, CYP3A4 (1 nmol/mL), CYP2C9, CYP2E1, CYP3A5 (2 nmol/mL), flavin-containing monooxygenase (FMO3) (5 mg protein/mL), or pHLS9 (20 mg microsomal protein/mL), UDP-glucuronosyltransferase (UGT) reaction mixture solution A (25 mM UDP-glucuronic acid), and UGT reaction mixture solution B (250 mM Tris HCl, 40 mM MgCl<sub>2</sub>, and 125 μg/mL alamethicin) were obtained from Corning (Amsterdam, Netherlands). After delivery, the enzymes were thawed at 37°C, aliquoted, snap-frozen in liquid nitrogen, and stored at -80°C until use.

### Identification of phase I and II metabolites

CP-F and THF-F incubations were conducted as described earlier (14) with minor modifications. Briefly, preincubation was done for 10 min at 37°C with pHLS9 (2 mg microsomal protein/mL), 25 μg/mL alamethicin (UGT reaction mixture solution B), 90 mM phosphate buffer (pH 7.4), 2.5 mM Mg<sup>2+</sup>, 2.5 mM isocitrate, 0.6 mM NADP<sup>+</sup>, 0.8 U/mL isocitrate dehydrogenase, 100 U/mL superoxide dismutase. Afterwards, 2.5 mM UDP-glucuronic acid (UGT reaction mixture solution A), 40 μM PAPS, 1.2 mM SAM, 1 mM DTT, 10 mM GSH, and 2.5 μM substrate were added. The amount of organic

solvent was < 1% (15). All given concentrations are concentrations in the final incubation mixtures (300  $\mu$ L final volume).

Reactions were started by addition of the substrate (CP-F or THF-F). The reaction mixtures were incubated for 360 min and 30  $\mu$ L samples were taken after 1, 15, 30, 45, 60, 75, 90, 180, and 360 min. Reactions were terminated by addition of 10  $\mu$ L ice-cold acetonitrile containing trimipramine- $d_3$  (5  $\mu$ M) as internal standard (IS). Thereafter, the samples were cooled for 30 min at  $-20^\circ\text{C}$ , centrifuged at  $18,407\times g$  for 2 min, the supernatants transferred to autosampler vials, and analyzed by LC-HRMS/MS. Incubations without NADP<sup>+</sup> were prepared for the identification of metabolites formed by NADP<sup>+</sup> independent enzymes. Blank incubations without substrate and control incubations without pHLS9 were conducted to confirm the absence of interfering and non-metabolically formed compounds, respectively. All incubations were done in duplicate.

### Elucidation of metabolic stability in pHLS9

Experiments for assessing metabolic stability were based on a previously published study (16). All statistical evaluations were done with Graph Pad Prism 5.00 (GraphPad Software, San Diego, USA). The natural logarithm of the peak area ratios of CP-F or THF-F and the IS were plotted versus time, respectively. The cut-off was set to 90 min, due to decreasing enzyme activity after a period of time. The slope of the linear regression of each compound was used to calculate the *in vitro* half-life. A t-test was done to confirm that the remaining compound concentrations in control incubations after 360 min were not significantly different from the initial concentrations determined in samples taken after 1 min.

Metabolic stability was calculated using equations 1 and 2 (17-19). Clearance was calculated by using the parallel tube model with (equation 4) and without (equation 5) free fraction in plasma. Clearance was also calculated by using the well-stirred model with (equation 6) and without (equations 7, 8) free fraction in plasma.

$$(1) t_{1/2, \text{ min}} = \frac{\ln 2}{k}$$

$$(2) \ln[\text{peak area ratio}]_{\text{remaining}} = \ln[\text{peak area ratio}]_{\text{initial}} - k \times t$$

$$(3) \text{CL}_{\text{int}}, \text{ mL/min/kg} = \frac{\ln 2}{t_{1/2}} \times \frac{[V]_{\text{incubation}}}{[P]_{\text{incubation}}} \times \frac{[\text{Liver}]}{[\text{BW}]} \times \text{SF}$$

$$(4) \text{CL}_{\text{h}}, \text{ mL/min/kg} = Q \times \left( 1 - e^{\left( \frac{-f_u \times \text{CL}_{\text{int}}}{Q} \right)} \right)$$

$$(5) \text{CL}_{\text{h}}, \text{ mL/min/kg} = Q \times \left( 1 - e^{\left( \frac{-\text{CL}_{\text{int}}}{Q} \right)} \right)$$

$$(6) \text{CL}_{\text{h}}, \text{ mL/min/kg} = \frac{Q \times f_u \times \text{CL}_{\text{int}}}{Q + f_u \times \text{CL}_{\text{int}}}$$

$$(7) \text{CL}_{\text{h}}, \text{ mL/min/kg} = \frac{Q \times \text{CL}_{\text{int}}}{Q + \text{CL}_{\text{int}}}$$

$$(8) \text{ER}_{\text{h}} = \frac{\text{CL}_{\text{h}}}{Q}$$

$t_{1/2}$  = in vitro half-life,  $k$  = slope of the linear regression fit,  $\text{CL}_{\text{intr}}$  = intrinsic clearance,  $[V]_{\text{incubation}}$  = incubation volume = 0.3 mL,  $[P]_{\text{incubation}}$  = amount of S9 protein in the incubation = 0.6 mg,  $\frac{[\text{Liver}]}{[\text{BW}]}$  = liver weight normalized by body weight = 26 g/kg (20), SF = scaling factor S9 protein per gram of liver = 121 mg/g (21),  $\text{CL}_{\text{h}}$  = hepatic clearance,  $Q$  = hepatic blood flow rate in human = 20 mL/min/kg (22),  $f_u$  = free fraction in plasma, and  $\text{ER}_{\text{h}}$  = hepatic extraction ratio

## Isozyme activity screening

In accordance to a published study with minor modifications (23), CP-F or THF-F (2.5  $\mu\text{M}$ ) were incubated with CYP1A2, CYP2A6, CYP2B6, CYP2C8, CYP2C9, CYP2C19, CYP2D6, CYP2E1, CYP3A4, CYP3A5 (50 pmol/mL each), or FMO3 (0.25 mg protein/mL) for 30 min at 37°C. All given concentrations are concentrations in the final incubation mixture (250  $\mu\text{L}$  final volume). Further components of the incubation mixtures were 90 mM phosphate buffer (pH 7.4), 5 mM  $\text{Mg}^{2+}$ , 5 mM isocitrate, 1.2 mM NADP<sup>+</sup>, 0.5 U/mL isocitrate dehydrogenase, and 200 U/mL superoxide dismutase. CYP2A6 and CYP2C9 incubations were done after replacing phosphate buffer with tris buffer, as recommended by the manufacturer. Reactions were started after addition of the enzymes and terminated at 1, 5, 10, 15, 20, 25, and 30 min taking 30  $\mu\text{L}$  samples and adding 10  $\mu\text{L}$  ice-cold acetonitrile. Afterwards, the samples were centrifuged at 18,407 $\times$ g for 5 min, the supernatants transferred to autosampler vials, and analyzed by LC-HRMS/MS. A blank incubation without substrate and a negative control without enzyme were done to confirm the absence of interfering compounds and to identify non-metabolically formed compounds. All incubations were done in duplicate.

## Determination of plasma protein binding

Ultrafiltration was done in accordance to published procedures (24, 25). A volume of 50  $\mu\text{L}$  methanolic CP-F and THF-F solution (final concentration 0.5  $\mu\text{M}$ ) was spiked into 450  $\mu\text{L}$  fresh pooled human plasma and then incubated for 30 min at 37°C. Thereafter, a 100  $\mu\text{L}$  sample (global approach, GA) was taken and transferred into a new reaction tube. The remaining sample was transferred into an ultrafiltration device and centrifuged at 1,600 $\times$ g for 35 min. A volume of 50  $\mu\text{L}$  of the ultrafiltrate (UF) was transferred in a new reaction tube. All samples were precipitated by adding 50  $\mu\text{L}$  ice-

cold acetonitrile containing trimipramine-d<sub>3</sub> (2.5 μM) as IS, cooled for 30 min at -20°C, and centrifuged for 2 min at 18,407×g before measurement. Ultrafiltration was done in triplicate, respectively. Lipophilicity (log *P*) was calculated with ChemDraw Professional 16.0.1.4 (PerkinElmer, Waltham, USA).

Following equations were used to calculate the PPB:

$$(9) f_u = \frac{\text{peak area ratio} \left( \frac{CP-F_{UF} \text{ or } THF-F_{UF} \times 2}{IS_{UF}} \right)}{\text{peak area ratio} \left( \frac{CP-F_{GA} \text{ or } THF-F_{GA}}{IS_{GA}} \right)}$$

The factor of 2 in the numerator is due to the sample volume of the GA being twice that of the UF.

$$(10) \text{PPB, \%} = (1 - f_u) \times 100$$

### Rat urine samples for toxicological detectability

Male wistar rats (Charles River, Sulzfeld, Germany) were used for detectability studies in accordance to the German law for animal protection. Studies have been approved by an ethics committee (Landesamt für Verbraucherschutz, Saarbrücken, Germany). Single oral low doses of 0.01 mg/kg CP-F or THF-F were administered to the rats. The dosage was based on previous low dose detectability studies of other fentanyl analogous (13). Rats had water ad libitum during the collection of urine over a period of 24 hours. Urine was caught separately from feces. Before compound administration, blank urine was collected to confirm the absence of distracting compounds. Creatinine values were determined by an immunoassay in blank urine and in the urine collected after NSO administration.

### Detectability in urine after precipitation

In accordance to an established procedure (26), a volume of 200  $\mu\text{L}$  rat urine was precipitated with 1 mL ice-cold acetonitrile, shaken for 2 min, and centrifuged at  $18,407\times g$  for 2 min. Thereafter, the supernatants were evaporated to dryness under nitrogen stream at  $70^{\circ}\text{C}$ , reconstituted in 100  $\mu\text{L}$  eluent mixture A and B (50:50% v/v, see LC-HRMS/MS settings). The samples were analyzed by using the MS parameters described in LC-HRMS/MS settings and by the same settings but using positive/negative switching and no inclusion list (27).

### Detectability in urine after glucuronidase cleavage and solid phase extraction

Glucuronidase cleavage was performed by incubating 200  $\mu\text{L}$  rat urine with 2,6666 U/mL BG Turbo glycerol free, 80  $\mu\text{L}$  instant buffer I, 210  $\mu\text{L}$  distilled water, and 30  $\mu\text{L}$  methanol (600  $\mu\text{L}$  final volume) at  $50^{\circ}\text{C}$  for 10 min. For solid phase extraction (SPE), the HCX cartridges were previously conditioned with 1 mL methanol and 1 mL distilled water. Thereafter, cartridges were washed with 1 mL distilled water and 1 mL 0.01 M hydrochloric acid. A mixture of 1 mL freshly prepared methanol and aqueous ammonia 33% (98:2, v/v) was used to elute the compounds from the cartridges into reaction tubes. After evaporation to dryness under a nitrogen stream at  $70^{\circ}\text{C}$ , the samples were reconstituted in 50  $\mu\text{L}$  eluent mixture A and B (50:50%, v/v, see LC-HRMS/MS settings). The samples were analyzed by using the MS parameters described in LC-HRMS/MS settings and by the same settings but using positive/negative switching and no inclusion list (27).

### LC-HRMS/MS settings

A Thermo Fisher Scientific (TF, Dreieich, Germany) Dionex UltiMate 3000 RS pump consisting of a degasser, a quaternary pump, and an UltiMate autosampler, coupled to a TF Q-Exactive Plus system equipped with a heated electrospray ionization (HESI)-II source were used. An external mass calibration was done prior to analysis according to the manufacturer's recommendations. The injection volume was 1  $\mu$ L for all samples. Gradient elution was performed on a TF Accucore PhenylHexyl column (100 mm x 2.1 mm, 2.6  $\mu$ m) as described in a previous study (27). The mobile phases were composed of 2 mM aqueous ammonium formate containing formic acid (0.1%, v/v, pH 3, eluent A) and 2 mM ammonium formate solution with acetonitrile: methanol (1:1, v/v), water (1%, v/v), and formic acid (0.1%, v/v, eluent B). Initially, the flow rate was set to 500  $\mu$ L/min for 10 min followed by 800  $\mu$ L/min for 10–13.5 min. The gradient was programmed as follows: 0–1 min hold 99% A, 1–10 min to 1% A, 10–11.5 min hold 1% A, and 11.5–13.5 min hold 99% A. The following HESI-II source conditions were used: heater temperature, 320°C; ion transfer capillary temperature, 320°C; spray voltage, 4.0 kV; ionization mode, positive; sheath gas, 60 arbitrary units (AU); auxiliary gas, 10 AU; sweep gas, 0 AU; and S-lens RF level, 50.0. Mass spectrometry was performed using full scan data and a subsequent data-dependent acquisition (DDA) with priority to mass-to-charge ratios ( $m/z$ ) of parent compounds and their expected metabolites. The settings for full scan data acquisition were the following: resolution, 35,000; microscans, 1; automatic gain control (AGC) target, 1e6; maximum injection time (IT), 120 ms; and scan range,  $m/z$  50–750. Inclusion lists of CP-F or THF-F and their expected metabolites, respectively, were prepared for the DDA mode and following settings were selected: option “pick others”, enabled; dynamic exclusion, 5 seconds; resolution, 17,500; microscans, 1; isolation window, 1.0  $m/z$ ; loop count, 5; AGC target, 2e5; maximum IT, 250 ms; high collision dissociation cell with stepped normalized collision

energy, 17.5, 35.0, 52.5; exclude isotopes, on; spectrum data type, profile; and underfill ratio, 1%. Most likely formed metabolites such as hydroxy, dihydroxy, and *N*-dealkyl metabolites (phase I) as well as sulfates, glucuronides (phase II) were components of the inclusion lists. ChemSketch 2010 12.01 (ACD/Labs, Toronto, Canada) was used for structure drawings of hypothetical metabolites and exact mass calculations. TF Xcalibur Qual Browser software version 2.2 SP1.48 was used for data processing. Automated peak integration was done with following settings: peak detection algorithm, INCOS; baseline window, 40; area noise factor, 5; and peak noise factor, 10.

## Results and discussion

### Metabolic stability in pHLS9

The substrate depletion strategy was used to determine the metabolic stability of CP-F and THF-F. As recommended, low substrate concentrations of 2.5  $\mu\text{M}$  were picked to achieve a linear metabolism rate during incubation (17). T-tests for significance between the natural logarithm of the peak area ratios of incubations after 1 min and control incubations after 360 min showed no differences. All metabolic stability data are summarized in Table S1 in the Electronic Supplementary Material (ESM). The *in vitro* half-lives of CP-F and THF-F were calculated to be 13.8 min and 67.5 min, respectively.  $CL_{\text{int}}$  of CP-F was 64 mL/min/kg and 17 mL/min/kg in case of THF-F, which could be classified as high and moderate, respectively (28). Calculations of hepatic clearances were done using the well-stirred and parallel tube model with and without considering PPB, because disregarding binding values for basic compounds often lead to more accurate predictions of human clearance (18). Well-stirred and parallel tube model with  $f_u$  resulted in an identical  $CL_h$  of 0.6 mL/min/kg for CP-F. By

comparing these results with the calculations of  $CL_h$  without  $f_u$ , the  $CL_h$  values of 19.2 mL/min/kg in the well-stirred and 15.2 mL/min/kg in the parallel tube model were much higher. Predicted  $CL_h$  of THF-F were 3.6 mL/min/kg for the well-stirred and 3.9 mL/min/kg for the parallel tube model. Using well-stirred model without  $f_u$ ,  $CL_h$  yielded in 9.2 mL/min/kg and parallel tube in 11.5 mL/min/kg. Thus, hepatic clearance calculations considering PPB could lead to underestimation of the in vivo  $CL_h$  of both compounds but especially of CP-F. In accordance to Rogge and Taft (29), the  $ER_h$  of 0.96 for CP-F can be rated as high and the value of 0.46 for THF-F as intermediate. These results indicate that especially CP-F most likely undergoes pronounced first-pass extraction resulting in a reduced bioavailability.

### In vitro identification of phase I and II metabolites

Qualitative metabolism studies are essential to identify suitable targets for toxicological screenings in biosamples. Especially, since parent compounds are often not excreted into urine or only in very small amounts (30). Metabolites were identified by mining the  $MS^1$  data for the exact precursor ions (PI) of the expected metabolites. Afterwards, the metabolites were tentatively identified by comparing their fragmentation patterns in  $MS^2$  to those of the parent compounds.

Two studies are available on the qualitative metabolic fate of CP-F and THF-F. Astrand et al. studied the phase I and II metabolism of CP-F in human hepatocytes (11). Krotulski et al. investigated the phase I metabolites of THF-F in pooled human liver microsomes, post-mortem blood, and urine (6).

The current study using pHLS9 fraction revealed in total 12 phase I metabolites of CP-F and 13 phase I metabolites of THF-F. Amongst them two CP-F metabolites and seven THF-F metabolites which were described for the first time. No phase II metabolites

could be identified. In comparison to literature, only the THF-F metabolite formed by ring opening at the tetrahydrofuran moiety in humans previously described by Krotulski et al. could not be found (6). This metabolite, however, was the less abundant one detected in the blood and urine samples. The measured accurate masses of PI and characteristic fragment ions (FIs), relative intensities, calculated exact masses, elemental composition, mass deviation errors of the most abundant fragment ions, and retention time (RT) of all metabolites are listed in Table S2 (CP-F) and S3 (THF-F) in the ESM. The metabolites were sorted by increasing mass and RT. MS<sup>2</sup> spectra of the parent compounds and their metabolites, which were described for the first-time compared to literature are shown in Figure 2 (CP-F) and 3 (THF-F). Figure 3 also shows some previously discussed and tentatively identified metabolites, which were more in detail characterized in the present study. All other MS<sup>2</sup> spectra are given in Figure S1 (CP-F) and S2 (THF-F) in the ESM.

The exact masses will be used for discussion in the following sections. Most abundant but less specific fragments of both CP-F (PI at  $m/z$  377.2587) and THF-F (PI at  $m/z$  379.2380) were the FI at  $m/z$  188.1433, representing the phenyl ring linked with the ethyl group to the piperidine ring, and FI at  $m/z$  105.0698, formed after elimination of the piperidine ring. The latter contained the phenyl ring plus ethyl moiety. More specific for CP-F was the FI at  $m/z$  256.1695, which consisted of the phenyl coupled to the amide, cyclopentyl ring and a part of the piperidine ring. Another specific FI representing only the cyclopentyl ring was the FI at  $m/z$  69.0698. The corresponding specific fragments of THF-F were the FI at  $m/z$  258.1488 and 71.0491 differing in one oxygen atom at the ring compared to the MS<sup>2</sup> spectrum of CP-F. First-time described CP-F metabolites were the two dihydroxy isomers M10 and M11 (PI at  $m/z$  409.2485, each). Both hydroxy groups were located at the cyclopentyl ring, which was

characterized by the FI at  $m/z$  83.0491. It consisted of the mono hydroxylated cyclopentyl ring with one double bond formed after loss of water.

Seven additional metabolites were identified for THF-F. M19 (PI at  $m/z$  395.2329) was formed by oxidation of the nitrogen in the piperidine ring and characterized by FI at  $m/z$  189.1386 containing the methyl piperidine group linked to the phenyl ring via the amine after amide cleavage. M18 (PI at  $m/z$  395.2329) occurred through hydroxylation at the piperidine ring or ethyl linker, although the exact position could not be determined based on the fragmentation, as shown for other fentanyl derivatives (12, 31). It was represented by the FI at  $m/z$  186.1277, which corresponded to the FI at  $m/z$  188.1433 minus two hydrogen atoms representing an additional double bond formed after loss of water. M15 (PI at  $m/z$  393.2172) was the corresponding oxo metabolite of M17 (PI at  $m/z$  395.2329) and their MS<sup>2</sup> spectra were in accordance to each other, except the loss of water indicated by the FI at  $m/z$  377.2223. Three oxo-hydroxy isomers (M20, M21, M22, PI at  $m/z$  409.2121, each) could be identified. M22 was formed after dihydroxylation at the tetrahydrofuran ring and oxidation of one hydroxy moiety, which showed the same MS<sup>2</sup> spectrum as the corresponding oxo metabolite M15. M20 was hydroxylated at the phenyl ring linked to the piperidine ring and at the tetrahydrofuran ring followed by oxidation of the latter. A characteristic FI was the FI at  $m/z$  204.1382, which correlated to the FI at  $m/z$  188.1433 containing an additional oxygen atom. M21 was also hydroxylated at the phenyl ring, but the keto group was located at the ethyl linker characterized by the FI at  $m/z$  258.1488. This part was not altered compared to the parent compound. The MS<sup>2</sup> spectrum of the dihydroxy isomer M24 (PI at  $m/z$  411.2281) was characterized by the FI at  $m/z$  281.2012, which contained the 4-anilino-*N*-phenethylpiperidine (4-ANPP) part of THF-F. Although the hydroxy isomer M17 and dihydroxy isomer M23 were already identified by Krotulski et al., they only postulated

a vague position of the hydroxy groups (6). Due to the MS<sup>2</sup> spectrum of M17, the hydroxy group could be determined to be located at the tetrahydrofuran ring, which corresponded to the dihydroxy isomer M24. In terms of M23, one hydroxylation occurred at the phenyl ring and the other at the ethyl spacer represented by the FI at *m/z* 220.1328, which differed from FI at *m/z* 188.1433 by two additional oxygen atoms. Krotulski et al. supposed that M14 was hydroxylated at the amide nitrogen (6), but based on the MS<sup>2</sup> spectrum of M14, it was not evident where the hydroxylation occurred. Most likely, the hydroxylation took place at the phenyl ring next to the amide nitrogen, as reported for other fentanyl derivatives (12, 31, 32).

During storage of the stock solutions over four weeks, an increasing signal of the *N*-deacyl-metabolite (4-ANPP, M2), a precursor in the synthesis of fentanyl and their analogous (33, 34) was observed. To avoid formation, only freshly prepared solutions were used. However, M2 was identified solely in incubations without NADP<sup>+</sup>. This might be explained as follows. In the presence of NADP<sup>+</sup>, M2 most probably gets quickly further metabolized, as in case of THF-F by the formation of M14, and/or other metabolizing steps are pronounced.

Several metabolites of CP-F (M3, M8) and THF-F (M15, M17, M19, M20, M21, M22, M23) were only identified in the isozyme incubations (see below) and not in pHLS9 incubations, most likely due to low concentrations in pHLS9 incubations. It is expected that these are minor metabolites, because pHLS9 represents the relative CYP isozyme amounts within the human liver. Due to the unavailability of certified reference materials for the metabolites, validation experiments such as sensitivity and matrix effects were not able to be completed for this qualitative study and matrix effects can not be excluded in these results. No interfering compounds were identified in blank and control incubations.

## Isozyme mapping

Isozyme mapping can provide insights into possible interaction risks caused by interindividual variability of polymorphically expressed isozymes, drug-drug, or drug-food interactions. The involvement of individual isozymes in formation of the most abundant metabolites in comparison to pHLS9 is summarized in Table S4. The absence of interfering or non-metabolically formed compounds was confirmed by blank and negative control incubations. The isozymes mainly involved in CP-F and THF-F phase I metabolism were the polymorphically expressed isozyme CYP2D6 and the isozyme CYP3A4. The formation rates of the three most abundant metabolites and the change in amount of parent compound in pHLS9, CYP2D6, or CYP3A4 incubations is given in Figure 4.

The hydroxy isomer (M7) was the most abundant CP-F metabolite in vitro. Formation was catalyzed by CYP2D6 and CYP3A4 but also by CYP2C8 and CYP2C19. Furthermore, CYP2D6 was involved in the formation of another hydroxy metabolite (M6), the oxo metabolite (M5), and the dihydroxy isomers (M10, M11). CYP3A4 catalyzed the formation of the *N*-dealkyl metabolite (M1), the *N*-dealkyl-hydroxy isomers (M3, M4), the hydroxy isomers (M6, M7, M8), and the *N*-oxide (M9). The most abundant in vitro THF-F metabolite was the dihydroxy isomer (M24), which was only found in CYP2D6 incubations. CYP2D6 was also involved in the formation of the oxo metabolite (M15), the two hydroxy isomers (M16, M17), the oxo-hydroxy isomers (M20, M21, M22), and the dihydroxy isomer (M23). The *N*-dealkyl metabolite (M13), the hydroxy isomers (M17, M18), and the *N*-oxide (M19) were identified in CYP3A4 incubations.

Based on these observations and considering the high  $ER_h$  of CP-F, a higher risk of increasing drug levels and thus intoxications might be expected in CYP2D6 poor metabolizers or in case of certain drug-drug interactions involving CYP2D6 and/or CYP3A4 inhibitors. Interactions with other drugs of abuse may occur e.g. with methylenedioxy- (35) or 2,5-dimethoxyamphetamine-derivates (36), which particularly act as CYP2D6 inhibitors.

Table 1 compares the contribution of isozymes on the phase I metabolism of CP-F and THF-F to their contribution on the phase I metabolism of fentanyl and some derivatives. CYP2D6 and CYP3A4 were the two isozymes contributing to the majority of phase I metabolic reactions of fentanyl and the given derivatives.

### Determination of plasma protein binding

Toxicodynamic effects of drugs depend on their free fraction in plasma, which is highly correlated with their PPB. Only the unbound drug is toxicological active, can be(re)distributed into tissue, and excreted (37). The used ultrafiltrate devices consisted of a regenerated cellulose membrane, which was shown to overcome the non-specific binding as disadvantage compared to equilibrium dialysis (38). For CP-F,  $f_u$  was 0.01 and for THF-F,  $f_u$  was 0.26. This resulted in 99% and 74% PPB, respectively, which corresponded to their log  $P$  values (4.7 and 3.3, respectively). Although other factors e. g. ionization state can influence the PPB lipophilicity connection (39), a correlation has already been shown for the NSO U-48800 (40). Effects on the toxicodynamics and toxicokinetics such as reduced clearance might be expected for drugs with PPB exceeding 70% (37). The elimination route and active transport into the hepatocytes may also have an impact on the clearance (41), which should be further investigated. Furthermore, the simultaneous intake of multiple drugs of abuse with high binding

affinity to plasma proteins such as cannabinoids (25) or phenethylamine derivatives (42) could lead to a greater  $f_u$  by replacement from the binding site and therefore to a higher risk of toxicity (25).

### Detectability of metabolites in rat urine

The low dose studies in rats were done to investigate the detectability of the parent compounds and/or their metabolites in urine samples by LC-HRMS/MS SUSAs. Urinary creatinine values before and after administration were 63 and 93 mg/dL for CP-F and 34 and 44 mg/dL for THF-F, respectively.

Neither metabolites nor parent compounds were identified after urine precipitation (UP). A more targeted approach for analysis of the UP samples by adding an inclusion list containing the analytes of interest to the MS method, allowed only the detection of the THF-F dihydroxy isomer M24. Therefore, another sample preparation should be used, consisting of a glucuronidase cleavage followed by SPE. This resulted in the detection of the dihydroxy isomer M10 of CP-F and the oxo metabolite M15 and dihydroxy isomer M24 in case of THF-F. The parent compounds were not detected. Based on these findings, a focus on the described metabolites after a dedicated sample preparation should be used for reliable identification of a THF-F or CP-F intake. Similar findings were published for other fentanyl derivatives (13).

### Conclusions

The presented study revealed the toxicokinetic characteristics of the two NSO CP-F and THF-F. CP-F showed a shorter  $t_{1/2}$  in pHLS9 than THF-F with 13.8 min compared to 67.5 min. The resulting  $CL_{int}$  and  $ER_h$  were rated as high for CP-F and intermediate in case of THF-F. Both fentanyl analogous underwent mainly *N*-dealkylation,

hydroxylation, and dihydroxylation. Isozyme mapping identified CYP2D6 and CYP3A4 to be mainly catalyzing the phase I metabolism of both compounds. Therefore, an elevated risk of intoxications due to drug-drug interactions and particularly for CYP2D6 poor metabolizers cannot be excluded. CP-F showed a high PPB of 99% whereas THF-F had a PPB of 74%. The simultaneous intake of different drugs with high binding affinity to plasma proteins may lead to a higher risk of toxicity. Detectability studies in rat urine showed that neither parent compounds nor metabolites are detectable with LC-HRMS/MS SUSA unless a more targeted approach is used. In that case, metabolites should be included in the screening, as they are expected to be mainly or even exclusively excreted into urine in contrast to the parent compounds.

### **Acknowledgements**

The authors would like to thank Thomas P. Bambauer, Cathy M. Jacobs, Sascha K. Manier, Frederike Nordmeier, Gabriele Ulrich, Armin A. Weber, and the EU funded project ADEBAR (IZ25-5793-2016-27) for their support.

## References

1. EMCDDA. European Drug Report 2018. *Publications of the European Union* [serial online]. Available from: European Monitoring Centre for Drugs and Drug Addiction, Luxembourg.
2. EMCDDA. Fentanils and synthetic cannabinoids: driving greater complexity into the drug situation. An update from the EU Early Warning System. Publications Office of the European Union, Luxembourg, 2018
3. Section ULaS. Current NPS Threats, Volume 1, March 2019. [https://www.unodc.org/pdf/opioids-crisis/Current\\_NPS\\_Threats\\_-\\_Volume\\_1.pdf](https://www.unodc.org/pdf/opioids-crisis/Current_NPS_Threats_-_Volume_1.pdf), 2019
4. O'Donnell JK, Halpin J, Mattson CL, et al. Deaths Involving Fentanyl, Fentanyl Analogs, and U-47700 - 10 States, July-December 2016. *MMWR Morb Mortal Wkly Rep* 2017;66:1197-202
5. Giorgetti A, Centola C, Giorgetti R. Fentanyl novel derivative-related deaths. *Hum Psychopharmacol* 2017;32
6. Krotulski AJ, Papsun DM, Friscia M, et al. Fatality Following Ingestion of Tetrahydrofuranlylfentanyl, U-49900 and Methoxy-Phencyclidine. *J Anal Toxicol* 2018;42:e27-e32
7. Helander A, Backberg M, Signell P, et al. Intoxications involving acrylfentanyl and other novel designer fentanyls - results from the Swedish STRIDA project. *Clin Toxicol (Phila)* 2017;55:589-99
8. Wilde M, Pichini S, Pacifici R, et al. Metabolic Pathways and Potencies of New Fentanyl Analogs. *Front Pharmacol* 2019;10
9. Baumann MH, Majumdar S, Le Rouzic V, et al. Pharmacological characterization of novel synthetic opioids (NSO) found in the recreational drug marketplace. *Neuropharmacology* 2018;134:101-7
10. Addiction EMCfDaD. Report on the risk assessment of N-phenyl- N-[1-(2-phenylethyl)piperidin-4-yl]oxolane-2-carboxamide in the framework of the Council Decision on new psychoactive substances. Vol. Risk Assessments, Publications Office of the European Union, Luxembourg. <http://www.emcdda.europa.eu/system/files/publications/9124/Risk%20assessment%20THF-F.pdf>, 2018
11. Astrand A, Toreskog A, Watanabe S, et al. Correlations between metabolism and structural elements of the alicyclic fentanyl analogs cyclopropyl fentanyl, cyclobutyl fentanyl, cyclopentyl fentanyl, cyclohexyl fentanyl and 2,2,3,3-tetramethylcyclopropyl fentanyl studied by human hepatocytes and LC-QTOF-MS. *Arch Toxicol* 2019;93:95-106
12. Steuer AE, Williner E, Staeheli SN, et al. Studies on the metabolism of the fentanyl-derived designer drug butyrfentanyl in human in vitro liver preparations and authentic human samples using liquid chromatography-high resolution mass spectrometry (LC-HRMS). *Drug Test Anal* 2017;9:1085-92
13. Meyer MR, Dinger J, Schwaninger AE, et al. Qualitative studies on the metabolism and the toxicological detection of the fentanyl-derived designer drugs 3-methylfentanyl and isofentanyl in rats using liquid chromatography-linear ion trap-mass spectrometry (LC-MS(n)). *Anal Bioanal Chem* 2012;402:1249-55
14. Richter LHJ, Maurer HH, Meyer MR. New psychoactive substances: Studies on the metabolism of XLR-11, AB-PINACA, FUB-PB-22, 4-methoxy-alpha-PVP, 25-I-NBOMe, and meclonazepam using human liver preparations in comparison to primary human hepatocytes, and human urine. *Toxicol Lett* 2017;280:142-50

15. Chauret N, Gauthier A, Nicoll-Griffith DA. Effect of common organic solvents on in vitro cytochrome P450-mediated metabolic activities in human liver microsomes. *Drug Metab Dispos* 1998;26:1-4
16. Wagmann L, Manier SK, Eckstein N, et al. Toxicokinetic studies of the four new psychoactive substances 4-chloroethcathinone, N-ethylnorpentylone, N-ethylhexedrone, and 4-fluoro-alpha-pyrrolidinohexiophenone. *Forensic Toxicology* 2019;in press
17. Baranczewski P, Stanczak A, Sundberg K, et al. Introduction to in vitro estimation of metabolic stability and drug interactions of new chemical entities in drug discovery and development. *Pharmacol Rep* 2006;58:453-72
18. Obach RS. Prediction of human clearance of twenty-nine drugs from hepatic microsomal intrinsic clearance data: An examination of in vitro half-life approach and nonspecific binding to microsomes. *Drug Metab Dispos* 1999;27:1350-9
19. Benet LZ, Liu S, Wolfe AR. The Universally Unrecognized Assumption in Predicting Drug Clearance and Organ Extraction Ratio. *Clin Pharmacol Ther* 2018;103:521-5
20. Davies B, Morris T. Physiological parameters in laboratory animals and humans. *Pharm Res* 1993;10:1093-5
21. Houston JB, Galetin A. Methods for predicting in vivo pharmacokinetics using data from in vitro assays. *Curr Drug Metab* 2008;9:940-51
22. Boxenbaum H. Interspecies variation in liver weight, hepatic blood flow, and antipyrine intrinsic clearance: extrapolation of data to benzodiazepines and phenytoin. *J Pharmacokinet Biopharm* 1980;8:165-76
23. Wagmann L, Meyer MR, Maurer HH. What is the contribution of human FMO3 in the N-oxygenation of selected therapeutic drugs and drugs of abuse? *Toxicol Lett* 2016;258:55-70
24. Fung EN, Chen YH, Lau YY. Semi-automatic high-throughput determination of plasma protein binding using a 96-well plate filtrate assembly and fast liquid chromatography-tandem mass spectrometry. *J Chromatogr B Analyt Technol Biomed Life Sci* 2003;795:187-94
25. Mardal M, Gracia-Lor E, Leibnitz S, et al. Toxicokinetics of new psychoactive substances: plasma protein binding, metabolic stability, and human phase I metabolism of the synthetic cannabinoid WIN 55,212-2 studied using in vitro tools and LC-HR-MS/MS. *Drug Test Anal* 2016;8:1039-48
26. Wissenbach DK, Meyer MR, Remane D, et al. Development of the first metabolite-based LC-MS(n) urine drug screening procedure-exemplified for antidepressants. *Anal Bioanal Chem* 2011;400:79-88
27. Helfer AG, Michely JA, Weber AA, et al. Orbitrap technology for comprehensive metabolite-based liquid chromatographic-high resolution-tandem mass spectrometric urine drug screening - exemplified for cardiovascular drugs. *Anal Chim Acta* 2015;891:221-33
28. McNaney CA, Drexler DM, Hnatyshyn SY, et al. An automated liquid chromatography-mass spectrometry process to determine metabolic stability half-life and intrinsic clearance of drug candidates by substrate depletion. *Assay Drug Dev Technol* 2008;6:121-9
29. Rogge M, Taft DR. *Preclinical Drug Development*. CRC Press 2009
30. Wagmann L, Maurer HH. Bioanalytical Methods for New Psychoactive Substances. *Handb Exp Pharmacol* 2018;252:413-39

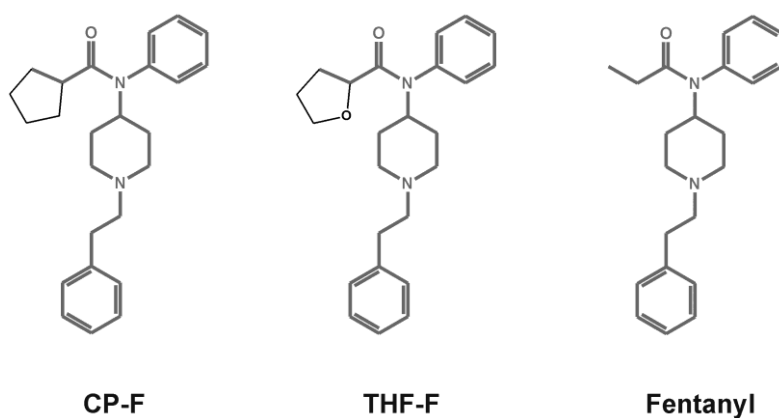
31. Watanabe S, Vikingsson S, Roman M, et al. In Vitro and In Vivo Metabolite Identification Studies for the New Synthetic Opioids Acetylfentanyl, Acrylfentanyl, Furanylfentanyl, and 4-Fluoro-Isobutyrylfentanyl. *AAPS J* 2017;19:1102-22
32. Nordmeier F, Richter LHJ, Schmidt PH, et al. Studies on the in vitro and in vivo metabolism of the synthetic opioids U-51754, U-47931E, and methoxyacetylfentanyl using hyphenated high-resolution mass spectrometry. *Sci Rep* 2019;9:13774
33. Valdez CA, Leif RN, Mayer BP. An efficient, optimized synthesis of fentanyl and related analogs. *PLoS One* 2014;9:e108250
34. Gupta PK, Laxmi M, Kumaran G, et al. A method for the preparation of fentanyl. Vol. Patent, International Publication Number WO2009116084A3, 2009
35. Dinger J, Meyer MR, Maurer HH. In vitro cytochrome P450 inhibition potential of methylenedioxy-derived designer drugs studied with a two-cocktail approach. *Arch Toxicol* 2016;90:305-18
36. Ewald AH, Maurer HH. 2,5-Dimethoxyamphetamine-derived designer drugs: studies on the identification of cytochrome P450 (CYP) isoenzymes involved in formation of their main metabolites and on their capability to inhibit CYP2D6. *Toxicol Lett* 2008;183:52-7
37. Lindup WE, Orme MC. Clinical pharmacology: plasma protein binding of drugs. *Br Med J (Clin Res Ed)* 1981;282:212-4
38. Kratzer A, Kees F, Dorn C. Unbound fraction of fluconazole and linezolid in human plasma as determined by ultrafiltration: Impact of membrane type. *J Chromatogr B Analyt Technol Biomed Life Sci* 2016;1039:74-8
39. Zhivkova ZD. Quantitative Structure - Pharmacokinetics Relationships for Plasma Protein Binding of Basic Drugs. *J Pharm Pharm Sci* 2017;20:349-59
40. Gampfer TM, Richter LHJ, Schaper J, et al. Toxicokinetics and analytical toxicology of the abused opioid U-48800 - in vitro metabolism, metabolic stability, isozyme mapping, and plasma protein binding. *Drug Test Anal* 2019
41. Howard ML, Hill JJ, Galluppi GR, et al. Plasma protein binding in drug discovery and development. *Comb Chem High Throughput Screen* 2010;13:170-87
42. Richter LHJ, Menges J, Wagmann L, et al. In vitro toxicokinetics and analytical toxicology of three novel NBOME derivatives: phase I and II metabolism, plasma protein binding, and detectability in standard urine screening approaches studied by means of hyphenated mass spectrometry. *Forensic Toxicology* 2019
43. Guitton J, Buronfosse T, Desage M, et al. Possible involvement of multiple cytochrome P450s in fentanyl and sufentanil metabolism as opposed to alfentanil. *Biochem Pharmacol* 1997;53:1613-9

**Table 1.** Summary of the isozymes mainly involved in the phase I metabolism of cyclopentanoyl-fentanyl (CP-F), tetrahydrofuranoyl-fentanyl (THF-F), fentanyl, and several other fentanyl derivatives. Cytochrome P450 (CYP); \*, mainly involved

Compound	CYP			
	2C19	2D6	3A4	3A5
3-Methylfentanyl (13)	*		*	*
Butyrfentanyl (12)		*	*	
CP-F		*	*	
Fentanyl (43)			*	
Isofentanyl (13)	*	*	*	*
THF-F		*	*	

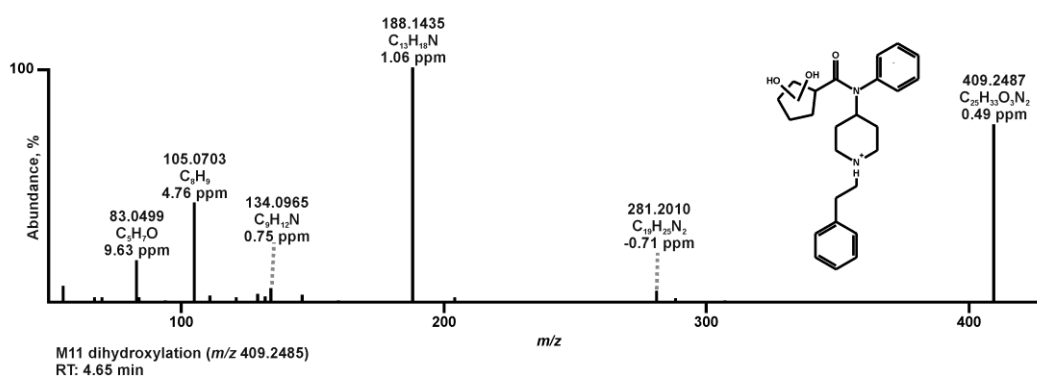
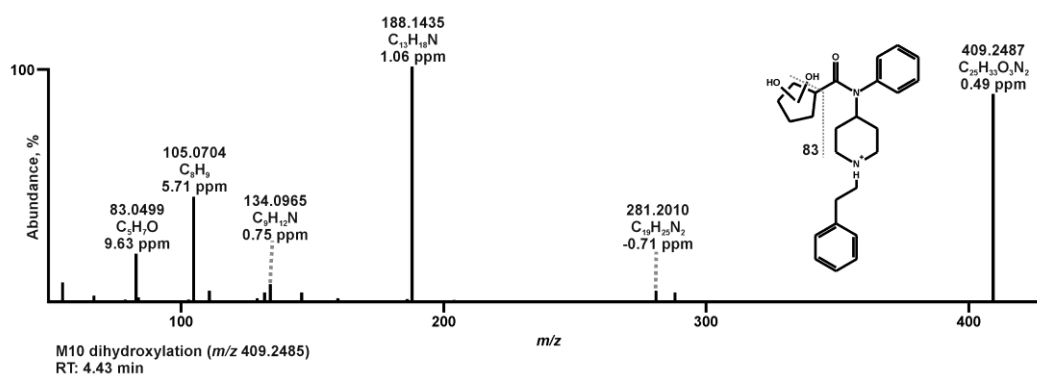
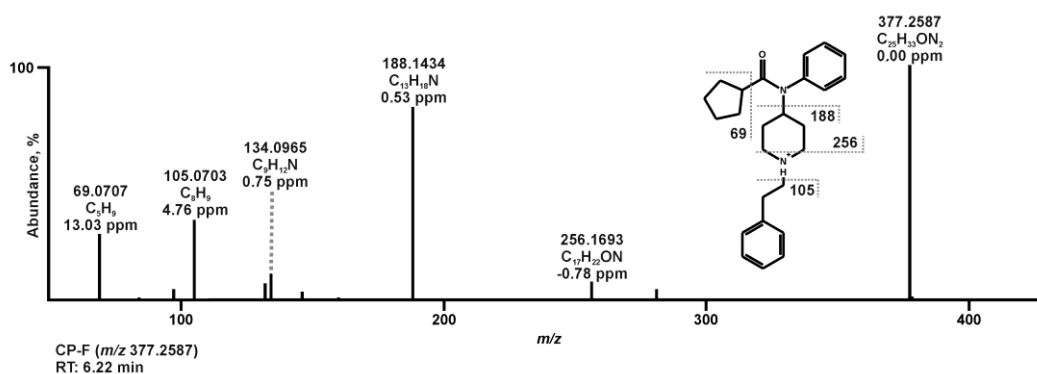
### Legends to Figures

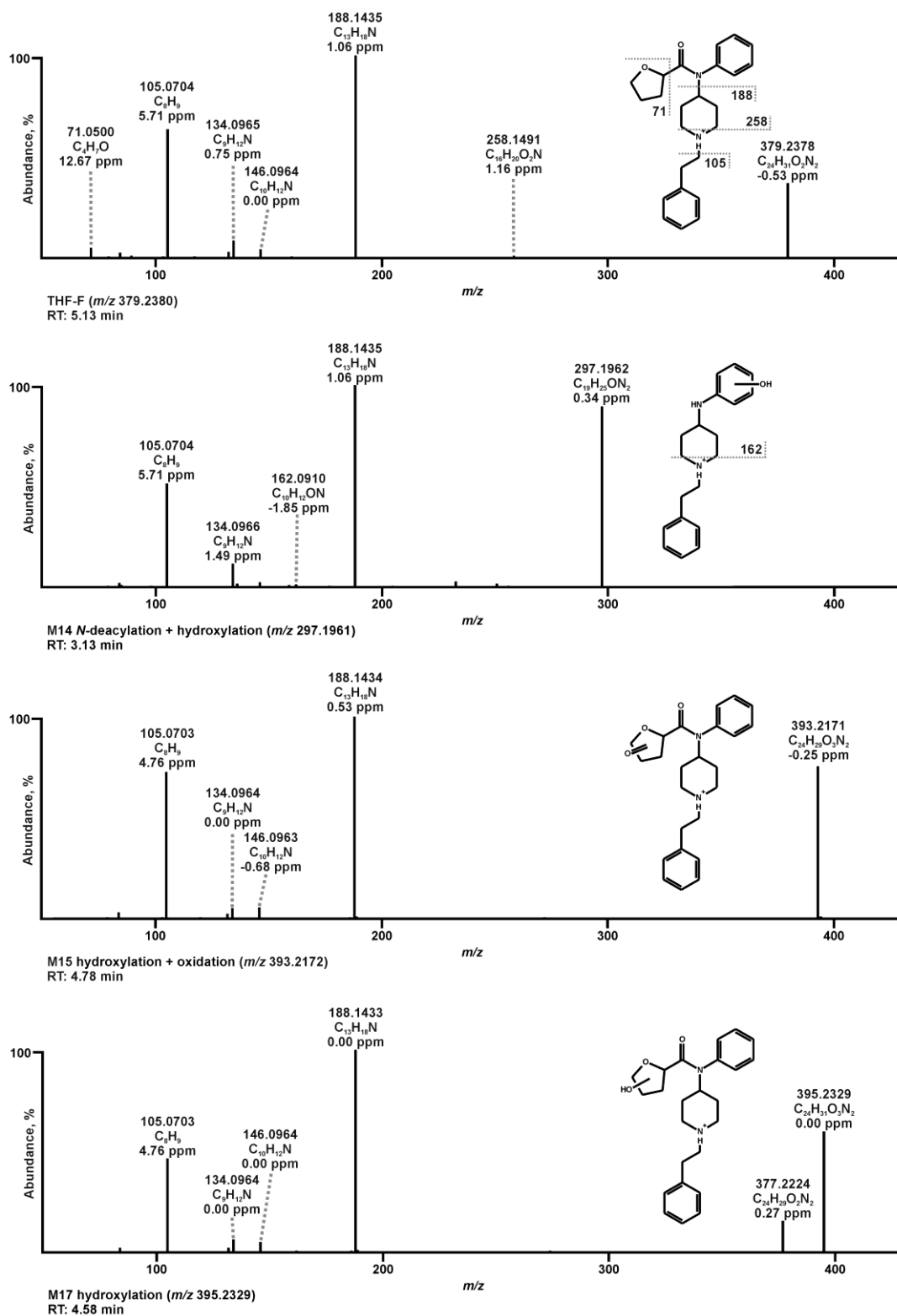
**Figure 1.** Chemical structures of cyclopentanoyl-fentanyl (CP-F), tetrahydrofuranoyl-fentanyl (THF-F), and fentanyl. The fentanyl core is highlighted in red/bold.



**Figure 2.** MS<sup>2</sup> spectra of cyclopentanoyl-fentanyl (CP-F) and the CP-F metabolites described for the first-time. Identified by means of liquid chromatography high-resolution tandem mass spectrometry (LC-HRMS/MS) after pooled human liver S9

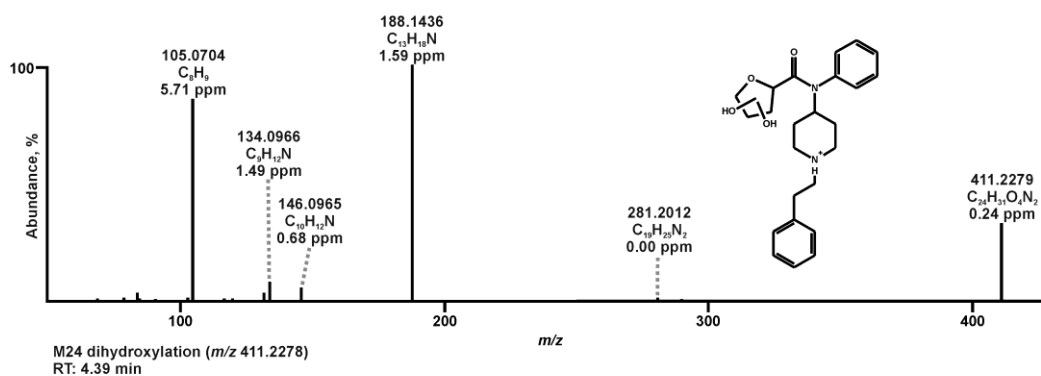
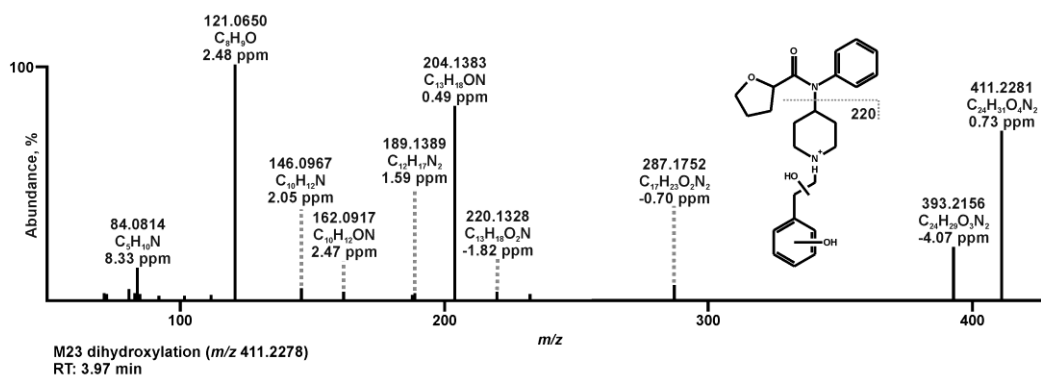
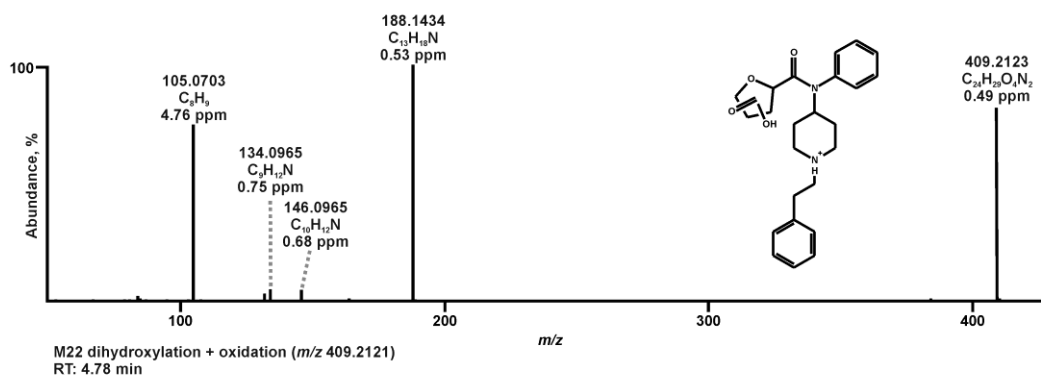
fraction (pHLS9) and/or isozyme incubations sorted by increasing precursor ions (PI) and retention times (RT).





**Figure 3.** MS<sup>2</sup> spectra of tetrahydrofuranoyl-fentanyl (THF-F) and the THF-F metabolites described for the first time and identified by means of liquid chromatography high-resolution tandem mass spectrometry (LC-HRMS/MS) after

pooled human liver S9 fraction (pHLS9) and/or isozyme incubations sorted by increasing precursor ions (PI) and retention times (RT). Already published metabolites are also included with altered positions of the hydroxy groups.



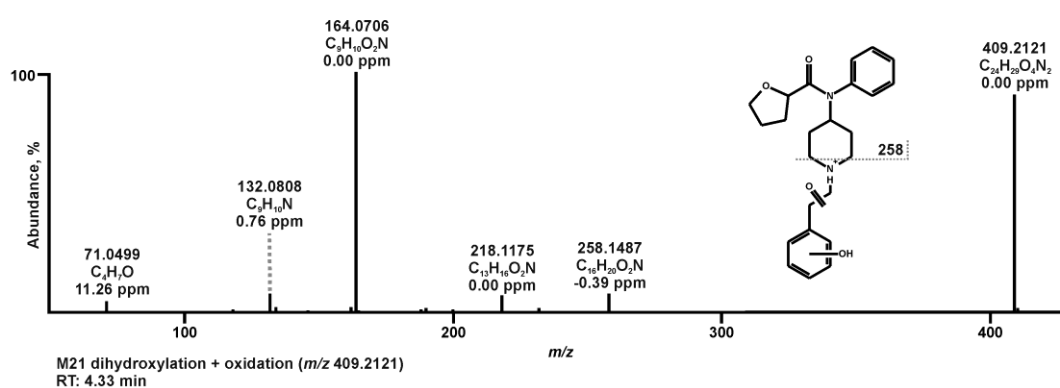
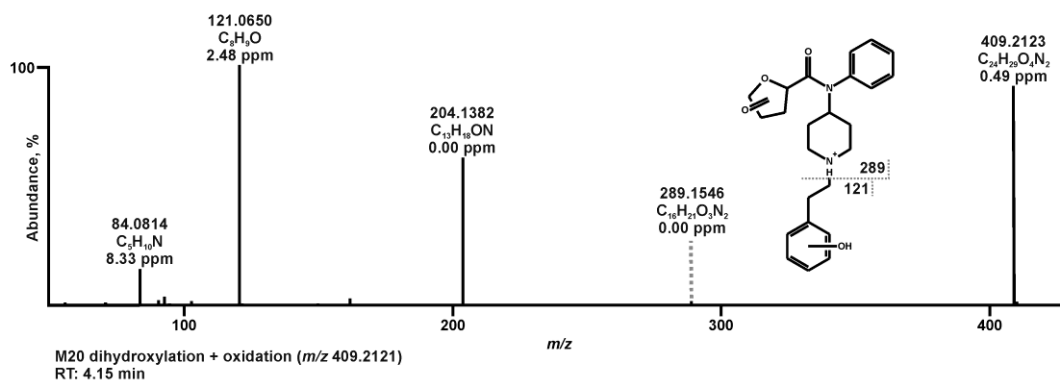
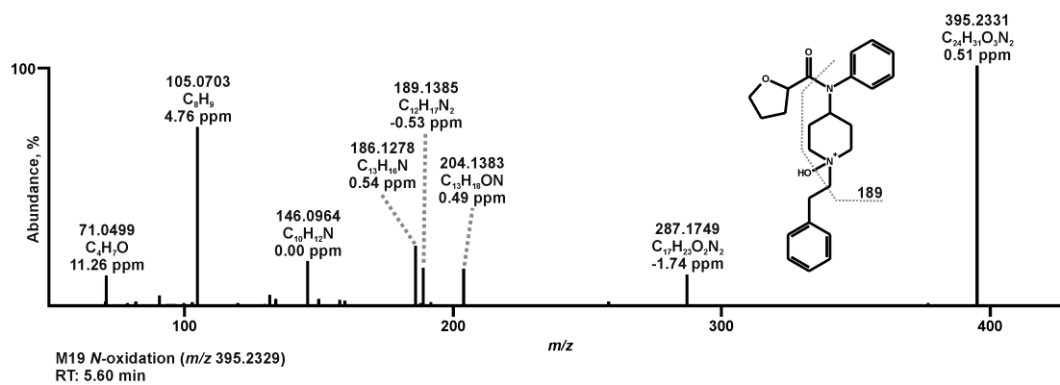
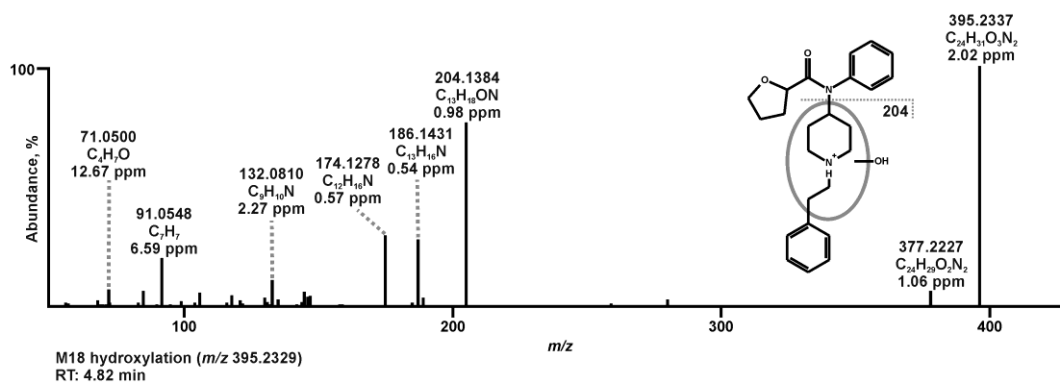
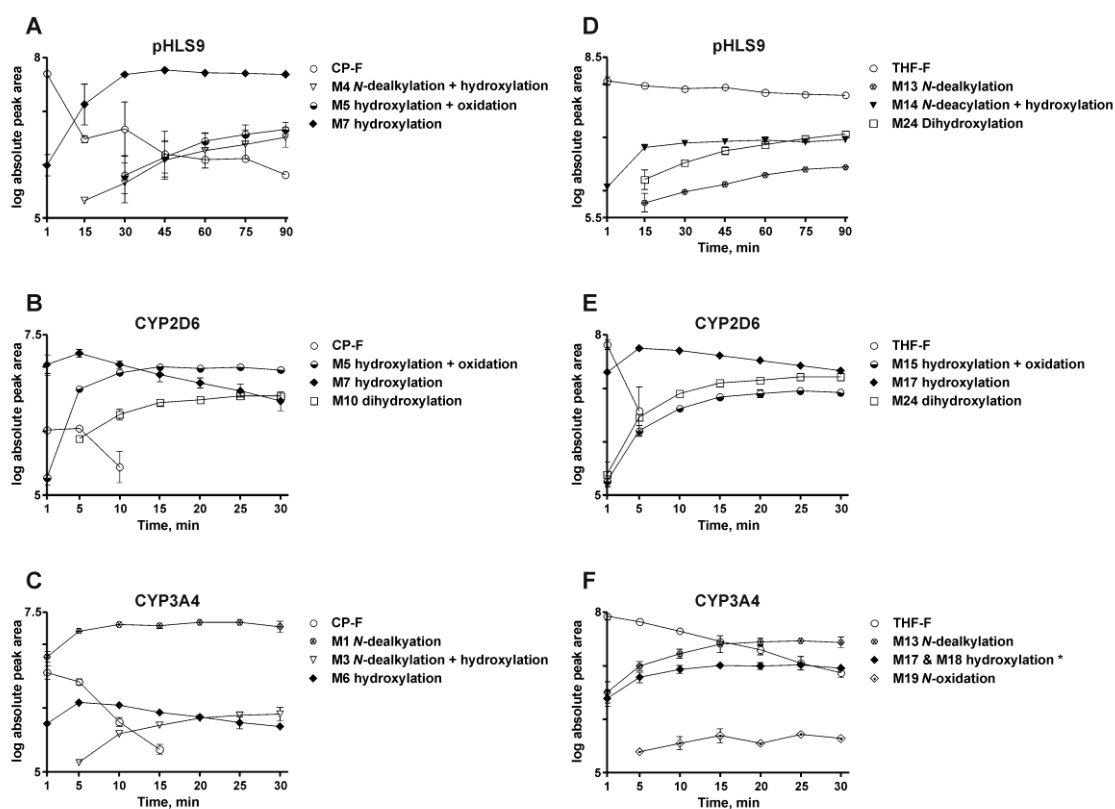


**Figure 4.** Formation rates of the three most abundant metabolites in proportion to the alteration of cyclopentanoyl-fentanyl (CP-F, A-C) and tetrahydrofuranoyl-fentanyl (THF-F, D-F) concentrations in pooled human liver S9 fraction (pHLS9, A, D) and in the two mainly involved isozyme incubations cytochrome P450 (CYP)2D6 (B, E), and CYP3A4 (C, F). In (F) the metabolite marked by an asterisk consisted of two inseparably metabolites with the described liquid chromatography high-resolution tandem mass spectrometry (LC-HRMS/MS) settings. If marks are missing for certain time points, no signals were detectable.



### 3.3 Toxicokinetics and toxicodynamics of the fentanyl homologs cyclopropanoyl-1-benzyl-4'-fluoro-4-anilinopiperidine and furanoyl-1- benzyl-4-anilinopiperidine<sup>65</sup>

(DOI: 10.1007/s00204-020-02726-1)

**Authors Contributions** Tanja M. Gampfer conducted the in vitro toxicokinetic experiments, analyzed the in vitro/ in vivo metabolism data, and took the lead in writing the manuscript; Yu-Mi Park and Jennifer Herrmann developed and conducted the experiments with the zebrafish larvae, analyzed the MTC assay and supported with scientific discussions; Annelies Cannaert and Christophe P. Stove developed and conducted the  $\mu$ -opioid receptor activity screening, supported with scientific discussion, and wrote the corresponding publication part. Svenja Fischmann and Folker Westphal characterized and provided the investigated new psychoactive substances and supported with scientific discussion; Markus R. Meyer and Lea Wagmann supported with scientific discussions, the design of the experiments, and research supervision.



# Toxicokinetics and toxicodynamics of the fentanyl homologs cyclopropanoyl-1-benzyl-4'-fluoro-4-anilinopiperidine and furanoyl-1-benzyl-4-anilinopiperidine

Tanja M. Gampfer<sup>1</sup> · Lea Wagmann<sup>1</sup> · Yu Mi Park<sup>2,5</sup> · Annelies Cannaert<sup>3</sup> · Jennifer Herrmann<sup>2</sup> · Svenja Fischmann<sup>4</sup> · Folker Westphal<sup>4</sup> · Rolf Müller<sup>2</sup> · Christophe P. Stove<sup>3</sup> · Markus R. Meyer<sup>1</sup>

Received: 12 February 2020 / Accepted: 26 March 2020 / Published online: 5 April 2020  
© The Author(s) 2020

## Abstract

The two fentanyl homologs cyclopropanoyl-1-benzyl-4'-fluoro-4-anilinopiperidine (4F-Cy-BAP) and furanoyl-1-benzyl-4-anilinopiperidine (Fu-BAP) have recently been seized as new psychoactive substances (NPS) on the drugs of abuse market. As their toxicokinetic and toxicodynamic characteristics are completely unknown, this study focused on elucidating their in vitro metabolic stability in pooled human liver S9 fraction (pHLS9), their qualitative in vitro (pHLS9), and in vivo (zebrafish larvae) metabolism, and their in vitro isozyme mapping using recombinant expressed isoenzymes. Their maximum-tolerated concentration (MTC) in zebrafish larvae was studied from 0.01 to 100  $\mu\text{M}$ . Their  $\mu$ -opioid receptor (MOR) activity was analyzed in engineered human embryonic kidney (HEK) 293 T cells. In total, seven phase I and one phase II metabolites of 4F-Cy-BAP and 15 phase I and four phase II metabolites of Fu-BAP were tentatively identified by means of liquid chromatography high-resolution tandem mass spectrometry, with the majority detected in zebrafish larvae. *N*-Dealkylation, *N*-deacylation, hydroxylation, and *N*-oxidation were the most abundant metabolic reactions and the corresponding metabolites are expected to be promising analytical targets for toxicological analysis. Isozyme mapping revealed the main involvement of CYP3A4 in the phase I metabolism of 4F-Cy-BAP and in terms of Fu-BAP additionally CYP2D6. Therefore, drug-drug interactions by CYP3A4 inhibition may cause elevated drug levels and unwanted adverse effects. MTC experiments revealed malformations and changes in the behavior of larvae after exposure to 100  $\mu\text{M}$  Fu-BAP. Both substances were only able to produce a weak activation of MOR and although toxic effects based on MOR activation seem unlikely, activity at other receptors cannot be excluded.

**Keywords** In vitro and in vivo metabolism · Metabolic stability · LC–HRMS/MS · Zebrafish larvae · In vitro  $\mu$ -opioid receptor activity

**Electronic supplementary material** The online version of this article (<https://doi.org/10.1007/s00204-020-02726-1>) contains supplementary material, which is available to authorized users.

✉ Markus R. Meyer  
markus.meyer@uks.eu

- <sup>1</sup> Department of Experimental and Clinical Toxicology, Institute of Experimental and Clinical Pharmacology and Toxicology, Center for Molecular Signaling (PZMS), Saarland University, 66421 Homburg, Germany
- <sup>2</sup> Department of Microbial Natural Products (MINS), Helmholtz Institute for Pharmaceutical Research Saarland (HIPS), Saarland University, 66123 Saarbrücken, Germany

## Introduction

More and more compounds intended to be consumed as substitutes and/or alternatives to classic opioids such as heroin are brought into the drugs of abuse market (Beardsley and

- <sup>3</sup> Laboratory of Toxicology, Department of Bioanalysis, Faculty of Pharmaceutical Sciences, Ghent University, 9000 Ghent, Belgium
- <sup>4</sup> State Bureau of Criminal Investigation Schleswig-Holstein, 24116 Kiel, Germany
- <sup>5</sup> Environmental Safety Group, Korea Institute of Science and Technology (KIST) Europe, 66123 Saarbrücken, Germany

Zhang 2018). They are summarized under the term new synthetic opioids (NSO) and have markedly contributed to the dramatic rise in overdose deaths amongst opioid abusers (Fagiola et al. 2018; Guerrieri et al. 2017; Muller et al. 2019; Sharma et al. 2019; Solimini et al. 2018). This is partly due to their nM affinity at the  $\mu$ -opioid receptor (MOR) and their enhanced brain penetration owing to higher lipophilicity, but the influence of other toxicodynamic effects cannot be excluded as they were often not characterized prior to abuse (Baumann et al. 2018). Limited data are also available concerning their toxicokinetics, which is important amongst other factors in forensic and clinical toxicology and doping control for developing analytical procedures to detect these compounds in human biosamples (Wagmann and Maurer 2018). Furthermore, the knowledge about the toxicokinetics and toxicodynamics of emerging NSO and other drugs of abuse is essential for law enforcement personnel and policymakers to allow thorough risk assessment (Evans-Brown and Sedefov 2018).

The two fentanyl homologs cyclopropanoyl-1-benzyl-4'-fluoro-4-anilinopiperidine (4F-Cy-BAP) and furanoyl-1-benzyl-4-anilinopiperidine (Fu-BAP) have been seized in Europe and were intended to be brought onto the market as NSO (EMCDDA 2018). Their chemical structures, in comparison to fentanyl, are given in Fig. 1. Fu-BAP is structurally related to furanylfentanyl, which was risk assessed by the EMCDDA in 2017 (EMCDDA 2017). Furanylfentanyl differs from Fu-BAP by replacement of the phenylethylamine part with phenylmethanamine. So far, nothing is known about the toxicokinetic and toxicodynamic characteristics of 4F-Cy-BAP and Fu-BAP. However, *N*-(1-benzylpiperidin-4-yl)-arylacetamides, structurally related compounds, were described to be potent agonists at the sigma receptor (Huang et al. 2001), with an affinity of *N*-(1-benzylpiperidin-4-yl)-arylacetamide at the sigma1 and sigma2 receptor of 3.9 and 240 nM, respectively. Fu-BAP and related compounds were also identified as antagonists at

the acetylcholine M2 and M3 receptor with  $K_i$  values of 794 and 100 nM for Fu-BAP, respectively (Diouf et al. 2002).

To close the knowledge gap concerning their toxicokinetics and toxicodynamics, the present study aimed to elucidate the toxicokinetics of these compounds, including in vitro metabolism in pooled human liver S9 fraction (pHLS9) incubations in comparison to in vivo metabolites identified using the zebrafish larvae model, isozyme mapping, and the determination of plasma protein binding (PPB). Toxicodynamic properties should include characterizing the MOR activity in engineered human embryonic kidney (HEK) 293 T cells as well as maximum-tolerated concentration (MTC) studies in zebrafish larvae.

## Materials and methods

### Chemicals and reagents

4F-Cy-BAP and Fu-BAP were provided as citrate salts for research purposes from the EU-project ADEBAR/State Bureau of Criminal Investigation Schleswig–Holstein (Kiel, Germany). Chemical purity and identity of the compounds were verified by mass spectrometry (MS) and nuclear magnetic resonance analysis. Stock solutions in methanol (1 mg/mL) or DMSO were freshly prepared before each experiment. Hydromorphone was purchased as hydromorphone HCl from Fagron (Nazareth, Belgium). Fentanyl was obtained as a free base from LGC Chemicals (Wesel, Germany). Trimipramin-d<sub>3</sub>, isocitrate, isocitrate dehydrogenase, superoxide dismutase, 3'-phosphoadenosine-5'-phosphosulfate (PAPS), S-(5'-adenosyl)-L-methionine (SAM), dithiothreitol (DTT), reduced glutathione (GSH), magnesium chloride (MgCl<sub>2</sub>), potassium dihydrogen phosphate (KH<sub>2</sub>PO<sub>4</sub>), dipotassium hydrogen phosphate (K<sub>2</sub>HPO<sub>4</sub>), tris hydrochloride, fetal bovine serum (FBS), and poly-d-lysine were from Sigma Aldrich (Taufkirchen, Germany/Overijse, Belgium) and NADP<sup>+</sup> from Biomol (Hamburg, Germany). Centrifuge devices were obtained from Merck (Darmstadt, Germany). Dulbecco's Modified Eagle's Medium (DMEM; GlutaMAX™), Opti-MEM® I Reduced Serum Medium, penicillin–streptomycin (5.000 U/mL) and amphotericin B (250 µg/mL) were purchased from Thermo Fisher Scientific (Pittsburg, PA, USA). The Nano-Glo® Live Cell reagent, which was used for the readout of the MOR bioassay, was procured from Promega (Madison, WI, USA). Acetonitrile (LC–MS grade), methanol (LC–MS grade), ammonium formate (analytical grade), formic acid (LC–MS grade), and all other reagents and chemicals (analytical grade) were from VWR (Darmstadt, Germany). Zebrafish embryos were obtained from in-house bred adult zebrafish of the AB wild-type line. The baculovirus-infected insect cell microsomes (Supersomes) containing

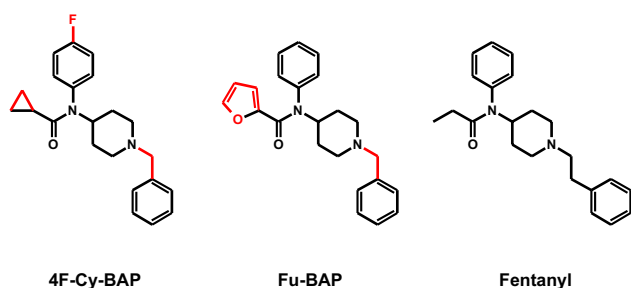


**Fig. 1** Chemical structures of cyclopropanoyl-1-benzyl-4'-fluoro-4-anilinopiperidine (4F-Cy-BAP), furanoyl-1-benzyl-4-anilinopiperidine (Fu-BAP), and fentanyl. Structural deviations from fentanyl are highlighted in red (online version only)

human cDNA-expressed flavin-containing monooxygenase 3 (FMO3) (5 mg protein/mL), CYP1A2, CYP2A6, CYP2B6, CYP2C8, CYP2C19, CYP2D6, CYP3A4 (1 nmol/mL), CYP2C9, CYP2E1, or CYP3A5 (2 nmol/mL), as well as pooled human liver microsomes (pHLM, 20 mg microsomal protein/mL, 330 pmol total CYP/mg protein), pooled human liver S9 fraction (pHLS9; 20 mg microsomal protein/mL), UGT reaction mixture solution A (25 mM UDP-glucuronic acid), and UGT reaction mixture solution B (250 mM Tris HCl, 40 mM MgCl<sub>2</sub>, and 125 µg/mL alamethicin) were supplied by Corning (Amsterdam, The Netherlands). After delivery, the enzymes were thawed at 37 °C, aliquoted, snap-frozen in liquid nitrogen, and stored at –80 °C until use.

### In vitro metabolic stability, identification of in vitro metabolites, and plasma protein binding

According to a previous study (Gampfer et al. 2019), pHLS9 (2 mg microsomal protein/mL) was preincubated for 10 min at 37 °C with 25 µg/mL alamethicin (UGT reaction mixture solution B), 90 mM phosphate buffer (pH 7.4), 2.5 mM Mg<sup>2+</sup>, 2.5 mM isocitrate, 0.6 mM NADP<sup>+</sup>, 0.8 U/mL isocitrate dehydrogenase, 100 U/mL superoxide dismutase. Thereafter, 2.5 mM UDP-glucuronic acid (UGT reaction mixture solution A), 40 µM PAPS, 1.2 mM SAM, 1 mM DTT, 10 mM GSH was added. To ensure a linear metabolism during incubation, the compound concentrations were set at 2.5 µM (Baranczewski et al. 2006). The given concentrations are concentrations in the final incubation mixtures (300 µL final volume). All incubations were done in duplicate. The organic solvent content was kept below 1% (v/v) (Chauret et al. 1998).

Reactions were initiated after addition of 4F-Cy-BAP or Fu-BAP and continued for 360 min. Meanwhile, 30 µL samples were taken after 1, 15, 30, 45, 60, 75, 90, 180, and 360 min, respectively. Reactions were stopped by adding 10 µL ice-cold acetonitrile. Afterwards, the samples were cooled for 30 min at –20 °C, centrifuged at 18,407×g for 2 min, and the supernatants were transferred to autosampler vials, and measured by liquid chromatography high-resolution tandem MS (LC–HRMS/MS). In order to identify metabolites formed by NADP<sup>+</sup> independent enzymes, incubations without NADP<sup>+</sup> were also performed. Blank incubations without substrate and control incubations without enzyme (pHLS9) were prepared to examine whether interfering or non-metabolically formed compounds were present.

Metabolic stability was determined by declining substrate concentration (Wagmann et al. 2019), plotting the natural logarithm of the absolute peak area ratios of 4F-Cy-BAP or Fu-BAP versus time, respectively. In vitro half-lives were calculated by the slope of the respective linear regression. A *t*-test was done to confirm that there was no significant

difference between the compound concentration at 360 min in control incubations and the initial concentrations in the pHLS9 incubations at 1 min. GraphPad Prism 5.00 (GraphPad Software, San Diego, USA) was used for statistical calculations with the following defined settings: unpaired; two-tailed; significance level, 0.05; confidence intervals, 99%.

In vitro half-life ( $t_{1/2}$ ) and intrinsic clearance ( $CL_{int}$ , Eq. 1–3) were determined in accordance to Baranczewski et al. (2006). Hepatic clearance ( $CL_h$ ) was predicted using parallel tube model with (Eq. 4) and without (Eq. 5) free fraction in plasma ( $f_u$ ) and well-stirred model with (Eq. 6) and without (Eq. 7)  $f_u$  (Obach 1999). Calculations of hepatic extraction ratio ( $ER_h$ , Eq. 8) were based on Eqs. 5 and 7 (Mehvar 2018).

$$t_{1/2, \text{ min}} = \frac{\ln 2}{k} \quad (1)$$

$$\ln[\text{peak area ratio}]_{\text{remaining}} = \ln[\text{peak area ratio}]_{\text{initial}} - k \times t \quad (2)$$

$$CL_{int, \text{ mL/min/kg}} = \frac{\ln 2}{t_{1/2}} \times \frac{[V]_{\text{incubation}}}{[P]_{\text{incubation}}} \times \frac{[\text{Liver}]}{[\text{BW}]} \times \text{SF} \quad (3)$$

$$CL_h, \text{ mL/min/kg} = Q \times \left( 1 - e^{\left( \frac{-f_u \times CL_{int}}{Q} \right)} \right) \quad (4)$$

$$CL_h, \text{ mL/min/kg} = Q \times \left( 1 - e^{\left( \frac{-CL_{int}}{Q} \right)} \right) \quad (5)$$

$$CL_h, \text{ mL/min/kg} = \frac{Q \times f_u \times CL_{int}}{Q + f_u \times CL_{int}} \quad (6)$$

$$CL_h, \text{ mL/min/kg} = \frac{Q \times CL_{int}}{Q + CL_{int}} \quad (7)$$

$$ER_h = \frac{CL_h}{Q} \quad (8)$$

$t_{1/2}$  = in vitro half-life,  $k$  = slope of the linear regression fit,  $CL_{int}$  = intrinsic clearance,  $[V]_{\text{incubation}}$  = incubation volume = 0.3 mL,  $[P]_{\text{incubation}}$  = amount of S9 protein in the incubation = 0.6 mg,  $\frac{[\text{Liver}]}{[\text{BW}]}$  = liver weight normalized by body weight = 26 g/kg (Davies and Morris 1993), SF = scaling factor S9 protein per gram of liver = 121 mg/g (Houston and Galetin 2008),  $CL_h$  = hepatic clearance,  $Q$  = hepatic blood flow rate in human = 20 mL/min/kg (Boxenbaum 1980),  $f_u$  = free fraction in plasma, and  $ER_h$  = hepatic extraction ratio.

PPB studies were done as described earlier (Fung et al. 2003; Mardal et al. 2016). Methanolic 4F-Cy-BAP and

Fu-BAP solution (final concentration 0.5  $\mu\text{M}$ ) were spiked into fresh pooled human plasma (500  $\mu\text{L}$  final volume). As human blood concentrations of both compounds were unknown, the selected plasma concentration was based on an average value of two intoxications with the synthetic opioid THF-F (Helander et al. 2017; Krotulski et al. 2018). After the incubation was conducted for 30 min at 37  $^{\circ}\text{C}$ , a volume of 100  $\mu\text{L}$  (global approach, GA) was taken and transferred into a new reaction tube. The remaining sample was transferred into an ultrafiltrate device and centrifuged at 1600 $\times g$  for 35 min. Thereafter, a volume of 100  $\mu\text{L}$  of the ultrafiltrate (UF) was transferred to a new reaction tube. All samples were precipitated by adding a volume of 50  $\mu\text{L}$  of ice-cold acetonitrile containing trimipramine- $d_3$  (2.5  $\mu\text{M}$ ) as internal standard (IS). This was done as there was no deuterated 4F-Cy-BAP or Fu-BAP available and trimipramine- $d_3$  was shown to be suitable as IS. Afterwards, they were cooled for 30 min at  $-20$   $^{\circ}\text{C}$ , centrifuged for 2 min at 18,407 $\times g$ , and measured by LC-HRMS/MS. Ultrafiltration was done in triplicate.

Calculations of PPB were done using the following equations:

$$f_u = \frac{\text{peak area ratio} \left( \frac{4\text{F-Cy-BAP}_{\text{UF}} \text{ or Fu-BAP}_{\text{UF}}}{\text{IS}_{\text{UF}}} \right)}{\text{peak area ratio} \left( \frac{4\text{F-Cy-BAP}_{\text{GA}} \text{ or Fu-BAP}_{\text{GA}}}{\text{IS}_{\text{GA}}} \right)} \quad (9)$$

$$\text{PPB, \%} = (1 - f_u) \times 100 \quad (10)$$

### Isozyme mapping

As described elsewhere (Wagmann et al. 2016) with minor modifications, 4F-Cy-BAP and Fu-BAP (2.5  $\mu\text{M}$ ) were incubated with CYP1A2, CYP2A6, CYP2B6, CYP2C8, CYP2C9, CYP2C19, CYP2D6, CYP2E1, CYP3A4, CYP3A5 (50 pmol/mL each), FMO3 (0.25 mg protein/mL), respectively, or pHLM (1 mg protein/mL) as positive control for 30 min at 37  $^{\circ}\text{C}$ . All given concentrations are concentrations in the final incubation mixtures (100  $\mu\text{L}$  final volume). In addition, the incubation mixtures contained 90 mM phosphate buffer (pH 7.4), 5 mM  $\text{Mg}^{2+}$ , 5 mM isocitrate, 0.5 U/mL isocitrate dehydrogenase, 1.2 mM  $\text{NADP}^+$ , and 200 U/mL superoxide dismutase. CYP2A6 and CYP2C9 incubations were conducted using Tris buffer instead of phosphate buffer, according to the manufacturer's recommendation. In a preliminary test, reactions were started by adding the enzymes and stopped after 30 min by transferring a volume of 30  $\mu\text{L}$  into new reaction tubes, which contained 10  $\mu\text{L}$  ice-cold acetonitrile. Before analysis, the samples were centrifuged at 18,407 $\times g$  for 5 min and the supernatants were transferred into autosampler vials. In a second

test, only the involved isozymes and pHLM were incubated under identical conditions as described above (250  $\mu\text{L}$  final volume). Reactions were stopped after 1, 5, 10, 15, 20, 25, and 30 min. Blank incubations without substrate and negative control incubations without enzymes were conducted to examine whether interfering or non-metabolically formed compounds were present. All incubations were done in duplicate.

### Maximum-tolerated concentration (MTC) studies in zebrafish larvae

Following the study of Richter et al. (2019a), zebrafish maintenance and all experiments with larvae were performed according to internal protocols based on standard methods (Westerfield 2007). Zebrafish larvae were raised at 28  $^{\circ}\text{C}$  in Danieau's medium consisting of 17 mM NaCl, 2 mM KCl, 0.12 mM  $\text{MgSO}_4$ , 1.8 mM  $\text{Ca}(\text{NO}_3)_2$ , 1.5 mM HEPES, and 1.2  $\mu\text{M}$  methylene blue. MTC studies were performed by placing the collected embryos in 6-well plates with 10 embryos per well in 2 mL Danieau's medium. Zebrafish larvae at 4 days post-fertilization (dpf) were exposed to 4F-Cy-BAP and Fu-BAP dissolved in Danieau's medium containing 1% (v/v) DMSO (waterborne exposition). Final compound concentrations were 0.01, 0.1, 1, 10, 50, and 100  $\mu\text{M}$ . A negative control without drug was prepared, to exclude morphological malfunctions caused by DMSO (Xiong et al. 2017). The well plates remained over 24 h in the incubator at 28  $^{\circ}\text{C}$ . All drug exposure tests were done with 20 larvae. During exposure, the larvae were monitored using a LEICA M205 FA stereo microscope (Leica Mikrosysteme Vertrieb GmbH, Wetzlar, Germany).

### In vivo identification of metabolites

In compliance with an already described procedure (Richter et al. 2019a), 4F-Cy-BAP or Fu-BAP were administered to the zebrafish larvae (4 dpf) via medium. One well of a 6-well plate contained 10 zebrafish larvae and 2 mL of Danieau's medium spiked with the compound (100  $\mu\text{M}$  4F-Cy-BAP or 80  $\mu\text{M}$  Fu-BAP final concentrations, respectively). Drug exposure lasted for 24 h at 28  $^{\circ}\text{C}$ . Afterwards, the larvae and surrounding medium were collected separately and the medium was frozen at  $-20$   $^{\circ}\text{C}$  until use. Twenty larvae (from two wells) were transferred into a reaction tube, washed twice with 1 mL medium and euthanized by placing the tubes in ice water for 15 min. After the wash solution was removed, larvae were snap-frozen in liquid nitrogen, followed by lyophilization, and stored at  $-20$   $^{\circ}\text{C}$  until use.

Extraction of the medium was conducted by precipitation of 50  $\mu\text{L}$  medium with 50  $\mu\text{L}$  acetonitrile containing 0.1% (v/v) formic acid, shaking for 2 min, and cooling for 30 min at  $-20$   $^{\circ}\text{C}$ . Before analysis, the samples were centrifuged at

18,407×g for 2 min and the supernatant was transferred to an autosampler vial. Twenty larvae (one tube) were extracted with 50 µL methanol and shaken for 2 min. After centrifugation at 18,407×g for 2 min, the supernatant was transferred to an autosampler vial. All above described experiments were prepared and analyzed in triplicate. Blank zebrafish larvae ( $n=2$ ) were incubated in the medium without drugs and analyzed along with their blank medium to identify interfering compounds. Furthermore, a control medium sample containing only the drug in Danieau's medium was prepared, respectively, for the detection of compound degradations during incubation.

### In vitro $\mu$ -opioid (MOR) receptor activity

To assess the in vitro biological activity of 4F-Cy-BAP and Fu-BAP, a live cell-based reporter assay was used that monitors functional complementation of a split nanoluciferase (NanoLuc Binary Technology) following agonist-induced recruitment of a  $\beta$ -arrestin 2 ( $\beta$ arr2) protein (fused to a small part of NanoLuc) to MOR (fused to a large part of NanoLuc). Details regarding the development of the stable cell line used here have been reported elsewhere (Cannaert et al. 2017, 2018).

Engineered HEK 293 T cells were routinely maintained at 37 °C, 5% CO<sub>2</sub>, under humidified atmosphere in DMEM supplemented with 10% heat-inactivated FBS, 100 U/mL of penicillin, 100 µg/mL of streptomycin and 0.25 µg/mL of amphotericin B. Stability of the cell lines was followed by flow cytometric analysis. For experiments, cells were plated on poly-D-lysine coated 96-well plates at  $5 \times 10^4$  cells/well and incubated overnight. The cells were washed twice with Opti-MEM® I Reduced serum medium to remove any remaining FBS and 100 µL of Opti-MEM® I was added. The Nano-Glo Live Cell reagent, a non-lytic detection reagent containing the cell permeable furimazine substrate, was prepared by diluting the Nano-Glo Live Cell substrate 20-fold using Nano-Glo LCS Dilution buffer, and 25 µL was added to each well. Subsequently, the plate was placed in the TriStar2 LB 942 multimode microplate reader (Berthold Technologies GmbH & Co., Germany). Luminescence was monitored during the equilibration period until the signal stabilized (15 min). We added 20 µL per well of test compounds, present as 6.75×stocks (as 20 µL was added to 135 µL in total) in Opti-MEM® I. The luminescence was continuously measured for 120 min. Solvent controls were run in all experiments. Curve fitting and statistical analyses were performed using GraphPad Prism. The concentration–response curves were generated from experiments performed in triplicate, the data points representing the mean area under the curve (AUC) ± standard error of mean (SEM). All results were normalized to the maximal activity ( $E_{\max}$ ) of hydromorphone (= 100%), used as the reference compound.

Curve fitting of concentration – effect curves via nonlinear regression was employed to determine the potency ( $EC_{50}$ ) and the efficacy ( $E_{\max}$ ).

### LC–HRMS/MS system

The used Thermo Fisher Scientific (TF, Dreieich, Germany) Dionex UltiMate 3000 RS pump was composed of a degasser, a quaternary pump, and an UltiMate autosampler and connected to a TF Q-Exactive Plus system equipped with a heated electrospray ionization source (HESI)-II. A volume of 1 µL was injected for all samples. Gradient elution was performed as described earlier (Helfer et al. 2015), using a TF Accucore PhenylHexyl column (100 mm×2.1 mm, 2.6 µm). The composition of the mobile phases was: 2 mM aqueous ammonium formate containing formic acid (0.1%, v/v, pH 3, eluent A) and 2 mM ammonium formate solution with acetonitrile:methanol (1:1, v/v), water (1%, v/v), and formic acid (0.1%, v/v, eluent B). At first, the flow rate was set to 500 µL/min for a period of 10 min followed by 800 µL/min for 10–13.5 min. The gradient was stepped from 0 to 1 min hold 99% A, 1–10 min to 1% A, 10–11.5 min hold 1% A, and 11.5–13.5 min hold 99% A. HESI-II source settings were: heater temperature, 320 °C; ion transfer capillary temperature, 320 °C; spray voltage, 4.0 kV; ionization mode, positive; sheath gas, 60 arbitrary units (AU); auxiliary gas, 10 AU; sweep gas, 0 AU; and S-lens RF level, 50.0. External mass calibrations were done in advance before analysis as recommended by the manufacturer. Identification and quantification of parent compounds and metabolites were performed using full scan data and a subsequent data-dependent MS<sup>2</sup> (dd-MS<sup>2</sup>) mode with an inclusion list containing the exact masses of the respective parent compound and its presumed metabolites. Expected phase I metabolites such as hydroxy, dihydroxy or *N*-dealkyl metabolites and phase II e.g. sulfates, glucuronides were the inclusion lists. Full scan data acquisition was conducted as follows: resolution, 35,000; microscans, 1; automatic gain control (AGC) target, 1e<sup>6</sup>; maximum injection time (IT), 120 ms; and scan range, *m/z* 50–750. The following settings for the dd-MS<sup>2</sup> mode were defined: option “pick others”, enabled; dynamic exclusion, disabled; resolution, 17,500; microscans, 1; isolation window, 1.0 mass-to-charge ratio (*m/z*); loop count, 5; AGC target, 2e<sup>5</sup>; maximum IT, 250 ms; high collision dissociation cell with stepped normalized collision energy, 17.5, 35.0, 52.5; exclude isotopes, on; spectrum data type, profile; and underfill ratio, 1%. Chemical structure drawings of presumed metabolites and exact mass calculations were prepared by ChemSketch 2010 12.01 (ACD/Labs, Toronto, Canada). Data handling was performed by TF Xcalibur Qual Browser software version 2.2. Automated peak integration settings were as follows: mass tolerance, 5 ppm; peak detection

algorithm, INCOS; baseline window, 40; area noise factor, 5; and peak noise factor, 10.

## Results

### In vitro metabolic stability and PPB

Metabolic stability data are summarized in Table S1 in the Electronic Supplementary Material (ESM). Non-metabolic compound degradation during the pHLS9 incubations could be excluded by control incubations as the *t*-tests did not show a significant difference between the parent compound concentration after 360 min in control incubations and the initial concentrations after 1 min. Based on decreasing enzyme activities after 2 h of incubation, the cut-off value for determination of in vitro half-lives was defined to be 90 min (Baranczewski et al. 2006). Since the half-life of 4F-Cy-BAP was longer than 90 min, no clearance values and  $ER_h$  were calculated. The half-life of Fu-BAP was 71 min, resulting in a  $CL_{int}$  of 15 mL/min/kg. Calculations of  $f_u$  gave values of 0.02 for 4F-Cy-BAP and 0.05 in terms of Fu-BAP resulting in a PPB of 98% (4F-Cy-BAP) and 95% (Fu-BAP).  $CL_h$  predictions of Fu-BAP in consideration of  $f_u$  resulted in 0.7 mL/min/kg in both models. In disregard of  $f_u$ ,  $CL_h$  values were 10.6 mL/min/kg, calculated with the parallel tube and 8.6 mL/min/kg with the well-stirred model, which gave  $ER_h$  values of 0.5 and 0.4, respectively.

### Identification of in vitro and in vivo metabolites

To avoid redundancies and to ease readability, results of in vitro and in vivo metabolite identification will be combined in the following section. Metabolites were identified by mining the data recorded in full-scan mode for their on beforehand calculated exact precursor ions (PIs). Subsequently, the spectra of the tentative metabolites obtained from the dd-MS<sup>2</sup> mode were compared to that of the respective parent compound. All metabolites are listed in Table S2 in the ESM along with their metabolite ID, PI recorded in MS<sup>1</sup>, characteristic fragment ions (FIs) in MS<sup>2</sup>, relative intensities, calculated exact masses, elemental composition, mass deviation errors of the most abundant FIs, and retention time (RT). The in vitro and in vivo metabolic pathways of 4F-Cy-BAP and Fu-BAP are depicted in Fig. 2 and Fig. 3, respectively. In total, 7 phase I and 1 phase II metabolites of 4F-Cy-BAP and 15 phase I and 4 phase II metabolites in case of Fu-BAP were tentatively identified. The MS<sup>2</sup> spectra of 4F-Cy-BAP or Fu-BAP and their three most abundant in vitro and in vivo metabolites are given in Figs. 4 and 5, respectively. In addition, the MS<sup>2</sup> spectra of the lower

abundant metabolites are represented in Fig. S1 (4F-Cy-BAP) and Fig. S2 (Fu-BAP) in the ESM.

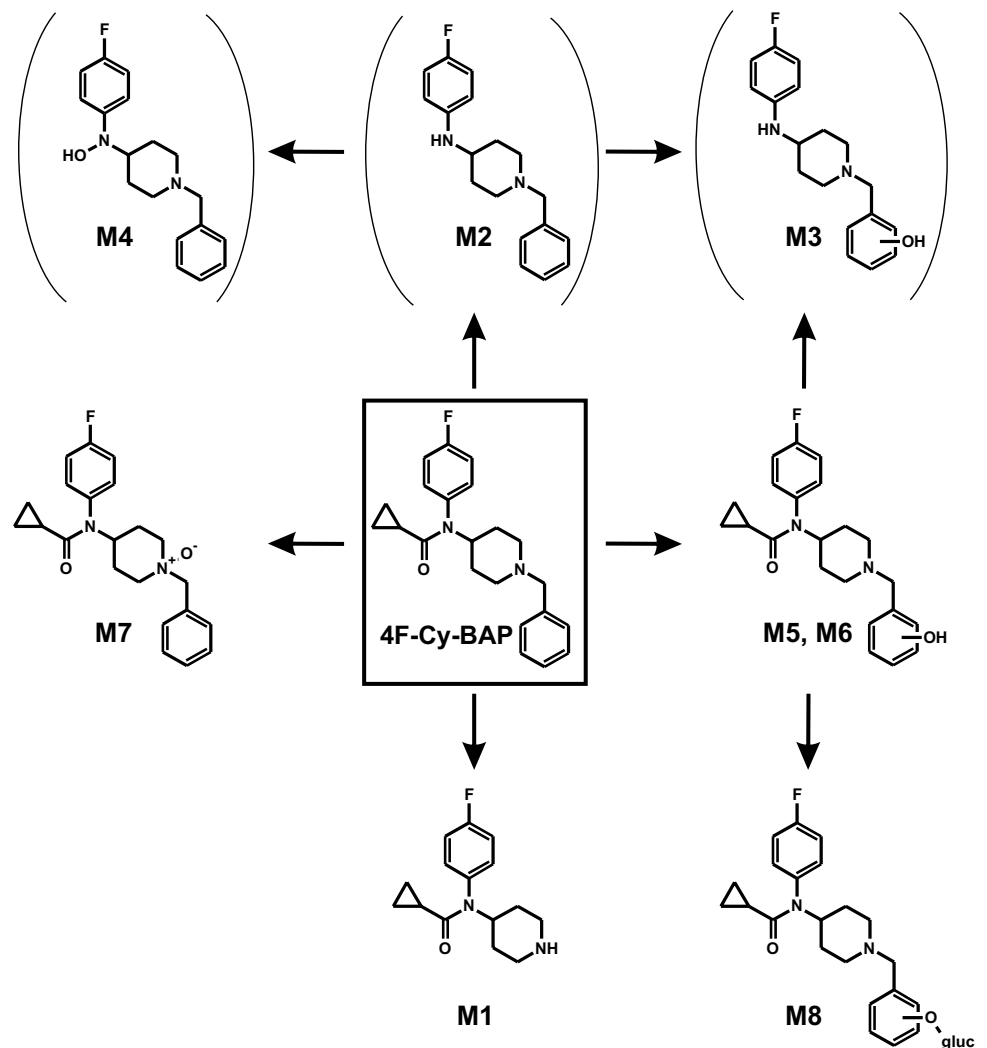
In the following section, only exact masses will be used for the characterization of parent compounds and their respective metabolites. High abundant but less characteristic FIs of 4F-Cy-BAP (PI at  $m/z$  353.2023) as well as Fu-BAP (PI at  $m/z$  361.1910) were FIs at  $m/z$  174.1277 and at  $m/z$  91.0542. The former fragment originated from the benzyl piperidine part of the compounds and the latter of the phenyl coupled to the methyl spacer after piperidine cleavage. A distinctive fragment of 4F-Cy-BAP was the FI at  $m/z$  246.1288, which was generated after the separation of the piperidine nitrogen plus benzyl part. Another prominent FI at  $m/z$  69.0334 contained the cyclopropyl and carbonyl moiety formed after amide cleavage. Equally, distinguishing FIs of Fu-BAP were the less abundant FI at  $m/z$  254.1175 and the FI at  $m/z$  95.0127, which differed from the MS<sup>2</sup> fragments of 4F-Cy-BAP through substitution of the cyclopropyl with the furanyl group.

One of the most abundant metabolites of 4F-Cy-BAP was M1 (PI at  $m/z$  263.1554), which originated from *N*-dealkylation at the piperidine nitrogen. A characteristic FI was FI at  $m/z$  180.0819, which consisted of the fluorophenyl linked to the cyclopropyl moiety. M2 (PI at  $m/z$  285.1761), showed a similar fragmentation pattern as the parent compound, except for the missing FI at  $m/z$  69.0334, which represented the cyclopropyl and carbonyl moiety. *N*-oxidation of the piperidine nitrogen led to the formation of M7 (PI at  $m/z$  369.1972). The characteristic FI at  $m/z$  98.0600 correlated with FI at  $m/z$  84.0807 varying in one oxygen and two missing hydrogen atoms.

The Fu-BAP metabolite M9 (PI at  $m/z$  267.1855) emerged from *N*-deacylation at the amide. Its MS<sup>2</sup> spectrum was similar to that of the parent compound, except for the FI at  $m/z$  95.0127, which originated from the furanyl part. M10 (PI at  $m/z$  271.1441) was formed by *N*-dealkylation at the piperidine nitrogen and specified by FI at  $m/z$  188.0706, which was generated after separation of the piperidine. M15 (PI at  $m/z$  377.1859) was one of two hydroxy isomers, with the hydroxy group located at the phenyl part, which was part of the benzyl moiety. The FI at  $m/z$  107.0491 corresponded to the FI at  $m/z$  91.0548, which was altered by one oxygen atom. Both hydroxy isomers (M15, M16) were distinguishable from each other by different RT and intensities.

The *N*-deacyl hydroxy metabolite of 4F-Cy-BAP, M3 (PI at  $m/z$  301.1710) was formed by *N*-deacylation at the amide and followed by hydroxylation at the phenyl, which was represented by the prominent FI at  $m/z$  107.0491. *N*-Deacylation followed by *N*-oxidation of the linker nitrogen between piperidine and fluorophenyl led to the formation of M4 (PI at  $m/z$  301.1710). A characteristic FI of M4 was FI at  $m/z$  193.1135, which was matched with the fluorophenyl part linked to the piperidine ring with one double bond indicating

**Fig. 2** In vitro and in vivo metabolic pathways of 4F-Cy-BAP. Metabolites in brackets are considered to be artifacts



loss of water. The two hydroxy isomers M5 and M6 (PI at  $m/z$  369.1972) were formed by hydroxylation at the phenyl part. As already described for the Fu-BAP metabolite M15, M5 and M6 were characterized by the same FI at  $m/z$  107.0491. A differentiation between both isomers was possible by different RT. The phase II metabolite M8 (PI at  $m/z$  545.2293) was formed by glucuronidation of M5 or M6, which was also identified by the FI at  $m/z$  107.0491.

M11 and M12 (PI at  $m/z$  283.1804) were two Fu-BAP metabolites formed by *N*-deacylation plus hydroxylation. M12 was the equivalent *N*-deacyl metabolite of M15 or M16, which was characterized by FI at  $m/z$  107.0491. The hydroxylation of M11 (PI at  $m/z$  283.1804) occurred at the phenyl, which was designated by FI at  $m/z$  192.1258 originating from elimination of the benzyl part. M13 (PI at  $m/z$  305.1495) was formed by *N*-dealkylation and dihydrodiol formation by epoxidation of one double bond at the furanyl, followed by a non-enzymatic hydrolysis. Identification of M13 followed FI at  $m/z$  166.0862, which contained the phenyl linked to a remaining part of the furanyl. M14 (PI

at  $m/z$  363.1373) stemmed from M11 through sulfation of the hydroxy group and their MS<sup>2</sup> spectra were in accordance to each other. The second hydroxy isomer M16 (PI at  $m/z$  377.1859) showed a similar fragmentation pattern as M15. M17 (PI at  $m/z$  377.1859) originated from *N*-oxidation of the piperidine nitrogen, which was also specified with FI at  $m/z$  98.0600, as already described for M7 of 4F-Cy-BAP. The 2,5-dihydroxypent-2-enal metabolite M18 (PI at  $m/z$  381.2172) occurred through oxidative opening of the furan ring, which was identified by FI at  $m/z$  363.2067 and FI at  $m/z$  174.1277. The former fragment indicated a loss of water and due to the presence of the latter, which was unchanged compared to parent compound, the water loss was located at the opened furan ring. Aromatic dihydroxylation led to the formation of M19 (PI at  $m/z$  393.1808), with the hydroxy groups located at the phenyl being part of the benzyl. The specific FI at  $m/z$  123.0440 represented the dihydroxylated benzyl moiety, which differed in two oxygen atoms to the FI at  $m/z$  91.0548. The dihydrodiol metabolite M20 (PI at  $m/z$  395.1965) was characterized due to the

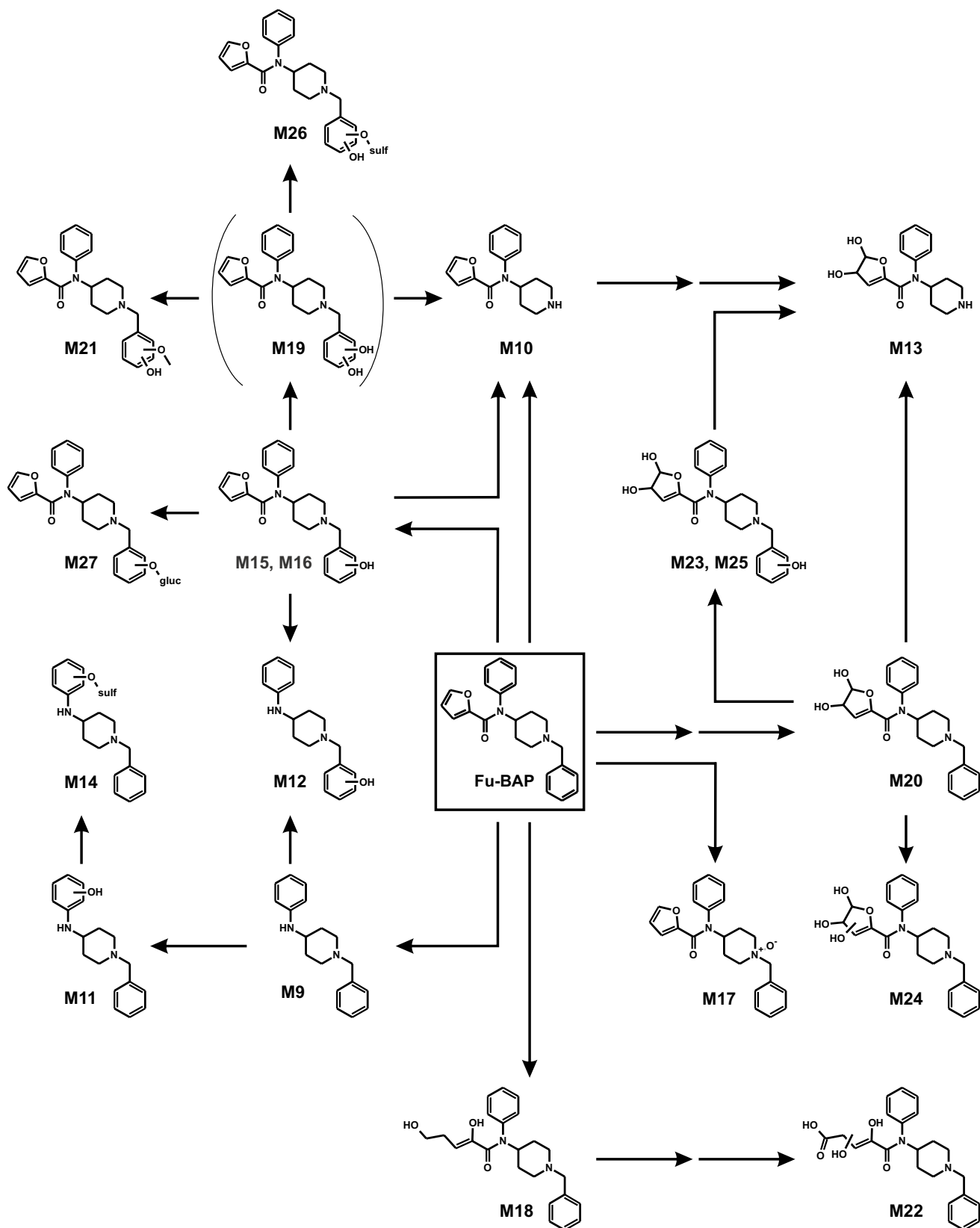


**Fig. 3** In vitro and in vivo metabolic pathways of Fu-BAP. For reasons of clarity, some arrows of expected metabolization steps are not shown. The metabolite in brackets is considered to be an artifact

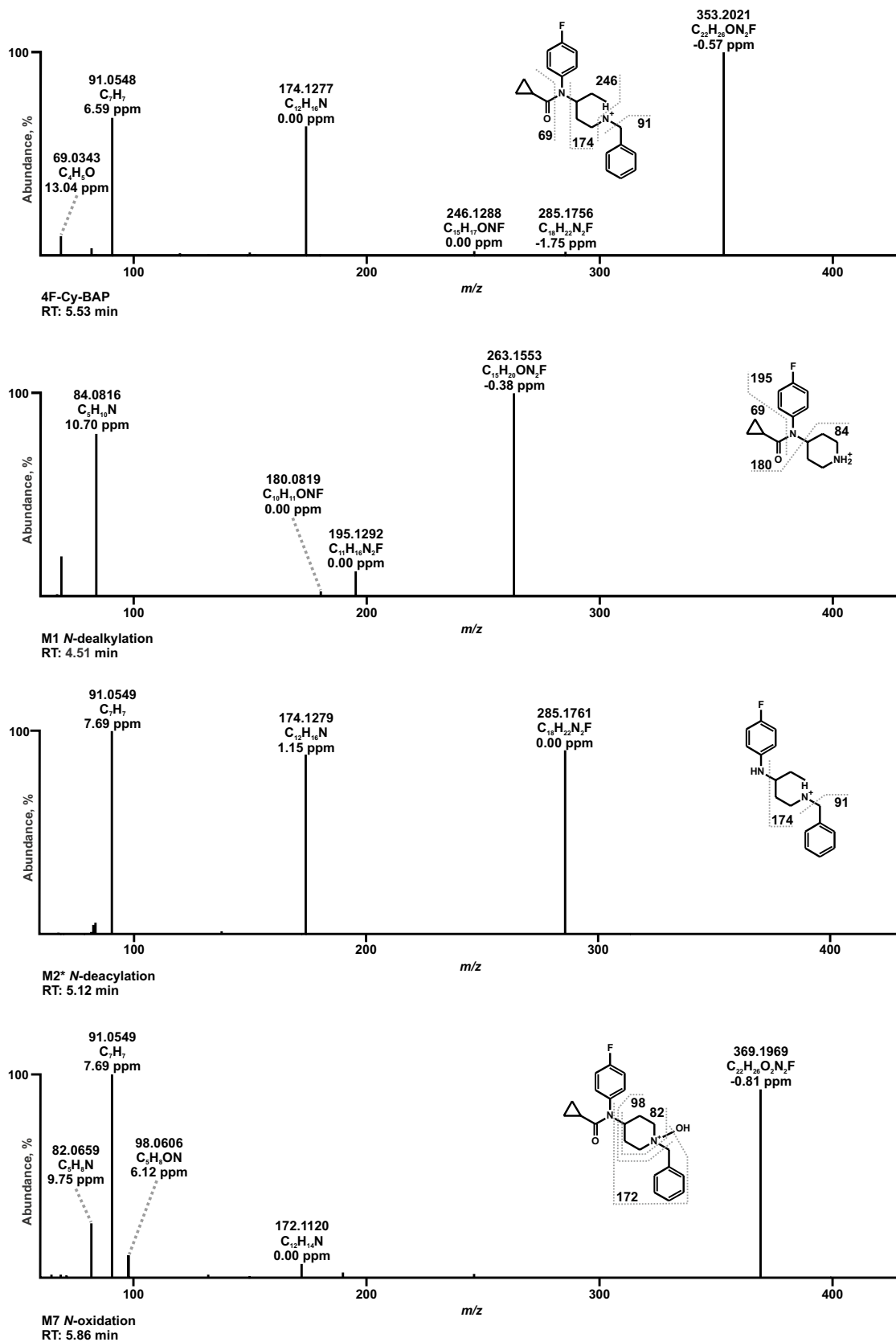


**Fig. 4** MS<sup>2</sup> spectra of 4F-Cy-BAP and its most abundant metabolites identified in all investigated in vitro and in vivo models, sorted by increasing precursor ion masses and retention times (RT). The metabolite marked with an asterisk is considered to be an artifact

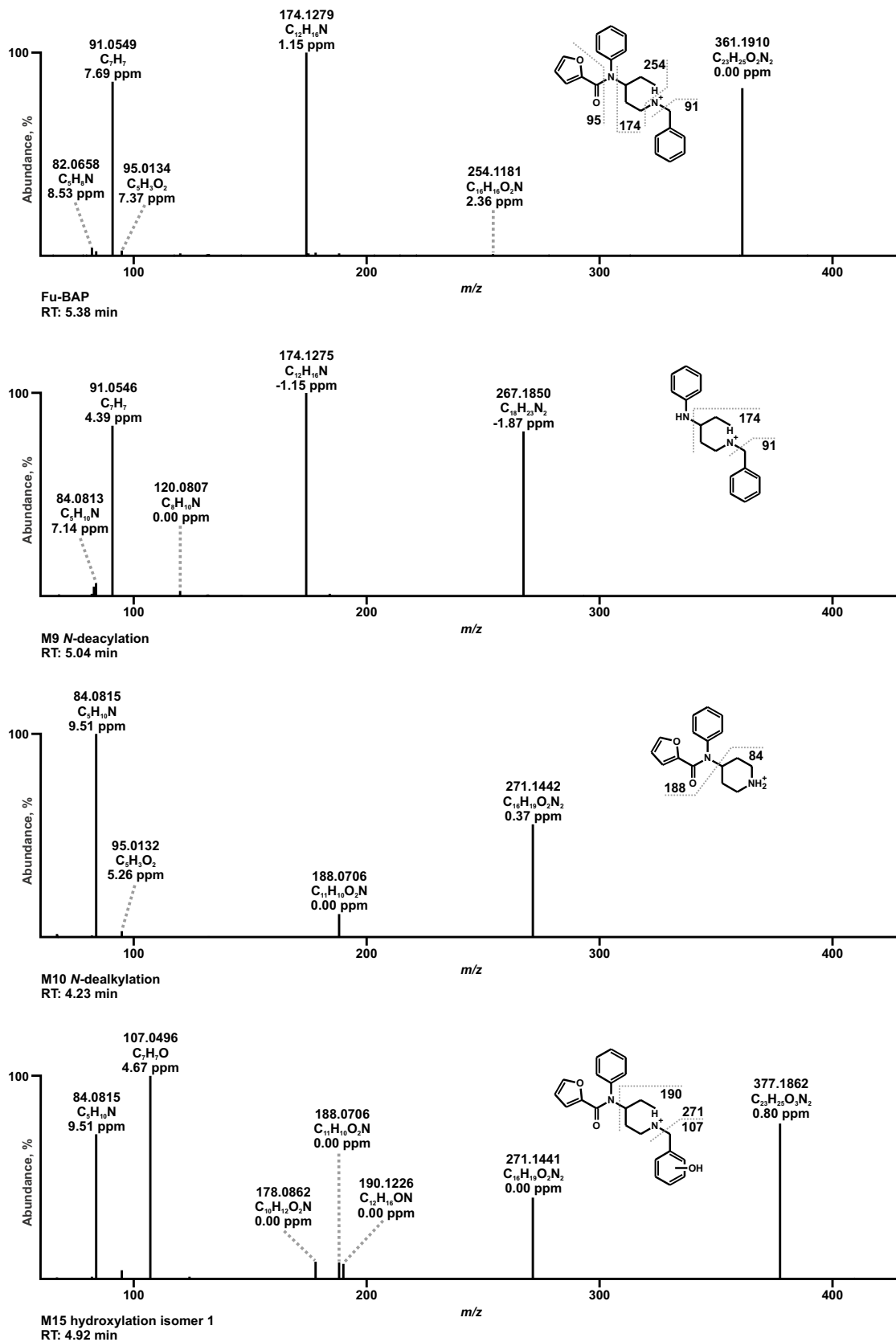


**Fig. 5** MS<sup>2</sup> spectra of Fu-BAP and its most abundant metabolites identified in all investigated in vitro and in vivo models, sorted by increasing precursor ion masses and retention times (RT)

absence of FI at  $m/z$  95.0127, which was assigned to the furanyl part. M21 (PI at  $m/z$  407.1965) occurred through methylation of one hydroxy group at the catechol structure of M19. The pronounced FI at  $m/z$  137.0597 corresponded to FI at  $m/z$  107.0491, which was altered by one additional methoxy group. The dihydroxy-5-oxopent-3-enoic acid metabolite M22 (PI at  $m/z$  411.1914) originated from oxidative furan ring opening, oxidation of the terminal hydroxy group to carboxylic acid, and an additional hydroxylation at the opened side chain as described for the saturated furan ring of a fentanyl analogue (Kanamori et al. 2019). The low abundant FI at  $m/z$  367.2016, which indicated an elimination of carbon dioxide, was used for its characterization. Based on its  $MS^2$  spectrum, the hydroxy group could be attached to position 2 or 3 at the chain, but the exact position was not locatable. M23, M24, and M25 (PI at  $m/z$  411.1914) were three dihydrodiol-hydroxy isomers. In case of M23 and M25 the hydroxy group was determined at the phenyl, which belonged to the benzyl moiety, by means of FI at  $m/z$  107.0491. Although the hydroxy group of M24 was located at the furanyl part, due to the presence of FI at  $m/z$  267.1855, which resulted from the cleavage of the furanyl moiety, the precise structure of the furanyl residue was not determinable. Therefore, the most likely ring-closed structure is given for M24. The phase II metabolite M26 (PI at  $m/z$  473.1376) was formed by sulfation of one hydroxy group of M21. It was specified by the FI at  $m/z$  203.0008, which correlated to the FI at  $m/z$  123.0440, differing in one sulfate group. M27 (PI at  $m/z$  553.2180) was the corresponding phase II metabolite of M15 or M16, which was formed by glucuronidation of the hydroxy group. The prominent FI at  $m/z$  107.0491 was used for identification. In the negative control incubations of all in vitro models and in the zebrafish larvae control media, the *N*-deacyl-metabolites M2 and M9 were also present with similar peak intensities as in the corresponding incubations with enzymes. However, in incubations without  $NADP^+$  solely the peak intensity of M9 increased. Blank incubations confirmed the absence of interfering compounds.

## Isozyme mapping

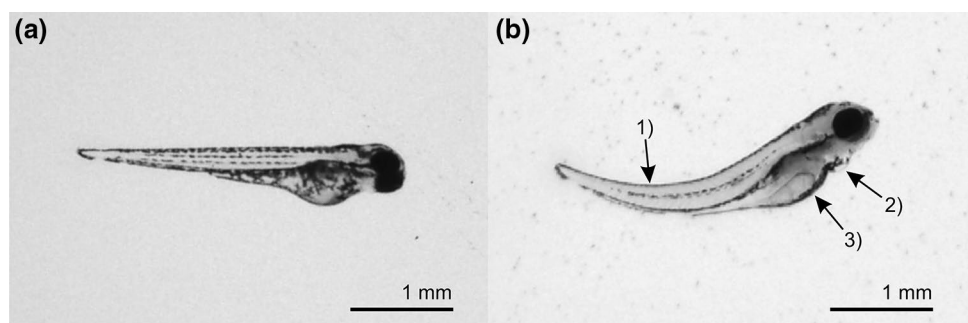
Blank incubations confirmed the absence of interfering compounds. The involvement of single isozymes compared to pHLS9 and pHLM incubations of both compounds is listed in Table S3 in the ESM.

*N*-Dealkyl 4F-Cy-BAP (M1) was present in incubations of CYP1A2, CYP2C19, CYP3A4, and CYP3A5. Furthermore, CYP2C19 catalyzed the formation of the two hydroxy isomers (M5, M6). The former (M5) was also formed by CYP2D6. CYP3A4 and CYP3A5 contributed to the emergence of the *N*-oxide (M7). Equally, several isozymes catalyzed the formation of the *N*-dealkyl Fu-BAP (M10), namely CYP1A2, CYP2C8, CYP2C19, CYP2D6, and CYP3A4. Apart from that, CYP2C8 was only involved in the formation of the *N*-oxide (M17). CYP2C19 contributed to numerous different steps, amongst them the formation of the two hydroxy isomers (M15, M16), the *N*-oxide (M17), and the furan ring opened 2,5-dihydroxypent-2-enal metabolite (M18). CYP2D6 was involved in the formation of the dihydrodiol metabolite (M20), the furan ring opened dihydroxy-5-oxopent-3-enoic acid metabolite (M22), as well as the dihydrodiol-hydroxy metabolite (M24). CYP3A4 was another considerable isozyme, catalyzing, besides M10 the formation of the hydroxy isomer (M15), the *N*-oxide (M17), and the dihydrodiol-hydroxy metabolite (M24).

## MTC studies in zebrafish larvae

Survival rates of the 4 dpf larvae exposed for 24 h to both compounds at concentrations of 0.01, 0.1, 1, 10, 50, and 100  $\mu$ M were 100%. However, after treatment with 100  $\mu$ M Fu-BAP, 80% of the larvae showed malformations and changes in behavior. An influence of DMSO could be excluded by the negative control incubation. Figure 6 shows a larva in control Danieau's medium (a) or treated with 100  $\mu$ M Fu-BAP (b), both containing 1% (*v/v*) DMSO. Visible morphological changes manifested in a spinal curvature (1), abnormal pericardial edema (2), and a dark brown colored yolk sac (3), which has already been described e.g.

**Fig. 6** Microscopic image of two zebrafish larvae (a) in control medium (Danieau's medium) plus 1% DMSO and (b) in Danieau's medium containing 100  $\mu$ M Fu-BAP plus 1% DMSO. Morphological malfunctions were a spinal curvature (1), abnormal pericardial edema (2), and a dark brown colored yolk sac (3)



for environmental toxins (Seok et al. 2008). Furthermore, various larvae were observed, which showed random body vibrations, a fast heartbeat, and slow movements after touching. To prevent toxic effects in subsequent in vivo experiments, the Fu-BAP concentration was reduced to 80  $\mu\text{M}$  for the metabolism study. However, still 20% of the larvae exhibited morphological/behavioral changes after exposure to 80  $\mu\text{M}$  Fu-BAP in the metabolism study.

### Determination of the in vitro activity at MOR

Analysis of the in vitro MOR activation potential of 4F-Cy-BAP and Fu-BAP showed an  $E_{\text{max}}$  of 5.98% and 0.98%, respectively, compared to the reference compound hydromorphone ( $E_{\text{max}}$  of 100%) and fentanyl ( $E_{\text{max}}$  of 180%), as presented in Fig. 7 and also summarized in Table S4 in the ESM along with their  $\text{EC}_{50}$  values.

## Discussion

### In vitro metabolic stability, predicted in vivo clearance, and PPB

Metabolic stability was characterized by  $t_{1/2}$ ,  $\text{CL}_{\text{int}}$ ,  $\text{CL}_{\text{h}}$ , and  $\text{ER}_{\text{h}}$ .  $\text{CL}_{\text{int}}$  differs from  $\text{CL}_{\text{h}}$  in the independence of physiological factors, such as hepatic blood flow and drug binding (Baranczewski et al. 2006). In vitro  $t_{1/2}$  was determined by decreasing 4F-Cy-BAP or Fu-BAP amounts during incubation with pHLS9 from 1 till 90 min. As several incubations were prepared at once, the first samples had to be taken at  $t = 1$  min.  $\text{CL}_{\text{int}}$  of Fu-BAP was rated to be low in accordance to McNaney et al. (2008). No half-life and clearance values of 4F-Cy-BAP could be determined as it demonstrated only weak metabolic degradation.

$\text{CL}_{\text{h}}$  was predicted by parallel tube and well-stirred model. The parallel tube model describes the liver as a set of tubes representing a sinusoid, with the drug concentration exponentially decreasing in the direction of the hepatic

vein (Choi et al. 2019). However, the liver is considered as a single, well-mixed compartment with a fixed drug concentration in the well-stirred model (Segers et al. 2019).  $\text{CL}_{\text{h}}$  values of Fu-BAP were identical in both models by considering  $f_{\text{u}}$ .  $\text{CL}_{\text{h}}$  predictions without  $f_{\text{u}}$  led to much higher values in both models.

$\text{ER}_{\text{h}}$  estimations provide insight into the oral bioavailability of drugs under consideration of  $Q_{\text{h}}$  (Benet and Zia-Amirhosseini 1995). The calculated  $\text{ER}_{\text{h}}$  was based on  $\text{CL}_{\text{h}}$  values without  $f_{\text{u}}$  and it could be classified as intermediate in both models in accordance to Rogge and Taft (2009). As expected, no significant differences between both models were found, because this is rather the case for high  $\text{ER}_{\text{h}}$  drugs (Mehvar 2018).

Based on the free drug theory (Bohnert and Gan 2013), toxicokinetic effects of drugs, e.g. distribution or excretion, depends on their  $f_{\text{u}}$ , which is strongly linked with their PPB. As both compounds showed a high PPB of more than 90%, a simultaneous intake with other drugs of abuse with similar high PPB such as cannabinoids (Mardal et al. 2016) or NBOMes (Richter et al. 2019b) could lead to an accumulation and adverse effects by displacement from the binding site. Moreover, a PPB higher than 70% is expected to have an impact on e.g. the clearance (Lindup and Orme 1981). However, another study indicated that in particular, clearance predictions of basic compounds based on in vitro measurement are more consistent with in vivo data regardless of any drug binding (Obach 1999). In addition, other influencing factors must be considered, e.g. active transport into the hepatocytes or elimination route (Smith et al. 2010).

### Comparison of in vitro and in vivo metabolites

Although in vitro metabolism studies may have some advantages, e.g. cost-effectivity or feasibility, there is often a discrepancy between the metabolites identified in vitro to those in human (Richter et al. 2019a). As no human samples after intake of 4F-Cy-BAP or Fu-BAP were available, an additional in vivo assay should confirm possible main targets

**Fig. 7** Concentration-dependent interaction of  $\mu$ -opioid (MOR) receptor with  $\beta$ -arrestin 2 ( $\beta\text{arr}2$ ) protein upon stimulation with hydromorphone (HM), fentanyl, 4F-Cy-BAP and Fu-BAP in (a) full concentration curves or (b) zoom on lower part of the graph. Data are given as mean receptor activation  $\pm$  SEM ( $n = 3$ ), normalized to the  $E_{\text{max}}$  (maximal activity) of HM ( $= 100\%$ )

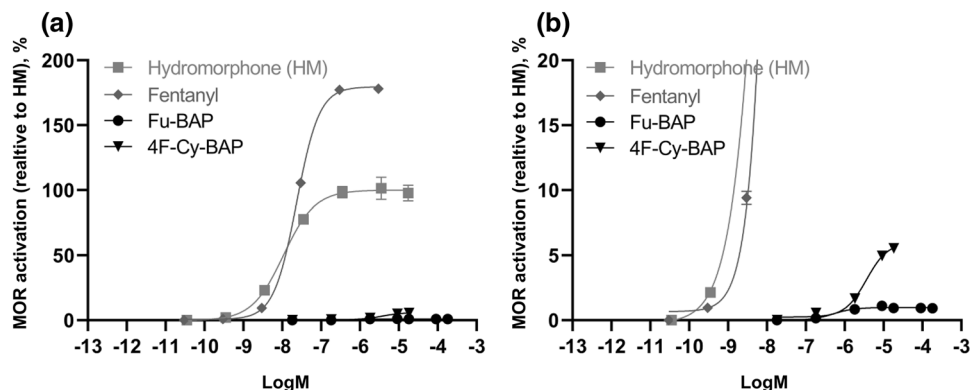


**Table 1** List of 4F-Cy-BAP and Fu-BAP metabolites, respectively detected in zebrafish larvae incubations, pHLS9 or pHLM incubations, which were rated from + to + + + according to their absolute peak areas

Parent compound Metabolite ID	Metabolic reaction	In vivo		In vitro	
		Zebrafish larvae		pHLS9 6 h	pHLM 0.5 h
		Larvae extract 24 h	Medium 24 h		
<b>4F-Cy-BAP</b>					
M1	<i>N</i> -Dealkylation	+++	+	++	++
M2*	<i>N</i> -Deacylation	+++	+++	+	+
M3*	<i>N</i> -Deacylation + hydroxylation	++	+	+	+
M4*	<i>N</i> -Deacylation + <i>N</i> -oxidation	+++	N.D	N.D	N.D
M5	Hydroxylation isomer 1	++	+	N.D	N.D
M6	Hydroxylation isomer 2	N.D	N.D	N.D	N.D
M7	<i>N</i> -Oxidation	+++	N.D	+	++
M8	Hydroxylation + glucuronidation	+	N.D	N.D	–
<b>Fu-BAP</b>					
M9	<i>N</i> -Deacylation	+++	++	++	++
M10	<i>N</i> -Dealkylation	+++	+	++	++
M11	<i>N</i> -Deacylation + hydroxylation isomer 1	+	N.D	++	++
M12	<i>N</i> -Deacylation + hydroxylation isomer 2	++	N.D	+	+
M13	<i>N</i> -Dealkylation + epoxidation + hydrolyze (dihydrodiol)	+	N.D	N.D	N.D
M14	<i>N</i> -Deacylation + hydroxylation + sulfation	++	N.D	N.D	–
M15	Hydroxylation isomer 1	+++	+	+	+
M16	Hydroxylation isomer 2	N.D	N.D	N.D	N.D
M17	<i>N</i> -Oxidation	+++	N.D	+	++
M18	Oxidation (furan ring open)	+++	+	N.D	+
M19*	Dihydroxylation	+	N.D	N.D	N.D
M20	Epoxidation + hydrolyze (dihydrodiol)	++	N.D	++	+
M21	Dihydroxylation + methylation	++	N.D	N.D	–
M22	Oxidation (furan ring open, carboxylic acid) + hydroxylation	N.D	N.D	N.D	N.D
M23	Epoxidation + hydrolyze + hydroxylation isomer 1	+	N.D	N.D	N.D
M24	Epoxidation + hydrolyze + hydroxylation isomer 2	N.D	N.D	N.D	N.D
M25	Epoxidation + hydrolyze + hydroxylation isomer 3	+	N.D	N.D	N.D
M26	Dihydroxylation + sulfation	+	N.D	N.D	–
M27	Hydroxylation + glucuronidation	++	N.D	N.D	–

Metabolite IDs correspond to Table S2 in the ESM

*N.D.* not detected

\*Considered to be artifacts, — formation with the given incubation conditions not possible

for toxicological screenings. Comparison of the identified in vitro and in vivo metabolites in all investigated models of 4F-Cy-BAP and Fu-BAP are summarized in Table 1. The largest number of 4F-Cy-BAP and Fu-BAP metabolites (7 and 16, respectively) were identified in the zebrafish larvae extracts. These metabolites included all metabolites previously detected in the pHLS9 and pHLM incubations as well as in the zebrafish larvae media plus two novel 4F-Cy-BAP and eight Fu-BAP metabolites. However, all phase II metabolites were exclusively identified in zebrafish larvae extracts. This finding is due to the missing cofactors for the phase II enzymes in the pHLM incubations. In the case of pHLS9

incubations, the lower substrate concentration and shorter incubation time compared to the zebrafish larvae experiments are expected to be the main causes.

As shown in Fig. 8, the in vitro formation of the *N*-deacyl-metabolite of 4F-Cy-BAP (M2) had its peak already within the first minute of incubation and declined afterwards most likely due to further biotransformation to M3. However, its formation was also observed in stock solutions after long-term storage and negative control incubations and thus, it may be also of artificial nature. Its subsequent metabolites (M3, M4) were also marked to be possible artifacts e.g. in Table 1. Similar findings were observed for Fu-BAP.

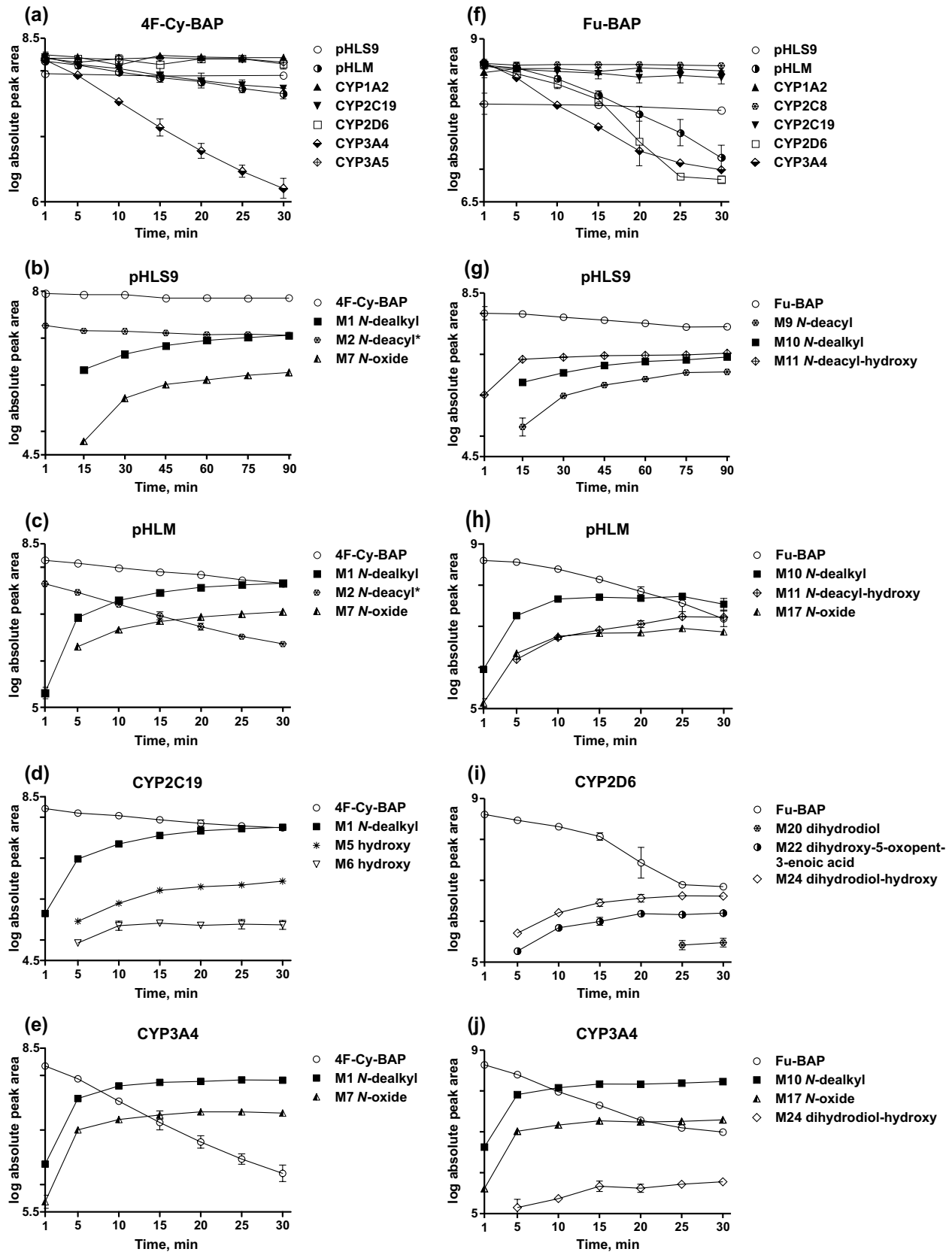


**Fig. 8** Changes of the amount of parent compounds in pHLS9, pHLM, and isozyme incubations (a) 4F-Cy-BAP and (f) Fu-BAP are presented as changes in the logarithm of the absolute peak areas as a function of time (min). The formation rates of the three most abundant metabolites are depicted in comparison to the changes of the logarithmic absolute peak areas of parent compounds (4F-Cy-BAP, b–e) and (Fu-BAP, g–j) in pHLS9 b, g, pHLM c, h, CYP2C19 d, CYP2D6 i or CYP3A4 e, j. The metabolite marked with an asterisk is considered to be an artifact. If data points are missing, no signal was detected

However, based on an increasing peak intensity of M9 in absence of NADP<sup>+</sup>, M9 and all metabolites derived thereof were presented as metabolites. Some metabolites (M6, M16, M22, M24) were solely detected in single isozyme incubations and therefore considered as minor metabolites. Moreover, it can be assumed that the origin of the Fu-BAP metabolite M19 was artificial because the retention time correlated with that of M26. Nevertheless, M19 was obliged to be a precursor of the phase II metabolites M21 and M26, but most probably with another RT. Suitable analytical targets for toxicological urine screenings should be the *N*-dealkyl metabolites (M1, M10) and the *N*-deacyl metabolites (M2, M9) of both compounds, and additionally 4F-Cy-BAP *N*-oxide (M7), as well as hydroxy Fu-BAP (M15).

### Involvement of CYP2D6, CYP3A4, and other isozymes in phase I steps

Isozyme mapping is essential for the prediction of possible interactions, e.g. drug-drug interactions, or interindividual variations by different expressions of isozymes. Figure 8 summarizes the change in the amount of each parent compound in the incubations of pHLS9, pHLM, and in incubations of all involved isozymes. The formation rates of the three most abundant metabolites and the change in amount of each parent compound in pHLS9, pHLM, CYP2C19 or CYP2D6, and CYP3A4 incubations are also given in Fig. 8. In particular, 4F-Cy-BAP was mainly metabolized by CYP3A4, which may result in increased drug levels and intoxications after co-consumption of CYP3A4 inhibitors, e.g. tryptamines (Dinger et al. 2016). Due to the additional involvement of CYP2D6 in the Fu-BAP metabolism, inhibition of CYP3A4 is expected to be less substantial if the user is not a CYP2D6 poor metabolizer.

### In vitro MOR receptor activity

The receptor activation was evaluated via the interaction between  $\beta$ arr2, a cytosolic protein, and the G-protein coupled MOR. Both  $\beta$ arr2 and MOR are fused to an inactive part of nanoluciferase. When MOR is activated by a ligand,  $\beta$ arr2 is recruited to the receptor, allowing interaction of

the complementary nanoluciferase subunits, yielding a functional enzyme that generates a bioluminescent signal in the presence of the substrate furimazine (Cannaert et al. 2019). In vitro MOR activity analysis of 4F-Cy-BAP and Fu-BAP revealed that these compounds were only able to activate MOR to a limited extent. Also the EC<sub>50</sub> values of both compounds were strongly reduced compared to hydromorphone and fentanyl.

These findings are not surprising as in vivo studies in mice and rat showed that the replacement of the *N*-phenethyl group with a *N*-benzyl group resulted in a strong reduction in anti-nociceptive activity (Casy et al. 1969; Casy and Huckstep 1988). Moreover, the *N*-benzyl analog of fentanyl (benzylfentanyl) was originally listed in the US as a Scheduled I controlled substance, but was removed from the list as the Drug Enforcement Administration (DEA) indicated that this compound was inactive at MOR (DEA and DoJ 2010), in line with our unpublished findings.

## Conclusion

The current study focused on the toxicokinetic and toxicodynamic properties of the fentanyl homologs 4F-Cy-BAP and Fu-BAP. As 4F-Cy-BAP was metabolically much more stable with an in vitro  $t_{1/2}$  greater than 90 min, no clearances and ER<sub>h</sub> were calculated. Predicted CL<sub>int</sub> and ER<sub>h</sub> values of Fu-BAP were classified as low and intermediate, respectively. The higher in vitro metabolic stability of 4F-Cy-BAP was confirmed by a smaller number of metabolites formed in vitro and in vivo in comparison to Fu-BAP. Overall, seven phase I and one phase II metabolites of 4F-Cy-BAP and 15 phase I and four phase II metabolites for Fu-BAP were identified, with the majority detected in zebrafish larvae. In particular, *N*-dealkylation, hydroxylation, *N*-oxidation, and *N*-deacylation were the main metabolic reactions. Therefore, these metabolites should be considered as useful targets for toxicological urine screenings. CYP3A4 and, in the case of Fu-BAP, additionally CYP2D6, were the two isozymes mainly involved in their in vitro phase I metabolism. Based on these findings, drug-drug interactions leading to CYP3A4 inhibition may cause an accumulation especially of 4F-Cy-BAP. CYP2D6 poor metabolizers could be equally affected by drug-drug interactions after intake of Fu-BAP. A simultaneous intake together with high protein bound drugs could lead to adverse reactions by displacement from the binding site. Treatment of larvae with Fu-BAP revealed malformations and changes in behavior. Only a weak activity at MOR ( $E_{max}$  values of 5.98% and 0.98% compared to HM, respectively) could be observed in vitro but strong agonism or antagonism at other

receptors such as the sigma1, sigma2 or acetylcholine M2 and M3 receptors cannot be excluded and should be investigated.

**Acknowledgements** Open Access funding provided by Projekt DEAL. The authors would like to thank Cathy M. Jacobs, Gabriele Ulrich, Armin A. Weber and the EU funded project ADEBAR (IZ25-5793-2016-27) for their support. A. Cannært and C. Stove acknowledge funding from the Research Foundation-Flanders (FWO; 12Y9520N) and the Ghent University—Special Research Fund (grants no. 01N00814 and 01J15517).

## Compliance with ethical standards

**Conflict of interest** The authors declare that they have no conflict of interest.

**Open Access** This article is licensed under a Creative Commons Attribution 4.0 International License, which permits use, sharing, adaptation, distribution and reproduction in any medium or format, as long as you give appropriate credit to the original author(s) and the source, provide a link to the Creative Commons licence, and indicate if changes were made. The images or other third party material in this article are included in the article's Creative Commons licence, unless indicated otherwise in a credit line to the material. If material is not included in the article's Creative Commons licence and your intended use is not permitted by statutory regulation or exceeds the permitted use, you will need to obtain permission directly from the copyright holder. To view a copy of this licence, visit <http://creativecommons.org/licenses/by/4.0/>.

## References

- Baranczewski P, Stanczak A, Sundberg K et al (2006) Introduction to in vitro estimation of metabolic stability and drug interactions of new chemical entities in drug discovery and development. *Pharmacol Rep* 58(4):453–472
- Baumann MH, Majumdar S, Le Rouzic V et al (2018) Pharmacological characterization of novel synthetic opioids (NSO) found in the recreational drug marketplace. *Neuropharmacology* 134(Pt A):101–107. <https://doi.org/10.1016/j.neuropharm.2017.08.016>
- Beardsley PM, Zhang Y (2018) Synthetic opioids. *Handb Exp Pharmacol* 252:353–381. [https://doi.org/10.1007/164\\_2018\\_149](https://doi.org/10.1007/164_2018_149)
- Benet LZ, Zia-Amirhosseini P (1995) Basic principles of pharmacokinetics. *Toxicol Pathol* 23(2):115–123. <https://doi.org/10.1177/019262339502300203>
- Bohnert T, Gan LS (2013) Plasma protein binding: from discovery to development. *J Pharm Sci* 102(9):2953–2994. <https://doi.org/10.1002/jps.23614>
- Boxenbaum H (1980) Interspecies variation in liver weight, hepatic blood flow, and antipyrine intrinsic clearance: extrapolation of data to benzodiazepines and phenytoin. *J Pharmacokinet Biopharm* 8(2):165–176
- Cannaert A, Deventer M, Fogarty M, Mohr ALA, Stove CP (2019) Hide and seek: overcoming the masking effect of opioid antagonists in activity-based screening tests. *Clin Chem* 65(12):1604–1605. <https://doi.org/10.1373/clinchem.2019.309443>
- Cannaert A, Franz F, Auwarter V, Stove CP (2017) Activity-based detection of consumption of synthetic cannabinoids in authentic urine samples using a stable cannabinoid reporter system. *Anal Chem* 89(17):9527–9536. <https://doi.org/10.1021/acs.analchem.7b02552>
- Cannaert A, Vasudevan L, Friscia M, Mohr ALA, Wille SMR, Stove CP (2018) Activity-based concept to screen biological matrices for opiates and (synthetic) opioids. *Clin Chem* 64(8):1221–1229. <https://doi.org/10.1373/clinchem.2018.289496>
- Casy AF, Hassan MM, Simmonds AB, Staniforth D (1969) Structure-activity relations in analgesics based on 4-anilinopiperidine. *J Pharm Pharmacol* 21(7):434–440. <https://doi.org/10.1111/j.2042-7158.1969.tb08284.x>
- Casy AF, Huckstep MR (1988) Structure-activity studies of fentanyl. *J Pharm Pharmacol* 40(9):605–608. <https://doi.org/10.1111/j.2042-7158.1988.tb05318.x>
- Chauret N, Gauthier A, Nicoll-Griffith DA (1998) Effect of common organic solvents on in vitro cytochrome P450-mediated metabolic activities in human liver microsomes. *Drug Metab Dispos* 26(1):1–4
- Choi GW, Lee YB, Cho HY (2019) Interpretation of non-clinical data for prediction of human pharmacokinetic parameters: in vitro-in vivo extrapolation and allometric scaling. *Pharmaceutics*. <https://doi.org/10.3390/pharmaceutics11040168>
- Davies B, Morris T (1993) Physiological parameters in laboratory animals and humans. *Pharm Res* 10(7):1093–1095
- DEA, DoJ (2010) Correction of code of federal regulations: removal of temporary listing of benzylfentanyl and thenylfentanyl as controlled substances. In: [https://www.deadiversion.usdoj.gov/fed\\_regs/rules/2010/fr06292.htm](https://www.deadiversion.usdoj.gov/fed_regs/rules/2010/fr06292.htm). Accessed 29 June 2010
- Dinger J, Woods C, Brandt SD, Meyer MR, Maurer HH (2016) Cytochrome P450 inhibition potential of new psychoactive substances of the tryptamine class. *Toxicol Lett* 241:82–94. <https://doi.org/10.1016/j.toxlet.2015.11.013>
- Diouf O, Gadeau S, Chelle F et al (2002) A new series of M3 muscarinic antagonists based on the 4-amino-piperidine scaffold. *Bioorg Med Chem Lett* 12(18):2535–2539. [https://doi.org/10.1016/s0960-894x\(02\)00487-0](https://doi.org/10.1016/s0960-894x(02)00487-0)
- EMCDDA (2017) Report on the risk assessment of *N*-phenyl-*N*-[1-(2-phenylethyl)piperidin-4-yl]furan-2-carboxamide (furanlylfentanyl) in the framework of the council decision on new psychoactive substances. In: publications office of the european union. [https://www.emcdda.europa.eu/system/files/publications/6712/20176480\\_TDAK17002ENN\\_PDF.pdf](https://www.emcdda.europa.eu/system/files/publications/6712/20176480_TDAK17002ENN_PDF.pdf). Accessed Dec 2017
- EMCDDA (2018) EU Early Warning System Formal Notification—Furanlylfentanyl.
- Evans-Brown M, Sedefov R (2018) Responding to new psychoactive substances in the European union: early warning, risk assessment, and control measures. *Handb Exp Pharmacol* 252:3–49. [https://doi.org/10.1007/164\\_2018\\_160](https://doi.org/10.1007/164_2018_160)
- Fagiola M, Hahn T, Avella J (2018) Five Postmortem case reports with qualitative analysis of cyclopropylfentanyl by LC–MS–MS. *J Anal Toxicol*. <https://doi.org/10.1093/jat/bky094>
- Fung EN, Chen YH, Lau YY (2003) Semi-automatic high-throughput determination of plasma protein binding using a 96-well plate filtrate assembly and fast liquid chromatography-tandem mass spectrometry. *J Chromatogr B Analyt Technol Biomed Life Sci* 795(2):187–194
- Gampfer TM, Richter LHJ, Schaper J, Wagmann L, Meyer MR (2019) Toxicokinetics and analytical toxicology of the abused opioid U-48800 - in vitro metabolism, metabolic stability, isozyme mapping, and plasma protein binding. *Drug Test Anal*. <https://doi.org/10.1002/dta.2683>
- Guerrieri D, Rapp E, Roman M, Druid H, Kronstrand R (2017) Postmortem and toxicological findings in a series of furanyl-fentanyl-related deaths. *J Anal Toxicol* 41(3):242–249. <https://doi.org/10.1093/jat/bkw129>
- Helander A, Backberg M, Signell P, Beck O (2017) Intoxications involving acrylfentanyl and other novel designer fentanyls—results from the Swedish STRIDA project. *Clin Toxicol (Phila)* 55(6):589–599. <https://doi.org/10.1080/15563650.2017.1303141>

- Helfer AG, Michely JA, Weber AA, Meyer MR, Maurer HH (2015) Orbitrap technology for comprehensive metabolite-based liquid chromatographic-high resolution-tandem mass spectrometric urine drug screening—exemplified for cardiovascular drugs. *Anal Chim Acta* 891:221–233. <https://doi.org/10.1016/j.aca.2015.08.018>
- Houston JB, Galetin A (2008) Methods for predicting in vivo pharmacokinetics using data from in vitro assays. *Curr Drug Metab* 9(9):940–951
- Huang Y, Hammond PS, Wu L, Mach RH (2001) Synthesis and structure-activity relationships of *N*-(1-benzylpiperidin-4-yl)arylacetamide analogues as potent sigma1 receptor ligands. *J Med Chem* 44(25):4404–4415. <https://doi.org/10.1021/jm010384j>
- Kanamori T, Segawa H, Yamamuro T, Kuwayama K, Tsujikawa K, Iwata YT (2019) Metabolism of a new synthetic opioid tetrahydrofuranyl fentanyl in fresh isolated human hepatocytes: detection and confirmation of ring-opened metabolites. *Drug Test Anal.* <https://doi.org/10.1002/dta.2743>
- Krotulski AJ, Papsun DM, Friscia M, Swartz JL, Holsey BD, Logan BK (2018) Fatality following ingestion of tetrahydrofuranyl fentanyl, U-49900 and methoxy-phencyclidine. *J Anal Toxicol* 42(3):e27–e32. <https://doi.org/10.1093/jat/bkx092>
- Lindup WE, Orme MC (1981) Clinical pharmacology: plasma protein binding of drugs. *Br Med J (Clin Res Ed)* 282(6259):212–214. <https://doi.org/10.1136/bmj.282.6259.212>
- Mardal M, Gracia-Lor E, Leibnitz S, Castiglioni S, Meyer MR (2016) Toxicokinetics of new psychoactive substances: plasma protein binding, metabolic stability, and human phase I metabolism of the synthetic cannabinoid WIN 55,212–2 studied using in vitro tools and LC–HR–MS/MS. *Drug Test Anal* 8(10):1039–1048. <https://doi.org/10.1002/dta.1938>
- McNaney CA, Drexler DM, Hnatyshyn SY et al (2008) An automated liquid chromatography-mass spectrometry process to determine metabolic stability half-life and intrinsic clearance of drug candidates by substrate depletion. *Assay Drug Dev Technol* 6(1):121–129. <https://doi.org/10.1089/adt.2007.103>
- Mehvar R (2018) Clearance concepts: fundamentals and application to pharmacokinetic behavior of drugs. *J Pharm Pharm Sci* 21(1s):88s–102s. <https://doi.org/10.18433/jpps29896>
- Muller D, Neurath H, Neukamm MA et al (2019) New synthetic opioid cyclopropylfentanyl together with other novel synthetic opioids in respiratory insufficient comatose patients detected by toxicological analysis. *Clin Toxicol (Phila)* 57(9):806–812. <https://doi.org/10.1080/15563650.2018.1554187>
- Obach RS (1999) Prediction of human clearance of twenty-nine drugs from hepatic microsomal intrinsic clearance data: an examination of in vitro half-life approach and nonspecific binding to microsomes. *Drug Metab Dispos* 27(11):1350–1359
- Richter LHJ, Herrmann J, Andreas A et al (2019a) Tools for studying the metabolism of new psychoactive substances for toxicological screening purposes - A comparative study using pooled human liver S9, HepaRG cells, and zebrafish larvae. *Toxicol Lett* 305:73–80. <https://doi.org/10.1016/j.toxlet.2019.01.010>
- Richter LHJ, Menges J, Wagmann L et al (2019b) In vitro toxicokinetics and analytical toxicology of three novel NBOME derivatives: phase I and II metabolism, plasma protein binding, and detectability in standard urine screening approaches studied by means of hyphenated mass spectrometry. *Forensic Toxicol* 38(1):141–159. <https://doi.org/10.1007/s11419-019-00498-7>
- Rogge M, Taft DR (2009) *Preclinical Drug Development*. CRC Press
- Segers K, Declerck S, Mangelings D, Heyden YV, Eeckhaut AV (2019) Analytical techniques for metabolomic studies: a review. *Bioanalysis* 11(24):2297–2318. <https://doi.org/10.4155/bio-2019-0014>
- Seok SH, Baek MW, Lee HY et al (2008) In vivo alternative testing with zebrafish in ecotoxicology. *J Vet Sci* 9(4):351–357. <https://doi.org/10.4142/jvs.2008.9.4.351>
- Sharma KK, Hales TG, Rao VJ, NicDaeid N, McKenzie C (2019) The search for the "next" euphoric non-fentanyl novel synthetic opioids on the illicit drugs market: current status and horizon scanning. *Forensic Toxicol* 37(1):1–16. <https://doi.org/10.1007/s11419-018-0454-5>
- Smith DA, Di L, Kerns EH (2010) The effect of plasma protein binding on in vivo efficacy: misconceptions in drug discovery. *Nat Rev Drug Discov* 9(12):929–939. <https://doi.org/10.1038/nrd3287>
- Solimini R, Pichini S, Pacifici R, Busardo FP, Giorgetti R (2018) Pharmacotoxicology of non-fentanyl derived new synthetic opioids. *Front Pharmacol* 9:654. <https://doi.org/10.3389/fphar.2018.00654>
- Wagmann L, Manier SK, Eckstein N, Maurer HH, Meyer MR (2019) Toxicokinetic studies of the four new psychoactive substances 4-chloroethcathinone, *N*-ethylnorpentylone, *N*-ethylhexedrone, and 4-fluoro-alpha-pyrrolidinohexiophenone. *Forensic Toxicol* 38(1):59–69. <https://doi.org/10.1007/s11419-019-00487-w>
- Wagmann L, Maurer HH (2018) Bioanalytical methods for new psychoactive substances. *Handb Exp Pharmacol* 252:413–439. [https://doi.org/10.1007/164\\_2017\\_83](https://doi.org/10.1007/164_2017_83)
- Wagmann L, Meyer MR, Maurer HH (2016) What is the contribution of human FMO3 in the *N*-oxygenation of selected therapeutic drugs and drugs of abuse? *Toxicol Lett* 258:55–70. <https://doi.org/10.1016/j.toxlet.2016.06.013>
- Westerfield M (2007) *The Zebrafish book a guide for the laboratory use of Zebrafish Danio\* (Brachydanio) Rerio*, 5th edn. University of Oregon Press, Eugene
- Xiong X, Luo S, Wu B, Wang J (2017) Comparative developmental toxicity and stress protein responses of dimethyl sulfoxide to rare minnow and zebrafish embryos/larvae. *Zebrafish* 14(1):60–68. <https://doi.org/10.1089/zeb.2016.1287>

**Publisher's Note** Springer Nature remains neutral with regard to jurisdictional claims in published maps and institutional affiliations.

### **3.4 Cytotoxicity, metabolism, and isozyme mapping of the synthetic cannabinoids JWH-200, A-796260, and 5F-EMB-PINACA studied by means of in vitro systems<sup>66</sup>**

(DOI: 10.1007/s00204-021-03148-3)

**Authors Contributions** Tanja M. Gampfer conducted the experiments, analyzed the data, and wrote the manuscript; Anouar Belkacemi and Veit Flockerzi aided in interpreting the results of the cell culture experiments and supported with scientific discussion; Markus R. Meyer and Lea Wagmann supported with scientific discussions, the design of the experiments, and research supervision.



# Cytotoxicity, metabolism, and isozyme mapping of the synthetic cannabinoids JWH-200, A-796260, and 5F-EMB-PINACA studied by means of in vitro systems

Tanja M. Gampfer<sup>1</sup> · Lea Wagmann<sup>1</sup> · Anouar Belkacemi<sup>2</sup> · Veit Flockerzi<sup>2</sup> · Markus R. Meyer<sup>1</sup>

Received: 5 July 2021 / Accepted: 19 August 2021 / Published online: 28 August 2021  
© The Author(s) 2021

## Abstract

Intake of synthetic cannabinoids (SC), one of the largest classes of new psychoactive substances, was reported to be associated with acute liver damage but information about their hepatotoxic potential is limited. The current study aimed to analyze the hepatotoxicity including the metabolism-related impact of JWH-200, A-796260, and 5F-EMB-PINACA in HepG2 cells allowing a tentative assessment of different SC subclasses. A formerly adopted high-content screening assay (HCSA) was optimized using a fully automated epifluorescence microscope. Metabolism-mediated effects in the HCSA were additionally investigated using the broad CYP inhibitor 1-aminobenzotriazole. Furthermore, phase I metabolites and isozymes involved were identified by in vitro assays and liquid chromatography–high-resolution tandem mass spectrometry. A strong cytotoxic potential was observed for the naphthoylindole SC JWH-200 and the tetramethylcyclopropanoylindole compound A-796260, whereas the indazole carboxamide SC 5F-EMB-PINACA showed moderate effects. Numerous metabolites, which can serve as analytical targets in urine screening procedures, were identified in pooled human liver microsomes. Most abundant metabolites of JWH-200 were formed by *N*-dealkylation, oxidative morpholine cleavage, and oxidative morpholine opening. In case of A-796260, most abundant metabolites included an oxidative morpholine cleavage, oxidative morpholine opening, hydroxylation, and dihydroxylation followed by dehydrogenation. Most abundant 5F-EMB-PINACA metabolites were generated by ester hydrolysis plus additional steps such as oxidative defluorination and hydroxylation. To conclude, the data showed that a hepatotoxicity of the investigated SC cannot be excluded, that metabolism seems to play a minor role in the observed effects, and that the extensive phase I metabolism is mediated by several isozymes making interaction unlikely.

**Keywords** Synthetic cannabinoids · Cytotoxicity · HepG2 · Imaging · Isozyme mapping · Metabolism

## Introduction

The ongoing emergence of new psychoactive substances (NPS) on the drugs of abuse market remains an analytical challenge for clinical and forensic toxicologists. Moreover, numerous case reports of intoxications or even deaths after

intake of synthetic cannabinoids (SC) demonstrate the threat on public health (Adamowicz et al. 2019; Bolt and Hengstler 2021; Hvozdoovich et al. 2020). Some reports associated their intake with liver failure, but knowledge about their hepatotoxic potential is sparse or even unknown (Solimini et al. 2017). Several in vitro strategies to assess the hepatotoxicity have been published using the hepatoma cell lines HepG2 or HepaRG, primary human hepatocytes, or rat hepatocytes (Dias da Silva et al. 2019; Luethi et al. 2017; O'Brien and Edvardsson 2017; Richter et al. 2019a; Roque Bravo et al. 2021). Most of them tested single cytotoxicity biomarkers in individual experiments, e.g., cell viability, collapse of mitochondrial membrane potential, increase of reactive oxygen or nitrogen species, damage on mitochondrial redox activity, leakage of lactate dehydrogenase (LDH) or cell death (Dias da Silva et al. 2019; Luethi et al. 2017; Roque Bravo et al. 2021). To prevent false-negative or -positive outcomes and

✉ Markus R. Meyer  
markus.meyer@uks.eu; m.r.meyer@mx.uni-saarland.de

<sup>1</sup> Department of Experimental and Clinical Toxicology, Institute of Experimental and Clinical Pharmacology and Toxicology, Center for Molecular Signaling (PZMS), Saarland University, 66421 Homburg, Germany

<sup>2</sup> Department of Experimental and Clinical Pharmacology, Institute of Experimental and Clinical Pharmacology and Toxicology, Center for Molecular Signaling (PZMS), Saarland University, 66421 Homburg, Germany

to gain a deeper insight into intracellular processes, it is favorable to monitor multiple parameters at a subcellular level within the same experiment using high-content screening assays (HCSA) (O'Brien and Edvardsson 2017; Richter et al. 2019a). Advantages of HCSA include a high degree of automation, affordability, high sample throughput, analysis of multiple biomarkers during one run, as well as a higher sensitivity compared to the traditional assays (O'Brien and Edvardsson 2017; Richter et al. 2019a). However, the specificity of the HCSA is reduced compared to the “classical” assays (O'Brien and Edvardsson 2017; Richter et al. 2019a). In 2019, Richter et al. adopted a HCSA method to analyze the hepatotoxicity of nine different NPS including synthetic cathinones and the SC 5F-PB-22 in HepG2 cells. 5F-PB-22 was shown to possess the strongest cytotoxic characteristics of all investigated NPS (Richter et al. 2019a).

However, as this HCSA method revealed some shortcomings regarding reproducibility, user friendliness, and sample throughput, the current study aimed to optimize the assay using a fully automated epifluorescence microscope. The optimized HCSA should then be used to study the cytotoxic properties of the SC JWH-200 (1-[2-(4-morpholinyl)ethyl]-3-(1-naphthoyl)-indole), A-796260 ([1-[2-(4-morpholinyl)ethyl]-indol-3-yl]-(2,2,3,3-tetramethylcyclopropyl)-methanone), and 5F-EMB-PINACA (ethyl-2-[[1-(5-fluoropentyl)-indazole-3-carbonyl]amino]-3-methyl-butanoate), which belong to different structural SC subclasses. JWH-200, a naphthoylindole class SC appeared on the market in 2009 (EMCDDA 2009), whereas the tetramethylcyclopropanoylindole compound A-796260 emerged in 2011 (Helander 2017). First reports about the indazole carboxamide type SC 5F-EMB-PINACA can be found in 2016 (DEA 2019). Structural compositions of investigated SC are given in Fig. 1. As not only parent compounds may cause hepatotoxic effects but also their metabolites (Dias da Silva et al. 2019; Roque Bravo et al. 2021), metabolism-based effects were also assessed. Moreover, the phase I metabolism of the SC was investigated, as knowledge about screening targets, crucial in analytical toxicology, is limited. The only exception is JWH-200, which has been investigated by De

Brabanter et al. (2013) in pooled human liver microsomes (pHLM) and in urine of liver-humanized mice identifying 11 metabolites and isomers deduced therefrom. In the current study, also an isozyme mapping together with the identification of in vitro phase I metabolites was performed and analyzed by liquid chromatography–high-resolution tandem mass spectrometry (LC–HRMS/MS) to determine the involvement of single isozymes and initial metabolic steps to predict possible drug interactions.

## Materials and methods

### Chemicals and reagents

JWH-200, A-796260, and 5F-EMB-PINACA were purchased from Cayman Chemical (Ann Arbor, MI, USA) with a purity of 98.3% or higher. 5F-PB-22 was obtained from Lipomed (Weil am Rhein, Germany) and fluvastatin from LGC Standards (Wesel, Germany). 2- to 100-fold-concentrated stock solutions of JWH-200, A-796260, and 5F-EMB-PINACA were prepared in dimethyl sulfoxide (DMSO) and sterile filtered. Sterile stock solutions of Fluvastatin and 5F-PB-22 originated from a previous study (Richter et al. 2019a), which were also prepared 200-fold concentrated in DMSO. Hoechst33342, ionomycin, RPMI 1640 medium supplemented with GlutaMAX, sterile filters suitable for DMSO, and Tetramethylrhodamine, methyl ester (TMRM) were obtained from Life Invitrogen (Darmstadt, Germany). TOTO-3 was supplied by Thermo Fisher Scientific (Schwerte, Germany). HepG2 cells were obtained from the German collection of microorganism and cell cultures (DSMZ, Braunschweig, Germany). 1-Aminobenzotriazole (ABT), dipotassium hydrogen phosphate ( $K_2HPO_4$ ), DMSO, ethylenediaminetetraacetic acid (EDTA), FCCP, isocitrate, isocitrate dehydrogenase, magnesium chloride ( $MgCl_2$ ), penicillin, poly-L-lysine (PLL), potassium dihydrogen phosphate ( $KH_2PO_4$ ), superoxide dismutase, streptomycin, tris hydrochloride, Triton X-100, and trypsin were purchased from Sigma-Aldrich (Taufkirchen, Germany). Calcium chloride ( $CaCl_2$ ) and 4-(2-hydroxyethyl)-1-piperazineethanesulfonic acid (HEPES) were obtained by AppliChem (Darmstadt, Germany). Potassium chloride (KCl) was bought from Grüssing (Filsum, Germany). The 75 cm<sup>2</sup> culture flasks were from Sarstedt (Nümbrecht, Germany). CAL-520 and NADP<sup>+</sup> were obtained from Biomol (Hamburg, Germany). The 96-well half area high-content imaging plates, acetonitrile (LC–MS grade), methanol (LC–MS grade), ammonium formate (analytical grade), formic acid (LC–MS grade), and all other reagents and chemicals (analytical grade) were from VWR International (Darmstadt, Germany). The baculovirus-infected insect cell microsomes (Supersomes) containing human cDNA-expressed flavin-containing monooxygenase

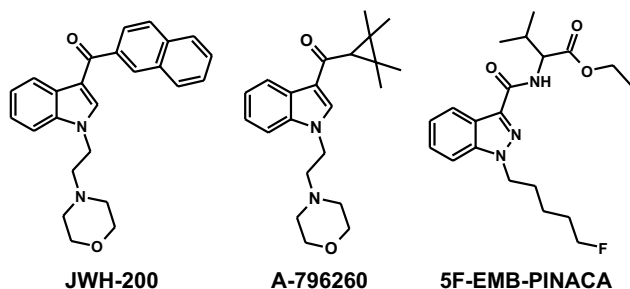


**Fig. 1** Structural composition of the investigated synthetic cannabinoids JWH-200, A-796260, and 5F-EMB-PINACA

3 (FMO3) (5 mg protein/mL), CYP1A2, CYP2A6, CYP2B6, CYP2C8, CYP2C19, CYP2D6, CYP3A4, CYP3A5 (1 nmol/mL), CYP2C9, and CYP2E1 (2 nmol/mL), as well as pHLM (20 mg microsomal protein/mL, 330 pmol total CYP/mg protein, 35 donors) and fetal bovine serum (FBS) were supplied by Corning (Amsterdam, The Netherlands). Enzymes were thawed at 37 °C, aliquoted, snap-frozen in liquid nitrogen, and stored at –80 °C until use.

### Cell culture

As recently described by Richter et al. (2019a), HepG2 cultures were maintained at 37 °C with 95% humidity and 5% CO<sub>2</sub> atmosphere in an incubator (Binder, Tuttlingen, Germany). Cells were handled under sterile conditions using a laminar flow bench class II (Thermo Fisher Scientific, Schwerte, Germany). According to the manufacturer's recommendation, cells were cultivated in RPMI medium with 100 U/mL penicillin, 100 µg/mL streptomycin, and 10% (v/v) FBS (medium plus supplements) as additives within 75 cm<sup>2</sup> culture flasks. PBS solution (137 mM NaCl, 2.7 mM KCl, 1.5 mM KH<sub>2</sub>PO<sub>4</sub>, 8.1 mM Na<sub>2</sub>HPO<sub>4</sub>, pH 7.4) and 0.05% (v/v) trypsin EDTA solution were used to passage cells every 3–4 days. Passage number 5 till 9 were used for all experiments. Single HepG2 stocks were cryopreserved and stored in liquid nitrogen at –160 °C until use.

### Cell plate preparation

According to Richter et al. (2019a) and with minor modifications, 96-well half area high-content imaging plates were coated with PLL by adding 100 µL aqueous PLL solution (100 µg/mL) and incubation for 30 min under laminar air flow at room temperature (21 °C). Thereafter, plates were washed once with 150 µL autoclaved water and twice with 150 µL medium plus supplements. Cells were counted using a hemocytometer (Carl Roth, Karlsruhe, Germany). Afterwards, cells were seeded in a density of 1500 or 1750 cells/well by transferring 100 µL of the cell suspension to the precoated well plates. Cell plates were ready for drug treatment after incubation of 24 h at 37 °C with 95% humidity and 5% CO<sub>2</sub> atmosphere.

### HCSA optimization and quality controls

As positive controls, the following reagents were used: mitochondrial uncoupler FCCP, calcium ionophore ionomycin, and membrane perturbing detergent Triton X-100. Fluvastatin and the SC 5F-PB-22 were used for method optimization and verification. All given concentrations in the following passages are final concentrations. Based on previous results, fluvastatin was incubated in four (0.14, 1.23, 3.7, and 11.1 µM) and 5F-PB-22 in seven concentrations (1.95, 3.91,

7.81, 15.6, 31.3, 62.5, and 125 µM) (Richter et al. 2019a). Before drug treatment, drug dilutions were freshly prepared in tubes using medium plus supplements. Then, 75 µL of the supernatants from the cell plates were removed and 50 µL of the drug solutions were added. Furthermore, each cell plate contained wells without drug but 0.5% (v/v) DMSO in medium plus supplements (blank incubations). Cell plates were incubated for either 48 h or 72 h at 37 °C with 95% humidity and 5% CO<sub>2</sub> atmosphere. Afterwards, supernatants were removed, and cells were loaded with 75 µL of a fluorescence dyes cocktail consisting of 0.8 µM Hoechst33342, 1 µM CAL-520, 20 nM TMRM, and 1 µM TOTO-3 in medium plus supplements. After an incubation for another hour at 37 °C with 95% humidity, 5% CO<sub>2</sub> atmosphere and protected from light, cells were washed three times with 50 µL ringer solution (140 mM NaCl, 2.8 mM KCl, 2 mM MgCl<sub>2</sub>, 1 mM CaCl<sub>2</sub>, 10 mM HEPES, pH 7.4), but the last 50 µL remained on the cells during measurement.

Negative controls were performed as described above by incubating cells in medium plus supplements (untreated), or additional 0.5% (v/v) DMSO. Each positive control was prepared in ringer solution in the following concentrations: FCCP, 100 µM; ionomycin, 10 µM; Triton X-100, 0.05% (v/v). After addition to the cell plate with the last washing step, positive controls remained on the cells during measurement. All incubations were done fivefold.

### Cytotoxicity (pre)screening and CYP inhibition

To assess the cytotoxicity of JWH-200, A-796260, and 5F-EMB-PINACA and potential metabolism-related effects, cell plates were prepared as described above, but incubations were conducted with final drug concentrations of 7.81 and 125 µM with or without 100 µM ABT. The given ABT concentration was based on the CYP inhibition in the HepaRG experiment by Yokoyama et al. (2018). Negative controls without test compound (blank incubations) but with additional ABT were performed to examine if one of the parameters were affected by ABT. If a strong or moderate cytotoxic potential was assigned, the SC was incubated again as defined below at seven concentrations (1.95, 3.91, 7.81, 15.6, 31.3, 62.5, and 125 µM) without ABT. All incubations were done fivefold.

### Microscope settings for HCSA

A Lionheart FX Automated Microscope (BioTek, BT, Bad Friedrichshall, Germany) equipped with an incubation chamber was used for cell plate analysis. During analysis, the incubation conditions were kept constant at 37 °C and lids were left on the cell plates to prevent evaporation. Images were recorded by a 20x/0.45 (semi-apochromat) objective. Hoechst33342 was captured in the first channel

using the autofocus mode followed by all other dyes. Camera settings were as follows: LED value, 1 (Hoechst33342 and CAL-520) and 2 (TMRM and TOTO-3); camera gain, 24 dB; integration time (IT), Hoechst33342, 240 ms; TMRM, 1000–1550 ms; CAL-520, 200–564 ms; TOTO-3, 600–794 ms. Before each measurement, ITs were controlled using blank incubations and if necessary adapted. Each plate was analyzed within 60 min by collecting six images per well in two rows and three columns with a fixed distance in between. BT Gen5 Image Prime 3.09 software was used for data handling including image analysis.

### Image analysis

Prior to analysis, images were manually inspected for quality issues such as blurriness or artifacts by the nuclei fluorescence of Hoechst33342 and if necessary excluded. Number and area of regions identified by Hoechst33342, and its total fluorescence intensity were used to determine the cell count as measure for cell proliferation, nuclear size, and nuclear intensity. Mitochondrial membrane potential was determined by the total fluorescence intensity of TMRM, the fluorogenic calcium-sensitive dye CAL-520 intensity was used to identify cytosolic calcium levels. TOTO-3, which only binds to cellular DNA when the integrity of the plasma membrane is disrupted, was used to monitor plasma membrane integrity. For data normalization, an average value was calculated for each parameter per well using the total number of images after image inspection. Thereafter, each parameter except of the cell count was normalized to the cell count.

### Statistical analysis

Data of image analysis were exported to Microsoft Excel 2016 (Microsoft Corporation, WA, USA) to normalize the cell count to the number of appropriate images per well. A comparison between two different treatment groups was done using a two-tailed student's test considering *P* values < 0.05 as statically significant (95% confidence interval). If more than two different treatment groups were compared to each other one-way ANOVA followed by either Dunnett's or Tukey's post hoc test was applied with a significance level of 0.05 (95% confidence interval). A Dunnett's test was done to compare control data to all other experiment data, while a Tukey's test compared all data with each other. Statistical analysis and *P* values were obtained by GraphPad Prism 5.00 (GraphPad Software, San Diego, CA, USA).

### Assessment of cytotoxic potential by prescreening

Assessment criteria for cytotoxicity were based on the study by Richter et al. (2019a) using adjusted concentrations as follows: a strong cytotoxic potential was defined when at

least two parameters were significantly impaired at a low concentration (7.81  $\mu\text{M}$ ). A moderate cytotoxic potential was defined when two parameters were significantly affected and one of these at a concentration of 7.81  $\mu\text{M}$ . Both ratings were considered as a positive result. A negative result was defined when parameters were only significantly influenced at a high concentration (125  $\mu\text{M}$ ).

### Isozyme mapping and in vitro phase I metabolism

Incubation conditions followed an established protocol (Wagmann et al. 2016). Details are outlined in the Electronic Supplementary Material (ESM).

### LC–HRMS/MS apparatus for identification of metabolites

Analysis was performed according to a previously published study (Gampfer et al. 2019) and further details can be found in the ESM.

## Results

### Method optimization

Quality control incubations were performed to exclude any effects derived from 0.5% DMSO on the tested parameters and to check the maximal or minimal fluorescence response of each dye. As positive controls, FCCP a protonophore and mitochondrial uncoupler, ionomycin a calcium ionophore, and Triton X-100 a membrane perturbing detergent were used. Figure 2a shows images of HepG2 cells stained with Hoechst33342, TMRM, CAL-520, and TOTO-3 and Fig. 2b measured effects on the six different parameters after incubation of untreated cells, treated with 0.5% DMSO or with a corresponding positive control. Comparisons between untreated cells and cells treated with 0.5% DMSO showed no statistically significant differences in all six investigated parameters, whereas cells treated with one of the positive controls showed significant differences compared to untreated cells. As expected, a decreasing fluorescence intensity of TMRM was observed in incubations with FCCP and an increasing fluorescence intensity of CAL-520 and TOTO-3 in incubations with ionomycin and Triton X-100, respectively.

Dose–response plots of the six parameters after incubation with fluvastatin (a) and 5F-PB-22 (b) are shown in Fig. S1 in the ESM. As expected, fluvastatin significantly decreased the cell count from a concentration of 1.23  $\mu\text{M}$  in comparison to blank incubations. Although no significance could be stated for the other five parameters, a general trend is apparent except for the plasma membrane integrity. Thus,

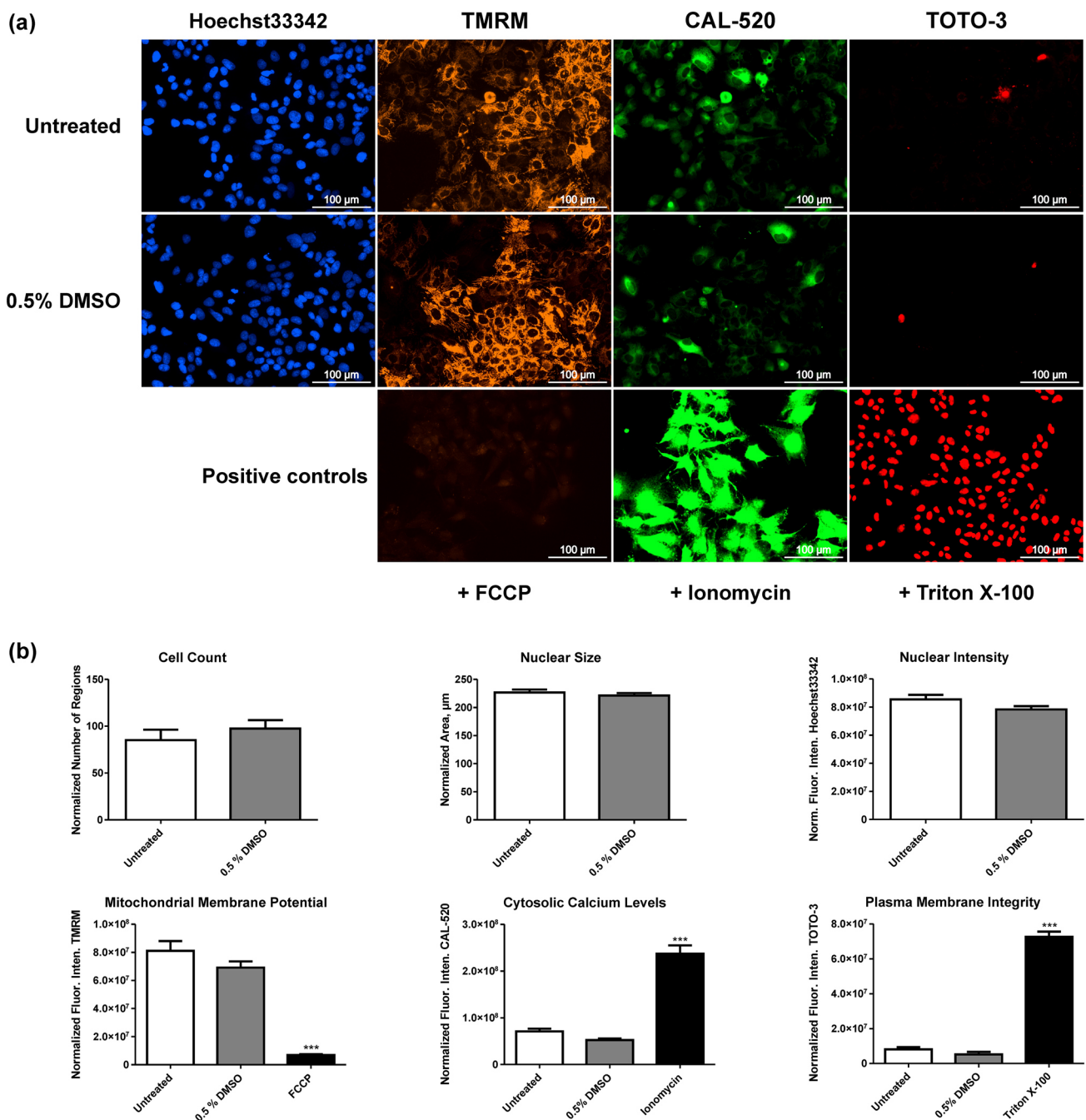


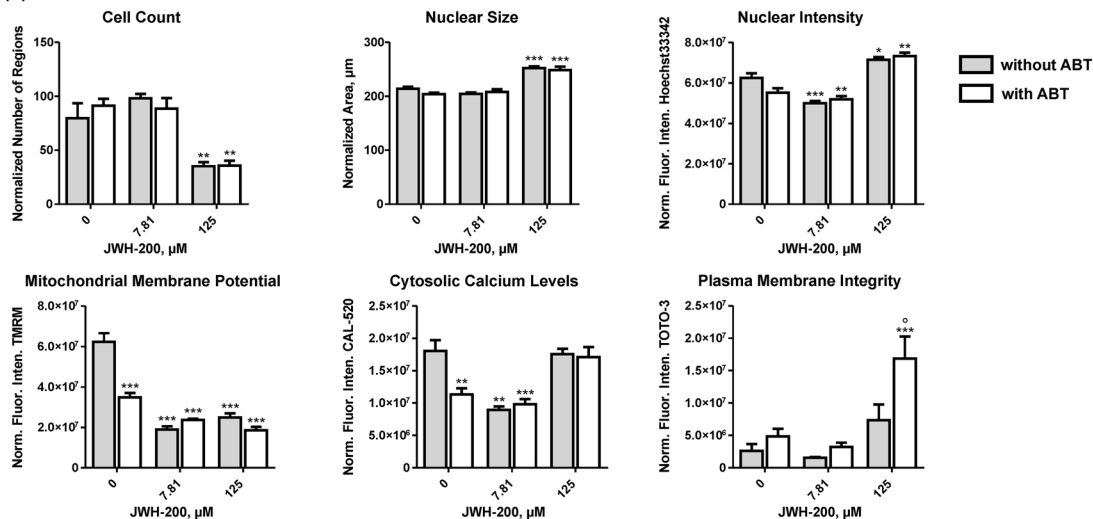
**Fig. 2** Fluorescence microscopic images of cells incubated with Hoechst33342, TMRM, CAL-520, and TOTO-3 (a) and measured effects on the six parameters (cell count, nuclear size, nuclear intensity, mitochondrial membrane potential, cytosolic calcium levels, and plasma membrane integrity) (b) obtained by incubation of cells without treatment, with 0.5% DMSO, and the corresponding positive control (FCCP, ionomycin, or Triton X-100). All parameters were

normalized to the cell count except for the cell count, which was normalized to the number of appropriate images. Values are expressed as mean  $\pm$  standard error of the mean (SEM;  $n=5$ ). Statistical analysis was done using either a *t*-test or one-way ANOVA followed by Dunnett's post hoc test (\*\*\*,  $P < 0.001$  compared to untreated cells). Norm. Fluor. Inten., normalized fluorescence intensity

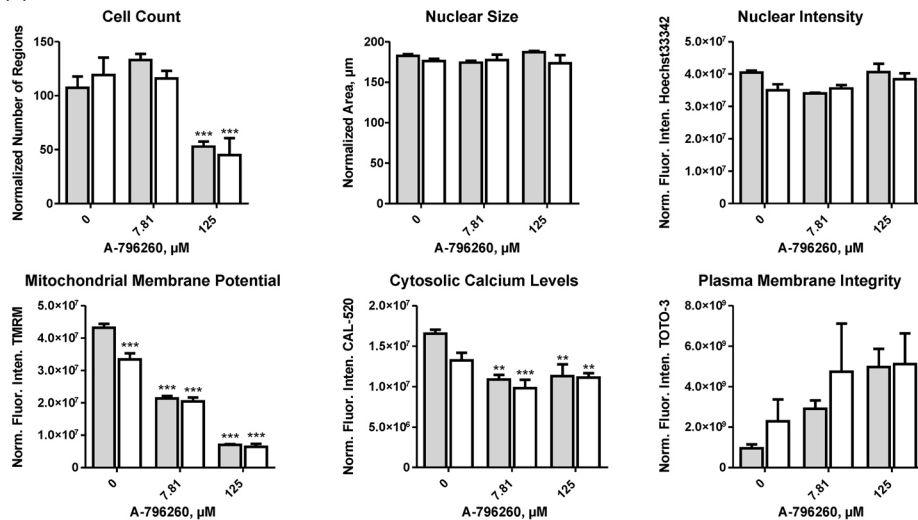
changes manifest in a decrease of the nuclear size, a hyperpolarization of the mitochondrial membrane, and an increase

of the nuclear intensity by chromatin condensation and a rise of intracellular calcium levels.

**(a) JWH-200**



**(b) A-796260**



**(c) 5F-EMB-PINACA**

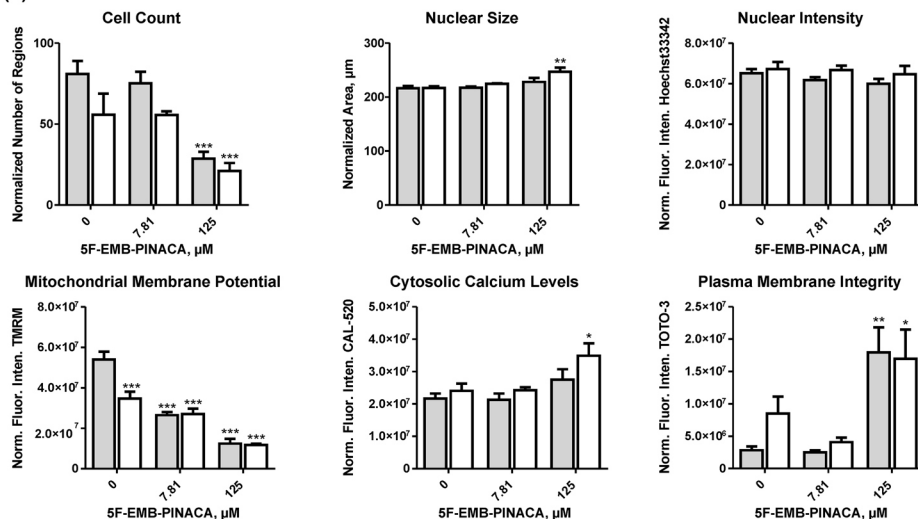


**Fig. 3** Dose–response plots of JWH-200 (a), A-796260 (b), and 5F-EMB-PINACA (c) obtained by incubation at two different concentrations (7.81 and 125  $\mu\text{M}$ ) and blank incubations without test compound with and without the cytochrome P450-inhibitor 1-aminobenzotriazole (ABT), respectively. Changes of different parameters (cell count, nuclear size, nuclear intensity, mitochondrial membrane potential, cytosolic calcium levels, and plasma membrane integrity) are plotted in relation to blank incubations (100%). All parameters were normalized to the cell count except the cell count, which was normalized to the number of appropriate images. Values are expressed as mean  $\pm$  standard error of the mean (SEM;  $n=5$ ). Statistical analysis was done using one-way ANOVA followed by Tukey's post hoc test ( $***P<0.001$ ,  $**P<0.01$ ,  $*P<0.05$  compared to blank incubation;  $^{\circ}P<0.05$  compared to incubations with identical treatment without ABT). Norm. Fluor. Inten., normalized fluorescence intensity

Referring to 5F-PB-22, significant variations of treated cells were observed by a decrease of the cell count from a concentration of 15.63  $\mu\text{M}$ , the nuclear intensity from 1.95  $\mu\text{M}$ , the mitochondrial membrane potential from 1.95  $\mu\text{M}$  and the cytosolic calcium from 31.25  $\mu\text{M}$  compared to blank incubations, respectively. However, the nuclear size remained unaffected by 5F-PB-22 and although the overall trend of the plasma membrane integrity decreased through increasing TOTO-3 fluorescence the different values were highly variable.

### Cytotoxicity (pre)screening with metabolism-based effects

Results of the cytotoxicity prescreening are presented in Fig. 3a–c, which were determined by incubation of each JWH-200, A-796260, and 5F-EMB-PINACA at concentrations of 7.81  $\mu\text{M}$  and 125  $\mu\text{M}$  with or without the CYP inhibitor ABT. Based on the criteria defined above, a strong cytotoxic potential was assigned for JWH-200 and A-796260, whereas 5F-EMB-PINACA showed only a moderate potential. Incubations with additional ABT showed no significant effects compared to incubations at equal SC concentrations but without ABT except for JWH-200 at 125  $\mu\text{M}$ , which adversely affected the plasma membrane integrity. For negative control incubations containing ABT but no SC, a reduced mitochondrial membrane potential and in case of the negative control of JWH-200 also decreased intracellular calcium levels were observed compared to blank incubations.

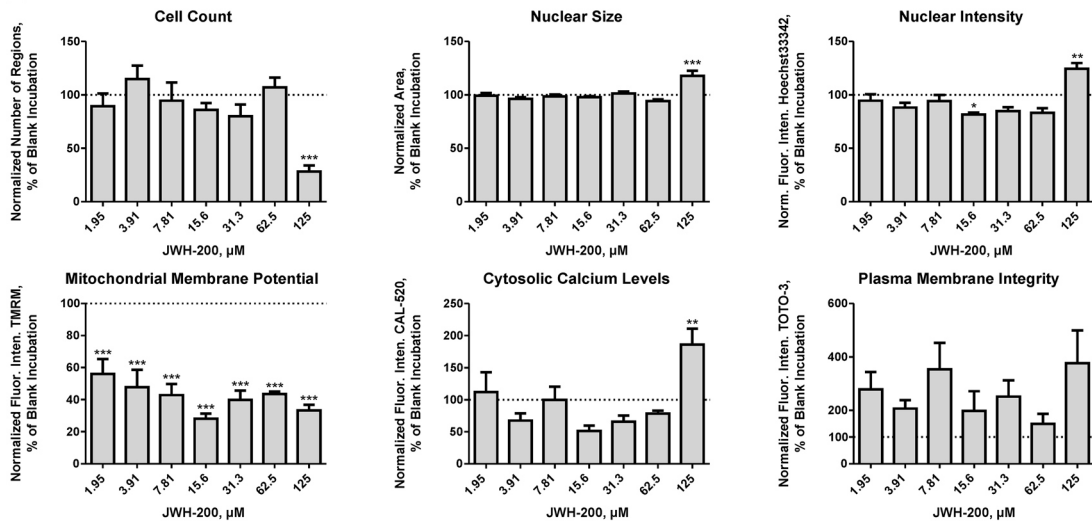
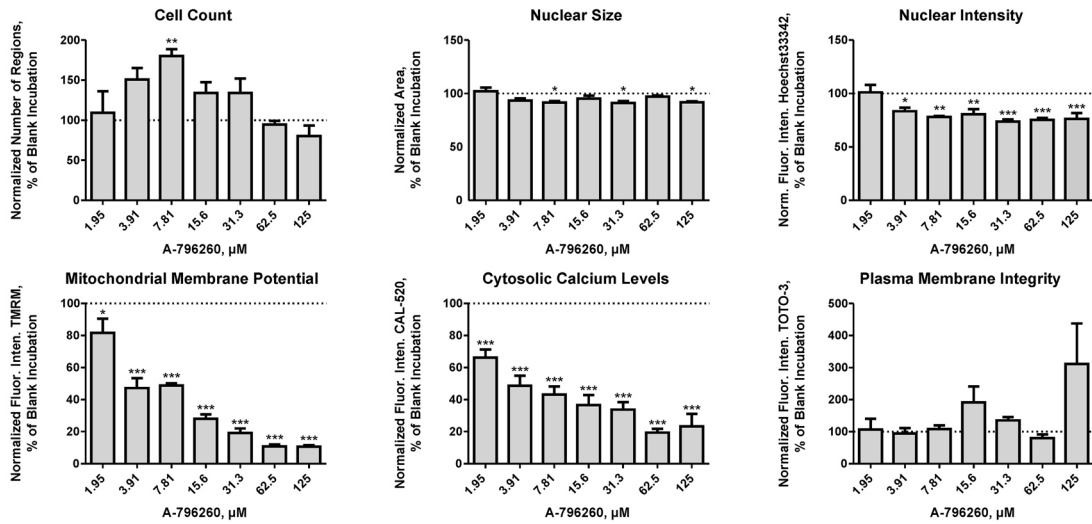
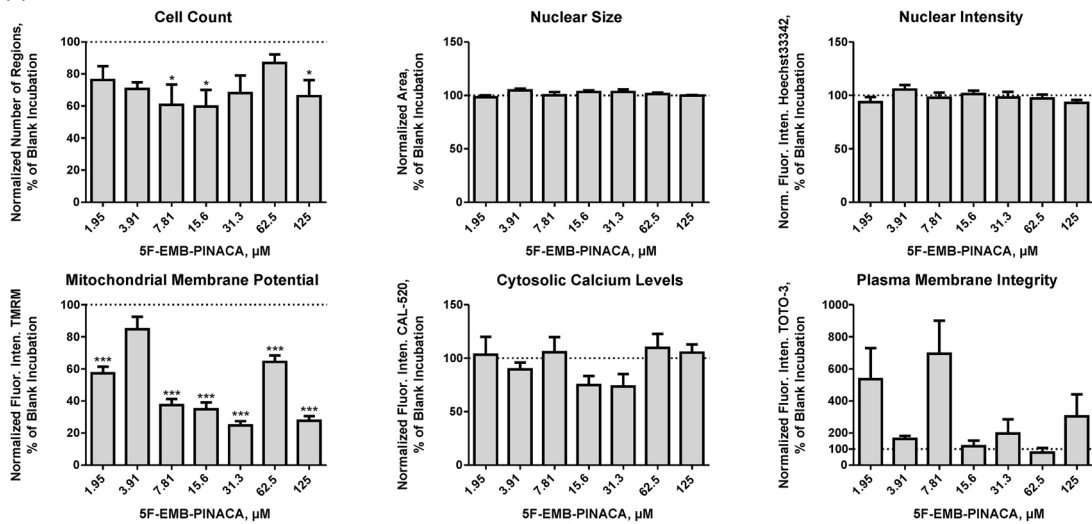
Results of the cytotoxicity screening after incubation of JWH-200 (a), A-796260 (b), and 5F-EMB-PINACA (c) in seven concentrations from 1.95 to 125  $\mu\text{M}$  are given in Fig. 4. JWH-200 significantly reduced the cell count and mitochondrial membrane potential at a concentration of 125 and 1.95  $\mu\text{M}$ , respectively. Furthermore, the nuclear size, nuclear intensity, and intracellular calcium levels increased at 125  $\mu\text{M}$ . Whereas the plasma membrane integrity showed

a high variability with no significant changes. A-796260 significantly impaired the nuclear intensity at 3.91  $\mu\text{M}$  and the mitochondrial membrane potential and cytosolic calcium levels at 1.95  $\mu\text{M}$ , respectively. Initially, the cell count increased at 7.81  $\mu\text{M}$ ; however, afterwards a downward trend was observed. Besides, A-796260 barely affected the nuclear size and the increase of TOTO-3 fluorescence intensity was not significant. In case of 5F-EMB-PINACA, at first the cell count was significantly reduced at 7.81  $\mu\text{M}$ , but then reversed with increasing concentration and declined again at 125  $\mu\text{M}$ . Similar variations were also detected for the mitochondrial membrane potential, which first decreased at 1.95  $\mu\text{M}$  followed by an increase and renewed reduction at 7.81  $\mu\text{M}$ . No significance could be determined for the nuclear size, nuclear intensity, intracellular calcium levels, and plasma membrane integrity after treatment with 5F-EMB-PINACA.

### In vitro phase I metabolites

All detected phase I metabolites of JWH-200, A-796260, and 5F-EMB-PINACA in pHLM or isozyme incubations along with their metabolite identification number, the calculated exact mass of the protonated molecule, elemental composition, retention time, and the three most abundant fragment ions (FIs) recorded in the HRMS<sup>2</sup> mode are given in Table S1–S3 in the ESM, respectively.

All incubations including negative controls of each JWH-200 and A-796260 contained one hydroxy-metabolite (MA21 and MB17) with similar signal intensities, thus both were most likely of an artificial origin. In negative control incubations of 5F-EMB-PINACA, no degradation products were detected. In the current study, 28 phase I metabolites of JWH-200 were found in all incubations. Observed metabolic reactions included a *N*-dealkylation (MA1), together with hydroxylation (MA4), oxidative morpholine cleavage (MA2), and additional oxidation to carboxylic acid (MA3), or hydroxylation (MA5–MA7), or dihydrodiol formation by epoxidation and non-enzymatic hydrolysis (MA8). Further metabolites were generated by oxidative opening of the morpholine ring (MA9, MA12, and MA13), together with either hydroxylation (MA10, MA11, and MA24), or dihydrodiol formation (MA14). Other biotransformation steps resulted in a hydroxylation and subsequent oxidation to a ketone (MA15 and MA17), dihydroxylation followed by dehydrogenation (MA16), hydroxylation (MA18–MA23) followed by dehydrogenation and dihydrodiol formation (MA25), dihydroxylation (MA25) as well as dihydrodiol formation (MA27 and MA28). The four most abundant metabolites in pHLM incubations were *N*-dealkylated (MA1), oxidative morpholine cleaved (MA2), and oxidative morpholine opened (MA9 and MA13).

**(a) JWH-200****(b) A-796260****(c) 5F-EMB-PINACA**

**Fig. 4** Dose–response plots of JWH-200 (a), A-796260 (b), and 5F-EMB-PINACA (c) obtained by incubation of cells at seven concentrations of the respective test compound (1.95, 3.91, 7.81, 15.6, 31.3, 62.5, and 125  $\mu$ M) and blank incubations without test compound. Changes of cell parameters (cell count, nuclear size, nuclear intensity, mitochondrial membrane potential, cytosolic calcium levels, and plasma membrane integrity) are plotted in relation to blank incubations (100%). All parameters were normalized to the cell count except the cell count, which was normalized to the number of appropriate images. Values are expressed as mean  $\pm$  standard error of the mean (SEM;  $n=5$ ). Statistical analysis was done using one-way ANOVA followed by Dunnett's post hoc test ( $***P < 0.001$ ,  $**P < 0.01$ ,  $*P < 0.05$  compared to blank incubation). Norm. Fluor. Inten., normalized fluorescence intensity

In case of A-796260, a total number of 22 phase I metabolites were identified, which originated partly from a *N*-dealkylation (MB1) and additional hydroxylation (MB3), oxidative morpholine cleavage (MB2), also together with hydroxylation (MB4 and MB5), oxidative morpholine opening (MB6, MB9, and MB10) plus hydroxylation (MB7, MB19, and MB20). Moreover, metabolites were formed by hydroxylation followed by dehydrogenation (MB8), plus additional hydroxylation (MB12), or oxidation (MB13), dihydroxylation and subsequent dehydrogenation (MB11), hydroxylation (MB14–MB18), and dihydroxylation (MB21 and MB22). The four most abundant metabolites in pHLM incubations were as follows: oxidative morpholine cleavage (MB2), oxidative morpholine opening (MB6), dihydroxylation followed by dehydrogenation (MB11), and hydroxylation (MB14).

Concerning 5F-EMB-PINACA, 23 metabolites were detected, which originated from a *N*-dealkylation (MC2) and simultaneous ester hydrolysis (MC1) or together with hydroxylation (MC3 and MC4), ester hydrolysis and oxidative defluorination (MC5) followed by further oxidation to carboxylic acid (MC8), and lactone formation with or without previous ester hydrolysis (MC6). Other specified metabolites included the ester hydrolysis (MC7) along with hydroxylation (MC9–MC11), oxidative defluorination (MC12) either together with hydroxylation and oxidation to a ketone (MC14) or subsequent oxidation to carboxylic acid (MC15). Besides, metabolites were generated by hydroxylation (MC16–MC18) followed by dehydrogenation (MC13) or oxidation to carboxylic acid (MC20), as well as dihydroxylation (MC21–MC23) followed by oxidation to a ketone (MC19). The four most abundant metabolites in pHLM incubations included metabolites generated by ester hydrolysis (MC7) plus additional metabolic steps such as oxidative defluorination (MC5), oxidative defluorination to carboxylic acid (MC8), and hydroxylation (MC9).

## Isozyme mapping of initial phase I steps

Results of the isozyme mapping of initial phase I metabolites in comparison to pHLM incubations of JWH-200, A-796260, and 5F-EMB-PINACA are summarized in Table S4–S6 in the ESM.

*N*-Dealkylation (MA1) of JWH-200 was catalyzed by CYP1A2, CYP3A4, and CYP3A5, whereas the metabolite generated by oxidative morpholine cleavage (MA2) was only found in CYP3A4 and CYP3A5 incubations. Several isozymes were involved on the oxidative morpholine ring opening (MA9, MA12, and MA13), namely CYP1A2, CYP2B6, CYP2C8, CYP2C19, CYP2D6, CYP3A4, and CYP3A5. All aforementioned isozymes also contributed to the formation of the monohydroxy metabolites (MA18–MA23) but CYP2B6 was replaced by CYP2C9. Metabolites formed by a dihydrodiol formation (MA27 and MA28) were detected in CYP1A2, CYP2C19, CYP3A4, and CYP3A5 incubations.

Similar to JWH-200, *N*-dealkyl-A-796260 (MB1) and the metabolite formed by oxidative morpholine cleavage (MB2) were both formed by CYP3A4 and CYP3A5 and additional by CYP1A2 in case of *N*-dealkyl-A-796260 (MB1). Furthermore, the isozymes which contributed to the oxidative morpholine ring opening of A-796260 (MB6, MB9, and MB10) were in accordance with that of JWH-200 except for CYP2B6. Monohydroxy metabolites (MB14–MB18) were formed by various isozymes including CYP1A2, CYP2C8, CYP2C9, CYP2D6, CYP3A4, and CYP3A5.

The following isozymes were involved on the formation of *N*-dealkylated 5F-EMB-PINACA (MC2): CYP1A2, CYP2B6, CYP2C19, CYP3A4, and CYP3A5. The ester hydrolysis product (MC7) was the only initial metabolite detected in positive control incubations. Moreover, metabolic reactions such as the oxidative defluorination (MC12) or hydroxylation (MC16–MC18) were in turn catalyzed by numerous isozymes. The former metabolite (MC12) was present in incubations of CYP1A2, CYP2B6, CYP2C8, CYP2C9, CYP2C19, CYP2D6, and CYP3A5. These isozymes also contributed to the hydroxylation of 5F-EMB-PINACA (MC16–MC18) except for CYP2D6 which was substituted by CYP3A4.

## Discussion

### HCSA optimization

To overcome some drawbacks of a previously developed HCSA method (Richter et al. 2019a) such as reproducibility, user friendliness, and sample throughput, an optimized HCSA method should first be developed. With the improved HCSA method using a fully automated epifluorescence

microscope, all parameters could be analyzed for statistical significance. Although O'Brien and Edvardsson (2017) mentioned, that at least 3 days of cell treatment with test compounds is needed for HepG2 cytotoxicity testing, it was necessary to reduce the treatment from 72 to 48 h to prevent cells from unpredictable cell growth such as multilayer formations. Furthermore, work load and duration of the experiment could thus be reduced. To prove the suitability of the method, two formerly tested compounds showing a high cytotoxic potential, fluvastatin and 5F-PB-22, were reanalyzed (Richter et al. 2019a). Statin induced hepatotoxicity is still not fully understood, but various triggers have been debated such as blockage of the cholesterol biosynthesis, decreasing levels of isoprenoids, e.g., ubiquinone and quite likely the inhibition of the 3-Hydroxy-3-methylglutaryl-coenzyme A reductase leading to reduced formation of mevalonate and its metabolites such as farnesol and geranylgeraniol (Diaz and O'Brien 2006). In the previous study, fluvastatin significantly affected the cell count and nuclear size at concentration of 11.12  $\mu\text{M}$  and the nuclear intensity at 100  $\mu\text{M}$ . In general, the remaining three parameters, namely mitochondrial membrane potential, cytosolic calcium levels, and plasma membrane integrity were not tested for significance. However, the mitochondrial membrane potential was reduced with increasing concentration, cytosolic calcium levels showed a peak at 11.12  $\mu\text{M}$  and the plasma membrane integrity was inconsistent (Richter et al. 2019a). Concerning the present study, only the cell count showed a statistical significance, which could be due to the high variances induced by the strongly reduced cell count since all other parameters were normalized to cell count. As a consequence, the seeded cell number was adjusted from 1500 to 1750 cell per well for all subsequent tests. The prior 5F-PB-22 experiment revealed a significantly decreased cell count and nuclear intensity at 1.95  $\mu\text{M}$  and nuclear size at 3.9  $\mu\text{M}$ . Mitochondrial membrane potential was reduced with increasing 5F-PB-22 concentration, whereas cytosolic calcium levels and plasma membrane integrity were increased (Richter et al. 2019a). Similar to Richter et al. (2019a) the cell count and mitochondrial membrane potential decreased in the current assay. In case of the nuclear intensity, initially the fluorescence intensity was reduced as determined by Richter et al. (2019a); however, it increased at a concentration of 125  $\mu\text{M}$ . The decreased nuclear intensity at lower concentrations could be explained by an intercalation of 5F-PB-22 into DNA, as already reported for other drugs such as doxorubicin (O'Brien and Edvardsson 2017). As Hoechst33342 is a DNA-binding fluorescence dye, Hoechst33342 and 5F-PB-22 compete for the binding site at the DNA. The elevated nuclear intensity at a high concentration could be reasoned by chromatin condensation caused by DNA degradation (O'Brien and Edvardsson 2017). In the present study, the nuclear size after treatment of 5F-PB-22

was barely impaired and the plasma membrane integrity declined rather unstable through increased fluorescence intensity. Those divergent results in comparison to the previous study (Richter et al. 2019a) might be explained by the reduced treatment time. Contrary to Richter et al. (2019a) the cytosolic calcium levels of 5F-PB-22 decreased, which has not yet been described for SC in literature, except for neuronal cells (Zhuang et al. 2005). Another explanation could be the presence of active transporters in living cells removing CAL-520 from the cytosol as postulated by Richter et al. (2019a).

### Cytotoxicity of the tested synthetic cannabinoids

Two different evaluation strategies to assess the cytotoxic potential of drugs and/or NPS following a HCSA were described in the literature (O'Brien and Edvardsson 2017; Richter et al. 2019a). The approach developed by O'Brien and Edvardsson (2017) depends on known maximum blood concentrations ( $C_{\text{max}}$ ) values, which are usually unavailable, due to the lack of controlled studies for ethical reasons. Moreover, no plasma concentrations or consumer dosages have yet been described. Solely for JWH-018, a JWH-200 derivative,  $C_{\text{max}}$  values after inhalation of a 2 or 3 mg dose were published ranging from 0.009 to 0.03  $\mu\text{M}$  (Toennes et al. 2017). Therefore, a first cytotoxicity estimation was done using a prescreening at a low and high concentration (7.81 and 125  $\mu\text{M}$ ) following the procedure proposed by Richter et al. (2019a). Since the result of the pretest was positive for all three SC, they were again incubated at seven different concentrations (1.95–125  $\mu\text{M}$ ) to gain a deeper insight into cytotoxic effects. To date, none of the investigated SC was analyzed for its hepatotoxicity. With regard to hepatotoxic properties of structural related SC, only a few studies are available (Giuliano et al. 2009; Koller et al. 2013; Richter et al. 2019a). Apart from 5F-PB-22, which showed a strong cytotoxic potential (Richter et al. 2019a), the morpholino derivative WIN 55,212-2 was examined in HepG2 cells (Giuliano et al. 2009). In this study cell viability using a 3-(4,5-dimethylthiazol-2-yl)-2,5-diphenyltetrazolium bromide reduction assay, mitochondrial membrane potential using 3,3-dihexyloxycarbocyanine, and morphological apoptotic changes using Hoechst33258 were investigated among others (Giuliano et al. 2009). WIN 55,212-2 concentrations ranged from 1 to 10  $\mu\text{M}$  and cells were treated for 16, 24, 36, 48, or 72 h depending on the assay. Effects on the cell viability (–25%) were already observed after 24 h of treatment with 10  $\mu\text{M}$  WIN 55,212-2, which increased with treatment time and was about 10% of control cells after 72 h (Giuliano et al. 2009). Collapse of mitochondrial membrane potential was induced after 16 h of treatment with 10  $\mu\text{M}$  and increased with treatment time (Giuliano

et al. 2009). Furthermore, at 36 h of treatment with 10  $\mu\text{M}$  WIN 55,212-2, an increased number of cells were observed showing typical apoptotic features such as condensed or fragmented nuclei (Giuliano et al. 2009). In another work by Koller et al. (2013), naphthylindole compounds such as JWH-018, JWH-073, JWH-122, and JWH-210 were investigated in HepG2 cells among others using a LDH leakage assay and changes of mitochondrial functions were assessed by alterations of the succinate dehydrogenase activity of the cells with the 2,3-bis(2-methoxy-4-nitro-5-sulfophenyl)-5-[(phenyl-amino)carbonyl]-2H-tetrazolium hydroxide (XTT) assay (Koller et al. 2013). No damage on the cell membrane of HepG2 cells by LDH leakage could be determined after a 24 h treatment for all investigated SC (10–100  $\mu\text{M}$ ). Whereas, JWH-018 and JWH-122 were positive in the XTT assay in HepG2 cells (Koller et al. 2013). Thus, data about a potential hepatotoxicity of SC are still limited and the current study partly closes this gap by providing insights into the cytotoxic effect of some SC belonging to different subclasses. JWH-200 and A-796260 show some structural similarities such as the 4-morpholinylethyl moiety linked to the indole group. However, JWH-200 consisted of a naphthyl head group, which is substituted by a 2,2,3,3-tetramethylcyclopropyl (TMCP) in case of A-796260. By contrast, 5F-EMB-PINACA, which is composed of a fluoro pentyl chain and an indazole core linked to an ethyl-methylbutanoate moiety, showed no structural overlap with the aforementioned SC. According to the criteria given above, a strong cytotoxic potential was assigned for the naphthylindole JWH-200 and the tetramethylcyclopropanoylindole A-796260, whereas the indazole carboxamide 5F-EMB-PINACA showed only moderate cytotoxic effects. Overall, the results of the pretest were in close consistency with those of the subsequent screening except for few parameters, which showed high variances or an unexpected outcome. Contradictory results of the cell count may be due to inaccuracies during cell seeding. In part, the calcium levels showed substantial differences and similarly to 5F-PB-22, A-796260 revealed an unexpected reduction of CAL-520 fluorescence intensity, which were already discussed above. However, there was no plausible explanation for variations of the plasma membrane integrity, hence this parameter seems less suited as a reliable indicator of cytotoxicity. In addition, the nuclear size appears rather inadequate as the automated software had sometimes difficulties in distinguishing two or more nuclei from each other. Nonetheless, a general recommendation to not consider parameters such as the plasma membrane integrity in the future might not be given, as this should be first evaluated on further NPS classes. As already reported by Richter et al. (2019a), the mitochondrial potential was found to be

the most sensitive parameter, and therefore, the best choice to monitor a potential cytotoxicity.

Some reports about possible SC induced liver injuries can be found in the literature (Abouchdid et al. 2016; Shahbaz et al. 2018; Sheikh et al. 2014). However, cannabinoid receptor type 2 (CB<sub>2</sub>) agonists, as it is the case for A-796260 (Yao et al. 2008), have been associated with liver diseases such as obesity-associated inflammation and insulin resistance (Sherpa et al. 2015). In general, an elevated risk of liver injuries is assumed for consumers with intake of high doses or with additional risk factors. Considering that the latest generations of SC show a higher potency and efficiency at the in vitro CB<sub>1</sub> receptor or CB<sub>2</sub> as older ones (Krotulski et al. 2021; Lie et al. 2021), such as JWH-200 or A-796260, lower consumer doses of more recent compounds might be expected. One might also suppose, that SC concentrations in blood do not generally reflect their concentrations in hepatocytes, based on different blood and liver contents of the JWH-200 homolog JWH-210 in a pig model (Schaefer et al. 2017).

### Metabolism-based effects on the cytotoxicity

The hepatotoxicity of NPS may be mediated not only by the parent compounds but also by their metabolites, thus the metabolism-related impact was investigated using the broad CYP inhibitor ABT (Dias da Silva et al. 2019; Roque Bravo et al. 2021). Based on the current findings of the isozyme mapping, various isozymes were involved in the SC metabolism and the use of single isozyme inhibitors appeared not to be appropriate. Since only the plasma membrane integrity seemed impaired after treatment with ABT and JWH-200 in a high concentration, the outcome might indicate that the formed metabolites might be less toxic than the corresponding parent compounds. Another reason might be that HepG2 cells are known for their limited metabolic ability due to low gene expression of CYP enzymes (Hart et al. 2010). However, a few studies have been reported, that metabolites are detectable in HepG2 cell incubates (Richter et al. 2019a, 2017; Wagmann et al. 2021). To substantiate these assumptions, HepG2 incubates should have been analyzed for SC metabolites, which represents the main limitation of the current study.

However, according to a comparative study for drug metabolism-based hepatotoxic effects in HepG2, HepaRG, and primary human hepatocytes by Yokoyama et al. (2018), HepaRG cells should be the most suitable ones for analysis of metabolism-based cytotoxicity. Unlike primary human hepatocytes, HepaRG showed a stable expression of CYP enzymes but this major drawback of inter-individual variability of primary human hepatocytes could be overcome using pooled human hepatocytes (Yokoyama et al. 2018). Furthermore, a recent study revealed considerable

differences between HepaRG and primary human hepatocytes among others with respect to CYP enzymes and transporter levels (Hammer et al. 2021). Alternatively, primary rat hepatocytes have been used to examine metabolism mediated effects (Dias da Silva et al. 2019; Roque Bravo et al. 2021) but the predictions of human toxicity deduced from mammalian cells have been reported to be lower than human cell lines in HCSA (O'Brien and Edvardsson 2017).

## Identification of metabolites

Even though investigations of metabolism-related effects in the HCSA indicated the formation of less toxic metabolites in HepG2 cells for all SC, identification of metabolites is crucial to figure out potential screening targets essential in analytical toxicology. Metabolites were tentatively identified by comparison of HRMS<sup>2</sup> spectra and fragmentation patterns of the parent compounds to those of putative metabolites. Owing to the large number of detected metabolites, some representatives were selected to exemplify the general identification approach using the exact, calculated masses. HRMS<sup>2</sup> spectra of JWH-200, A-796260, and 5F-EMB-PINACA and their metabolites, which are discussed in detail in the following, are given in Figs. 5, 6 and 7, respectively. All other HRMS<sup>2</sup> spectra of identified metabolites are depicted in Fig. S2 (JWH-200), S3 (A-796260), and S4 (5F-EMB-PINACA) in the ESM.

### JWH-200

In case of JWH-200, a general comparison between metabolites identified in the current study and by De Brabanter et al. is hardly possible due to variations in pHLM reaction conditions such as an extended incubation time and elevated substrate and enzyme concentrations, sparse availability of HRMS<sup>2</sup> spectra, and different sample preparation steps such as additional solid phase extraction (De Brabanter et al. 2013). However, differences turned out in the non-detectability of metabolites formed by hydroxylation and subsequent dehydrogenation at the morpholine and by hydroxylation at the morpholine plus dihydrodiol formation after epoxidation and non-enzymatic hydrolysis at the naphthalene. As a note, none of them was found in the urine of the liver-humanized mice (De Brabanter et al. 2013). Additional steps were identified by previously undescribed precursor masses such as the *N*-dealkylation (MA1), together with hydroxylation at the naphthalene (MA4), oxidative morpholine ring opening plus hydroxylation also at the naphthalene (M10 and M11), oxidative morpholine cleavage plus dihydrodiol formation (MA14), hydroxylation at the morpholine followed by dehydrogenation together with dihydrodiol formation (MA24), and dihydroxylation at the morpholine or ethyl part (MA26).

The fragmentation pattern of JWH-200 with a protonated precursor ion (PI) at  $m/z$  385.1910 showed two high abundant FIs at  $m/z$  155.0491 and at  $m/z$  114.0913. The former one corresponded to the naphthalene with vicinal carbonyl group after elimination of the indole moiety and the latter FI belonged to the morpholine plus ethyl spacer formed by cleavage of the indole at the indole's nitrogen atom. A lower abundant FI at  $m/z$  145.0647 derived from FI at  $m/z$  155.0491 by a loss of CO and addition of water. In addition, the FI at  $m/z$  70.0651 resulted from FI  $m/z$  114.0913 by opening of the morpholine ring and elimination of the C<sub>2</sub>H<sub>4</sub>O group (− 44.0262 u).

The HRMS<sup>2</sup> spectrum of *N*-dealkyl-JWH-200 (MA1) with PI at  $m/z$  315.1491 contained two FIs with  $m/z$  at 155.0491 and at 145.0647, which were both consistent with those of the parent compound. However, their spectra differed in the low abundant FI at  $m/z$  144.0647, which was only present in the spectrum of MA1. This fragment was composed of the indole ring plus carbonyl moiety by cleavage of the naphthalene. Two of three isomers formed by oxidative ring opening and hydroxylation (M10 and M11) with PI at  $m/z$  375.1703 indicated a loss of an ethylene at the morpholine, which was confirmed by FI at  $m/z$  88.0756 comprising the remaining part of the morpholine linked to the ethyl group. Whereas the third one (MA23) with PI at  $m/z$  403.1652 was identified by FI at  $m/z$  116.0706, which correlated with FI at  $m/z$  114.0913 by loss of a methylene plus one additional oxygen atom. Although the oxidative ring opening mechanism at the morpholine ring is not known in detail it could be explained by the speculative pathway described by Denissen et al. (1994). Based on the FI at  $m/z$  171.0440 in the spectra of all three isomers, which corresponded to FI at  $m/z$  155.0491 by a shift of one oxygen (+ 15.9949 u) the hydroxylation occurred at the naphthalene. One metabolite generated by hydroxylation followed by dehydrogenation and dihydrodiol formation with PI at  $m/z$  417.1808 (MA24) was characterized first by FI at  $m/z$  189.0551 representing a dihydrodiol formation at the naphthalene plus vicinal carbonyl. This FI also derived from the aforementioned FI at  $m/z$  155.0491 altered by two more oxygen and hydrogen atoms. Second, FI at  $m/z$  112.0756 suggested a loss of water after a hydroxylation at the morpholine by a shift of two hydrogen atoms compared to FI at  $m/z$  114.0913.

### A-796260

In the spectrum of A-796260 with the PI at  $m/z$  355.2380 a prominent FI at  $m/z$  125.0960 was detected, originating from the TMCP ring attached to the vicinal carbonyl group after elimination of the indole part. In accordance with JWH-200, FI at  $m/z$  114.0913 was generated by the separation of the indole ring linked to the TMCP consisting of the morpholine plus ethyl spacer. Furthermore, the loss of CO (− 27.9949

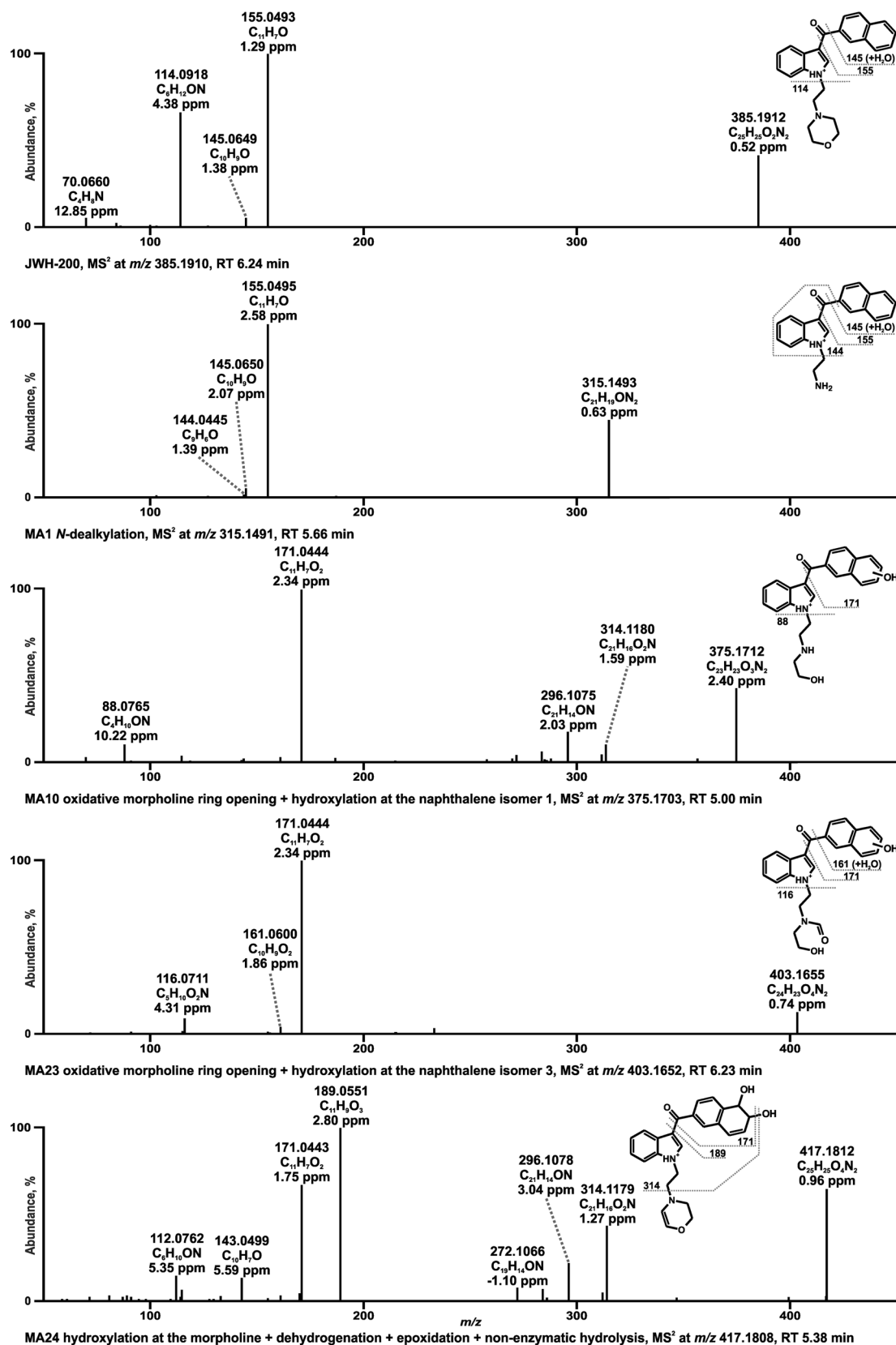


**Fig. 5** HRMS<sup>2</sup> spectra of JWH-200 and selected metabolites identified in pooled human liver microsomes or isozyme incubations. Metabolites are ordered by increasing mass and retention time (RT). Metabolite IDs correspond to Table S1. JWH-200 metabolite (MA)

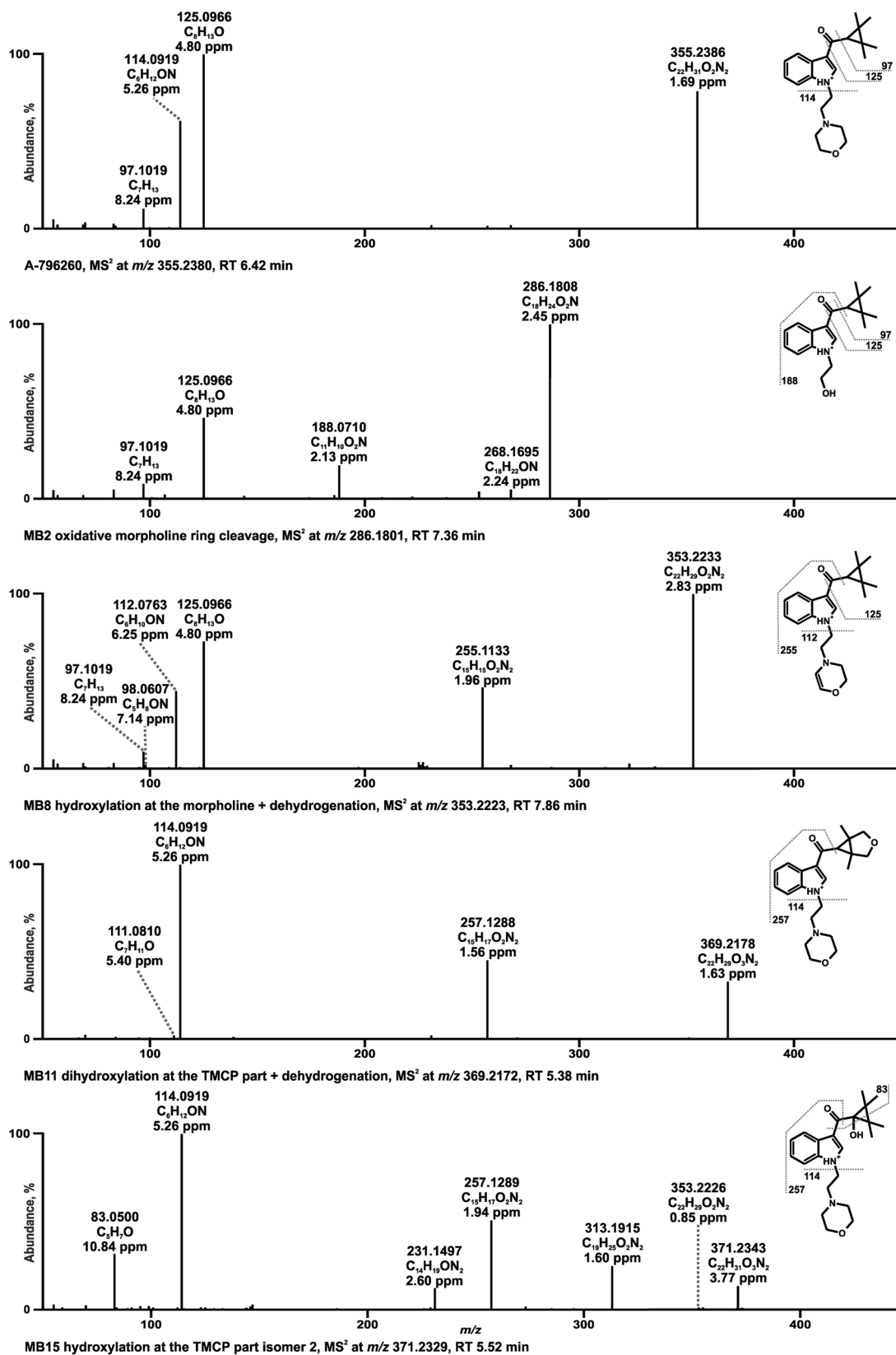


**Fig. 6** HRMS<sup>2</sup> spectra of A-796260 and selected metabolites identified in pooled human liver microsomes or isozyme incubations. Metabolites are ordered by increasing mass and retention time (RT).

Metabolite IDs correspond to Table S2. A-796260 metabolite (MB), tetramethylcyclopropyl (TMCP)

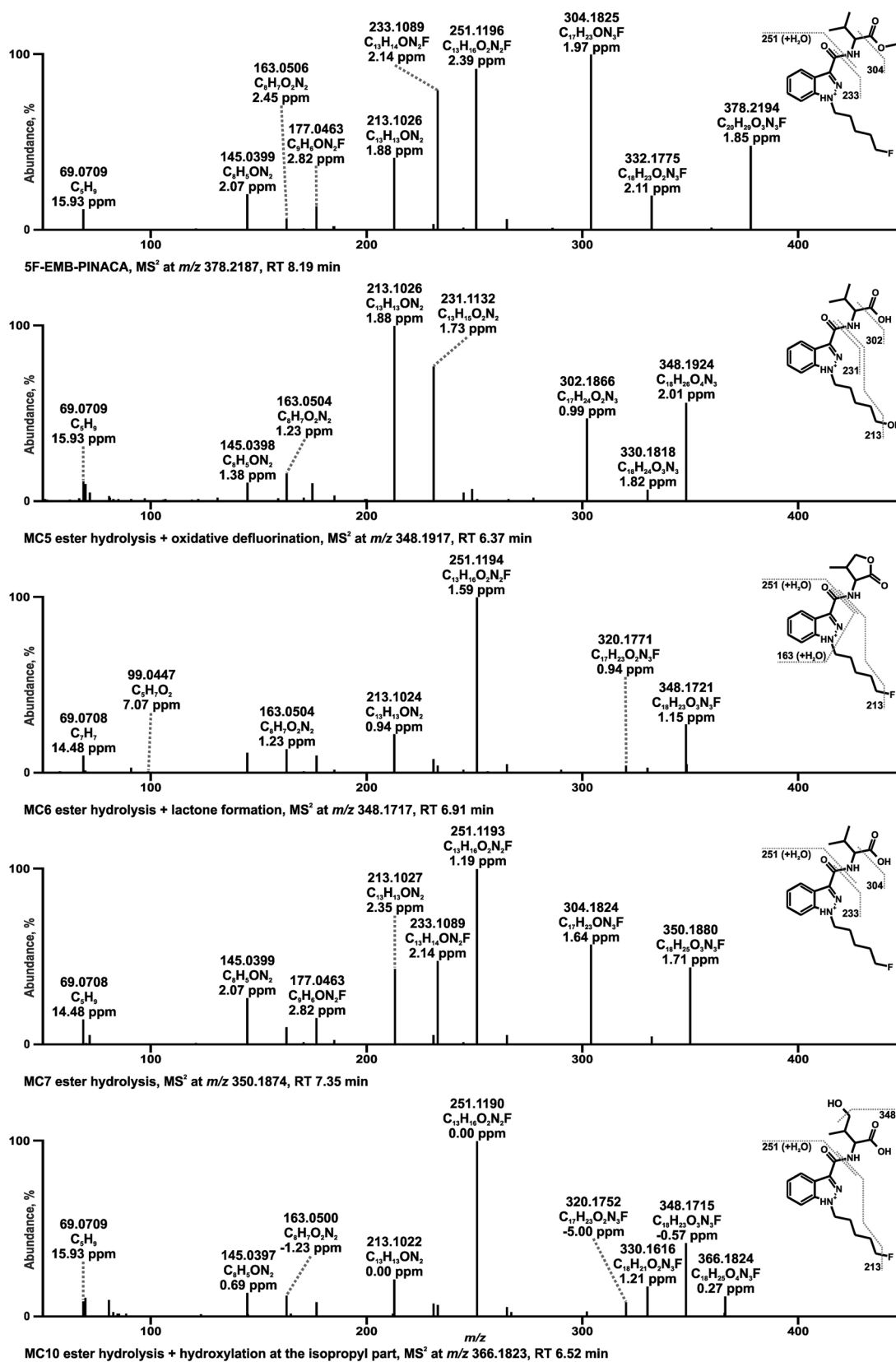


**Fig. 7** HRMS<sup>2</sup> spectra of 5F-EMB-PINACA and selected metabolites identified in pooled human liver microsomes or isozyme incubations. Metabolites are ordered by increasing mass and retention time (RT).

Metabolite IDs correspond to Table S3. 5F-EMB-PINACA metabolite (MC)

u) from FI at  $m/z$  125.0960 led to the FI at  $m/z$  97.1011 corresponding to the TMCP part. Fragmentation of the metabolite formed by oxidative cleavage of the morpholine ring (MB2) with PI at  $m/z$  286.1801 resulted in a specific FI at  $m/z$  188.0706 which occurred from a split of the TMCP moiety. As above mentioned for JWH-200, FI at  $m/z$  112.0756 in the HRMS<sup>2</sup> spectrum of dehydro-A-796260 (MB8) with PI at  $m/z$  353.2223 indicated a previous hydroxylation either on the morpholine ring or ethyl spacer with subsequent water elimination. Besides, the parallel occurrence of FI at  $m/z$  98.0607 varying from FI at  $m/z$  114.0913 by one methyl group ( $-16.0313$  u) suggested that the dehydrogenation happened at the morpholine ring. This finding was in line with dehydrogenated JWH-200 metabolite described by De Brabanter et al. (2013). Two possible metabolic reactions must be considered regarding MB11 with PI at  $m/z$  369.2172. Either it involved an aldehyde formation at the TMCP moiety or a dihydroxylation and subsequent dehydrogenation resulting in a cyclization as postulated for the structural related compound XLR-11 in human hepatocytes (Wohlfarth et al. 2013). Both formations could be justified by FI at  $m/z$  111.0804 deriving from FI at  $m/z$  97.1011 by one more oxygen and two less hydrogen atoms. However, as aldehydes are highly reactive and might be altered before detection, the more likely structure of MB11 is given in Fig. 7. MB15 with PI at  $m/z$  371.2329 represented one of three metabolites with the hydroxy group located at the TMCP ring or vicinal carbonyl (MB14–MB16). Hence, the following reaction positions were possible for a hydroxylation: one of the methyl substituents, the alpha carbon to the carbonyl group and the carbonyl carbon leading to a hemiketal formation as described by Wohlfarth et al. (2013). Regarding MB15, it was presumed to be hydroxylated at the alpha carbon to the carbonyl group, firstly due to FI at  $m/z$  353.2223, which indicated a loss of water. This led to a putative opening of the cyclopropyl ring. Second, the FI at  $m/z$  313.1910 suggested an elimination of  $C_3H_4$  ( $-40.0302$  u) from the opened TMCP ring, which was specific for MB15.

### 5F-EMB-PINACA

The fragmentation pattern of 5F-EMB-PINACA with PI at  $m/z$  378.2187 showed an initial ethanol loss due to an ester cleavage by FI at  $m/z$  332.1775. Cleavage at the carbonyl carbon of the ester moiety resulted in a loss of CO ( $-27.9949$  u) representing by FI at  $m/z$  304.1825. On that basis, FI at  $m/z$  233.1084 was formed by breaking of the amide bond between the carbonyl carbon and the nitrogen atom. The FI at  $m/z$  213.1022 derived therefrom by cleavage of the hydrogen fluoride (HF) at the pentyl side chain. A different mechanism was assumed for the formation of FI at  $m/z$  251.1190, which was shifted by

a mass of  $+18.0106$  u compared to FI at  $m/z$  233.1084, which corresponded to the mass of water. As discussed for the methyl ester homologs 5F-ADB and 4F-MDMB-BINACA (Richter et al. 2019b; Wagmann et al. 2020) a rearrangement reaction by ester cleavage and subsequent nucleophilic attack of the oxygen at the indazole nitrogen atom in the second position was most likely the cause. The same mass shift was observed for FIs at  $m/z$  145.0396 and 163.0502 consisting of the vicinal carbonyl group to the indazole moiety coupled to the fluoro pentyl chain. A fluorine rearrangement was supposed to be involved in the emergence of FI at  $m/z$  177.0458, which was shifted by  $-C_4H_8$  from FI at  $m/z$  233.1084. Diao et al. identified exact the same fragment in the spectra of derivatives with a pentyl fluoride side chain such as FUBIMINA and THJ-2201 and postulated the formation of an acyl fluoride without exact mechanism. Furthermore, the cleavage between alpha and beta carbon atom to the indazole led to a butenyl loss (Diao et al. 2016). Finally, FI at  $m/z$  69.0698 could be explained by the pentenyl side chain after loss of the indazole part and HF.

One metabolite generated by oxidative defluorination together with ester hydrolysis (MC5) with PI at  $m/z$  348.1917 was identified due to the absence of the fragment originating from an ester hydrolysis by mass shift of 28.0313 u from the parent mass, which was present in all spectra of metabolites with an intact ester group. In addition, FI at  $m/z$  302.1863 differed from FI at  $m/z$  304.1825 by one more oxygen and one less fluorine atom. MC6 with a PI at  $m/z$  348.1717 was suspected to be formed after ester hydrolysis by a cyclization to a lactone as postulated for 4F-MDMB-BINACA by Wagmann et al. (2020). Although an ester hydrolysis followed by dehydrogenation would be also possible (Haschimi et al. 2019; Krotulski et al. 2019), the fact that FI at  $m/z$  320.1769 was present in the spectra of both MC6 as well as MC10 (ester hydrolysis + hydroxylation at the isopropyl part), but not in that of the ester hydrolysis (MC7) supports the assumption of a lactone formation. Similar to 4F-MDMB-BINACA, FI at  $m/z$  99.0440 corresponded to the lactone part after cleavage between alpha carbon and amide nitrogen atom (Wagmann et al. 2020). The aforementioned ester hydrolysis product with PI at  $m/z$  350.1874 was identified by the FI at  $m/z$  304.1825, which was already stated for the parent mass. MC10 with PI at  $m/z$  366.1823 originated, as above mentioned from an ester hydrolysis and hydroxylation at the isopropyl part. The unaltered FI at  $m/z$  251.1190 compared to the parent spectrum ruled out a hydroxylation at the indazole or fluoro pentyl part. Besides, the mass shift of  $-18.0106$  u leading to 348.1717 indicated a water loss, which pointed out that the hydroxylation happened at the isopropyl part.

## Isozyme mapping

The initial metabolic steps of all three SC were primarily catalyzed by CYP3A4 and CYP3A5, but various other isozymes were additionally involved. In case of 5F-EMB-PINACA, due to the presence of human carboxylesterases only in pHLM, the ester hydrolysis (MC7) was exclusively found in pHLM incubations but not during the isozyme mapping. All other initial metabolites were only detected in pHLM incubations in combination with the ester hydrolysis (data not shown), thus, an esterase activity screening of 5F-EMB-PINACA might give further insights (Meyer et al. 2015; Wagmann et al. 2020). As the extensive phase I metabolism is mediated by several isozymes, drug–drug or drug–food interaction are unlikely.

## Conclusion

With a successfully optimized HCSA method, the cytotoxic potential of the SC JWH-200, A-796260, and 5F-EMB-PINACA was evaluated. The naphthylindole JWH-200 and tetramethylcyclopropanoylindole A-796260 showed the strongest cytotoxic effects, whereas the potential of indazole carboxamide 5F-EMB-PINACA was moderate. All SC caused a collapse of the mitochondrial membrane potential, which was found to be the most reliable/sensitive indicator. No metabolism-related impact was observed; however, the low enzymatic activity of HepG2 cells could be a limitation. Several phase I metabolites of the studied SC could be identified in pHLM or single isozyme incubations. Most abundant metabolites of JWH-200 in pHLM were formed by *N*-dealkylation, oxidative morpholine cleavage, and oxidative morpholine opening. Oxidative morpholine cleavage, oxidative morpholine opening, hydroxylation, and dihydroxylation followed by dehydrogenation were the most abundant metabolites of A-796260. 5F-EMB-PINACA underwent mainly ester hydrolysis plus additional metabolic steps such as oxidative defluorination, oxidative defluorination to carboxylic acid, and hydroxylation. The initial metabolic steps of all three SC were primarily catalyzed by CYP3A4 and CYP3A5 but several other isozymes were involved making interaction unlikely.

**Supplementary Information** The online version contains supplementary material available at <https://doi.org/10.1007/s00204-021-03148-3>.

**Acknowledgements** The authors are grateful for the patient guidance and support in cell culture by Heidi Löhr and Ute Soltek. Special thanks go to Joel Mailliet from BioTek, Bad Friedrichshall, Germany and Martin Simon-Thomas for their assistance with microscope setup. Sascha K. Manier for fruitful discussions regarding statistical approaches and Fabian Frankenfeld for proofreading. This work was supported by the Deutsche Forschungsgemeinschaft (DFG) SFB 894 (A.B. and V.F.) and the DFG project INST 256/414-1 FUGG (Q-Exactive Plus).

**Funding** Open Access funding enabled and organized by Projekt DEAL.

## Declarations

**Conflict of interest** The authors declare that they have no conflict of interest.

**Open Access** This article is licensed under a Creative Commons Attribution 4.0 International License, which permits use, sharing, adaptation, distribution and reproduction in any medium or format, as long as you give appropriate credit to the original author(s) and the source, provide a link to the Creative Commons licence, and indicate if changes were made. The images or other third party material in this article are included in the article's Creative Commons licence, unless indicated otherwise in a credit line to the material. If material is not included in the article's Creative Commons licence and your intended use is not permitted by statutory regulation or exceeds the permitted use, you will need to obtain permission directly from the copyright holder. To view a copy of this licence, visit <http://creativecommons.org/licenses/by/4.0/>.

## References

- Abouchedd R, Ho JH, Hudson S et al (2016) Acute toxicity associated with use of 5F-derivations of synthetic cannabinoid receptor agonists with analytical confirmation. *J Med Toxicol* 12(4):396–401. <https://doi.org/10.1007/s13181-016-0571-7>
- Adamowicz P, Meissner E, Maslanka M (2019) Fatal intoxication with new synthetic cannabinoids AMB-FUBINACA and EMB-FUBINACA. *Clin Toxicol (phila)* 57(11):1103–1108. <https://doi.org/10.1080/15563650.2019.1580371>
- Bolt HM, Hengstler JG (2021) Commemorating 85 years of publications on cannabis by archives of toxicology. *Arch Toxicol* 95(7):2231–2233. <https://doi.org/10.1007/s00204-021-03079-z>
- De Brabanter N, Esposito S, Tudela E et al (2013) In vivo and in vitro metabolism of the synthetic cannabinoid JWH-200. *Rapid Commun Mass Spectrom* 27(18):2115–2126. <https://doi.org/10.1002/rcm.6673>
- DEA (2019) 5F-AEB (5F-EMB-PINACA). Drug Enforcement Administration, Diversion Control Division Drug & Chemical Evaluation Section, U.S. Department of Justice. [https://www.deadiversion.usdoj.gov/drug\\_chem\\_info/5F-AEB.pdf](https://www.deadiversion.usdoj.gov/drug_chem_info/5F-AEB.pdf)
- Denissen JF, Grabowski BA, Johnson MK, et al. (1994) The orally active renin inhibitor A-74273. In vivo and in vitro morpholine ring metabolism in rats, dogs, and humans. *Drug Metab Dispos* 22(6):880–8
- Diao X, Scheidweiler KB, Wohlfarth A, Zhu M, Pang S, Huestis MA (2016) Strategies to distinguish new synthetic cannabinoid FUBIMINA (BIM-2201) intake from its isomer THJ-2201: metabolism of FUBIMINA in human hepatocytes. *Forensic Toxicol* 34:256–267. <https://doi.org/10.1007/s11419-016-0312-2>
- Dias da Silva D, Ferreira B, Roque Bravo R et al (2019) The new psychoactive substance 3-methylmethcathinone (3-MMC or methaphedrone) induces oxidative stress, apoptosis, and autophagy in primary rat hepatocytes at human-relevant concentrations. *Arch Toxicol* 93(9):2617–2634. <https://doi.org/10.1007/s00204-019-02539-x>
- Diaz D, O'Brien PJ (2006) Identifying human toxicity potential. *Eur Pharmaceut Rev*(4):1–8

- EMCDDA (2009) EMCDDA-Europole 2009 Annual Report Publications of the European Union. European Monitoring Centre for Drugs and Drug Addiction, Luxembourg
- Gampfer TM, Richter LHJ, Schaper J, Wagmann L, Meyer MR (2019) Toxicokinetics and analytical toxicology of the abused opioid U-48800—in vitro metabolism, metabolic stability, isozyme mapping, and plasma protein binding. *Drug Test Anal* 11(10):1572–1580. <https://doi.org/10.1002/dta.2683>
- Giuliano M, Pellerito O, Portanova P et al (2009) Apoptosis induced in HepG2 cells by the synthetic cannabinoid WIN: involvement of the transcription factor PPARgamma. *Biochimie* 91(4):457–465. <https://doi.org/10.1016/j.biochi.2008.11.003>
- Hammer H, Schmidt F, Marx-Stoelting P, Potz O, Braeuning A (2021) Cross-species analysis of hepatic cytochrome P450 and transport protein expression. *Arch Toxicol* 95(1):117–133. <https://doi.org/10.1007/s00204-020-02939-4>
- Hart SN, Li Y, Nakamoto K, Subileau EA, Steen D, Zhong XB (2010) A comparison of whole genome gene expression profiles of HepaRG cells and HepG2 cells to primary human hepatocytes and human liver tissues. *Drug Metab Dispos* 38(6):988–994. <https://doi.org/10.1124/dmd.109.031831>
- Haschimi B, Mogler L, Halter S et al (2019) Detection of the recently emerged synthetic cannabinoid 4F-MDMB-BINACA in “legal high” products and human urine specimens. *Drug Test Anal* 11(9):1377–1386. <https://doi.org/10.1002/dta.2666>
- Helander A (2017) Chapter 87—synthetic cannabinoid receptor agonists (Spice) as new recreational psychoactive substances. In: Preedy VR (ed) *Handbook of cannabis and related pathologies*. Academic Press, San Diego, pp 839–847
- Hvozdoovich JA, Chronister CW, Logan BK, Goldberger BA (2020) Case report: synthetic cannabinoid deaths in state of florida prisoners. *J Anal Toxicol* 44(3):298–300. <https://doi.org/10.1093/jat/bkz092>
- Koller VJ, Zlabinger GJ, Auwarter V, Fuchs S, Knasmueller S (2013) Toxicological profiles of selected synthetic cannabinoids showing high binding affinities to the cannabinoid receptor subtype CB(1). *Arch Toxicol* 87(7):1287–1297. <https://doi.org/10.1007/s00204-013-1029-1>
- Krotulski AJ, Mohr ALA, Kacinko SL et al (2019) 4F-MDMB-BINACA: A new synthetic cannabinoid widely implicated in forensic casework. *J Forensic Sci* 64(5):1451–1461. <https://doi.org/10.1111/1556-4029.14101>
- Krotulski AJ, Cannart A, Stove C, Logan BK (2021) The next generation of synthetic cannabinoids: detection, activity, and potential toxicity of pent-4-en and but-3-en analogues including MDMB-4en-PINACA. *Drug Test Anal* 13(2):427–438. <https://doi.org/10.1002/dta.2935>
- Lie W, Cheong EJY, Goh EML et al (2021) Diagnosing intake and rationalizing toxicities associated with 5F-MDMB-PINACA and 4F-MDMB-BINACA abuse. *Arch Toxicol* 95(2):489–508. <https://doi.org/10.1007/s00204-020-02948-3>
- Luethi D, Liechti ME, Krahenbuhl S (2017) Mechanisms of hepatocellular toxicity associated with new psychoactive synthetic cathinones. *Toxicology* 387:57–66. <https://doi.org/10.1016/j.tox.2017.06.004>
- Meyer MR, Schutz A, Maurer HH (2015) Contribution of human esterases to the metabolism of selected drugs of abuse. *Toxicol Lett* 232(1):159–166. <https://doi.org/10.1016/j.toxlet.2014.10.026>
- O'Brien PJ, Edvardsson A (2017) Validation of a multiparametric, high-content-screening assay for predictive/investigative cytotoxicity: evidence from technology transfer studies and literature review. *Chem Res Toxicol* 30(3):804–829. <https://doi.org/10.1021/acs.chemrestox.6b00403>
- Richter LHJ, Flockerzi V, Maurer HH, Meyer MR (2017) Pooled human liver preparations, HepaRG, or HepG2 cell lines for metabolism studies of new psychoactive substances? A study using MDMA, MDBD, butylone, MDPPP, MDPV, MDPB, 5-MAPB, and 5-API as examples. *J Pharm Biomed Anal* 143:32–42. <https://doi.org/10.1016/j.jpba.2017.05.028>
- Richter LHJ, Beck A, Flockerzi V, Maurer HH, Meyer MR (2019a) Cytotoxicity of new psychoactive substances and other drugs of abuse studied in human HepG2 cells using an adopted high content screening assay. *Toxicol Lett* 301:79–89. <https://doi.org/10.1016/j.toxlet.2018.11.007>
- Richter LHJ, Maurer HH, Meyer MR (2019b) Metabolic fate of the new synthetic cannabinoid 7'-N-5F-ADB in rat, human, and pooled human S9 studied by means of hyphenated high-resolution mass spectrometry. *Drug Test Anal* 11(2):305–317. <https://doi.org/10.1002/dta.2493>
- Roque Bravo R, Carmo H, Valente MJ et al (2021) From street to lab: in vitro hepatotoxicity of buphedrone, butylone and 3,4-DMMC. *Arch Toxicol* 95(4):1443–1462. <https://doi.org/10.1007/s00204-021-02990-9>
- Schaefer N, Kettner M, Laschke MW et al (2017) Distribution of synthetic cannabinoids JWH-210, RCS-4 and Delta 9-tetrahydrocannabinol after intravenous administration to pigs. *Curr Neuropharmacol* 15(5):713–723. <https://doi.org/10.2174/1570159X1566616111114214>
- Diversion Control Division Drug & Chemical Evaluation Section, U.S. Department of Justice [https://www.deadiversion.usdoj.gov/drug\\_chem\\_info/5F-AEB.pdf](https://www.deadiversion.usdoj.gov/drug_chem_info/5F-AEB.pdf)
- Shahbaz A, Gaviria REE, Shahid MF, Yasin MA, Ashraf A, Zaman MA (2018) Acute liver injury induced by synthetic cannabinoid abuse. *Cureus* 10(9):e3257. <https://doi.org/10.7759/cureus.3257>
- Sheikh IA, Luksic M, Ferstenberg R, Culpepper-Morgan JA (2014) Spice/K2 synthetic marijuana-induced toxic hepatitis treated with N-acetylcysteine. *Am J Case Rep* 15:584–588. <https://doi.org/10.12659/AJCR.891399>
- Sherpa D, Paudel BM, Subedi BH, Chow RD (2015) Synthetic cannabinoids: the multi-organ failure and metabolic derangements associated with getting high. *J Community Hosp Intern Med Perspect* 5(4):27540. <https://doi.org/10.3402/jchimp.v5.27540>
- Solimini R, Busardo FP, Rotolo MC et al (2017) Hepatotoxicity associated to synthetic cannabinoids use. *Eur Rev Med Pharmacol Sci* 21(1 Suppl):1–6
- Toennes SW, Geraths A, Pogoda W et al (2017) Pharmacokinetic properties of the synthetic cannabinoid JWH-018 and of its metabolites in serum after inhalation. *J Pharm Biomed Anal* 140:215–222. <https://doi.org/10.1016/j.jpba.2017.03.043>
- Wagmann L, Meyer MR, Maurer HH (2016) What is the contribution of human FMO3 in the N-oxygenation of selected therapeutic drugs and drugs of abuse? *Toxicol Lett* 258:55–70. <https://doi.org/10.1016/j.toxlet.2016.06.013>
- Wagmann L, Frankenfeld F, Park YM et al (2020) How to study the metabolism of new psychoactive substances for the purpose of toxicological screenings—a follow-up study comparing pooled human liver S9, HepaRG cells, and zebrafish larvae. *Front Chem* 8:539. <https://doi.org/10.3389/fchem.2020.00539>
- Wagmann L, Gampfer TM, Meyer MR (2021) Recent trends in drugs of abuse metabolism studies for mass spectrometry-based analytical screening procedures. *Anal Bioanal Chem*. <https://doi.org/10.1007/s00216-021-03311-w>
- Wohlfarth A, Pang S, Zhu M et al (2013) First metabolic profile of XLR-11, a novel synthetic cannabinoid, obtained by using human hepatocytes and high-resolution mass spectrometry. *Clin Chem* 59(11):1638–1648. <https://doi.org/10.1373/clinchem.2013.209965>
- Yao BB, Hsieh GC, Frost JM et al (2008) In vitro and in vivo characterization of A-796260: a selective cannabinoid CB2 receptor agonist exhibiting analgesic activity in rodent pain models. *Br J Pharmacol* 153(2):390–401. <https://doi.org/10.1038/sj.bjp.0707568>

- Yokoyama Y, Sasaki Y, Terasaki N et al (2018) Comparison of drug metabolism and its related hepatotoxic effects in HepaRG, cryopreserved human hepatocytes, and HepG2 cell cultures. *Biol Pharm Bull* 41(5):722–732. <https://doi.org/10.1248/bpb.17-00913>
- Zhuang SY, Bridges D, Grigorenko E et al (2005) Cannabinoids produce neuroprotection by reducing intracellular calcium release from ryanodine-sensitive stores. *Neuropharmacology*

48(8):1086–1096. <https://doi.org/10.1016/j.neuropharm.2005.01.005>

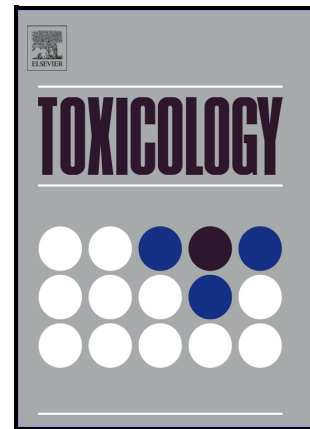
**Publisher's Note** Springer Nature remains neutral with regard to jurisdictional claims in published maps and institutional affiliations.

### **3.5 A simplified strategy to assess the cytotoxicity of new psychoactive substances in HepG2 cells using a high content screening assay - Exemplified for nine compounds<sup>67</sup>**

**Authors Contributions** Tanja M. Gampfer conducted the experiments, analyzed the data, and wrote the manuscript; Benedikt Pulver and Folker Westphal characterized and provided the investigated new psychoactive substances 4CN-CUMYL-BINACA, CUMYL-CBMICA, dibutylone, and ephylone; Veit Flockerzi aided in interpreting the results of the cell culture experiments and supported with scientific discussions; Markus R. Meyer and Lea Wagmann supported with scientific discussions, the design of the experiments, and research supervision.

A simplified strategy to assess the cytotoxicity of new psychoactive substances in HepG2 cells using a high content screening assay - Exemplified for nine compounds

Tanja M. Gampfer, Lea Wagmann, Benedikt Pulver, Folker Westphal, Veit Flockerzi, Markus R. Meyer



PII: S0300-483X(22)00170-6

DOI: <https://doi.org/10.1016/j.tox.2022.153258>

Reference: TOX153258

To appear in: *Toxicology*

Received date: 21 May 2022

Revised date: 27 June 2022

Accepted date: 11 July 2022

Please cite this article as: Tanja M. Gampfer, Lea Wagmann, Benedikt Pulver, Folker Westphal, Veit Flockerzi and Markus R. Meyer, A simplified strategy to assess the cytotoxicity of new psychoactive substances in HepG2 cells using a high content screening assay - Exemplified for nine compounds, *Toxicology*, (2022) doi:<https://doi.org/10.1016/j.tox.2022.153258>

This is a PDF file of an article that has undergone enhancements after acceptance, such as the addition of a cover page and metadata, and formatting for readability, but it is not yet the definitive version of record. This version will undergo additional copyediting, typesetting and review before it is published in its final form, but we are providing this version to give early visibility of the article. Please note that, during the production process, errors may be discovered which could affect the content, and all legal disclaimers that apply to the journal pertain.

## **A simplified strategy to assess the cytotoxicity of new psychoactive substances in HepG2 cells using a high content screening assay - Exemplified for nine compounds**

Tanja M. Gampfer<sup>1</sup>, Lea Wagmann<sup>1</sup>, Benedikt Pulver<sup>2,3,4</sup>, Folker Westphal<sup>2</sup>, Veit Flockerzi<sup>5</sup>, Markus R. Meyer<sup>1</sup>

1 Department of Experimental and Clinical Toxicology, Institute of Experimental and Clinical Pharmacology and Toxicology, Center for Molecular Signaling (PZMS), Saarland University, Homburg, Germany

2 State Bureau of Criminal Investigation Schleswig-Holstein, Forensic Science Institute, Kiel, Germany

3 Institute of Forensic Medicine, Forensic Toxicology, Medical Center-University of Freiburg, Faculty of Medicine, University of Freiburg, Freiburg, Germany

4 Herrmann Staudinger Graduate School, University of Freiburg, Freiburg, Germany.

5 Department of Experimental and Clinical Pharmacology, Institute of Experimental and Clinical Pharmacology and Toxicology, Center for Molecular Signaling (PZMS), Saarland University, Homburg, Germany

*Corresponding author:*

*Markus R. Meyer*

*Department of Experimental and Clinical Toxicology*

*Institute of Experimental and Clinical Pharmacology and Toxicology, Center for Molecular Signaling (PZMS), Saarland University*

*66421 Homburg, Germany*

*E-mail address: markus.meyer@uks.eu*

*Phone: +49 6841 1626430*

**Abstract**

New psychoactive substances (NPS) are an issue of global concern posing a serious threat to the healthcare systems. Consumption of some NPS has been associated with toxic effects on the liver amongst others. However, data concerning their (cyto-)toxicity are usually not available. For a straightforward assessment of their cytotoxic potential, a simplified strategy measuring six different cytotoxicity indicating parameters simultaneously by a high content screening assay (HCSA) was developed. Its applicability was further investigated using nine NPS from heterogeneous chemical classes. HepG2 cells were incubated with NPS for 48 h at a low and high concentration (7.81 and 125  $\mu\text{M}$ ), respectively. To study metabolism-mediated effects on their cytotoxicity, cells were additionally incubated with the unspecific cytochrome (CYP) P450 inhibitor 1-aminobenzotriazole. Four fluorescence dyes were used to monitor cell count, nuclear size, and nuclear intensity (all Hoechst33342), mitochondrial membrane potential (TMRM), cytoplasmic calcium levels (CAL-520), and plasma membrane integrity (TOTO-3). Amongst the investigated NPS, ephylone, CUMYL-CBMICA, and dibutylone showed a strong cytotoxic potential, affecting two parameters at 7.81  $\mu\text{M}$ . 5-MeO-MiPT showed moderate effects by impairing one parameter at 7.81 and one at 125  $\mu\text{M}$ . Furthermore, at the high concentration of 5-MeO-MiPT, an effect of metabolism on cytotoxicity was observed. The HCSA confirmed the cytotoxic potential of ephylone and 5-MeO-MiPT, as the investigated concentrations were in the range of their published blood concentrations which induced liver damages after intake. The mitochondrial membrane potential was the parameter with the highest sensitivity and thus considered as suitable "cytobiomarker". In turn, parameters showing a high variability or unexpected effects such as cytosolic calcium levels and plasma membrane integrity might be omitted in the future. Even though 5-MeO-MiPT showed metabolism-based effects, HepG2 are known to have limited metabolic activity compared to cell lines such as HepaRG. Therefore, in further experiments cell lines with higher CYP-expression needs to be included and findings compared. Nevertheless, the simplified HCSA-based strategy allowed to screen NPS from diverse chemical groups for a first assessment of the cytotoxic properties of the parent compound. This information is crucial for a thorough risk assessment of NPS not only for public health authorities.

**Keywords**

High-content screening assay, cytotoxicity, HepG2, imaging, new psychoactive substances, metabolism-based effects

Journal Pre-proof

## 1 Introduction

New psychoactive substances (NPS) are an issue of global concern posing a considerable challenge to drug policies and a serious threat for drug users. During the last years, the number of fatalities attributed to NPS increased remarkably and at the same time, most NPS seemed to trigger more serious adverse effects than traditionally established recreational drugs such as amphetamine, heroin, and cannabis (Kronstrand et al. 2018). Aside from clinical features concerning the central nervous and cardiovascular system also toxic effects on the liver have been associated with the consumption of NPS (Kronstrand et al. 2018). Products containing NPS are easily accessible via Internet retailers selling new compounds as so-called “legal highs” or “research chemicals” (Brandt et al. 2014), yet data about their toxicity are only limited or nonexistent leading to an unknown risk for consumers. To date, no official guidelines for *in vitro* cytotoxicity testing are available neither e.g., by the US Food and Drug Administration nor the European Medicines Agency. However, different *in vitro* models have been used to study the potential hepatotoxicity of NPS using the human hepatoma cell lines HepG2 or HepaRG and primary human or rat hepatocytes (Dias da Silva et al. 2019; Richter et al. 2019; Roque Bravo et al. 2021a; Roque Bravo et al. 2021b). In most of these studies, various cytotoxic parameters such as cell proliferation, leakage of constituents from injured cells e.g., lactate dehydrogenase, changes in mitochondrial membrane homeostasis, cell death, or increase of reactive oxygen or nitrogen species were analyzed in separate experiments by manual measurements. In contrast, approaches based on automated methods such as high-content screening assays (HCSA) can analyze different parameters in a single run. Hence, HCSA are less prone to give false positive or negative results by monitoring multiple parameters and, additionally, less labor-intensive, time-consuming, and resource requiring, than manual and/or single assays (O'Brien and Edvardsson 2017; Richter et al. 2019). Another advantage of HCSA might be single-cell microscopic imaging, which allows spatial resolution of cells on subcellular levels during analysis. Thus, changes in intracellular processes caused by cytotoxicity can be directly monitored e.g., apoptosis can be visualized and artifacts reduced such as occurred from extracellular fluorescence (O'Brien and Edvardsson 2017). Recently, an optimized HCSA using a fully automated microscope has been shown to be suitable to study the hepatotoxic properties of three synthetic cannabinoids (SC) together with their metabolism-based effects (Gampfer et al. 2021). However, this HCSA showed some drawbacks regarding its time requirement and effective use of resources. For a first assessment of the cytotoxicity of NPS, a fast and unsophisticated approach is needed. Therefore, this work aimed to develop a simplified HCSA-based strategy for a straightforward cytotoxicity assessment of NPS. Its applicability should be tested on nine

NPS belonging to different chemical classes such as the SC 4CN-CUMYL-BINACA, also known as 4CN-CUMYL-BUTINCA and CUMYL-CBMICA, the cathinone derivatives dibutylone, ephylone, and 4-MEAP, as well as the tryptamines 5-MeO-MiPT and 5-MeO-DALT, and the phenylethylamines 25C-NBOMe and 25I-NBOMe. Chemical structures of the investigated NPS are depicted in Figure 1. As not only parent compounds may induce cytotoxic effects but also their metabolites, the impact of the CYP-dependent metabolism should also be investigated. Finally, the six investigated parameters, namely cell count, nuclear size, nuclear intensity, mitochondrial membrane potential, cytoplasmic calcium levels, and plasma membrane integrity should be evaluated in terms of their suitability as cytobiomarker (O'Brien and Edvardsson 2017) for a cytotoxicity assessment.

## 2 Materials and methods

### 2.1 Chemicals and reagents

4CN-CUMYL-BINACA (CAS number 1631074-54-8), CUMYL-CBMICA (CAS number 2571070-88-5), dibutylone HCl (CAS number 17763-12-1), and ephylone HCl (CAS number 17763-02-9) were provided by the EU-funded project ADEBAR plus (grant number IZ25-5793-2019-33) for research purposes. 5-MeO-MiPT (CAS number 96096-55-8) was purchased by Cayman Chemical (Ann Arbor, MI, USA). 5-MeO-DALT (CAS number 928822-98-4), 4-MEAP HCl (CAS number 18297-05-7), 25C-NBOMe HCl (CAS number 1539266-19-7), and 25I-NBOMe HCl (CAS number 1043868-97-8) were obtained from LGC Standards (Wesel, Germany). The purity of all investigated NPS was higher than 98%. Stock solutions of NPS (200-fold concentrated) were prepared in dimethyl sulfoxide (DMSO) and sterile filtered. Hoechst33342, RPMI 1640 medium with GlutaMAX supplement, sterile filters suitable for DMSO, and Tetramethylrhodamine methyl ester (TMRM) were purchased from Life Invitrogen (Darmstadt, Germany). TOTO-3 was bought from Fisher Scientific (Schwerte, Germany). 1-Aminobenzotriazole (ABT), disodium hydrogen phosphate ( $\text{Na}_2\text{HPO}_4$ ), DMSO, ethylenediaminetetraacetic acid (EDTA), magnesium chloride ( $\text{MgCl}_2$ ), penicillin, phosphate buffered saline (PBS), poly-L-lysine (PLL), potassium dihydrogen phosphate ( $\text{KH}_2\text{PO}_4$ ), sodium chloride (NaCl), streptomycin, and trypsin were supplied by Sigma-Aldrich (Taufkirchen, Germany). Calcium chloride ( $\text{CaCl}_2$ ), 4-(2-hydroxyethyl)-1-piperazineethanesulfonic acid (HEPES), potassium chloride (KCl) as well as the 96-well half area high content imaging plates were supplied by VWR International (Darmstadt, Germany). The 75 cm<sup>2</sup> culture flasks were bought from Sarstedt (Nümbrecht, Germany) and CAL-520

was from Biomol (Hamburg, Germany). Fetal bovine serum (FBS) was purchased from Corning (Amsterdam, The Netherlands) and HepG2 cells were provided by the German collection of microorganism and cell cultures (DSMZ, Braunschweig, Germany). Single stocks were cryopreserved and stored in liquid nitrogen at  $-160^{\circ}\text{C}$  until use.

## 2.2 Cell culture

Experiments were carried out using the hepatoblastoma-derived cell line HepG2 as it is widely used and useful model in terms of HCSA to predict human toxicology (O'Brien and Edvardsson 2017). Also it might have some shortcomings regarding the metabolic activity of some CYP enzymes (Hart et al. 2010), it has been successfully used in the past not only to study the cytotoxic properties of xenobiotics (O'Brien and Edvardsson 2017; O'Brien et al. 2006) but also of NPS such as SC or cathinones (Gampfer et al. 2021; Richter et al. 2019). Briefly, cells were cultured at  $37^{\circ}\text{C}$  with 95% humidity and 5%  $\text{CO}_2$  atmosphere in an incubator (Binder, Tuttlingen, Germany), as recently described (Gampfer et al. 2021). A laminar flow bench class II (Fisher Scientific, Schwerte, Germany) was used for handling the cells under sterile conditions. Briefly, cells were cultivated in RPMI medium supplemented with 100 U/mL penicillin, 100  $\mu\text{g}/\text{mL}$  streptomycin, and 10% FBS (supplemented RPMI medium) within 75  $\text{cm}^2$  culture flasks following the manufacturer's recommendations. Cells were passaged every 3-4 days using PBS (137 mM NaCl, 2.7 mM KCl, 1.5 mM  $\text{KH}_2\text{PO}_4$ , 8.1 mM  $\text{Na}_2\text{HPO}_4$ , pH 7.4) and 0.05% trypsin EDTA solution. Experiments were conducted with passage numbers four to seven.

## 2.3 Cell plate preparation

In accordance with a previous study (Gampfer et al. 2021), 96-well half area high content imaging plates were coated with 100  $\mu\text{L}$  aqueous PLL solution (100  $\mu\text{g}/\text{mL}$ ) and incubated for 30 min at room temperature ( $21^{\circ}\text{C}$ ). Thereafter, plates were washed once with 150  $\mu\text{L}$  autoclaved water and twice with 150  $\mu\text{L}$  supplemented RPMI medium. Cells were counted by a hemocytometer (Carl Roth, Karlsruhe, Germany) and seeded in a density of 1750 cells/well by adding 100  $\mu\text{L}$  of the cell suspension to the precoated well plates. After incubation for 24 h at  $37^{\circ}\text{C}$  with 95% humidity and 5%  $\text{CO}_2$  atmosphere cell plates were prepared for drug treatment.

## 2.4 Drug preparation and treatment

Based on a recent study (Gampfer et al. 2021), dilutions of the NPS stock solutions with and without ABT were freshly prepared in tubes with supplemented RPMI medium (final concentrations 7.81 and 125  $\mu\text{M}$  NPS and 100  $\mu\text{M}$  ABT). The concentration of 100  $\mu\text{M}$  ABT was based on a CYP activity experiment using HepaRG cells (Yokoyama et al. 2018). A volume of 75  $\mu\text{L}$  of the supernatants was removed from the cell plates and 50  $\mu\text{L}$  of the NPS solution was added. Moreover, each cell plate contained wells without NPS but 0.5% DMSO in supplemented RPMI medium (blank) and with additional ABT (negative control) to assess any effects on the parameters derived therefrom. After incubation for 48 h at 37°C with 95% humidity and 5%  $\text{CO}_2$  atmosphere, the supernatants were removed and 75  $\mu\text{L}$  of a fluorescence dyes cocktail including 0.8  $\mu\text{M}$  Hoechst33342, 1  $\mu\text{M}$  CAL-520, 20 nM TMRM, and 1  $\mu\text{M}$  TOTO-3 in supplemented RPMI medium were added. Cell plates were incubated protected from light for 1 h at 37°C with 95% humidity and 5%  $\text{CO}_2$  atmosphere before washing the cells three times with 50  $\mu\text{L}$  ringer solution (140 mM NaCl, 2.8 mM KCl, 2 mM  $\text{MgCl}_2$ , 1 mM  $\text{CaCl}_2$ , 10 mM HEPES, pH 7.4). The last 50  $\mu\text{L}$  remained on the cells during measurement. All incubations were done fivefold.

## 2.5 Microscope parameters

Cell plates were measured with a Lionheart FX Automated Microscope (BioTek, BT, Bad Friedrichshall, Germany) equipped with an environmental control cover. During image acquisition, the incubation conditions were kept constant at 37°C without extra  $\text{CO}_2$ . Microplate lids were left on the cell plates to prevent evaporation. The 20x/0.45 (semi-apochromat) objective was used for image recording. Each dye was excited and its fluorescence was recorded at excitation and emission wavelengths of 377 and 447 nm for Hoechst33342, 469 and 525 nm for CAL-520, 531 and 593 nm for TMRM, and 628 and 685 nm for TOTO-3. In the process, Hoechst33342 was captured in the first channel by the autofocus mode followed by CAL-520, TMRM, and TOTO-3. The following camera settings were used: camera gain, 24 dB; LED value, 1 (Hoechst33342 and CAL-520) and 2 (TMRM and TOTO-3); integration time (IT), Hoechst33342, 240 ms; TMRM, 1000 ms; CAL-520, 300 ms; TOTO-3, 600 ms. The IT was checked before measuring the cell plate by blanks and, if necessary adapted. Six images per well were recorded in two rows and three columns with a gap of 500  $\mu\text{m}$  in between. Each compound was measured within 60 min.

## 2.6 Data capture and image analysis

The following data were collected for each image using the BT Gen5 Image Prime 3.09 software: number and average area of objects recorded with Hoechst33342 as well as its total fluorescence intensity were used to assess cell count, nuclear size, and nuclear intensity; CAL-520 total fluorescence intensity was defined as intracellular calcium levels; mitochondrial membrane potential was measured as total fluorescence intensity of TMRM; the plasma membrane integrity was monitored by TOTO-3 total fluorescence intensity. All images were analyzed by applying pre-processing filters and intensity thresholds to define nuclei as individual units or regions of interest. Afterwards, images were manually inspected by the nuclei fluorescence Hoechst33342 to identify and exclude images containing a blurriness or artifacts if necessary. Thereafter, an average value of each parameter per well was automatically calculated based on the remaining number of images. Total fluorescence intensities of Hoechst33342, CAL-520, TMRM, and TOTO-3 were normalized by dividing through the number of objects per well. After the data were transferred to Microsoft Excel 2016 (Microsoft Corporation, WA, USA), the number of objects was normalized to the number of used images per well.

## 2.7 Statistical analysis

Data are presented as mean  $\pm$  standard error of the mean (SEM) and statistical analysis was performed by GraphPad Prism 5.00 (GraphPad Software, San Diego, CA, USA). A one-way ANOVA followed by Tukey's post hoc test was used with a significance level of 0.05 (95% confidence interval) to compare blank incubations with all other incubations and pure NPS incubations with the same concentrated NPS incubations containing additional ABT.

## 2.8 Relevance of the concentration and criteria for evaluation of cytotoxic potential

Cytotoxic potentials of drugs should be estimated based on maximum serum concentrations ( $C_{\max}$ ), amongst others (O'Brien and Edvardsson 2017). However,  $C_{\max}$  values for NPS are usually not available as controlled human studies are not feasible due to ethical concerns. Even intracellular concentrations of NPS are usually not published. For selection of the investigated NPS concentrations, published plasma/blood concentrations of case reports were considered for 4CN-CUMYL-BINACA (0.001 – 0.094  $\mu\text{M}$ ) (Yeter 2017), dibutylone (0.037 – 5.1  $\mu\text{M}$ ) (Krotulski et al. 2018), ephylone (0.035 – 9.5  $\mu\text{M}$ ) (Giachetti et al. 2020), 5-MeO-MiPT (0.650 – 13.7  $\mu\text{M}$ ) (Grafinger et al. 2017), 25C-NBOMe (0.008  $\mu\text{M}$ ) (Morini et al. 2017), and 25I-NBOMe (0.001 – 0.073  $\mu\text{M}$ ) (Hermanns-Clausen et al. 2017; Poklis et

al. 2014). No case reports with plasma/blood concentrations were available for CUMYL-CBMICA, 4-MEAP, and 5-MeO-DALT. Final assessment criteria for cytotoxic potential were as follows (Gampfer et al. 2021): when at least two parameters showed significant changes at a concentration of 7.81  $\mu\text{M}$ , a strong cytotoxic potential was observed; when two parameters were significantly affected and one of them at the low concentration (7.81  $\mu\text{M}$ ) a moderate cytotoxic potential was observed; no cytotoxic potential was observed when only one parameter was impaired or several ones but only at a high concentration (125  $\mu\text{M}$ ).

### **3 Results and Discussion**

#### **3.1 Assessment of NPS cytotoxic potential using a simplified high content screening assay**

Cytotoxicity assessments of NPS were previously performed by a prescreening using two different NPS concentrations followed by a screening in a full concentration range for compounds with a positive cytotoxic prescreening (Gampfer et al. 2021). This strategy seems to be too resource-intensive and time-consuming for a rough assessment of cytotoxic characteristics, considering the dynamic shifts of NPS on the drug market. Therefore, experiments were carried out incubating HepG2 cells only at one low and one high NPS concentration. Even though it is expected that plasma/blood concentration for all the investigated NPS at least vary between different classes, we selected for all compounds the same test concentrations to allow a first straightforward estimation of a cytotoxic potential. However, in some cases a screening using a lower concentration range might be useful to gain a deeper insight.

Four fluorescence stains were used targeting different cellular marker to visualize changes on six cytobiomarker caused by NPS. Hoechst33342, a cell-permeable fluorescent dye specifically stains the nuclei of living cells. Thus, it is appropriate to monitor the total cell number as well as morphological changes at the nucleus induced by xenobiotics such as apoptosis or necrosis. Apoptosis has been characterized by an active, programmed process of autonomous cellular breakdown that avoids eliciting inflammation by cytoplasmic shrinkage, nuclear condensation, and controlled cleavage of DNA by the endonucleases. By contrast, a necrosis is described as passive, accidental cell death resulting from environmental perturbations with uncontrolled release of inflammatory cellular contents (Fink and Cookson 2005). Increasing or decreasing fluorescence signals of Hoechst33342 and a reduction or increase of nuclei volume may indicate such events. Additionally, xenobiotics may interact with DNA, which may

result in a decreasing fluorescence intensity, if Hoechst33342 and the xenobiotic compete for the same binding site at the DNA double strand (O'Brien and Edvardsson 2017).

The mitochondrial membrane potential generated by proton pumps is an essential component in the process of energy storage during oxidative phosphorylation. Together with the proton gradient, the mitochondrial membrane potential forms the transmembrane potential of hydrogen ions which is required to produce ATP (Zorova et al. 2018). TMRM is a lipophilic cationic dye which loads specifically into negative charged areas of the cell such as the mitochondria. If there is a malfunction in mitochondrial membrane potential, less TMRM accumulates, which led to a decreasing fluorescence signal of TMRM. An increasing TMRM signal has been associated with drugs that may be substrates for the p-glycoprotein (O'Brien and Edvardsson 2017).

Intracellular calcium signaling regulates numerous basic cellular processes including proliferation, differentiation, and cellular motility. Cells generate calcium signals by using both internal and external sources of calcium. The internal calcium storage is located within the membrane of the endoplasmic reticulum and sarcoplasmic reticulum. When stimuli such as xenobiotics binds to cell surface receptors (e.g., G-protein-coupled receptors), calcium is released from the internal stores through various channels, including inositol 1, 4, 5-trisphosphate receptor and members from ryanodine receptor families (Liao et al. 2021). Equally, an influx of calcium from the extracellular space is possibly caused by membrane-perturbing substances as there is a 10,000-fold gradient across the plasma membrane (O'Brien and Edvardsson 2017). Disturbance of this gradient may lead to dysfunction, activation of degenerative enzymes, and cell loss (Weber 2012). The calcium-binding dye CAL-520 consists of lipophilic blocking groups, enabling the dye to diffuse through the cell membrane. Once inside the cell, these lipophilic groups are cleaved by esterases, resulting in a negatively charged dye which is trapped inside the cell. As Hoechst33342, TOTO-3 binds to nucleic acid with the difference that it is cell-impermeable for healthy cells. If a damage occurs on the cell membrane, it could pass through and bind to double- and single-stranded DNA. Therefore, increased fluorescence signals of TOTO-3 are an indicator of apoptosis. In general, changes on parameters may undergo natural fluctuations as a response to other factors such as oxidative stress, however, this should not affect the outcome by treating negative control incubations like NPS incubations. Results of the HCSA, determined after incubating the cells for 48 h with ephylone (a), CUMYL-CBMICA (b), dibutylone (c), 5-MeO-MiPT (d), 4CN-CUMYL-BINACA (g), 5-MeO-DALT (h), and 4-MEAP (i) at concentrations of 7.81 and 125  $\mu$ M are shown in Figure 2 (a) – (i). According to

the assessment criteria stated above, a high cytotoxic potential was observed for ephylone, CUMYL-CBMICA, and dibutylone. The term “strong cytotoxic potential” used to classify the results from this *in vitro* assay refers to the highest probability of a cytotoxic effect *in vivo* for the respective compound. It should be noted that the *in vivo* cytotoxicity depends aside from the applied dose on several other toxicokinetic parameters e.g., adsorption, distribution, metabolism, and excretion. Such data are usually limited for NPS.

Ephylone induced a decrease in mitochondrial membrane potential and intracellular calcium concentrations at the low concentration as well as an increase in the cell count and reduction of the nuclear size at the high concentration, as depicted in Figure 3. Concerning the increased cell count of ephylone, variations during cell seeding could result in a low cell count in the blank incubations. Furthermore, reduced intracellular calcium concentrations were not expected. Instead, a decrease should have appeared with increasing cell damage through extracellular influx or release from intracellular compartments. This phenomenon has also already been observed earlier and might be explained by the active removal of CAL-520 via transport out of living cells (Richter et al. 2019).

The parameters, which were significantly affected by CUMYL-CBMICA at the low concentration included a decrease in the nuclear intensity, mitochondrial membrane potential, and intracellular calcium levels. However, the two latter parameters were not significantly changed at the high concentration. A decrease in nuclear intensity at 7.81  $\mu\text{M}$  could be due to intercalation of CUMYL-CBMICA into DNA and competition for the binding sites at the nucleic acid between the DNA stain Hoechst33342 and CUMYL-CBMICA. Such effects have also been observed for doxorubicin (O'Brien and Edvardsson 2017) or other SC (Gampfer et al. 2021). By contrast, a rise of the nuclear intensity at 125  $\mu\text{M}$  compared to 7.81  $\mu\text{M}$  could be explained by increasing chromatin condensation.

In terms of dibutylone, a dysfunction of the mitochondrial membrane potential and shrinkage of the nuclear size was induced at 7.81  $\mu\text{M}$ . The only slightly affected nuclear size at the low concentration might explain why no significant effects were measured at the high concentration.

For 5-MeO-MiPT a moderate cytotoxic potential was determined as the mitochondrial membrane homeostasis was significantly impaired at the low concentration and size increase of the nuclei was observed at 125  $\mu\text{M}$ . The NBOMe derivatives 25C-NBOMe and 25I-NBOMe strongly reduced the cell count at 125  $\mu\text{M}$ , thus no final cytotoxic potential could be assessed due to the lack of normalization. The increased mitochondrial membrane potential after 25C-NBOMe treatment at 125  $\mu\text{M}$  compared to the

decrease at the same concentration for 25I-NBOME might be an artifact caused by the low number of viable cells at this concentration. To further investigate these compounds, studies either after increasing the number of seeded cell or adjusting the highest test concentration to 50  $\mu\text{M}$  might be possible. However, published blood/plasma concentrations of the NBOME (0.87 – 73 nM) were far below the test concentrations (Poklis et al. 2014)

Incubations of 4CN-CUMYL-BINACA, 5-MeO-DALT, and 4-MEAP did not lead to findings indicating cytotoxic potential according to the defined criteria, although all of them affected the mitochondrial membrane potential at a low or in the case of 5-MeO-DALT at a high concentration. Additionally, 5-MeO-DALT increased the nuclear size but only at 125  $\mu\text{M}$ .

To date, none of the studied NPS has been analyzed for its hepatotoxic potential *in vitro*, but liver damage e.g., abnormal increase in liver size or liver transaminases, associated with their intake has been reported for some of them such as ephylone and 25I-NBOME (Costa et al. 2019; Thirakul et al. 2017; Wood et al. 2015; Zawilska et al. 2020). Furthermore, after intravenous application of 5-MeO-MiPT to mice at 0.27 and 2.7 mg/kg, acute toxicity to the liver was induced at 2.7 mg/kg (Altunci et al. 2021). Taking that into account along with the published plasma/blood concentrations, users consuming high doses of NPS are generally expected to be at high risk for hepatotoxicity. Also the simultaneous use of multiple NPS or a single NPS along with other drugs of abuse, as is often seen in clinical cases, may also increase the risk (Supervia et al. 2021).

### 3.2 Metabolism-based effects on the cytotoxicity

Cytotoxic effects may on the one hand be induced by the parent compound but on the other hand also by its metabolites. Therefore, the non-specific CYP inhibitor ABT was used to investigate CYP-dependent cytotoxic effects. Results obtained after incubation under the same conditions as described in section 3.1 but with addition of 100  $\mu\text{M}$  ABT are shown in Figure 2 (a) – (i). A significant change of the mitochondrial membrane potential was already observed in some ABT blank incubations, which may lead to the conclusion that ABT itself has already an effect on this parameter. Thus, the mitochondrial membrane potential may be inappropriate to monitor CYP-dependent effects via ABT. This effect on the cells may be explained as follows: CYP enzymes are membrane-bound heme-containing monooxygenases localized in mitochondria among others, while ABT acts as CYP enzyme blocker by forming adducts with this heme molecule (de Montellano 2018). Structural alterations of this heme

molecules in the mitochondria may explain the dysregulated mitochondrial membrane potential after ABT treatment.

5-MeO-MiPT was the only compound for which an effect of ABT could be observed on cytotoxicity indicating parameters. The nuclei were significantly increased at 125  $\mu$ M without ABT compared to incubations with ABT. Additionally, the nuclear intensity was significantly reduced in incubations at 125  $\mu$ M 5-MeO-MiPT plus ABT in comparison to incubations without ABT. All other tested NPS showed no significant changes of parameters. Similar studies on metabolism-based effects of three SC using HepG2 cells revealed that only JWH-200 caused a loss of plasma membrane integrity at 125  $\mu$ M with ABT compared to incubations without ABT (Gampfer et al. 2021).

One possible reason for this minor impact of CYP metabolism on the cytotoxicity might be that the metabolites formed are as toxic as their corresponding parent compounds. As mentioned above, HepG2 are limited in their metabolic capacity as e.g., demonstrated in a comparative study using HepG2, HepaRG, and cryopreserved human hepatocytes. HepG2 showed almost no basal drug metabolizing enzyme activities except for CYP2D6, CYP3A4, and UGT enzymes. Thus, HepaRG cells should be the best suited model for metabolism-based cytotoxicity screenings in general, as they express CYP enzymes without the major drawback of inter-individual variability as demonstrated for primary human hepatocytes (Yokoyama et al. 2018). However, HepaRG cells are more laborious as cell culture, hard to cultivate, and much expensive than HepG2 cells. Therefore, further studies should consider cell lines with CYP-expressing levels comparable to human hepatocytes such as HepaRG or alternatively CYP-overexpressing HepG2 cells and data compared (Chen et al. 2021). These studies should also include a more detailed investigation of the impact of ABT on the metabolism of the used cell lines e.g., by using different pre incubation times and different ABT concentrations as well as positive controls with known metabolic activation.

### **3.3 Evaluation of parameters**

The mitochondrial membrane potential was confirmed as the most sensitive biomarker and thus as most reliable indicator of potential cytotoxicity in a general screening as indicated in earlier studies (Gampfer et al. 2021; Richter et al. 2019). For assessments of the CYP-dependent metabolism on the cytotoxicity, this parameter seemed to be less suited as ABT already showed an effect even in blank incubations. All other parameters were only significantly affected by one or two out of nine NPS, respectively. Overall,

this might be due to that a longer incubation period of 72 h has been found to give higher sensitivity (O'Brien and Edvardsson 2017). However, a 72 h-treatment led to a non-reproducible cell growth and multilayer formations. Therefore, the incubation time was reduced from 72 h to 48 h (Gampfer et al. 2021).

The comparable high variation within the cell count might be explained by a too small number of seeded cells or an inhomogeneous cell suspension during seeding. Such a high variation also effects in turn the significance of other parameters, due their normalization to the cell count. Nonetheless, strong and robust effects can and could still be observed e.g., in case of the NBOMe compounds.

In terms of the nuclear size, one reason for few significant findings could be that the automated software sometimes had difficulties detecting two or more attached cells as individual ones, therefore, in some cases, the given cell area was measured larger as it should be. However, the nuclear size seems suitable as significant effects could be measured e.g., in case of ephylone.

Also the nuclear intensity could be considered as an appropriate biomarker of cytotoxicity. By monitoring the plasma membrane integrity, one significant result was observed, however, this was considered a false-positive result, as a declined fluorescence intensity of TOTO-3 in NPS incubations would imply a less damaged plasma membrane compared to blank incubations.

Based on these findings and similar observations from previous works (Gampfer et al. 2021; Richter et al. 2019), parameters showing a high variability or not reproducible results, seemed less suitable to monitor a possible cytotoxicity. Thus, these parameters may be omitted in future experiments. Consequently, evaluation criteria for a possible cytotoxicity must be adjusted, such as the criteria for a strong cytotoxic potential could be adopted from the current moderate cytotoxic classification (two affected parameters, one at high and one at a low concentration). For a moderate cytotoxic potential, at least one parameter should be affected at the low concentration. Additionally, costs and time could be saved by omitting two fluorescence dyes for the HCSA.

#### **4. Conclusions**

A simplified HCSA-based approach was developed and tested using nine NPS from various chemical classes. A strong cytotoxic potential was observed for ephylone, CUMYL-CBMICA, and dibutylone. 5-MeO-MiPT showed a moderate effect. An intake of ephylone and 5-MeO-MiPT was previously associated with liver injury such as an abnormal increase in liver size or in liver transaminases and

apoptosis through caspase-8 activity. Additionally, 5-MeO-MiPT + ABT incubations indicated a CYP-mediated cytotoxicity. The mitochondrial membrane potential was the parameter with the highest sensitivity and thus considered as suitable cytobiomarker and the cytosolic calcium levels and plasma membrane integrity might be omitted as cytobiomarker in the future. Further experiments should include cell lines with CYP- expressing levels comparable to human hepatocytes such as HepaRG or alternatively CYP-overexpressing HepG2 cells.

### **Acknowledgements**

We would like to thank the EU funded Project ADEBAR plus (grant no.: IZ25-5793-2019-33) for the supply of chemical standards as well as Carsten Schröder, Gabriele Ulrich, and Ute Soltek for their support and Matthias J. Richter for proofreading. We acknowledge support by the Deutsche Forschungsgemeinschaft (DFG, German Research Foundation) SFB 894 (V.F.).

### **Declaration of competing interest**

The authors declare that they have no known competing financial interests or personal relationships that could have influenced the work reported in this paper.

## References

- Altunci YA, Aydogdu M, Acikgoz E, et al. (2021) New Psychoactive Substance 5-MeO-MiPT In vivo Acute Toxicity and Hystotoxicological Study. *Balkan Med J* 38(1):34-42 doi:10.4274/balkanmedj.galenos.2020.2019.11.68
- Brandt SD, King LA, Evans-Brown M (2014) The new drug phenomenon. *Drug Test Anal* 6(7-8):587-97 doi:10.1002/dta.1686
- Chen S, Wu Q, Li X, et al. (2021) Characterization of cytochrome P450s (CYP)-overexpressing HepG2 cells for assessing drug and chemical-induced liver toxicity. *J Environ Sci Health C Toxicol Carcinog* 39(1):68-86 doi:10.1080/26896583.2021.1880242
- Costa JL, Cunha KF, Lanaro R, Cunha RL, Walther D, Baumann MH (2019) Analytical quantification, intoxication case series, and pharmacological mechanism of action for N-ethylnorpentylone (N-ethylpentylone or ephylone). *Drug Test Anal* 11(3):461-471 doi:10.1002/dta.2502
- de Montellano PRO (2018) 1-Aminobenzotriazole: A Mechanism-Based Cytochrome P450 Inhibitor and Probe of Cytochrome P450 Biology. *Med Chem (Los Angeles)* 8(3) doi:10.4172/2161-0444.1000495
- Dias da Silva D, Ferreira B, Roque Bravo R, et al. (2019) The new psychoactive substance 3-methylmethcathinone (3-MMC or metaphedrone) induces oxidative stress, apoptosis, and autophagy in primary rat hepatocytes at human-relevant concentrations. *Arch Toxicol* 93(9):2617-2634 doi:10.1007/s00204-019-02539-x
- Fink SL, Cookson BT (2005) Apoptosis, pyroptosis, and necrosis: mechanistic description of dead and dying eukaryotic cells. *Infect Immun* 73(4):1907-16 doi:10.1128/IAI.73.4.1907-1916.2005
- Gampfer TM, Wagmann L, Belkacemi A, Flockerzi V, Meyer MR (2021) Cytotoxicity, metabolism, and isozyme mapping of the synthetic cannabinoids JWH-200, A-796260, and 5F-EMB-PINACA studied by means of in vitro systems. *Arch Toxicol* 95(11):3539-3557 doi:10.1007/s00204-021-03148-3
- Giachetti AD, Kahl JH, Zaney ME, Hime GW, Boland DM (2020) Method Validation of Seven Synthetic Cathinones by LC-MS/MS Analysis and the Prevalence of N-Ethylpentylone in Postmortem Casework. *J Anal Toxicol* doi:10.1093/jat/bkaa194
- Grafinger KE, Hadener M, Konig S, Weinmann W (2017) Study of the in vitro and in vivo metabolism of the tryptamine 5-MeO-MiPT using human liver microsomes and real case samples. *Drug Test Anal* doi:10.1002/dta.2245
- Hart SN, Li Y, Nakamoto K, Subileau EA, Steen D, Zhong XB (2010) A comparison of whole genome gene expression profiles of HepaRG cells and HepG2 cells to primary human hepatocytes and human liver tissues. *Drug Metab Dispos* 38(6):988-94 doi:10.1124/dmd.109.031831
- Hermanns-Clausen M, Angerer V, Kithinji J, Grumann C, Auwarter V (2017) Bad trip due to 25I-NBOMe: a case report from the EU project SPICE II plus. *Clin Toxicol (Phila)* 55(8):922-924 doi:10.1080/15563650.2017.1319572
- Kronstrand R, Guerrieri D, Vikingsson S, Wohlfarth A, Green H (2018) Fatal Poisonings Associated with New Psychoactive Substances. *Handb Exp Pharmacol* 252:495-541 doi:10.1007/164\_2018\_110
- Krotulski AJ, Mohr ALA, Papsun DM, Logan BK (2018) Dibutylone (bk-DMBDB): Intoxications, Quantitative Confirmations and Metabolism in Authentic Biological Specimens. *J Anal Toxicol* 42(7):437-445 doi:10.1093/jat/bky022
- Liao J, Patel D, Zhao Q, Peng R, Guo H, Diwu Z (2021) A novel Ca(2+) indicator for long-term tracking of intracellular calcium flux. *Biotechniques* 70(5):271-277 doi:10.2144/btn-2020-0161
- Morini L, Bernini M, Vezzoli S, et al. (2017) Death after 25C-NBOMe and 25H-NBOMe consumption. *Forensic Sci Int* 279:e1-e6 doi:10.1016/j.forsciint.2017.08.028
- O'Brien PJ, Edvardsson A (2017) Validation of a Multiparametric, High-Content-Screening Assay for Predictive/Investigative Cytotoxicity: Evidence from Technology Transfer Studies and Literature Review. *Chem Res Toxicol* 30(3):804-829 doi:10.1021/acs.chemrestox.6b00403
- O'Brien PJ, Irwin W, Diaz D, et al. (2006) High concordance of drug-induced human hepatotoxicity with in vitro cytotoxicity measured in a novel cell-based model using high content screening. *Arch Toxicol* 80(9):580-604 doi:10.1007/s00204-006-0091-3
- Poklis JL, Devers KG, Arbefeville EF, Pearson JM, Houston E, Poklis A (2014) Postmortem detection of 25I-NBOMe [2-(4-iodo-2,5-dimethoxyphenyl)-N-[(2-methoxyphenyl)methyl]ethanamine] in fluids and tissues determined by high performance liquid chromatography with tandem mass spectrometry from a traumatic death. *Forensic Sci Int* 234:e14-20 doi:10.1016/j.forsciint.2013.10.015

- Richter LHJ, Beck A, Flockerzi V, Maurer HH, Meyer MR (2019) Cytotoxicity of new psychoactive substances and other drugs of abuse studied in human HepG2 cells using an adopted high content screening assay. *Toxicol Lett* 301:79-89 doi:10.1016/j.toxlet.2018.11.007
- Roque Bravo R, Carmo H, Valente MJ, et al. (2021a) 4-Fluoromethamphetamine (4-FMA) induces in vitro hepatotoxicity mediated by CYP2E1, CYP2D6, and CYP3A4 metabolism. *Toxicology* 463:152988 doi:10.1016/j.tox.2021.152988
- Roque Bravo R, Carmo H, Valente MJ, et al. (2021b) From street to lab: in vitro hepatotoxicity of buphedrone, butylone and 3,4-DMMC. *Arch Toxicol* 95(4):1443-1462 doi:10.1007/s00204-021-02990-9
- Supervia A, Ibrahim-Achi D, Miro O, et al. (2021) Impact of co-ingestion of ethanol on the clinical symptomatology and severity of patients attended in the emergency department for recreational drug toxicity. *Am J Emerg Med* 50:422-427 doi:10.1016/j.ajem.2021.08.046
- Thirakul P, L SH, K LB, J MP (2017) Clinical Presentation, Autopsy Results and Toxicology Findings in an Acute N-Ethylpentylone Fatality. *J Anal Toxicol* 41(4):342-346 doi:10.1093/jat/bkx004
- Weber JT (2012) Altered calcium signaling following traumatic brain injury. *Front Pharmacol* 3:60 doi:10.3389/fphar.2012.00060
- Wood DM, Sedefov R, Cunningham A, Dargan PI (2015) Prevalence of use and acute toxicity associated with the use of NBOMe drugs. *Clin Toxicol (Phila)* 53(2):85-92 doi:10.3109/15563650.2015.1004179
- Yeter O (2017) Identification of the Synthetic Cannabinoid 1-(4-cyanobutyl)-N-(2-phenylpropan-2-yl)-1H-indazole-3-carboxamide (CUMYL-4CN-BINACA) in Plant Material and Quantification in Post-Mortem Blood Samples. *J Anal Toxicol* 41(9):720-728 doi:10.1093/jat/bkx061
- Yokoyama Y, Sasaki Y, Terasaki N, et al. (2018) Comparison of Drug Metabolism and Its Related Hepatotoxic Effects in HepaRG, Cryopreserved Human Hepatocytes, and HepG2 Cell Cultures. *Biol Pharm Bull* 41(5):722-732 doi:10.1248/bpb.b17-00913
- Zawilska JB, Kacela M, Adamowicz P (2020) NBOMes-Highly Potent and Toxic Alternatives of LSD. *Front Neurosci* 14:78 doi:10.3389/fnins.2020.00078
- Zorova LD, Popkov VA, Plotnikov EY, et al. (2018) Mitochondrial membrane potential. *Anal Biochem* 552:50-59 doi:10.1016/j.ab.2017.07.009

## Legends to the figures

**Figure 1** Chemical structures of the investigated NPS.

**Figure 2** Dose-response plots of CUMYL-CBMICA (a), dibutylone (b), ephylone (c), 5-MeO-MiPT (d), 25C-NBOMe (e), 25I-NBOMe (f), 4CN-CUMYL-BINACA (g), 5-MeO-DALT (h), and 4-MEAP (i) obtained after incubation of HepG2 cells with NPS for 48 h in a low (7.81  $\mu$ M) and high (125  $\mu$ M) concentration and blank incubations without NPS both without (white bars) and with (grey bars) the cytochrome P450-inhibitor 1-aminobenzotriazol (ABT), respectively. Changes in different parameters (cell count, nuclear size, nuclear intensity, mitochondrial membrane potential, cytosolic calcium levels, and plasma membrane integrity) are plotted as absolute values. All parameters were normalized to the cell count except the cell count, which was normalized to the number of appropriate images. Values are expressed as mean  $\pm$  standard error of the mean (SEM; n = 5). Statistical analysis was done using one-way ANOVA followed by Tuckey's post-hoc test (\*\*\*,  $P < 0.001$ , \*\*,  $P < 0.01$ , \*,  $P < 0.05$  blank incubations without NPS and ABT versus all other incubations;  $^{\circ\circ}$ ,  $P < 0.01$ ,  $^{\circ}$ ,  $P < 0.05$  NPS incubations versus NPS incubations plus ABT at the same concentration). Norm. Fluor. Inten., normalized fluorescence intensity.

**Figure 3** Merged multifluorescence images of HepG2 cells obtained after 48 h exposure without NPS and ABT (blank) (a) and ephylone at 7.81 (b) or 125  $\mu$ M (c). Cell nuclei are stained blue (Hoechst33342). Mitochondrial membrane potential is depicted in orange (TMRM). Cytosolic calcium is represented by green (CAL-520) and damage on the plasma membrane is shown in magenta/pink (TOTO-3).

Fig 1

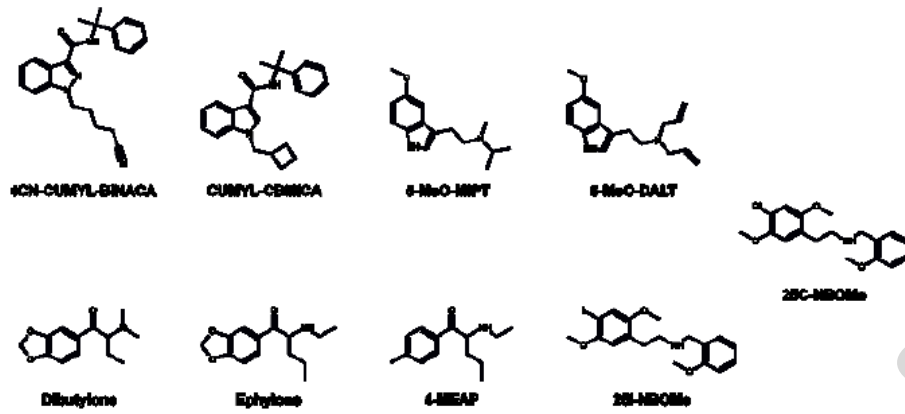
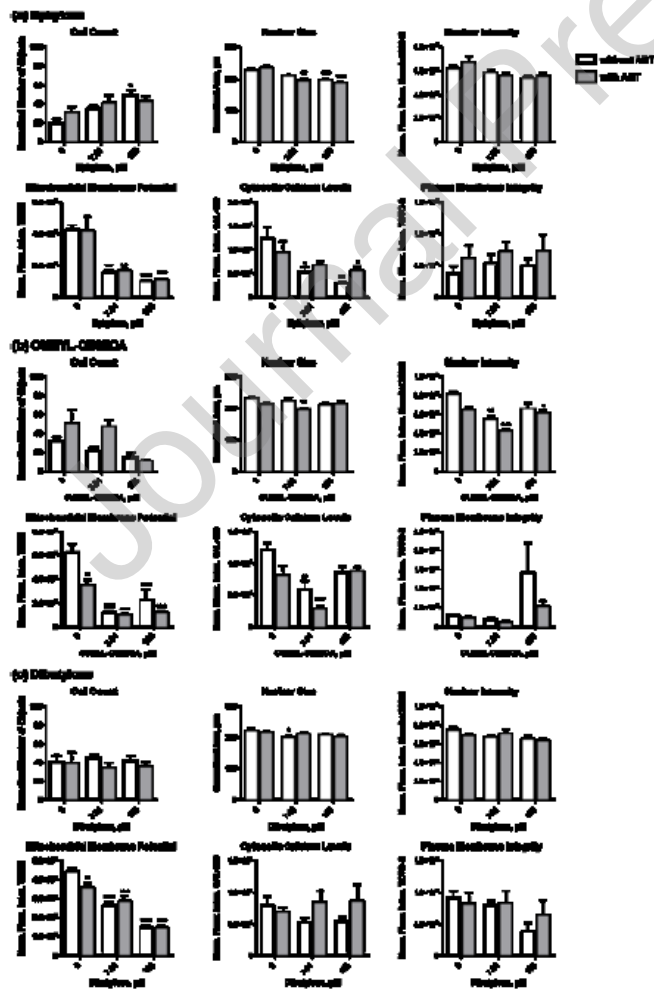
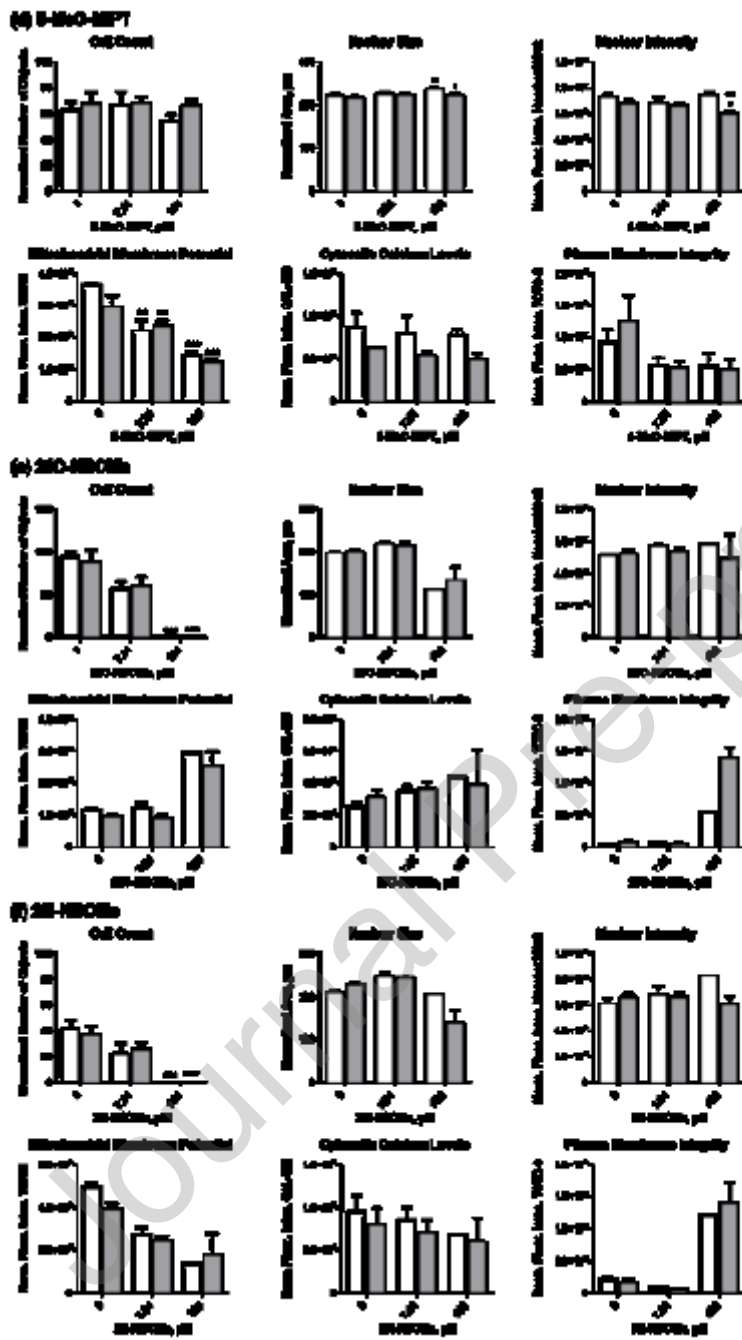


Fig 2 a



b)



c)

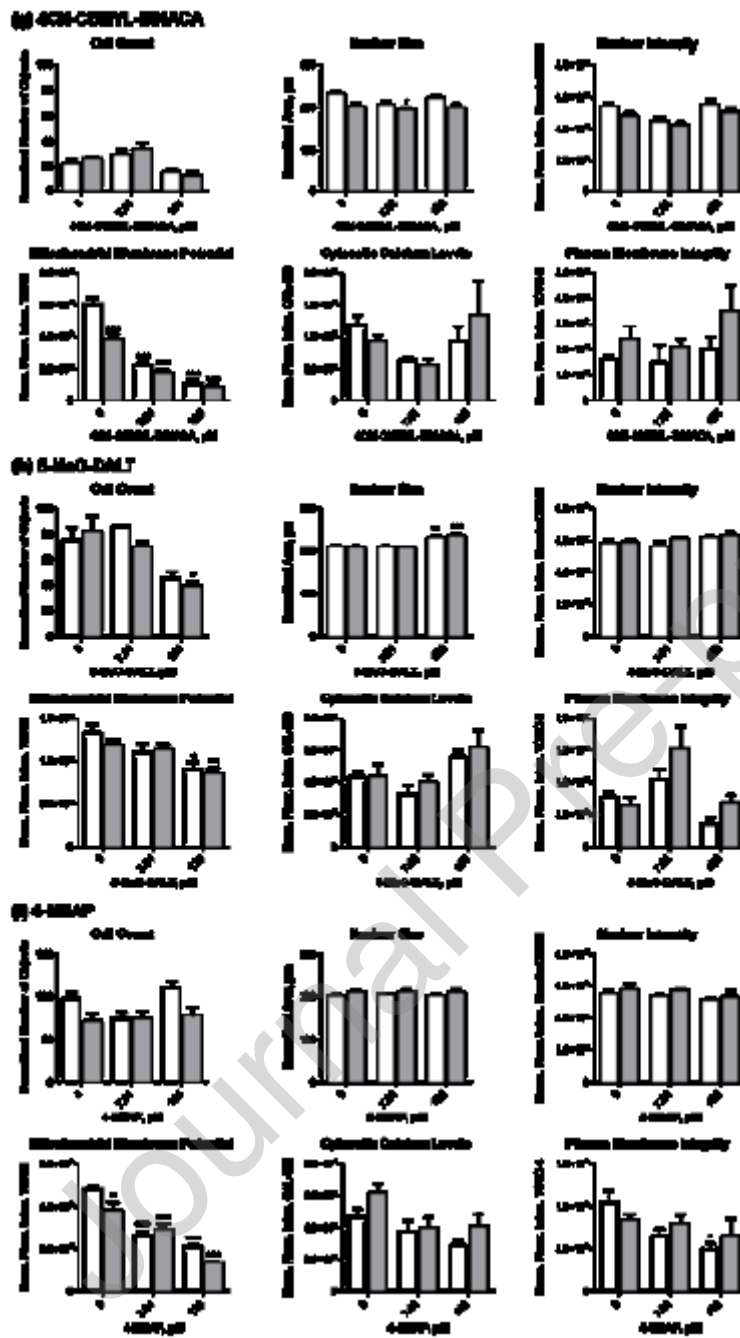
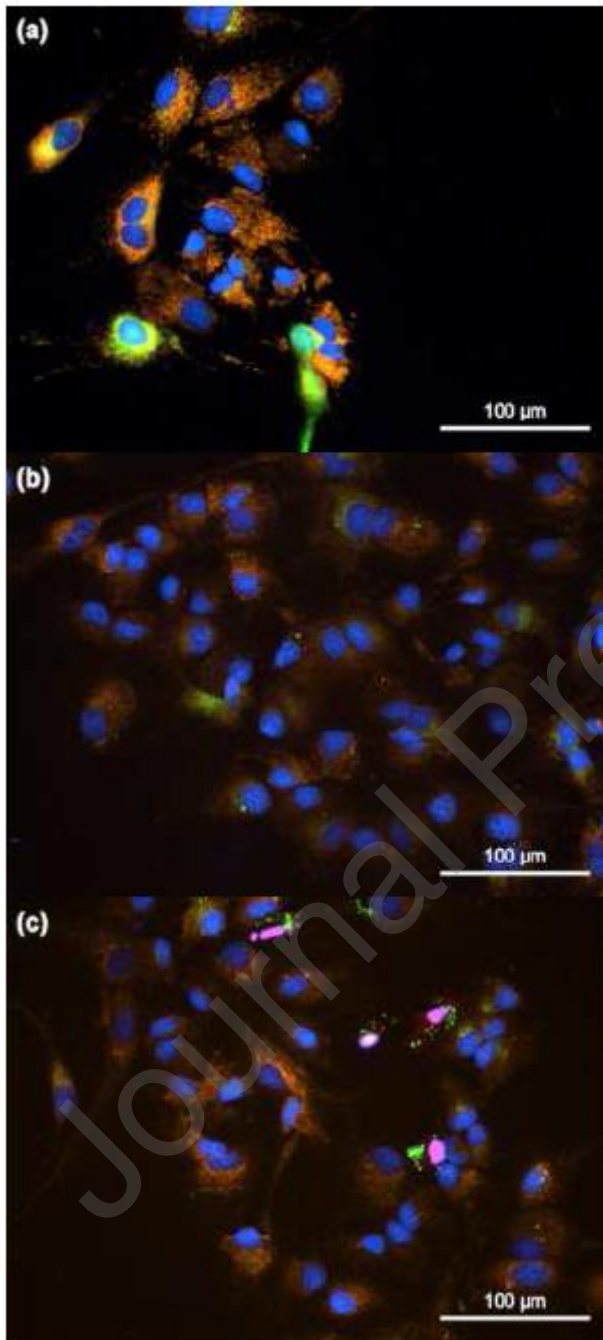
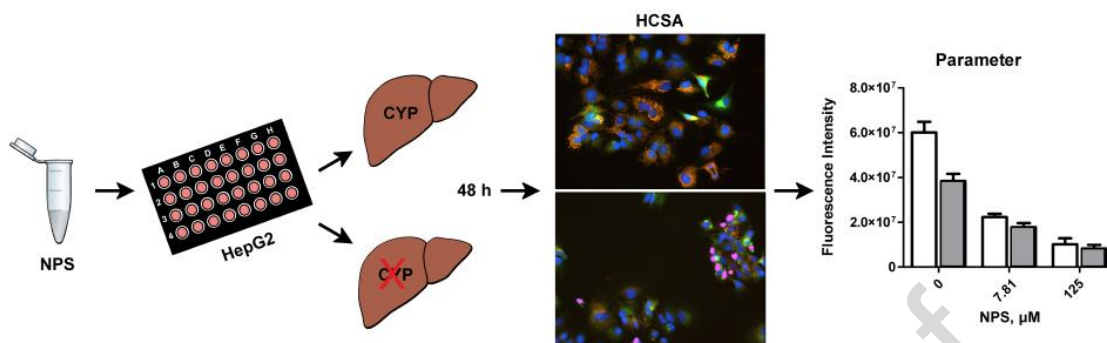


**Fig 3**



## Graphical abstract



## Highlights

- A simplified HCSA-based method was developed and tested using new psychoactive substances
- Significant cytotoxic potential was observed for two cathinone derivatives and one synthetic cannabinoid
- Metabolism-based effects on cytotoxicity were observed for one tryptamine derivative
- Mitochondrial membrane potential confirmed as most sensitive parameter

## 4. DISCUSSION AND CONCLUSIONS

In the first study, the in vitro metabolic stability and metabolism of the non-fentanyl derived new synthetic opioid (NSO) U-48800 were investigated using pHLS9. In vitro  $t_{1/2}$  and  $CL_{int}$  were computed and classified as moderate in comparison to the structurally similar NSO AH-7921.<sup>68</sup> However, in this study, pHLM was used instead of pHLS9, which contains significantly higher amounts of total CYP protein concentrations<sup>69</sup> Therefore, if pHLM is used instead of pHLS9, metabolic stability of U-48800 can be lower due to the potential higher metabolism rate in pHLM. Isozyme mapping of U-48800 revealed the particular involvement of CYP2C19 and CYP3A4 on its initial metabolic steps. As consequence, by inhibiting one of these isozymes, e.g., by drug-drug or drug-food interactions, or in case of a poor metabolizer of the polymorph expressed CYP2C19 may lead to increased U-48800 concentrations and elevated toxicity. It is expected that NSO are consumed in extremely low doses due to their high potency. Hence, detectability studies in rat urine after oral application of an estimated consumer dosage were performed by a standard urine precipitation (UP) procedure and targeted LC-HRMS/MS analysis.<sup>70,71</sup> Three metabolites were detected besides trace amounts of unaltered U-48800. The two phase I metabolites were formed by *N*-demethylation followed by hydroxylation whereas the phase II metabolite was formed by *N*-demethylation and dihydroxylation at the phenyl ring followed by methylation at one of the hydroxy groups. Based on these results and findings in human urine of structurally related compounds, the two *N*-demethyl-hydroxy metabolites and the parent compound should be considered as urinary screening targets. Additionally, the *N*-demethyl metabolite only identified in the in vitro experiments should be included, as it was the most abundant metabolite identified in human urine samples of structurally related compounds.<sup>36,72</sup> Based on the free fraction in plasma ( $f_u$ ) of U-48800, a

PPB of 92% was determined. PPB values above 70% are expected to influence toxicodynamic and toxicokinetic characteristics of a compound such as clearance. However, other influences such as the elimination route and active transport into hepatocytes may affect the clearance.<sup>73</sup> Moreover, drug-drug interactions may occur by displacement from the binding site of the plasma proteins.

Following the procedure from U-48800, in the second study the *in vitro* metabolic stability and metabolic pattern of the fentanyl related NSO cyclopentanoyl-fentanyl (CP-F) and tetrahydrofuranoyl-fentanyl (THF-F) were investigated using pHLS9. Values of *in vitro*  $t_{1/2}$  differed significantly between both NSO resulting in a high classification of  $Cl_{int}$  for CP-F and moderate in case of THF-F. These findings are most likely related to the replacement of one carbon atom in the cyclopentyl ring of CP-F by an oxygen atom in the THF-F molecule. Main *in vitro* metabolic reactions of both compounds included *N*-dealkylation, hydroxylation, and dihydroxylation. Among the 25 metabolites identified in total, 14 metabolites have already been identified in previous works and nine were described for the first time.<sup>74,75</sup> CYP2D6 and CYP3A4 particularly contributed to the initial metabolization of both NSO. By comparing these results with those of fentanyl and further derivatives, CYP2D6 and CYP3A4 seem to be the major players among others catalyzing initial phase I steps of fentanyl related compounds.<sup>76-78</sup> Detectability studies in rat urine using the same UP approach as applied for U-48800 produced no satisfactory results, as only one dihydroxy-metabolite of THF-F was detectable. Therefore, a more sophisticated approach should be used to confirm an intake of these NSO. After glucuronidase cleavage of the urine followed by SPE one dihydroxy metabolite of each CP-F and THF-F and additionally an oxo metabolite of THF-F could be detected. The structural difference of CP-F and THF-F at the ring system next to the amide moiety containing either a carbon or an oxygen atom may also explain why the PPB value of 99% determined for CP-F was much higher

compared to THF-F (74%). It is assumed that, PPB is highly reflected by physiochemical properties of a compound, besides ionization state or spatial configuration of a molecule.<sup>79,80</sup> Therefore, a high correlation between PPB and their lipophilicity is expected, which can be confirmed for CP-F and THF-F as calculated log *P*-values of 4.7 (CP-F) and 3.3 (THF-F) corresponded with their PPB. Simultaneous consumption of mainly CP-F with compounds exhibiting equally high binding affinity to plasma proteins may raise the risk of toxicity by displacement from the binding site.

In the third study, the metabolic stability of the two fentanyl homologs 4F-Cy-BAP and Fu-BAP was analyzed similarly according to the other NSO using pHLS9. The cut-off value for determining the in vitro half-life was set at 90 min due to decreasing enzyme activity after 2 h.<sup>34</sup> Consequently, for 4F-Cy-BAP the in vitro  $t_{1/2}$  could not be determined as it was longer than 90 min and thus it was not possible to compute  $CL_{int}$ . In accordance with McNaney et al.,  $Cl_{int}$  values of Fu-BAP can be rated as low.<sup>81</sup> In vitro metabolism of the two fentanyl homologs was studied using both pHLS9 and pHLM and compared to an in vivo zebrafish larvae model. The higher in vitro metabolic stability of 4F-Cy-BAP was confirmed by a smaller number of formed metabolites in all models in comparison to Fu-BAP. Introduction of the fluorine substituent at the phenyl ring of 4F-Cy-BAP can be discussed as main reason for its higher metabolic stability due its inductive/resonance (bond) or conformational and electrostatic (space) effects.<sup>82</sup> Most abundant metabolites of both compounds were formed by *N*-dealkylation, *N*-deacylation, hydroxylation, and *N*-oxidation, which may be suitable analytical targets in suspected intoxication cases. Notably, the majority of metabolites was detected in the zebrafish larvae model. A lower substrate concentration and shorter incubation time with pHLS9 in comparison to the zebrafish larvae experiments may be the cause for variations between both models. However, a comparative study on the metabolism of the SC 4F-MDMB-BINACA using

pHLS9, HepaRG, and zebrafish larvae revealed that the zebrafish larvae produced the largest number of metabolites underlining their potential as an alternative metabolism model.<sup>23</sup> Phase I metabolic reactions of 4F-Cy-BAP were mainly catalyzed by CYP3A4, whereas CYP2C19 was additionally involved in the formation of Fu-BAP metabolites. As a result, drug-drug interactions or in case of a CYP2C19 poor metabolizer may lead to toxic effects after their intake. PPB values of 4F-Cy-BAP and Fu-BAP were 98% and 95%. As discussed for CP-F, an intake of 4F-Cy-BAP and Fu-BAP together with other highly bound drugs may lead to displacement from the binding site and may increase the risk of drug-drug interactions. Especially since both compounds seem metabolically much more stable, which can even increase toxic risks.

In the fourth study, the *in vitro* phase I metabolism of three SC, JWH-200, A-796260, and 5F-EMB-PINACA, was investigated using pHLM. Numerous phase I metabolites of all three SC were identified, which may serve as target molecules for urine screenings in case of putative intoxications. The metabolic pattern of JWH-200 was already described by De Brabanter et al. in pHLM and in urine of liver-humanized mice, which differed in some metabolites from this study.<sup>83</sup> Possible explanations may be different incubation conditions and variations in sample preparation techniques. Both, JWH-200 and A-796260, consists of a morpholine moiety. Thus most abundant metabolic reactions of both compounds were found to be oxidative morpholine cleavage and oxidative morpholine opening. Apart from that, an additional main metabolite of JWH-200 was formed by *N*-dealkylation, whereas further high abundant metabolites of A-796260 were generated by mono- and dihydroxylation followed by dehydrogenation. Most abundant 5F-EMB-PINACA metabolites were formed via ester hydrolysis along with additional steps such as oxidative defluorination and hydroxylation. An isozyme mapping showed that various isozymes were involved in the biotransformation of all three SC making drug-drug interactions rather

unlikely. Additionally, an existing HCSA was optimized using a fully automated epifluorescence microscope to study cytotoxic propensity of the three SC. HepG2 cells were monitored for changes on the following six parameters: cell count, nuclear size, nuclear intensity, mitochondrial membrane potential, cytosolic calcium levels, and plasma membrane integrity. According to Richter et al., first a prescreening was performed using a low and high NPS concentration (7.81 and 125  $\mu\text{M}$ ) followed by a screening of serially doubled doses from a low to a high concentration range (1.95 – 125  $\mu\text{M}$ ) for compounds with a positive cytotoxic prescreening.<sup>53</sup> As all SC showed a positive result in the prescreening, subsequently a screening using a full concentration range was conducted. Based on the prescreening, evaluation criteria of a cytotoxic potential were as follows: if at least two parameters showed significant changes at a concentration of 7.81  $\mu\text{M}$ , a strong cytotoxic potential was assigned; if two parameters were significantly impaired and one of them at the low concentration (7.81  $\mu\text{M}$ ), a moderate cytotoxic potential was assigned; no cytotoxic potential was assigned, if parameters were only affected at the high concentration (125  $\mu\text{M}$ ). Accordingly, strong cytotoxic effects were observed for JWH-200 and A-796260, whereas 5F-EMB-PINACA showed moderate effects on HepG2 cells. The fact that not only parent compounds but also their metabolites may trigger toxic effects on cells led to further investigations on the impact of CYP-mediated metabolites thereon. For that purpose, the unspecific CYP inhibitor 1-aminobenzotriazole (ABT) was selected, which has been used, e.g., to examine metabolism-based effects of NPS from the amphetamine and cathinone type in primary rat hepatocytes.<sup>84,85</sup> JWH-200 was the only compound indicating metabolism-based effects by a significant loss in plasma membrane integrity, which manifested in an increased fluorescence intensity of TOTO-3 dye in high concentrated (125  $\mu\text{M}$ ) JWH-200 incubations containing additional ABT compared to incubations with JWH-200 alone. Even though the cytotoxicity HCS approach was

successfully optimized, with the overall concept being based on a prescreening followed by a screening in a whole concentration range, it seemed too extensive in laboratory work and costly for an initial assessment of cytotoxic properties of NPS regarding the ongoing fluctuation on the NPS market.

Therefore, in the last step, the cytotoxicity HCSA was simplified using only a low and high NPS concentration (7.81 and 125  $\mu\text{M}$ ) and applied on nine NPS from different classes. Following the same evaluation criteria as stated above: a strong cytotoxic potential was determined for ephylone, CUMYL-CBMICA, and dibutylone, whereas 5-methoxy-N-methyl-N-isopropyltryptamine (5-MeO-MiPT) showed moderate effects. Although both investigated phenylethylamine derivatives, 2-(4-chloro-2,5-dimethoxyphenyl)-N-(2-methoxybenzyl)-ethanamine (25C-NBOMe) and 2-(4-iodo-2,5-dimethoxyphenyl)-N-[(2-methoxyphenyl)methyl]-ethanamine (25I-NBOMe), strongly reduced the cell count at the high concentration, a relevant human toxicity is rather unlikely, as the published blood levels (0.87 - 73 nM) are far below the test concentrations.<sup>86</sup> No cytotoxic potential was observed for 4CN-CUMYL-BINACA, 5-methoxy-2-methyl-N,N-diallyltryptamine, and 2-(ethylamino)-1-(4-methylphenyl)-1-pentanone. Based on these results, an *in vivo* hepatotoxicity of ephylone and 5-MeO-MiPT described in literature can be confirmed *in vitro*.<sup>87,88</sup> CYP-derived effects on its cytotoxicity was only observed for 5-MeO-MiPT, by a significant reduction of the nuclear intensity in incubations at 125  $\mu\text{M}$  5-MeO-MiPT plus ABT in comparison to incubations without ABT indicating a higher toxicity of the potentially formed metabolites. Whereas the significant increase of the nuclear size in incubations with 125  $\mu\text{M}$  5-MeO-MiPT in comparison to incubations without ABT pointed towards a higher toxicity of the parent compound. Findings in this and preceding work revealed only in case of JWH-200 and 5-MeO-MiPT an involvement of CYP-mediated metabolism on the cytotoxicity. Even though Richter et al. were able to identify the most

abundant metabolites of different NPS after incubation with HepG2 cells, their limited metabolic activity may be a contributing factor on few significant results.<sup>29,53</sup> Likewise, HepG2 cell-based assays may underrate metabolite-mediated toxicity but also overestimate the significance of cell toxicity caused by parent compounds, which are rapidly metabolized in hepatocytes.<sup>59,89</sup> This may be particular relevant for the extensive metabolized SC or NBOMe compounds.<sup>14,90</sup> However, to confirm this assumption HepG2 cell incubates should have been analyzed for metabolites. Thus, future studies should include cell lines with a higher metabolic competence such as HepaRG cells or CYP-overexpressing HepG2. In both cytotoxicity investigations, inconsistent or opposite effects as expected were observed on some parameters, e.g., cell count or plasma membrane integrity. Improvements of the outcome parameters can potentially be achieved by combining the endpoint HCSA with a real-time analyzer, which monitors the proliferation rate and cell morphology continuously till the HCS analysis.<sup>60</sup> As expected from previous results, the mitochondrial membrane potential was identified as the most sensitive “cytobiomarker” in both investigations.<sup>53</sup> Having said that in some incubations ABT alone showed already a significant effect on the mitochondrial membrane potential, thus this parameter is not ideal to investigate metabolism-based effects under the given conditions.

Overall, results of the studies indicate that *in vitro* metabolism approaches are useful surrogates for *in vivo* models to identify possible biomarkers in human urine of different fentanyl and non-fentanyl NSO as well as SC. However, in terms of phase II metabolites or metabolites formed by consecutive reaction steps in *in vivo* models appear superior to *in vitro* systems as demonstrated by the findings of the BAP compounds in pHLS9 compared to zebrafish larvae. Given that NSO are often consumed in extremely low doses depending on their potency, development of sensitive analytical methods are needed to detect these compounds or their metabolites in authentic human urine samples. Such a method was

successfully implemented for CP-F and THF-F by glucuronidase cleavage followed by SPE. Studies on the *in vitro* PPB revealed that all fentanyl and non-fentanyl NSO as well as fentanyl homologs are bound with more than 70% to plasma proteins, which are expected to influence toxicodynamic and toxicokinetic characteristics of a compound. Especially, high PPB values in combination with low  $Cl_{int}$  as determined for CP-F, 4F-Cy-BAP, and Fu-BAP may even increase toxic risks by an additional prolonged dwell time in the body. Nevertheless, other clearance influencing factors not included in these studies, but not less important are their main elimination route or active transport into hepatocytes. Finally, a simplified HCSA approach was developed which allowed the straightforward assessment of NPS from different classes regarding their cytotoxic propensities on HepG2 cells. Even though metabolism-based effects were observed for JWH-200 and 5-MeO-MiPT using HepG2 cells further investigations are needed with cells exhibiting a higher metabolic activity than HepG2 cells such as HepaRG. This work clearly deepens the knowledge about NPS's toxicokinetic and cytotoxic properties, which are essential in the context of analytical confirmation after NPS consumption and to interpret clinical intoxication cases. Such data may be also valuable for authorities to build comprehensive risk assessments of NPS.

## 5. REFERENCES

1. UN. United Nations - Single Convention on Narcotic Drugs. 1961.
2. Feng LY, Battulga A, Han E, Chung H, Li JH. New psychoactive substances of natural origin: A brief review. *J Food Drug Anal.* 2017;25(3):461-471.
3. UNODC. New Psychoactive Substances Leaflet. 2020. [https://www.unodc.org/documents/scientific/NPS-Leaflet\\_WEB\\_2020.pdf](https://www.unodc.org/documents/scientific/NPS-Leaflet_WEB_2020.pdf). Accessed August 2022.
4. Helander A, Backberg M. Epidemiology of NPS Based Confirmed Overdose Cases: The STRIDA Project. *Handb Exp Pharmacol.* 2018;252:461-473.
5. Helander A, Bäckberg M. *New Psychoactive Substances*. Springer International Publishing; 2018.
6. UNODC. *Global SMART Update Volume 25*. [https://www.unodc.org/documents/scientific/GlobalSMART\\_25\\_web.pdf2021](https://www.unodc.org/documents/scientific/GlobalSMART_25_web.pdf2021).
7. EMCDDA. European Drug Report 2021. *Publications of of the European Union*. 2021. [http://www.emcdda.europa.eu/edr2020\\_en](http://www.emcdda.europa.eu/edr2020_en). Accessed August 2022.
8. Helander A, Bäckberg M, Beck O. Drug trends and harm related to new psychoactive substances (NPS) in Sweden from 2010 to 2016: Experiences from the STRIDA project. *PLoS One.* 2020;15(4):e0232038.
9. Zamengo L, Frison G, Bettin C, Sciarrone R. Understanding the risks associated with the use of new psychoactive substances (NPS): high variability of active ingredients concentration, mislabelled preparations, multiple psychoactive substances in single products. *Toxicol Lett.* 2014;229(1):220-228.
10. Reichel A, Lienau P. Pharmacokinetics in Drug Discovery: An Exposure-Centred Approach to Optimising and Predicting Drug Efficacy and Safety. *Handb Exp Pharmacol.* 2016;232:235-260.
11. Mak KK, Epemolu O, Pichika MR. The role of DMPK science in improving pharmaceutical research and development efficiency. *Drug Discov Today.* 2022;27(3):705-729.
12. Chung TDY, Terry DB, Smith LH. In Vitro and In Vivo Assessment of ADME and PK Properties During Lead Selection and Lead Optimization – Guidelines, Benchmarks and Rules of Thumb. In: Markossian S, Grossman A, Brimacombe K, et al., eds. *Assay Guidance Manual*. Bethesda (MD): Eli Lilly & Company and the National Center for Advancing Translational Sciences; 2004.
13. Meyer MR. New psychoactive substances: an overview on recent publications on their toxicodynamics and toxicokinetics. *Arch Toxicol.* 2016;90(10):2421-2444.

14. Diao X, Huestis MA. New Synthetic Cannabinoids Metabolism and Strategies to Best Identify Optimal Marker Metabolites. *Front Chem.* 2019;7:109.
15. Caspar AT, Gaab JB, Michely JA, Brandt SD, Meyer MR, Maurer HH. Metabolism of the tryptamine-derived new psychoactive substances 5-MeO-2-Me-DALT, 5-MeO-2-Me-ALCHT, and 5-MeO-2-Me-DIPT and their detectability in urine studied by GC-MS, LC-MS(n) , and LC-HR-MS/MS. *Drug Test Anal.* 2018;10(1):184-195.
16. Cone EJ, Tsadik A, Oyler J, Darwin WD. Cocaine metabolism and urinary excretion after different routes of administration. *Ther Drug Monit.* 1998;20(5):556-560.
17. Almazroo OA, Miah MK, Venkataramanan R. Drug Metabolism in the Liver. *Clin Liver Dis.* 2017;21(1):1-20.
18. Gómez-Lechón MJ, Lahoz A, Gombau L, Castell JV, Donato MT. In vitro evaluation of potential hepatotoxicity induced by drugs. *Curr Pharm Des.* 2010;16(17):1963-1977.
19. Yuan L, Kaplowitz N. Mechanisms of drug-induced liver injury. *Clin Liver Dis.* 2013;17(4):507-518, vii.
20. Seviour DK, Pelkonen O, Ahokas JT. Hepatocytes: the powerhouse of biotransformation. *Int J Biochem Cell Biol.* 2012;44(2):257-261.
21. Allen KR. Screening for drugs of abuse: which matrix, oral fluid or urine? *Ann Clin Biochem.* 2011;48(Pt 6):531-541.
22. Grafinger KE, Liechti ME, Liakoni E. Clinical value of analytical testing in patients presenting with new psychoactive substances intoxication. *Br J Clin Pharmacol.* 2020;86(3):429-436.
23. Wagmann L, Frankenfeld F, Park YM, et al. How to Study the Metabolism of New Psychoactive Substances for the Purpose of Toxicological Screenings-A Follow-Up Study Comparing Pooled Human Liver S9, HepaRG Cells, and Zebrafish Larvae. *Front Chem.* 2020;8:539.
24. Zeilinger K, Freyer N, Damm G, Seehofer D, Knöspel F. Cell sources for in vitro human liver cell culture models. *Exp Biol Med (Maywood).* 2016;241(15):1684-1698.
25. Ramboer E, Vanhaecke T, Rogiers V, Vinken M. Immortalized Human Hepatic Cell Lines for In Vitro Testing and Research Purposes. *Methods Mol Biol.* 2015;1250:53-76.
26. Yokoyama Y, Sasaki Y, Terasaki N, et al. Comparison of Drug Metabolism and Its Related Hepatotoxic Effects in HepaRG, Cryopreserved Human Hepatocytes, and HepG2 Cell Cultures. *Biol Pharm Bull.* 2018;41(5):722-732.
27. Hart SN, Li Y, Nakamoto K, Subileau EA, Steen D, Zhong XB. A comparison of whole genome gene expression profiles of HepaRG cells and HepG2 cells to

- primary human hepatocytes and human liver tissues. *Drug Metab Dispos.* 2010;38(6):988-994.
28. Richter LHJ, Maurer HH, Meyer MR. New psychoactive substances: Studies on the metabolism of XLR-11, AB-PINACA, FUB-PB-22, 4-methoxy-alpha-PVP, 25-I-NBOMe, and meclonazepam using human liver preparations in comparison to primary human hepatocytes, and human urine. *Toxicol Lett.* 2017;280:142-150.
  29. Richter LHJ, Flockenzi V, Maurer HH, Meyer MR. Pooled human liver preparations, HepaRG, or HepG2 cell lines for metabolism studies of new psychoactive substances? A study using MDMA, MDBD, butylone, MDPPP, MDPV, MDPB, 5-MAPB, and 5-API as examples. *J Pharm Biomed Anal.* 2017;143:32-42.
  30. Wagmann L, Gampfer TM, Meyer MR. Recent trends in drugs of abuse metabolism studies for mass spectrometry-based analytical screening procedures. *Anal Bioanal Chem.* 2021;413(22):5551-5559.
  31. Lee JY, Lee SY, Lee K, Oh SJ, Kim SK. Determination of species-difference in microsomal metabolism of amitriptyline using a predictive MRM-IDA-EPI method. *Chem Biol Interact.* 2015;229:109-118.
  32. Mardal M, Gracia-Lor E, Leibnitz S, Castiglioni S, Meyer MR. Toxicokinetics of new psychoactive substances: plasma protein binding, metabolic stability, and human phase I metabolism of the synthetic cannabinoid WIN 55,212-2 studied using in vitro tools and LC-HR-MS/MS. *Drug Test Anal.* 2016;8(10):1039-1048.
  33. Jones HM, Houston JB. Substrate depletion approach for determining in vitro metabolic clearance: time dependencies in hepatocyte and microsomal incubations. *Drug Metab Dispos.* 2004;32(9):973-982.
  34. Baranczewski P, Stanczak A, Sundberg K, et al. Introduction to in vitro estimation of metabolic stability and drug interactions of new chemical entities in drug discovery and development. *Pharmacol Rep.* 2006;58(4):453-472.
  35. Słoczyńska K, Gunia-Krzyżak A, Koczurkiewicz P, et al. Metabolic stability and its role in the discovery of new chemical entities. *Acta Pharm.* 2019;69(3):345-361.
  36. Nordmeier F, Doerr A, Laschke MW, et al. Are pigs a suitable animal model for in vivo metabolism studies of new psychoactive substances? A comparison study using different in vitro/in vivo tools and U-47700 as model drug. *Toxicol Lett.* 2020;329:12-19.
  37. Martignoni M, Groothuis GM, de Kanter R. Species differences between mouse, rat, dog, monkey and human CYP-mediated drug metabolism, inhibition and induction. *Expert Opin Drug Metab Toxicol.* 2006;2(6):875-894.
  38. Peters FT, Meyer MR. In vitro approaches to studying the metabolism of new psychoactive compounds. *Drug Test Anal.* 2011;3(7-8):483-495.

## References

39. Morales-Noé A, Esteve-Turrillas FA, Armenta S. Metabolism of third generation synthetic cannabinoids using zebrafish larvae. *Drug Test Anal.* 2022;14(4):594-603.
40. Wagmann L, Meyer MR. Reviewing toxicokinetics with a focus on metabolism of new psychoactive substances in the zebrafish (larvae) model. *WIREs Forensic Science.* 2022.
41. Jensen BP, Chin PK, Begg EJ. Quantification of total and free concentrations of R- and S-warfarin in human plasma by ultrafiltration and LC-MS/MS. *Anal Bioanal Chem.* 2011;401(7):2187-2193.
42. Kratochwil NA, Huber W, Muller F, Kansy M, Gerber PR. Predicting plasma protein binding of drugs: a new approach. *Biochem Pharmacol.* 2002;64(9):1355-1374.
43. Nilsson LB. The bioanalytical challenge of determining unbound concentration and protein binding for drugs. *Bioanalysis.* 2013;5(24):3033-3050.
44. Bohnert T, Gan LS. Plasma protein binding: from discovery to development. *J Pharm Sci.* 2013;102(9):2953-2994.
45. Smith SA, Waters NJ. Pharmacokinetic and Pharmacodynamic Considerations for Drugs Binding to Alpha-1-Acid Glycoprotein. *Pharm Res.* 2018;36(2):30.
46. Miida H, Noritake Y, Shimoda H, et al. Decrease in protein binding and its effect on toxicokinetics (TK)/toxicodynamics (TD) of diclofenac and propranolol in pregnant rats. *J Toxicol Sci.* 2008;33(5):525-536.
47. Suryanarayana P, Hari Priya K, Muktika T, Mukesh Chandra S, Pinaki S, Rakesh Kumar T. Chapter 12 - Drug–drug interactions and their implications on the pharmacokinetics of the drugs. *Advances in Pharmaceutical Product Development and Research.* 2022;2:291-322.
48. Wood DM, Sedefov R, Cunningham A, Dargan PI. Prevalence of use and acute toxicity associated with the use of NBOMe drugs. *Clin Toxicol (Phila).* 2015;53(2):85-92.
49. Simão AY, Antunes M, Cabral E, et al. An Update on the Implications of New Psychoactive Substances in Public Health. *Int J Environ Res Public Health.* 2022;19(8).
50. Shafi A, Berry AJ, Sumnall H, Wood DM, Tracy DK. New psychoactive substances: a review and updates. *Ther Adv Psychopharmacol.* 2020;10:2045125320967197.
51. Kronstrand R, Guerrieri D, Vikingsson S, Wohlfarth A, Green H. Fatal Poisonings Associated with New Psychoactive Substances. *Handb Exp Pharmacol.* 2018;252:495-541.
52. O'Brien PJ, Edvardsson A. Validation of a Multiparametric, High-Content-Screening Assay for Predictive/Investigative Cytotoxicity: Evidence from

- Technology Transfer Studies and Literature Review. *Chem Res Toxicol*. 2017;30(3):804-829.
53. Richter LHJ, Beck A, Flockerzi V, Maurer HH, Meyer MR. Cytotoxicity of new psychoactive substances and other drugs of abuse studied in human HepG2 cells using an adopted high content screening assay. *Toxicol Lett*. 2019;301:79-89.
  54. Gerets HH, Tilmant K, Gerin B, et al. Characterization of primary human hepatocytes, HepG2 cells, and HepaRG cells at the mRNA level and CYP activity in response to inducers and their predictivity for the detection of human hepatotoxins. *Cell Biol Toxicol*. 2012;28(2):69-87.
  55. Ding C, Li Y, Guo F, et al. A Cell-type-resolved Liver Proteome. *Mol Cell Proteomics*. 2016;15(10):3190-3202.
  56. Kammerer S. Three-Dimensional Liver Culture Systems to Maintain Primary Hepatic Properties for Toxicological Analysis In Vitro. *Int J Mol Sci*. 2021;22(19).
  57. Meijer M, Hendriks HS, Heusinkveld HJ, Langeveld WT, Westerink RH. Comparison of plate reader-based methods with fluorescence microscopy for measurements of intracellular calcium levels for the assessment of in vitro neurotoxicity. *Neurotoxicology*. 2014;45:31-37.
  58. Mandavilli BS, Aggeler RJ, Chambers KM. Tools to Measure Cell Health and Cytotoxicity Using High Content Imaging and Analysis. *Methods Mol Biol*. 2018;1683:33-46.
  59. Garside H, Marcoe KF, Chesnut-Speelman J, et al. Evaluation of the use of imaging parameters for the detection of compound-induced hepatotoxicity in 384-well cultures of HepG2 cells and cryopreserved primary human hepatocytes. *Toxicol In Vitro*. 2014;28(2):171-181.
  60. Single A, Beetham H, Telford BJ, Guilford P, Chen A. A Comparison of Real-Time and Endpoint Cell Viability Assays for Improved Synthetic Lethal Drug Validation. *J Biomol Screen*. 2015;20(10):1286-1293.
  61. Chu X, Cai X, Cui D, et al. In vitro assessment of drug-drug interaction potential of boceprevir associated with drug metabolizing enzymes and transporters. *Drug Metab Dispos*. 2013;41(3):668-681.
  62. Dias da Silva D, Ferreira B, Roque Bravo R, et al. The new psychoactive substance 3-methylmethcathinone (3-MMC or metaphedrone) induces oxidative stress, apoptosis, and autophagy in primary rat hepatocytes at human-relevant concentrations. *Arch Toxicol*. 2019;93(9):2617-2634.
  63. Gampfer TM, Richter LHJ, Schäper J, Wagmann L, Meyer MR. Toxicokinetics and analytical toxicology of the abused opioid U-48800 - in vitro metabolism, metabolic stability, isozyme mapping, and plasma protein binding. *Drug Test Anal*. 2019;11(10):1572-1580.
  64. Gampfer TM, Wagmann L, Richter MJ, Fischmann S, Westphal F, Meyer MR. Toxicokinetic Studies and Analytical Toxicology of the New Synthetic Opioids

- Cyclopentanoyl-Fentanyl and Tetrahydrofuranoyl-Fentanyl. *J Anal Toxicol.* 2020;44(5):449-460.
65. Gampfer TM, Wagmann L, Park YM, et al. Toxicokinetics and toxicodynamics of the fentanyl homologs cyclopropanoyl-1-benzyl-4-fluoro-4-anilinopiperidine and furanoyl-1-benzyl-4-anilinopiperidine. *Arch Toxicol.* 2020;94(6):2009-2025.
66. Gampfer TM, Wagmann L, Belkacemi A, Flockerzi V, Meyer MR. Cytotoxicity, metabolism, and isozyme mapping of the synthetic cannabinoids JWH-200, A-796260, and 5F-EMB-PINACA studied by means of in vitro systems. *Arch Toxicol.* 2021;95(11):3539-3557.
67. Gampfer TM, Wagmann L, Pulver B, Westphal F, Flockerzi V, Meyer MR. A simplified strategy to assess the cytotoxicity of new psychoactive substances in HepG2 cells using a high content screening assay - Exemplified for nine compounds. *Toxicology.* 2022:153258.
68. Wohlfarth A, Scheidweiler KB, Pang S, et al. Metabolic characterization of AH-7921, a synthetic opioid designer drug: in vitro metabolic stability assessment and metabolite identification, evaluation of in silico prediction, and in vivo confirmation. *Drug Test Anal.* 2016;8(8):779-791.
69. Wang X, He B, Shi J, Li Q, Zhu HJ. Comparative Proteomics Analysis of Human Liver Microsomes and S9 Fractions. *Drug Metab Dispos.* 2020;48(1):31-40.
70. UNODC. World Drug Report 2020. 2020.
71. Wissenbach DK, Meyer MR, Remane D, Weber AA, Maurer HH. Development of the first metabolite-based LC-MS(n) urine drug screening procedure-exemplified for antidepressants. *Anal Bioanal Chem.* 2011;400(1):79-88.
72. Krotulski AJ, Mohr ALA, Papsun DM, Logan BK. Metabolism of novel opioid agonists U-47700 and U-49900 using human liver microsomes with confirmation in authentic urine specimens from drug users. *Drug Test Anal.* 2018;10(1):127-136.
73. Howard ML, Hill JJ, Galluppi GR, McLean MA. Plasma protein binding in drug discovery and development. *Comb Chem High Throughput Screen.* 2010;13(2):170-187.
74. Astrand A, Toreskog A, Watanabe S, Kronstrand R, Green H, Vikingsson S. Correlations between metabolism and structural elements of the alicyclic fentanyl analogs cyclopropyl fentanyl, cyclobutyl fentanyl, cyclopentyl fentanyl, cyclohexyl fentanyl and 2,2,3,3-tetramethylcyclopropyl fentanyl studied by human hepatocytes and LC-QTOF-MS. *Arch Toxicol.* 2019;93(1):95-106.
75. Krotulski AJ, Papsun DM, Friscia M, Swartz JL, Holsey BD, Logan BK. Fatality Following Ingestion of Tetrahydrofuranlylfentanyl, U-49900 and Methoxy-Phencyclidine. *J Anal Toxicol.* 2018;42(3):e27-e32.
76. Steuer AE, Williner E, Staeheli SN, Kraemer T. Studies on the metabolism of the fentanyl-derived designer drug butyrfentanyl in human in vitro liver preparations

- and authentic human samples using liquid chromatography-high resolution mass spectrometry (LC-HRMS). *Drug Test Anal.* 2017;9(7):1085-1092.
77. Meyer MR, Dinger J, Schwaninger AE, et al. Qualitative studies on the metabolism and the toxicological detection of the fentanyl-derived designer drugs 3-methylfentanyl and isofentanyl in rats using liquid chromatography-linear ion trap-mass spectrometry (LC-MS(n)). *Anal Bioanal Chem.* 2012;402(3):1249-1255.
78. Guitton J, Buronfosse T, Desage M, Lepape A, Brazier JL, Beaune P. Possible involvement of multiple cytochrome P450S in fentanyl and sufentanil metabolism as opposed to alfentanil. *Biochem Pharmacol.* 1997;53(11):1613-1619.
79. Zhivkova ZD. Quantitative Structure - Pharmacokinetics Relationships for Plasma Protein Binding of Basic Drugs. *J Pharm Pharm Sci.* 2017;20(1):349-359.
80. Fauber BP, Rene O, de Leon Boenig G, et al. Reduction in lipophilicity improved the solubility, plasma-protein binding, and permeability of tertiary sulfonamide RORc inverse agonists. *Bioorg Med Chem Lett.* 2014;24(16):3891-3897.
81. McNaney CA, Drexler DM, Hnatyshyn SY, et al. An automated liquid chromatography-mass spectrometry process to determine metabolic stability half-life and intrinsic clearance of drug candidates by substrate depletion. *Assay Drug Dev Technol.* 2008;6(1):121-129.
82. Park BK, Kitteringham NR, O'Neill PM. Metabolism of fluorine-containing drugs. *Annu Rev Pharmacol Toxicol.* 2001;41:443-470.
83. De Brabanter N, Esposito S, Tudela E, et al. In vivo and in vitro metabolism of the synthetic cannabinoid JWH-200. *Rapid Commun Mass Spectrom.* 2013;27(18):2115-2126.
84. Roque Bravo R, Carmo H, Valente MJ, et al. From street to lab: in vitro hepatotoxicity of buphedrone, butylone and 3,4-DMMC. *Arch Toxicol.* 2021;95(4):1443-1462.
85. Roque Bravo R, Carmo H, Valente MJ, et al. 4-Fluoromethamphetamine (4-FMA) induces in vitro hepatotoxicity mediated by CYP2E1, CYP2D6, and CYP3A4 metabolism. *Toxicology.* 2021;463:152988.
86. Poklis JL, Devers KG, Arbefeville EF, Pearson JM, Houston E, Poklis A. Postmortem detection of 25I-NBOMe [2-(4-iodo-2,5-dimethoxyphenyl)-N-[(2-methoxyphenyl)methyl]ethanamine] in fluids and tissues determined by high performance liquid chromatography with tandem mass spectrometry from a traumatic death. *Forensic Sci Int.* 2014;234:e14-20.
87. Altunci YA, Aydogdu M, Acikgoz E, et al. New Psychoactive Substance 5-MeO-MiPT In vivo Acute Toxicity and Hystotoxicological Study. *Balkan Med J.* 2021;38(1):34-42.
88. Giachetti AD, Kahl JH, Zaney ME, Hime GW, Boland DM. Method Validation of Seven Synthetic Cathinones by LC-MS/MS Analysis and the Prevalence of N-Ethylpentylone in Postmortem Casework. *J Anal Toxicol.* 2020.

## References

89. Steinbrecht S, König R, Schmidtke KU, et al. Metabolic activity testing can underestimate acute drug cytotoxicity as revealed by HepG2 cell clones overexpressing cytochrome P450 2C19 and 3A4. *Toxicology*. 2019;412:37-47.
90. Zawilska JB, Kacela M, Adamowicz P. NBOMes-Highly Potent and Toxic Alternatives of LSD. *Front Neurosci*. 2020;14:78.

## 6. ABBREVIATIONS

2D	two-dimensional
3D	three-dimensional
4F-Cy-BAP	cyclopropanoyl-1-benzyl-4'-fluoro-4-anilinopiperidine
5-MeO-MiPT	5-methoxy-N-methyl-N-isopropyltryptamine
25C-NBOMe	2-(4-chloro-2,5-dimethoxyphenyl)-N-(2-methoxybenzyl)-ethanamine
25I-NBOMe	2-(4-iodo-2,5-dimethoxyphenyl)-N-[(2-methoxyphenyl)methyl]-ethanamine
ABT	1-aminobenzotriazole
$Cl_{int}$	intrinsic clearance
CP-F	cyclopentanoyl-fentanyl
CYP	cytochrome P450 monooxygenase
$f_u$	free fraction in plasma
Fu-BAP	furanoyl-1-benzyl-4-anilinopiperidine
LC-HRMS/MS	liquid chromatography coupled to high resolution mass spectrometry
HCSA	high-content screening assay
NPS	new psychoactive substances
NSO	new synthetic opioid
PHH	primary human hepatocytes

## Abbreviations

pHLM	pooled human liver microsomes
pHLS9	pooled human S9 fraction
PPB	plasma protein binding
SC	synthetic cannabinoid
SPE	solid phase extraction
SULT	sulfotransferases
$t_{1/2}$	half-life
THF-F	tetrahydrofuranoyl-fentanyl
UGT	uridine diphosphate glucuronyltransferases
UP	urine precipitation